STUDIES ON HETEROGENIZATION OF METAL COMPLEX CATALYSTS BY ENCAPSULATION IN ZEOLITES AND MESOPOROUS MATERIALS

A THESIS

SUBMITTED TO THE

UNIVERSITY OF PUNE

FOR THE DEGREE OF

DOCTOR OF PHILOSOPHY

IN

CHEMISTRY

BY

KAUSIK MUKHOPADHYAY

AT

HOMOGENEOUS CATALYSIS DIVISION
NATIONAL CHEMICAL LABORATORY
PUNE 411008
INDIA

DECEMBER 2003

DECLARATION BY RESEARCH GUIDE

Certified that the work incorporated in the thesis entitled: "**Studies on Heterogenization of Metal Complex Catalysts by Encapsulation in Zeolites and Mesoporous Materials**", submitted by Mr. Kausik Mukhopadhyay was carried out under my supervision. Such material as has been obtained from other sources has been duly acknowledged in the thesis.

December, 2003 **Dr. Raghunath V. Chaudhari**

Pune (Supervisor/ Research Guide)

DECLARATION BY RESEARCH SCHOLAR

I hereby declare that the thesis entitled "**Studies on Heterogenization of Metal Complex Catalysts by Encapsulation in Zeolites and Mesoporous Materials**", submitted for the Degree of Doctor of Philosophy to the University of Pune, has been carried out by me at the National Chemical Laboratory, Pune under the supervision of Dr. R. V. Chaudhari. The work is original and has not been submitted in part or full by me for any other degree or diploma to this or any other University.

Date: **Kausik Mukhopadhyay**

Dedicated to

My Parents,

My Teachers,

My Sister &

My Wife

ACKNOWLEDGEMENT

I wish to express my sincere gratitude and respect to Dr. R. V. Chaudhari, Head, Homogeneous Catalysis Division, National Chemical Laboratory (NCL) for his constant support, allowing and helping me to think and work independently, seed innovations to my work and constantly encouraging during the course of my work. I am will be remaining ever grateful to him for his teaching, guidance, friendship and wonderful personality.

I am grateful to Council of Scientific and Industrial Research (CSIR), India for the research fellowship. I am thankful to Dr. Paul Ratnasamy (ex-Director, NCL) and Dr. S. Sivaram, Director, NCL for allowing me to carry out research work and extending me all the possible infrastructural facilities from time to time in this institute of repute.

I take this opportunity to express my sincere gratitude to Dr. Rajiv Kumar, who was my mentor in understanding the subject of zeolites and my (un-official) co-guide, Dr. Ganapathy & Dr. Rajmohanan for rendering help and sharing knowledge in solid-state NMR of materials, Dr. A. V. Ramaswamy, Dr. Mandale, Dr. Gopinathan for their valuable help and suggestions in my research work. I am very much thankful to the Electron Microscope group, specially Dr. Sainkar for SEM and Dr. Bhadbhade, Mrs. Renu Parischa and Mr. Rajesh Gonnade for TEM, while helping me in every possible way through fruitful discussions.

I sincerely acknowledge Dr. R. Jaganathan, Dr. S. P. Gupte, Dr. G. S. Grover, Dr. C. V. Rode, Dr. R. M. Deshpande, Dr. V. M. Bhandari, Dr. A. A. Kelkar, Dr. V. V. Ranade, Mr. P. B. Jadkar, Mr. Ozarde and especially the divisional office staffs and Mr. Raheja for their valuable help and co-operation during my stay in NCL. I am also very much thankful to my senior colleagues Dr. A. Seayad, Dr. Jayasree Seayad, Dr. Suju P. Mathew and Dr. Vinod Nair for their helpful hand, sympathetic ears and making the lab feel like a family. Special thanks are to Dr. Amitava Sarkar, Dr. Murali Sastry and Dr. Priyabrata Mukherjee.

I would like to express my deep felt gratitude to my colleagues and friends, Subarno (ramu), Saptarshi (dadu), Mahua, Subhash, Arindam, Somnath, Sujata, Tarun, Anuradha, Bikash, Debasish (H) and Debasish (S), Dilip, Prabal, Sukhen, Deenu, Chitta, Senapati, Annyt, Babu, Rajaram, Khudiram, Subho, Kartick M, Saikat, Prabhash, Chaitali, Soumitro, Pradeep for spending such a wonderful time; the pleasure, joy and happiness we shared in drinks and food together, in roaming the peaceful, enchanting, fashionable and romantic city of Pune, watching movies together, chatting (Adda, as we call in Bengali) late nights in my room and doing everything in an unconventional and unprecedented way cannot be forgotten through out the rest of my life. I will miss the room-206-culture so much!!

I must thank my lab mates and friends, Yogesh, Sunil, Avinash, Srikanth, Manisha K, Manisha Kapote, Deepali, Manisha T, Anand S, Mahesh, Rajesh, Charu, Savita, Gunjal, Buwa, Anamika, Rita, Rashmi and Anand and all my junior colleagues who have joined now. I must thank all members of homogeneous catalysis division for such a friendly

and cheerful working atmosphere. I must also thank Sourav, Soma, Abhijit and Nalinava of IIT, Powaii and Ashwini, Sumant, Damodaran, Sachin, Anuji, Anuj, Jeetu (C) and many in NCL who are not named in person for their valuable suggestions and helping hands. Thanks to my Calcutta University batch-mates, Sarbani, Arijit and Arindam Basu, who have been so indispensable from my MSc days.

Special thanks to my graduation tutor, Dr. Swapan Sen Gupta from whom I learnt the aroma and taste of inorganic chemistry! His implausible way of teaching was so instrumental in building up my research career in chemistry and the knowledge he ushered still helps me to understand the basics of chemistry. I am indebted to my teachers, professors and staffs of Ramakrishna Mission Vidyapith Purulia, St. Xaviers College Calcutta, University Science College Calcutta and Presidency College Calcutta. The quality of education led the foundation stone of the cocktail of east-west culture.

I must be doing injustice if I don't mention three very special persons, who have been my friends and scientific colleagues and always beside me in my sunny and rainy days; Anirban, Bibhas and Debdut. Their help, cooperativeness, immensely friendly attitude and compromising nature have made me learnt so much from them. Thank you Debu in whichever way you have helped me and with your charming presence. Anirban, special thanks to you as I learnt so much from you about non-scientific subjects and discussions besides science and the way you work. And Bibhas, what more can I tell of you, you are such a wonderful brother, will be missing your delightful presence very much.

Baba, Maa and Sumi, I must thank you for the patience and belief you have shown on your naughty child; without your love, blessings, imparting culture, preparing marvelous cuisines, beatings and scolds it would have been impossible for this naughty child to obtain his PhD degree, that too in chemistry; due thanks and respect to my in-laws (Maa, Piya and Babai) who had so much love and faith in me. I am sure my granny and maternal uncle (baro-mama) would have been so happy this day if they were alive. May their souls rest in peace, their blessings and encouragement have always made me an optimist in any unknown areas I had ventured.

No words of appreciation can fulfill the status of my dear wife, Atashi. I should not belittle you by thanking, as you are so indispensable in my life. I must mention that my personal and professional life has changed being with you. The year 2000 was so special in every aspect, starting from the day we first met and the day we got married. I could not have completed my thesis without your love, respect, patience, appreciation, scientific discussions, faith, help and your letters from abroad, which kept my spirits alive. Never I felt you were so far away from me, the distance of Bonn and Pune being thousands of miles. It was you and only you who transformed my life radically in every possible way.

December 2003 *Kausik Mukhopadhyay*

CONTENTS

LIST OF CONTENTS

Page

LIST OF FIGURES

LIST OF TABLES

LIST OF SCHEMES

LIST OF ABBREVIATIONS

2D	Two Dimensional
3D	Three Dimensional
AAS	Atomic Absorption Spectroscopy
AFM	Atomic Force Microscopy
APTS	3-Aminopropyltrimethoxy silane
ATMS	Allyltrimethoxy silane
BE	Binding Energy
BET	Brunauer-Emmett-Teller
BJH	Barrett-Joyner-Halenda
BTME	Bis(trimethoxysilyl) ethane
BTSEY	1,2-Bis(triethoxysilyl) ethylene
CP	Cross Polarization
CTMABr or CTABr	Cetyltrimethylammonium bromide
DCM	Dichloromethane
EDT	Ethylenediaminetriacetic Acid
ESCA	Electron Spectroscopy for Chemical Analyses
FAU	Faujasite
FER	Ferrierite
FSM	Folded Sheet Materials
FTIR	Fourier Transform Infrared
GC	Gas Chromatography
GIS	Gismondite
HMS	Hexagonal Mesoporous Silica
HPA	Heteropolyacid
HRTEM	High Resolution Transmission Electron Microscopy
HSAB	Hard and Soft Acid and Base
IBPE	Isobutylphenylethanol
ICP-AES	Inductively Coupled Plasma with Atomic Emission Spectra

IUPAC	International Union for Pure and Applied Chemistry
MA	Molybdic Acid
MAS	Magic Angle Spinning
MCM	Mobil's Crystalline Material
MEK	Methylethylketone
MFI	Mobil's Five
MSU-V	Michigan State University - Vesicle
NMR	Nuclear Magnetic Resonance
ODTMA	Octadecyltrimethylammonium chloride
OTES	Octyltriethoxy siane
PEO	Polyethylene Oxide
PMA	Phosphomolybdic Acid
PMO	Periodic Mesoporous Organosilica
PPA	2-Phenylpropanoic Acid
PTA	Phosphotungstic Acid
PTES	Phenyltriethoxy silane
Pyca	Pyridine 2-Carboxylate
SAP	Supported Aqueous Phase
SAXS	Small Angle X-Ray Scattering
SBA	Santa Barbara Amorphous
SEM	Scanning Electron Microscopy
SLP	Supported Liquid Phase
TEM	Transmission Electron Microscopy
TEOS	Tetraethyl orthosilicate
TLK	Terrace–Ledge–Kink
TMA	Tetramethylammonium
TMOS	Trimethoxy silane
TMS	Tetramethylsilane
TOF	Turn Over Frequency
TON	Turn Over Number
TPA	Tetrapropylammonium

UOFMN	Unified Organically Functionalized Mesoporous Network
UV-Vis	Ultraviolet-Visible
VTES	Vinyltriethoxy silane
WA	Tungstic Acid
WAXS	Wide Angle X-Ray Scattering
Wk	Wilkinson's Catalyst, $HRh(CO)(PPh_3)_3$
XPS	X-Ray Photoelectron Spectroscopy
XRD	X-Ray Diffraction
ZSM	Zeolite Socony Mobil

Summary and Conclusions

The continuing sophistication in and ever changing landscape of molecular targets for a myriad of applications ranging from biology to materials science requires a continuing evolution of synthetic methods[1]. Zeolites, zeotypes and mesoporous materials are the novel materials, which meet the challenges of industrial applications abiding by the economic and environmental concerns. The discovery of these materials with their enormous practical utility led to synthesis, characterization and practical applications of these materials playing a pivotal role in chemistry, more importantly in catalysis.

Zeolites and zeotypes (molecular sieves) owing to their varied intrinsic properties (e.g. acidity, basicity, redox behaviour etc.), channel sizes, high surface areas, thermal and chemical stabilities and channel structures (shape selectivities) have been extensively used in oil refining, petrochemical and fine chemical industries for the past couple of decades, for producing bulk chemicals, fine chemicals and speciality chemicals[2]. However, with the limitation of micro-pore sizes (less than 13 Å), synthesis of complex organic molecules is inefficient, demanding a search for new materials with larger pore sizes. The discovery of a novel family of mesoporous materials called M41S has opened new opportunities in catalytic applications in this context. The M41S family has been generally classified into three different categories: MCM – 41 (hexagonal), MCM – 48 (cubic) and MCM – 50 (lamellar)[3]. These mesoporous materials have larger surface areas (> 700 m^2g^{-1}) and well-defined pore sizes (20 – 100 Å) and tenability to change the pore sizes have made them the most sought after materials of the last decade. The syntheses of these materials have expanded the applications of solid catalysts for developing new processes for fine and bulk chemicals.

Homogeneous catalysis is gaining considerable interest due to their high activity and selectivity at milder reaction conditions for a wide variety of reactions. However, their practical applications have been limited due to difficulties in achieving industrially viable catalyst-product separation[4]. In this context, encapsulation of metal complexes as a mean of "heterogenization" has particular significance. In this approach, the organometallic complex is encapsulated or anchored inside the pores of the inorganic inert matrices, e.g. zeolites, M41S materials, clay etc. in such a way that the complex is tightly bound inside the pores[5]. The prime requirement is stability of the encapsulated complex, so that it does not leach out of the catalyst pores to the liquid phase in the course of reaction, while retaining high

activity, selectivity and original configuration. In several reports, heterogeneous catalysis by encapsulated materials has been addressed for oxidation, hydrogenation, epoxidation and Heck reactions, but attempts to heterogenize some of the industrially relevant homogeneous catalysts for hydroformylation and carbonylation reactions have been very limited[6]. Also, a direct comparison of the encapsulated catalysts with their homogeneous counterparts has not been well investigated with meaningful quantitative data. It is envisaged that the metal complexes encapsulated in zeolites and mesoporous supports lead to very high metal dispersion and stable catalysts in addition to the possibility of tuning the selectivity. Similarly, the micro- and mesostructures could prevent leaching of metal complexes in solution, a serious problem with most of the "heterogenized" catalysts. Immobilized catalysts reported earlier, suffer either from lower selectivity and activity (TON), or low recyclability, or use expensive ligands and hence, not suitable for practical applications. Therefore, there is ample opportunity to explore development of new methods of heterogenization, which will eliminate the limitations of the state of the art methods. It is in this context that the encapsulation of metal complex catalysts provides an alternative approach opening up new vistas for the industrial applications in synthesis of speciality chemicals, fine chemicals. These catalysts could also have important applications in other homogeneous or organic reactions, wherein selectivity, catalyst-product separation and use of eco-friendly technologies is still a challenging task. The aim of this thesis was to investigate the approach of encapsulation or anchoring for heterogenization of industrially significant catalysts used in hydroformylation and carbonylation reactions.

The thesis is also aimed at characterization of the heterogeneous catalysts and investigation of the catalytic performance in comparison to the homogeneous and previously known heterogeneous catalysts. The specific problems chosen are:

- Synthesis of zeolites and mesoporous materials by employing heteropolyacids and metal oxoanions of group VI (molybdenum and tungsten) as novel promoters.
- Novel heterogeneous catalysts containing encapsulated $HRh(CO)(PPh_3)_3$ in different porous supports for hydroformylation of olefins to aldehydes.
- Novel heterogeneous catalysts containing encapsulated Pd-complex catalysts in different porous supports for hydrocarboxylation of olefins and alcohols to corresponding carboxylic acids.

- Metal complexes anchored on heteropolyacids tethered to zeolite and mesoporous materials for hydroformylation and hydrocarboxylation of alkenes.

Chapter 1 deals with a detailed literature survey on zeolites and mesoporous materials (as supports for encapsulation), encapsulation of homogeneous metal complex catalysts for hydroformylation and hydrocarboxylation of olefins. The merits and demerits of encapsulation in comparison to other methods of heterogenization have been discussed including the potential of these catalysts in practical applications. Based on these reviews, a scope of work of this thesis has been outlined.

Chapter 2 presents experimental results on synthesis of zeolites and mesoporous materials by employing heteropolyacids (HPA's) and metal oxoanions of group VI (molybdenum and tungsten) as new promoters. It was previously reported that addition of small amount of inorganic salts enhances the rates of zeolite crystallization by many folds. We observed dramatic increase in crystallization rates of zeolites, zeotypes and mesoporous materials by using catalytic amounts of HPA's and illustrated excellent crystallinity and high surface areas of the porous materials. These anions when used in catalytic amounts reduce the crystallization time for synthesis of these porous materials by many-folds. The observed trends for the crystallization rates of the synthesis of these porous materials can be explained on the basis of *soft and hard acid base* (SHAB) theory. Synthesis and characterization of these porous, inorganic supports by powder XRD, ^{29}Si MAS NMR, surface area measurements, AAS, SEM and TEM have been discussed along with optimum recommended conditions. The technique will thus be very much useful in the synthesis of various types of porous materials or other supported materials in a short duration and still recovering their exact physical characteristics.

Chapter 3 deals with novel heterogeneous catalyst systems containing encapsulated or immobilized $HRh(CO)(PPh_3)_3$ in different porous supports like NaY, MCM-41 and MCM-48 for hydroformylation of olefins to aldehydes. The preparation methods for encapsulation and characterization of these heterogenized solid catalysts by UV-VIS, FT-IR, ^{29}Si, ^{27}Al and ^{31}P (CP MAS) solid-state NMR spectroscopy, powder XRD, SEM, TEM (for analyzing the

porous phases and crystallinity before and after the reactions) and XPS (for retention of oxidation states of the metal complex after immobilization) have been discussed. ICP analyses of the catalysts before and after the reactions as well as the leaching of Rh under reaction conditions are also discussed. The encapsulated catalysts were found to be very stable, with excellent reusability (recycled 10 times without loosing activity) and produce high turn over numbers for hydroformylation of olefins to aldehydes. In case of styrene hydroformylation TON's were ~ 800, 1200 and 1300 with total aldehyde selectivity > 99% and n/iso ratio in a range of 2:3 and 3:7 for encapsulated $HRh(CO)(PPh_3)_3$ in MCM-41, NaY and MCM-48 supports respectively.

Chapter 4 deals with novel heterogeneous catalyst systems containing encapsulated Pd complex catalysts (e.g. Pd-pyca; pyca = pyridine carboxylic acid ligand) in different porous supports like NaY, MCM-41 and MCM-48 for hydrocarboxylation of olefins and alcohols to acids. It is demonstrated for the first time that the encapsulation methodology can be applied to palladium-catalyzed hydrocarboxylation of olefins and alcohols. Catalysts consisting of Pd-pyca or other Pd-complexes immobilized on MCM-41 and MCM-48 supports were found to give excellent activities and selectivities. Characterization of the heterogenized solid catalysts by FT-IR, solid-state NMR spectroscopy, powder XRD, SEM, TEM and XPS has also been discussed. The ICP analyses of the catalysts before and after the reactions as well as that of the liquid phase showed no leaching of Pd during the reaction. These catalysts showed excellent activity and selectivity for hydrocarboxylation (e.g. in hydrocarboxylation of styrene the TON for encapsulated Pd-pyca in MCM-41 was 5556) with 98% conversion and 99% selectivity for the branched carboxylic acid products.

Chapter 5 deals with unique heterogeneous catalyst systems containing metal complexes anchored on a zeolite Na-Y support tethered with heteropolyacids (HPA's). Many of the anchored homogeneous systems have drawbacks such as drop in activity and/or selectivity compared to homogeneously catalyzed reactions, due to leaching of the active species or the metal. A new technique was developed that circumvents these problems by allowing homogeneous catalysts containing cationic metal ion, a neutral mono- or bidentate ligand and an anionic counter ion to be anchored to a support. Here we describe for the first

time use of HPA's as the anchoring species between the support material (zeolite Na-Y) and the metal complex catalysts e.g. $HRh(CO)(PPh_3)_3$ and Pd-pyca and using the heterogeneous catalysts thus prepared for hydroformylation and hydrocarboxylation of linear and branched olefins. A major advantage of this *tethering* technique is that modifications on the ligand system are not necessary to anchor the catalyst to the support. Details on characterization of the catalysts as well as hydroformylation and hydrocarboxylation activity with exceptional stability by using tethered $HRh(CO)(PPh_3)_3$ and Pd-pyca complexes in zeolite matrix are discussed.

In conclusion, this thesis presents investigations on encapsulation and tethering as techniques of heterogenization of homogeneous catalysts. It is shown that both tethered and encapsulated Rh and Pd catalysts were found to be highly stable for hydroformylation and hydrocarboxylation reactions respectively. The activity and selectivity data on these catalysts indicate that desired selectivities can be tuned with appropriate choice of catalysts and supports. Extensive characterization studies of the catalysts before and after the reaction has led to confirmation of encapsulation of metal complexes in the pores or cages of the supports and allowed a correlation of catalyst activity and selectivity. The activity and selectivity observed for hydroformylation and hydrocarboxylation were found to be higher than conventional heterogeneous catalysts, though lower than homogeneous catalysts. This indicates the potential use of the encapsulation or tethered approach for practical applications, especially for high molecular weight complex organic compounds.

KEY REFERENCES

1. B. M. Trost, *Science* **1991**, *254*, 1471.
2. A. Corma, *Chem. Rev.* **1997**, *97*, 2373.
3. C. T. Kresge, M. E. Leonowicz, W. J. Roth, J. C. Vertulli, J. S. Beck, *Nature* **1992**, *359*, 710.
4. G.W. Parshall, *Homogeneous Catalysis*, Wiley Interscience, New York, **1980**.
5. (a) N. Herron, *Inorg. Chem*. **1986**, *25*, 4714; (b) D. S. Shephard, W. Zhou, T. Maschmeyer, J. W. Matters, C. L. Roper, S. Parsons, B. F. G. Johnson, M. J. Duer, *Angew. Chem. Int. Ed. Eng.* **1998**, *37*, 2719.
6. B. Cornils, W. A. Hermann, Eds. *Applied Homogeneous Catalysis with Organometallic Compounds*, VCH, **1996**, Volumes 1 and 2.

CHAPTER 1

INTRODUCTION AND LITERATURE REVIEW

1.1. GENERAL BACKGROUND

The continuing sophistication in and ever changing landscape of molecular targets for a myriad of applications ranging from biology to materials science requires a continuing evolution of synthetic methods. A key goal must be synthetic efficiency in transforming readily available starting materials to the final target [1].

Early 19th century saw many important discoveries in chemistry being made and it was noticed that a number of chemical reactions were affected by trace amounts of the substances that were not consumed during the reactions. It was observed that trace amount of acid could bring about hydrolysis of starch and low concentration of metal ions could effect the decomposition of hydrogen peroxide. Michael Faraday observed that platinum sponge was able to sustain the oxidation of ethanol vapour; the heat released making it white-hot, while J. W. Dobereinger discovered that platinum could catalyze the oxidation of hydrogen. In 1831 Peregrine Phillips patented the role of platinum in the oxidation of sulphur dioxide and later this became the basis for sulphuric acid manufacture [2-4].

The word *catalysis* came from the two Greek words, the prefix, *cata* meaning down, and the verb *lysein* meaning to split or break. A catalyst breaks down the normal forces that inhibit the reactions of the molecules; a widely accepted definition of catalyst being, '*a substance that increases the rate of approach to equilibrium of a chemical reaction without itself being substantially consumed in the reaction process*'. Catalysis is the phenomenon of a catalyst in action, wherein lowering of the activation energy is a fundamental principle that applies to all forms of catalysis – homogeneous, heterogeneous or enzymatic [1].

Broadly catalysis can be divided into five categories [5]:

a. **Homogeneous Catalysis**: Both the reactant and catalysts are present in the same phase (e.g. Carbonylation of methanol to acetic acid)
b. **Heterogeneous Catalysis**: Reactant and catalysts are present in separate phase, the catalyst is solid and the reactant either liquid or gas (e.g. Synthesis of gasoline from CO and H_2, known as Fischer-Tropsch synthesis)
c. **Bio Catalysis**: Also known as enzyme-catalysis. Mainly all body related reactions (e.g. α–amylase present in saliva hydrolyses α–1, 4 linkage of starch molecules to glucose)

d. **Electro Catalysis**: Catalyst as an electrode (e.g. fuel cell reactions for H_2 storage)

e. **Photo Catalysis**: Energy for reactions is from light source ($h\nu$) (e.g. TiO_2 photocatalytic purification and treatment of H_2O)

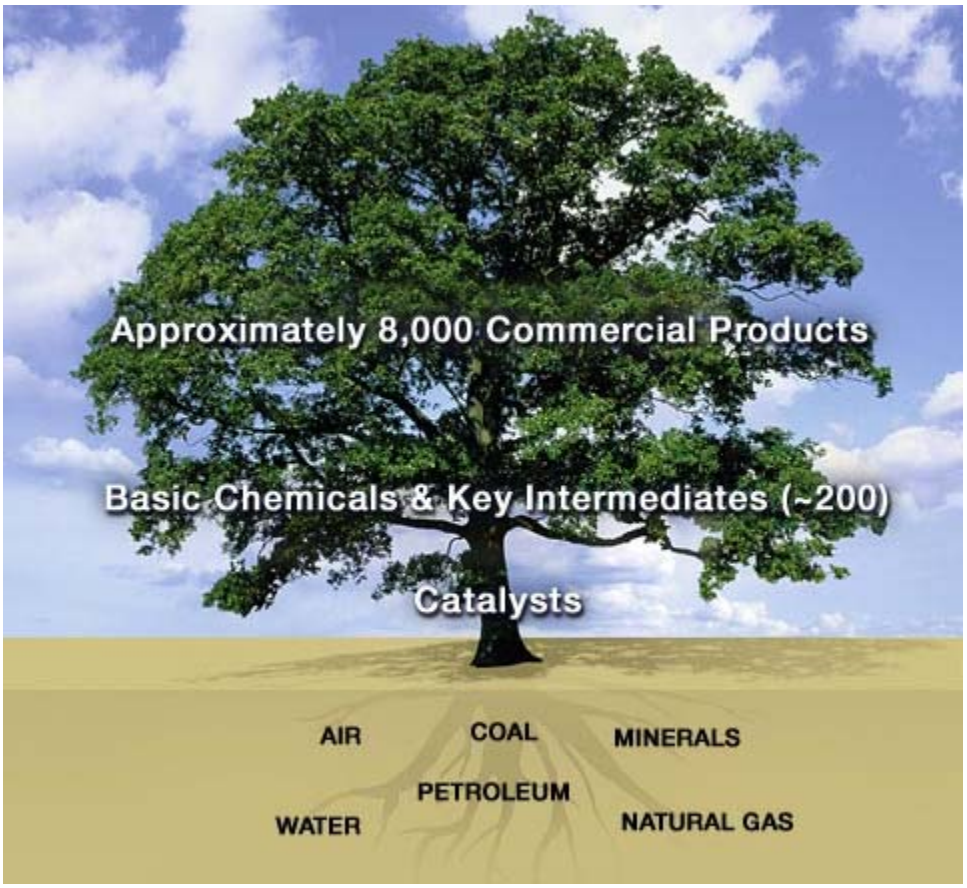

Scheme 1.1 A schematic presentation of Cata-Tree (source: BASF, Germany)

Nature performs many difficult chemical transformations essential to life, and among them majorities of the biological reactions is catalytic. Enzymes are nature's catalysts, which play a pivotal role for regioselective and stereoselective reactions producing almost no byproducts [6-a]. The ease with which nature performs these chemical syntheses has long been admired and envied by synthetic chemists. Ecological and environmental issues have forced industries all over the world to optimize their processes, so that they produce negligible side products. Since the discovery of catalysis phenomenon, catalysts are serving the purpose of selective chemical processing, which has desired commercial viability. Most

of the industrial reactions are catalytic and the number of chemical compounds produced world wide at the present time is roughly in the range of 20,000 to 30,000 [6-b].

Catalysis plays a key role in production of such a wide variety of products, which are having applications in food, clothing, drugs, plastics, agrochemicals, detergents, fuels etc. [7]. In addition to these, it plays an ever-expanding role in the balance of ecology and environment by providing cleaner alternative routes for stoichiometric technologies [8] by conversion of polluting emissions to harmless streams. Thus the importance of catalysis to society is obviously based on its great economic impact in the production of broad range of commodity products that improve our standards of living and quality of life. Usually, catalysts are categorized as homogeneous and heterogeneous, depending on the physical form in which they are used.

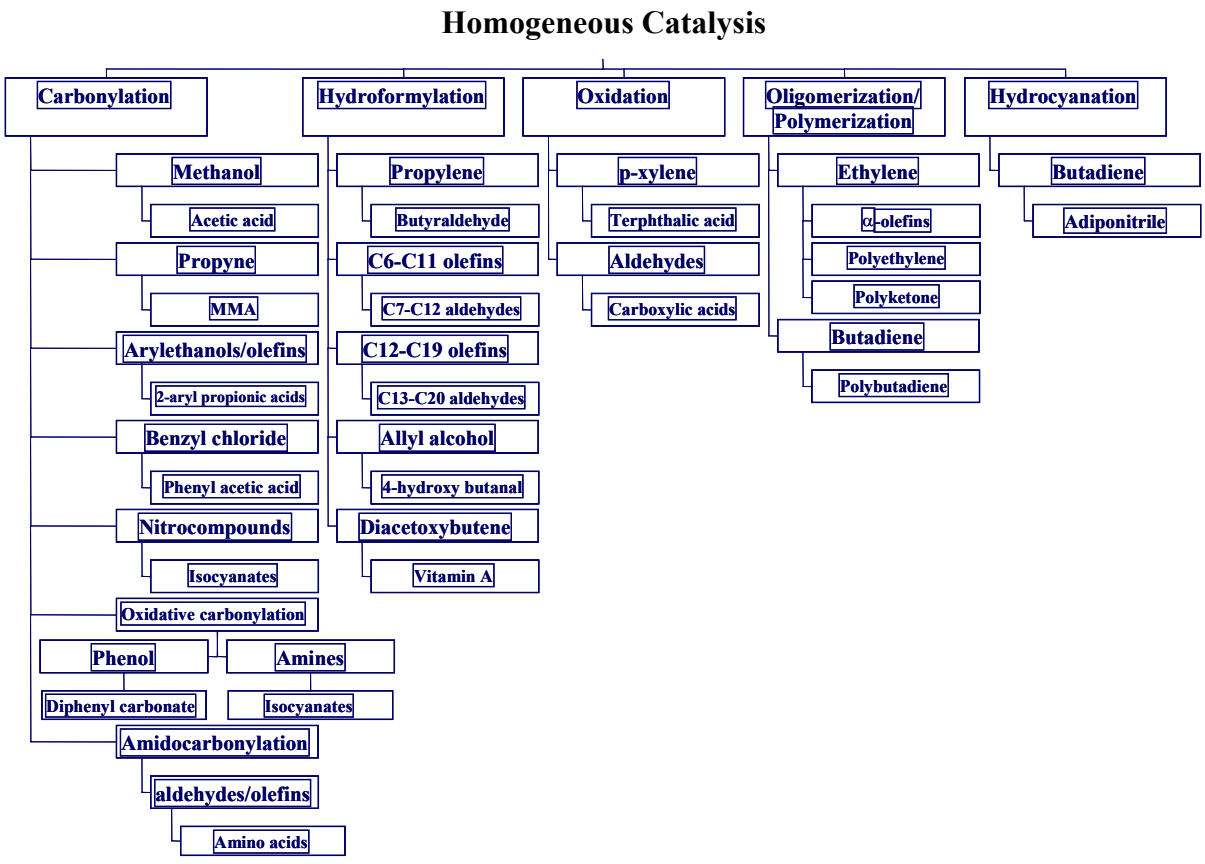

Scheme 1.2 A schematic presentation of important applications of homogeneous catalysis

1.2. HOMOGENEOUS CATALYSIS

Homogeneous catalysis, using soluble metal complexes, provides selective synthetic routes under mild operating conditions for valuable chemicals from basic organic precursors [9]. Some of the major reactions catalyzed by transition metal complexes are hydrogenation, oxidation, hydroformylation, carbonylation, carbon-carbon bond formation reactions such as Heck reaction, telomerization, co-polymerization and ring opening metathesis. Some of the important commercial applications of homogeneous catalysis are: hydroformylation of olefins to aldehydes/alcohols, carbonylation of methanol to acetic acid, synthesis of L-dopa by asymmetric hydrogenation, oxidation of p-xylene to terephthalic acid, hydrocyanation of butadiene to adiponitrile, ethylene oligomerization etc. [10]. Though homogeneous catalysis plays an extremely important role in highly efficient processes, yet there are some serious drawbacks, mainly in terms of catalyst-product separation from the reaction mixture and re-usability of the catalyst. These shortcomings have led to researchers investigate for new stable and easily separable catalyst systems. Thus, heterogeneous catalysis was born with a new look on the old portrait.

1.3. HETEROGENEOUS CATALYSIS

Heterogeneous catalysis has been the basis of most of the chemical processes so far, e.g. synthesis of ammonia, Ziegler-Natta polymerization etc. [11]. But, the approach to heterogenize of homogeneous catalysts was an invention that sorted out many challenging problems faced by the industry in recent years. Homogeneous catalysis by soluble metal complexes have wide ranging applications in a variety of reactions such as hydrogenation, oxidation, carbonylation, epoxidation, hydroformylation etc. [12]. The unique features of these catalysts are high selectivity and activity at milder operating conditions and better understanding on a molecular level. The demand for optically active drugs, agrochemicals and food products, for which homogeneous catalysis is the approach to develop cleaner catalytic routes, has further enhanced the importance of this subject [13]. Inspite of several attractive features and feasibility of new chemistry through homogeneous catalysis, their applications have been limited due to difficulties in achieving industrially viable catalyst-product separation.

Since, the present study has been done in the field of heterogeneous catalysis, further discussions will be mainly on the aspects of heterogeneous catalysis. Development of heterogeneous catalyst for any process is very important as it serves several advantages over the homogeneous catalyst system like, easy recovery of the catalysts, handling and preventing loss of the catalysts [14]. Although there are few drawbacks compared to the homogeneous catalysts (e.g. selectivity), heterogenization of the homogeneous catalysts is a need for industry to club all the advantages together.

1.4. HETEROGENIZATION OF HOMOGENEOUS CATALYSTS

Many homogeneous catalytic systems, though have many attractive properties, *viz*. high selectivity and activity, yet cannot be commercialized because of difficulties associated with the catalyst-product separation from catalyst system, procurement in usual conditions , thermally sensitive and reusability of the catalyst [14]. Hence, the homogeneous reactions that have been commercialized either involve volatile substrates and products or do not contain thermally sensitive organic ligands. The term heterogenization refers to a process, whereby a homogeneous transition metal complex (including free metal particles, biological molecules, organic species etc.) is either immobilized, or anchored, or incorporated or encapsulated in an inert organic (polymer) or inorganic support. These heterogeneous catalysts have a lot of advantages over their homogeneous analogues in:

(i) fixed-bed and continuous flow through operations,

(ii) complete commercial utility on a large scale owing to the economic debits of batch type operations and/or expense of catalyst recovery and recycle,

(iii) maintaining high selectivities and conversions (turn over frequency) of their homogeneous analogues for many reactions, and

(iv) preventing other side reactions e.g. dimerization, alkylation and aggregate formation of the catalyst complex, which normally occurs in solution.

To solve the problems occurring in homogeneous catalyst systems, new processes and catalyst designing are under investigation, which can be broadly divided into two types. In

the first case, a catalysts system is designed so that it is solubilized in a solvent that, under some conditions, is immiscible with the reaction products. These reactions involve two phases and are often referred to as ***Biphasic Systems*** [15]. The other type involves the metal complex catalyst or metal (in form of nanoparticles) anchored to some kind of soluble or insoluble support, and the separation is carried out by a filtration procedure. This type of process is known as ***Heterogenizing Homogeneous Catalysts*** [16].

1.4.1. ***Biphasic systems*** can be broadly classified as:

(a) **Aqueous Biphasic**: An example of this process is the commercialization for hydroformylation of propene using a ligand (Na-salt of triphenylphosphine) to make the rhodium-based catalyst soluble in water [17]. As most organic compounds do not mix with water, the reaction can be carried out in two phases with rapid mixing to ensure maximum contact between the catalyst and the substrate. After the reaction is over, the mixture is allowed to settle and the product decanted, leaving the catalyst in the aqueous phase. However, very low solubility of long chain alkenes in water, lowers the reaction rates and hence, commercialization of this process for production of detergent range aldehydes is not feasible. To solve this problem, recently, another approach has been reported [18], using the concept of derivatizing triphenylphosphine with polyethylene glycol chain. At room temperature, the rhodium phosphine derivative is soluble in water but not in organic solvents, however, upon heating, the polyether side chains undergo a phase transition and the complex becomes more soluble in the organic phase than in water. Hence, at the reaction temperature all the required components are dissolved in the organic phase, and when cooled, the phase transition is reversed allowing the catalyst to return to the aqueous phase; the organic phase, now devoid of rhodium complex, can be easily decanted.

(b) **Fluorous Biphasic:** Horvárth and co-workers proposed the use of fluorous biphasic systems to encounter the problem of different solubility experienced in the aqueous biphasic systems [19]. Using rhodium complexes of fluorinated phosphines in mixture of perfluorocyclohexane and toluene, Horvárth showed that good rates for hydroformylation of 1-octene with high selectivity (linear: branched = 8:1) could be obtained with limited

leaching of rhodium (4.2% after nine runs) in the reaction-substrate. But, almost 10% of 1-octene was lost through isomerization.

(c) **Supercritical Fluids:** Supercritical fluids (compressed gases above their crticial temperature) dissolve many low- to medium-polarity organic molecules and are fully miscible with permanent gases. If a catalyst can be dissolved, truly homogeneous catalysis can occur, as all reactant-contents are fully dissolved in one phase and no phase-transfer problems arise. Although the supercritical solvent can very simply be removed by decompression to a gas, this does not overcome the main separation problem, of the catalyst from the product. One elegant example, where this has been achieved is a hydrogenation reaction based on Ir-based catalyst and $scCO_2$ (the most commonly used supercritical fluid) [20]. The Ir-catalyst is soluble in $scCO_2$ in the presence of the substrate, but precipitates once the substrate has been used up. In an alternative process, temperature and pressure swings are used to participate the catalyst selectively; the product is thus recovered by decompression. This process has been successfully used for hydroformylation of various alkenes [21].

(d) **Ionic Liquids:** Ionic liquids are salts that are liquid at room temperature, or atleast at the reaction temperature. They have an extremely low vapor pressure and, depending on the design of ionic liquid, can dissolve or reject organic compounds. They also dissolve ionic catalysts. Hydroformylation reactions carried out in ionic liquids using a rhodium fluoro-functionalized ferrocenyl phosphines cationic complex in hexafluorophosphine anion ionic liquid system has shown excellent activity and selectivity, with advantage of catalyst separation from the product with minimal leaching (~ 10 parts per billion) [22]. Another way of using ionic liquids that has the potential for continuous-flow liquid operation is to support the ionic liquid as a film on a solid support (e.g. SiO_2) [23]. The catalyst is dissolved in the ionic liquid film, with an advantage that the surface area of the ionic liquid is greatly enhanced relative to its volume and the substrate can readily diffuse to the catalyst. One potential disadvantage of using ionic liquids containing PF_6^- or BF_4^- is that they react with traces of water to give species such as O_2 PF_2^- and the very highly reactive and corrosive HF thus produced can destroy the catalyst [24]. The environmental impact of these solvents (fluorous, ionic liquids) is, however, still unknown.

(e) **Supercritical Fluid-Ionic Liquid Biphasic:** An alternative way to extract the products from the ionic liquids with organic solvents is to coalesce the favourable properties of ionic liquids with those of supercritical fluids. $scCO_2$ has shown to be miscible with certain ionic liquids [25, 26] and extract many organic compounds from ionic liquids, allowing a genuinely continuous process to be developed. And ionic catalyst is dissolved in the ionic liquid in a stirred tank reactor. In a typical hydroformylation reaction [24], the alkene, permanent gases (CO and H_2) and $scCO_2$ are then passed into the reactor either separately or mixed. The reaction takes place and the products flow out of the reactor dissolved in $scCO_2$, which is decompressed to release the products. The CO_2 containing any excess of CO and H_2 can be recompressed for an emissionless and continuous process that requires no separation of the product from the solvent.

1.4.2. ***Supported Catalysts and Filtration*** systems can be broadly classified as:

(a) **Soluble supports:** The supports used to tether the catalyst may be soluble in the reaction media (e.g. soluble polymers), having the advantage that active sites are distributed through out the reaction solution [27,28]. The catalysts architecture can be similar to that of the efficient homogeneous catalyst that it is trying to mimic. In a recent example, anions of $[B(C_6H_3(CF_3)_2)_4]^-$ and Na-salt of water soluble phosphine anions were partially exchanged to obtain a polyelectrolyte that was used for hydroformylation of 1-octene [29]. The catalyst was separated from the product using ultra-filtration technique, good rates were obtained and 93% of the catalyst could be recycled. Losses were attributed to ligand oxidation during the batch process.

Dendrimers are large (2 to 4 nm) tree-like molecules with a persistent globular shape, which makes them more suitable for ultra-filtration than the soluble polymers, which may pass through the filtration membranes more easily. The metal-binding groups are usually on the exterior of the dendrimer but also may be buried inside shape-selective pockets. As membranes for enzyme ultra-filtration have channels ~ 1 nm in diameter, they allow the solvent and product of a catalytic system to pass through but reject the dendrimer-based catalyst. Often, dendrimers may have the advantage of exhibiting bidentate binding (through two donor atoms on the same dendrimer arm) to the metal [30]. The chelate-effect (ring-forming) will then ensure that leaching is minimized. Also, if the metal separates from its

dendrimer-bound ligand, it may be sequestered again rapidly by one of the many identical binding sites nearby. An advantage of using dendrimers is, they can show much higher selectivities to desired products than their small molecule analogues, as exemplified from hydroformylation of 1-octene giving a liner: branched selectivity ratio of 14:1 with 16 PPh_2 groups compared to 4:1 for a small molecule analogue [31]. In another recent report [32], dendrimers were anchored to silica beads or a polymer using a solid-phase organic approach and have been used for hydroformylation reactions; the catalyst was easily separated from the reaction products using conventional filtration.

(b) **Insoluble supports:** Metal complexes or ligands can be anchored onto or inside solid supports such as inorganic oxides (silica, alumina, microporous zeolites, mesoporous M41S and macroporous clay type materials), carbon, carbon nanotube, fullerene or polymers [33]. If the anchoring is covalent, it can be robust enough to withstand the harsh conditions of the catalytic reactions. As the ligand for binding the metal resides only on accessible sites of the solid and can be designed to protrude into the solvent, all catalytically active sites are available for reaction, allowing rates and selectivities comparable to those obtained with those obtained for the analogous homogeneous catalysts. The main problem is that the bonds between metal and ligand are often broken and reformed during catalytic reactions, leading to *leaching* of the metal from the catalyst in the product, thus decreasing the reaction rate and activity. Reduced leaching has been observed when a catalyst is encapsulated inside the zeolite pores (*ship-in-a-bottle* approach) or of mesoporous MCM-41 type materials [33,34]. Recently, heterogenized rhodium complex catalysts anchored to mesoporous materials have been reported for hydroformylation of various olefins showing good activity and high selectivity, but recyclability was a problem due to catalyst leaching [35]. In another survey, van Leuwen and co-workers have prepared Xantphos family of ligands supported to triethoxysilyl group and used for hydroformylation [36]. Though high activity and selectivity was achieved for alkene hydroformylation, yet it requires free phosphine in the reaction system showing leached metal ions, otherwise, without free phosphine the activity is lowered. The same group has also applied the catalyst for hydroformylation of 1-octene in a gas-like continuous flow system using $scCO_2$ [37], wherein, substrates and products were flowed over the catalyst. The reactant and gases (CO and H_2) are all fully soluble in $scCO_2$,

which can reach all active catalytic sites. Even the desired product nonanal, is also soluble in $scCO_2$ once it is formed. The only separation required is that of the product from unreacted starting material and any by-products and the CO_2 thus produced from the reactor depressurization, can be recompressed and recycled.

It is in this context, immobilization of metal complexes as a mean of "heterogenization" has particular significance. In this approach, the organometallic complex is encapsulated or anchored inside, or tethered to the pores and walls of the inorganic inert matrices, e.g. zeolites, M41S materials, clay etc. in such a way that the complex is tightly bound inside the pores [33]. The prime requirement is, the stability of the encapsulated complex such that it does not leach out of the catalyst pores to the liquid phase in the course of reaction, while retaining high activity, selectivity and the original configuration.

The tenability of these open framework structures in terms of pore size and shape, composition and electric fields have been exploited in a wide variety of applications. These microporous and mesoporous materials are being increasingly used as host materials to examine the adsorption properties, reactivity and dynamics of range of guest species. These investigations show that guest interactions with the internal surface of a zeolite host may be evaluated in terms of specific metal-ligand bonding interactions. The approach helps to better explain and exploit the reactivity and coordination properties of the zeolite internal surface for anchoring and self – assembly of a wide range of encapsulated guests, to name a few are metal cations, metal clusters, coordination compounds, metal carbonyls, organometallics, metal oxides and semiconductor nanoclusters [38]. The oxide framework plays a key role in complexing, coordinating, structure – directing, anchoring and stabilizing the guest species.

In several reports, heterogeneous catalysis by encapsulated materials, have been addressed for oxidation [39], hydrogenation [40] and asymmetric epoxidation [41] reactions, but attempts to heterogenize some of the industrially relevant homogeneous catalysts have been very limited. Also direct comparison of the encapsulated catalysts with their homogeneous counterparts has not been well investigated with meaningful quantitative data.

Researchers from Dupont [42] were among the early pioneers to exploit the chemistry of natural enzymes, adopt strategies and apply them to rational design of zeolite based catalysts as both mimics of natural enzymes and for processes of industrial interests. In an attempt to prepare analogues of hemoglobin and myoglobin, which reversibly bind O_2, cobalt

salen complexes were encapsulated in the supercages of zeolite-Y [42]. Such encapsulated complexes formed adducts with dioxygen, which were more stable than those formed by the same complexes in solution.

Romanonskii et al. first reported the synthesis of metallophthalocyanines inside the supercages of zeolite Na-Y in 1977 [43]. Because of the similarity in structure and chemical properties between metallophthalocyanine complexes, related porphyrin complexes as well as salen (N, N'- bis (salicylidene) ethylene diamine) complexes encapsulated in molecular sieves have also been performed. Parallel studies on intrazeolite organometallics and coordination complexes, as well as metal oxides have been reported [44]. There are two main approaches followed to create new redox active molecular sieves. In the first approach, the redox active transition metal ions have been incorporated by isomorphous substitution or ion exchange in the lattice of zeolites or aluminophosphate molecular sieves. In this way, heterogeneous Ti and V catalysts have been developed [45]. The second approach in creating the new redox active molecular sieves involves heterogenization of transition metal complexes with potential catalytic activity in zeolites or molecular sieves. Klier first formulated the interaction of transition metal cations and small ligands as intra-zeolite metal complex formation in zeolites [46] and considerable progress has been made, since then [47,48].

The encapsulation methods involved are limited by the ability of the complex to diffuse into the pores of the crystalline molecular sieve. But if the zeolite is synthesized around the metal complex, then only cage dimensions are important as far as the ligand size is concerned. However, the stability of the metal complex during the zeolite synthesis is a major requirement. The complex in this case, functions as a template. Several routes have been proposed to heterogenize transition metal complexes in zeolites. Apart from the above, another method is the anchoring on the zeolite surface of precursors of the desired complex through formation of new bonds [49].

1.5. MICROPOROUS AND MESOPOROUS SILICATES AS HOSTS FOR HOMOGENEOUS CATALYSTS

Catalyst designing is a very challenging task ahead of every chemist. The dream of every catalytic scientist is to synthesize a catalyst that carries out a desired chemical reaction selectively and at high rates to optimize the conversion from the reactants to the products. The main factors, which influence the catalyst performance, are the catalyst surface, metal-support interaction, support surface etc [3, 4]. It is in this context a prior art of heterogenizing homogeneous catalysts in microporous zeolites and mesoporous M41S type materials will be reviewed briefly.

1.5.1. IMMOBILIZATION OF METALS/ METAL COMPLEXES TO MICROPOROUS HOSTS – PRINCIPLES

1.5.1.1. Intrazeolite metal carbonyl cluster synthesis

Metal carbonyl clusters with nuclearity greater than three could potentially be encapsulated in faujasite (FAU) type zeolites. In this method, the reaction of CO/H_2 or CO/H_2O with metal ion exchanged Y type of zeolite has led to the encapsulation of the metal carbonyl cluster. The presence of H_2 or H_2O is necessary for the formation of the clusters by the reductive carboxylation of the intrazeolite metal ions. Anionic complexes could be easily encapsulated within the supercages of FAU type zeolites. Few examples of different types of carbonyl complexes encapsulated in zeolites by this method are: $Rh_6(CO)_{16}$, $Rh_4(CO)_{12}$, $Ir_6(CO)_{12}$ in Na-Y [50] etc.

1.5.1.2. Ligand synthesis method

This approach, which has been successful only for phthalocyanines is also known as ‘template synthesis method’. The ligands can be synthesized out of four identical or substituted dicyanobenzene molecules, which assemble around an intrazeolite metal ion that acts as a template. The synthesis involves heating zeolites X, Y, aluminophosphate VPI-5 modified with metal ions, metallocenes (Cp_2Ni, Cp_2Fe, $CpMn(CO)_3$, etc.) and metal carbonyl complexes ($Ni(CO)_4$, $Os_3(CO)_{12}$ etc.) with excess dicyanobenzene (DCB) in a bomb reactor between 150 – 350 °C or 180 °C, in the presence of a solvent [51]. The condensation of the

four DCB molecules around a metal ion to form a phthalocyanine (Pc) requires two reducing equivalents of, which may probably originate from H_2O or metal ions in the case of oraganometallic precursors. The synthesis of zeolite encapsulated phthalocyanine complexes of Cu, Co, Ni, Fe, Mn, Ru, Rh, Os, Ti, Li_2Pc and H_2Pc, perhalogenated phthalocyanines, t-butylphthalocyanines, nitrophthalocyanines. Co-porphyrins, Fe- and Mn-tetramethyl porphyrins, as well as tetraphenyl porphyrin complexes by the above method have been reported [52-b]. One disadvantage of the above method is the formation of aggregates during the synthesis, which hinders or limits encapsulation. Even though there are reports on the encapsulation if Fe- and Mn- tetramethyl and tetraphenyl porphyrins in zeolite Y by the above method, no convincing data on the intrazeolite formation of the phthalocyanine complexes have been reported.

1.5.1.3. Flexible ligand method

The flexible ligand method involves the diffusion of the ligands with one to five coordinating atoms into the zeolite pores, where, upon complexation with the metal ion, the resulting complex becomes too large to exit. This approach is especially well suited for the encapsulation of metal-Schiff-base complexes (e.g. Salen), as this ligand offers desires flexibility. The ligand should have a sufficiently low melting or sublimation point and should be small enough to enter the zeolite cavities. The void volume in the zolite is filled by homogeneously with the ligand molecules and these on heating form a complex with the cation and is sterically confined in the supercage. The ligand may bind in a bidentate or tetradentate fashion depending on the nature of the metal ion. The disadvantage of this method is the difficulty to control metal speciation; the zeolite often remains in the primary coordination sphere of the transition metal ion. A wide variety of Co, Fe, Rh, Ru, Mn and Pd complexes have been prepared according to this method within the supercages of faujasites [39-b,42,52-a,53].

1.5.1.4. Zeolite synthesis method

This method offers the advantage of encapsulating a well-defined metal complex without contamination by uncomplexed or partially complexed metal ions as well as free ligands. These problems are encountered using the template and flexible ligand approaches.

In this approach, the well-defined metal complex is added to the silica source prior to the gel formation. When a homogeneous dispersion results, the aluminate solution is added and the gel is aged prior to crystallization. However, if the metal complex is added to the aluminate solution or aluminophosphate gel, a heterogeneous mixture results and there is virtually no encapsulation in the zeolites. Metal phthalocyanines and perfluorophthalocyanines were encapsulated in Na-X during zeolite crystallization. In a similar way, metal complexes were also incorporated in ZSM-5 and mordenite [54]. The metal complex possibly plays the role of a template in directing the synthesis. The aggregation of the metal complexes in the aqueous synthesis medium can be overcome by careful design of the zeolite synthesis procedure. The disadvantages involved in this method are that the complex should be stable during all the stages of zeolite synthesis and crystallization, the complex should withstand the synthesis temperature of the gel while the zeolite is formed, the complex should be water soluble, otherwise, organic solvents in which it is soluble might hinder the crystallization of the zeolite thus, resulting in amorphous structures without any encapsulation. Further in the case of zeolite requiring a supplementary template molecule, removal of this template may necessiate calcinations or extraction by tedious methods, which may also damage the complex during the process.

1.5.1.5. Cationic exchange of the complexes

If the complex is cationic and if the zeolite has sufficient cationic exchange capacity, the complex can be directly exchanged from the aqueous solution; provided the complex is small enough to pass through the pores of the zeolite. This way $[Cu(ethylenediamene)_2]^{2+}$ was introduced into faujasite zeolites [55].

1.5.1.6. Ligand adsorption on metal ion exchanged zeolites

Adsorption of amines from aqueous solutions on transition metal containing zeolites is a typical example of this process [56]. The only controlling parameter in such synthesis procedures is the pH. A low pH results in protonation of the ligand, while a high pH may damage the zeolite structure. Impregnation of transition metal containing zeolites with NaCN solution results in entrapment of anionic $[Mn^{+} (CN)^{-}_{m}]^{n-m}$ chelates in anionic zeolites e.g. $[Co^{n+} (CN)^{-}_{m}]^{n-m}$ – Na-Y.

1.5.1.7. Tethering homogeneous catalysts by heteropolyacids-exchanged inorganic supports

Recently, a novel approach to immobilize homogeneous catalysts onto support materials (e.g. clay, carbon, La_2O_3, Al_2O_3, SiO_2) has been reported by Augustine et al. [57] in which, the organometallic complex is tethered inside the cavities of the porous, inorganic matrices so that the complex is tightly bound inside the pores and it does not leach out of the catalyst pores to the liquid phase in the course of a reaction. The authors have shown that high activity and enantioselectivity for the desired products when methyl 2-acetamidoacrylate was subjected to hydrogenation with a Rh(DiPamp) homogeneous catalyst tethered to various supports e.g. Montmorillonite K, Al_2O_3, carbon or Lanthana, at 25 °C and 1 atm. Pressure. This anchoring procedure has also been applied to achiral complexes with similar results. For instance, hydrogenation of 1-hexene over a Wilkinson's catalyst anchored to PTA treated Al_2O_3 proceeded 2–3 times faster than the corresponding homogeneously catalyzed reaction, even on the first use of the heterogenized material. A Rh(dppb) complex anchored to a PTA modified Al_2O_3 was used for several successive hydrogenations of 1-hexene with a combined substrate: catalyst ratio of about 8000: 1. An analysis of the product mixtures from these reactions found no detectable rhodium present.

One of the advantages of this approach to anchoring homogeneous catalysts is its apparent generality, in that this procedure can be used to anchor a variety of pre-formed active homogeneous catalysts onto a number of different supports. It is shown that the tethering technique leads to a true heterogeneous catalyst, which gives enhanced catalytic activity (often 2–3 faster than the corresponding homogeneously catalyzed reaction) and stability compared to other methods including encapsulation.

1.5.2. Immobilization of Metals/ Metal Complexes in Mesoporous Hosts – Principles

Surfactant-templated mesostructures have played a prominent role in materials chemistry during the last decade. The excitement began with the discovery of hexagonally ordered mesoporous silicate structures by Mobil Corp. (M41S materials) [58,59] and by Kuroda, Inagaki, and co-workers (FSM-16 materials) [60,61]. These materials initially appeared to be the 'Holy Grail' sought after by zeolite chemists of the time. They possessed

extremely high surface areas and easily accessible, uniformly sized pores. Most importantly, the pore sizes exceeded those attainable in zeolites and they could be tuned in the nanometer range by choosing an appropriate surfactant templating system, sometimes with a co-solvent or swelling agent. Thus, novel catalysts, sorbents, sensors, and host materials for large guest molecules were envisioned. However, the original mesoporous silicates and aluminosilicates exhibited a number of limitations, including lower hydrothermal stability and lower reactivity than zeolites with comparable compositions. They possessed relatively thin walls, which prevented incorporation of secondary pores within the walls, and they only formed fine particles. Yet, the ability to manipulate structures of porous solids on a nanometer scale in a controlled way proved to be so important to the research community, that many of these limitations have been addressed and overcome in the last few years. For example, the hydrothermal stability of mesoporous silicates has been improved by adding salts to the synthesis mixture [62] or by producing materials with thicker walls [63–73]. Structures with uniform pore sizes can now be formed throughout most of the mesopore size range, which encompasses 2–50 nm by International Union of Pure and Applied Chemistry (IUPAC) definition [74] One important way of modifying the physical and chemical properties of mesoporous silicates has been the incorporation of organic components, either on the silicate surface, as part of the silicate walls, or trapped within the channels [75,76]. Organic modification of the silicates permits precise control over the surface properties and pore sizes of the mesoporous sieves for specific applications, while at the same time stabilizing the materials towards hydrolysis. Bulk properties can also be affected by mixing inorganic and organic moieties in the mesostructures. The inorganic components can provide mechanical, thermal, or structural stability, whereas the organic features can introduce flexibility into the framework, or change, for example, the optical properties of the solid. Through the development of hybrid inorganic-organic mesoporous solids, much progress has been made in the last few years towards applications of mesoporous solids in a variety of fields. Mesoporous solids have been functionalized at specific sites, and were demonstrated to exhibit improved activity, selectivity, and stability in a large number of catalytic reactions and sorption processes. Herein, we describe grafting and co-condensation methods used to functionalize mesoporous silicates on the internal and external surfaces or within the walls. A number of designations have been used for mesoporous sieves. For mesoporous silicate

structures, some of those relevant to this review include MCM-41 (2D hexagonal, prepared under basic conditions using cationic surfactants) [59], MCM-48 (cubic, basic conditions, cationic surfactants) [59] FSM-16 (2D hexagonal, derived from the layered polysilicate kanemite) [61] HMS (acidic conditions with neutral amine templates) [63], SBA-1 (cubic, acidic conditions, cationic surfactants) [77,78] SBA-3 (2D hexagonal, acidic conditions, cationic surfactants)[77,78], SBA-15 (2D hexagonal, acidic conditions, prepared with block-copolymer templates) [69,71].

1.5.2.1. Grafting methods

Grafting, in this context, refers to post-synthesis modification of a pre-fabricated mesoporous support by attachment of functional molecules to the surface of the mesopores, usually after surfactant removal (Figure 1.1). Mesoporous silicates possess surface silanol (Si-OH) groups that can be present in high concentration and, like in amorphous silica, act as convenient anchoring points for organic functionalization [79-81]. Surface modification with organic groups is most commonly carried out by silylation, although modification of silanol groups is also possible by esterification, e.g., with ethanol [82,83]. Typically, silylation is accomplished by one of the following procedures [84]:

$$\equiv Si–OH + Cl–SiR_3 \rightarrow \equiv Si–OSiR_3 + HCl \quad (1)$$

$$\equiv Si–OH + R'O–SiR_3 \rightarrow \equiv Si–OSiR_3 + HOR' \quad (2)$$

$$2\ (\equiv Si–OH) + HN(SiR_3)_2\ 2 \equiv Si–OSiR_3 + NH_3 \quad (3)$$

Silylation occurs on free (≡Si–OH) and geminal silanol (=Si(OH)$_2$) groups, but hydrogen-bonded silanol groups are less accessible to modification because they form hydrophilic networks among themselves [85]. The original structure of the mesoporous support is generally maintained after grafting. If a high surface coverage with functional groups is desired, it is important to maintain a large number of surface silanol groups after removal of the surfactant. Surfactant removal is carried out either by calcination or by appropriate extraction methods. Calcination promotes condensation of unreacted silanol groups, and many surface groups are lost at typical calcinations temperatures (400–550 °C). The surface can be rehydrated by boiling calcined mesoporous silicate in water and removing

excess water by azeotropic distillation e.g., with toluene [86] or benzene [87]. The surface of calcined MCM-41 can also be rehydroxylated by acid hydrolysis [88] or by steam treatment [79]. Extraction processes (e.g., with acid/alcohol mixtures for cationic surfactants or with alcohols for neutral surfactants) minimize loss of surface silanols, although post-extraction thermal treatments can increase the surface reactivity for silylation and strengthen the walls through additional condensation. Zhao and Lu determined that, for MCM-41 samples in which the surfactant was removed by extraction, optimal out-gassing temperatures appeared to be between 400–450 °C [85]. At lower temperatures, a large number of silanols remain inaccessible to grafting because of hydrogen bonding between them; at much higher calcination temperatures, many silanol groups are lost due to condensation reactions.

Recently, supercritical fluids have been used as a reaction medium to deliver siloxanes to channel surfaces [89]. This method is particularly suited for smaller pore materials due to the low density, viscosity, and surface tension, and the high diffusivity of supercritical fluids, such as CO_2. When this technique was applied to mesoporous silica, a high degree of cross-linking was observed, resulting in an increase of the hydrolytic stability of the surface groups.

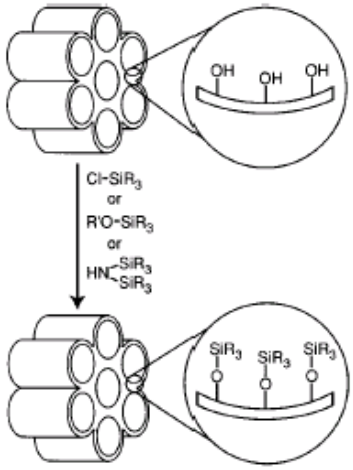

Figure 1.1. Functionalization of mesoporous silicates by grafting [Ref. 79-81]

1.5.2.1.1. Grafting with Passive Surface Groups

Grafting of the mesopore surfaces with groups that exhibit low reactivity, such as alkyl chains or phenyl groups, can be used to tailor the accessible pore sizes of mesoporous

solids, increase the surface hydrophobicity, passivate silanol groups, and thereby protect the framework towards hydrolysis. In their early work, Mobil researchers demonstrated that the pore sizes of MCM-41 could be reduced by trimethylsilylation [59,90]. Similar pore size tuning was carried out with FSM type mesoporous silicas [60,61], which contain fewer geminal silanols than MCM-41 [91].

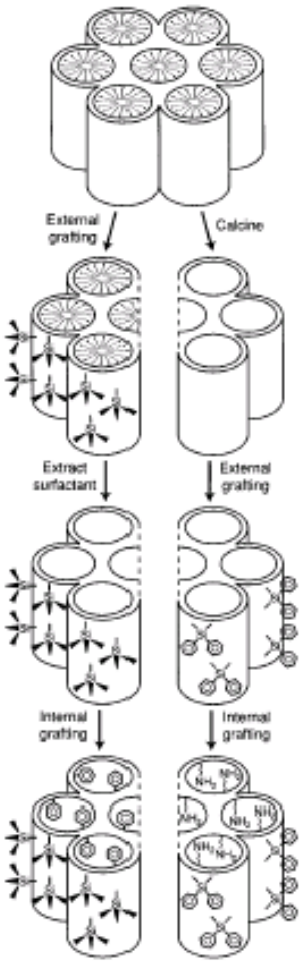

Figure 1.2. Methods of selective grafting on the external and internal surfaces of mesoporous silicates [91–93]

The pore diameters could be progressively decreased using longer alkyl chain lengths of chloroalkyldimethylsilanes. Alternatively, the apparent pore size of ordered mesoporous materials could be adjusted by varying the amount of grafted long-chain silylating agent [91]. It should be noted that pore size values, which are determined by gas adsorption measurements (typically nitrogen adsorption), depend strongly on the adsorption model that is used and also on the identity of the functional group. Jaroniec and co-workers demonstrated that low-pressure adsorption data are influenced by the presence of organic groups on mesoporous silica surfaces, making it possible to detect and sometimes quantify the organic species by gas adsorption techniques [92,93].

Zhao and Lu recently carried out a systematic study of the surface coverage obtained by silylating an MCM-41 surface with trimethylchlorosilane (TMCS) [85]. The maximum degree of surface coverage obtained was ca. 85 %. Silylation increased the hydrophobicity of the surface and strongly influenced the degree of water adsorption. Tatsumi et al. showed that trimethylsilylation of MCM-41 and MCM-48 improved their stability to moisture and mechanical compression [94]. It is remarkable that the additional siloxane groups protected the walls of the mesoporous solid even after removal of the methyl groups by calcination.

Anwander et al. functionalized the surface of MCM-41 with disilazane agents of the type $HN(SiR^1R_2^2)_2$ ($R^{1,2}$ = H, Me, Ph, vinyl, ^{n}Bu, ^{n}Oct) [84,95]. The size of the silylating groups affected the degree of silylation and the concurrent surface hydroxyl consumption. Best surface coverage was obtained with the sterically less demanding silyl groups. Hexamethyldisilazane functionalization was used to quantify the number of surface silanols, passivate surface silanols, and depolarize the surface for selective adsorption experiments. Multiple functionalization was carried out by consecutive or competitive silylation. The competitive silylation reactions demonstrated that the grafting rate depended on the steric bulkiness of the silyl groups of the silylamine, with preferential grafting of smaller groups.

1.5.2.1.2. Grafting with Reactive Surface Groups

A number of silane-coupling agents, such as those with olefins, nitriles, alkylthiols, alkyl amines, alkyl halides, epoxides, and some other surface groups, are reactive, permitting further functionalization. Olefins, such as vinyl groups, can be modified, e.g., by hydroboration [95] or bromination [96]. Nitriles can be hydrolyzed to form carboxylic acids,

and alkylthiols can be oxidized to sulfonic acids [97,98], which can be further employed as electrostatic anchoring points, e.g., for amino acids [99]. Surface amines may be derivatized, for example, by alkylation, nucleophilic aromatic substitution, or formation of amides or imines [100]. Functionalization of alkyl halides is possible by nucleophilic replacement of the halogen atom [101]. An example is given by Sutra and Brunel [102], who attached a Mn(III) Schiff-base complex (Mn–salen) to anMCM-41 surfacemodified with 3-chloropropylsilane moieties. In this type of reaction, HCl is produced and quaternization of the amine can occur as a side reaction. A milder method that is particularly suited to attachment of basic surface groups involves the reaction of oxirane surface (3-trimethoxylsilylpropoxymethyloxirane) groups with amines [103].

Balkus and co-workers functionalized MCM-41 with cobaltcomplexing ligands (ethylenediamine, diethylenetriamine, and ethylenediaminetriacetic acid (EDT)) [104]. The uniform, large pores of the MCM-41 support limited coordination of cobalt to adjacent ligands, avoiding random ligation, which may occur on amorphous silica. The EDT-complexed metal centers were shown to be redox active on the mesoporous silicate supports.

Anwander et al. developed a mild grafting method for chelating complexes using yttrium bis(dimethylsilyl) amide complexes as the anchoring groups [105]. These complexes were attached to the surface of MCM-41 by metal siloxide bond formation after elimination of the amine groups. The products acted as catalysts in a hetero Diels–Alder cyclization reaction.

1.5.2.1.3. Site-Selective Grafting

Multiple grafting has also been demonstrated. For example, if uncovered areas remain after silylation (e.g., hydrophilic sites) they can be passivated by trimethylsilylation [85,94]. Such passivation changes the hydrophobicity of the surface and thereby controls adsorption of polar/non-polar molecules.

In grafting reactions, the external surface is more easily accessible and is functionalized predominantly over the internal mesopore surface [106]. The functional groups on the external surface are again more accessible in subsequent reactions, leading to reduced selectivities in processes that benefit from pore confinement. To minimize involvement of the external surface in reaction processes and to optimize selectivity, it is

possible to passivate these surfaces first, before functionalizing the internal silanol groups. Controlled dual functionalization has been achieved by two different methods (Figure 1.2).

Shephard et al. assumed that silanol groups on the external surface of a calcined MCM-41 sample are kinetically more accessible for functionalization [107]. Calcined MCM-41 was modified first with Ph_2SiCl_2 to passivate the external surface and then with $(MeO)_3SiCH_2CH_2CH_2NH_2$ as an anchor for a redox- active ruthenium cluster. This cluster acted as a stain in high-resolution transmission electron microscopy (HRTEM) by which the authors concluded that the amine tethers were present almost entirely on the internal surface of MCM-41.

De Juan and Ruiz-Hitzky employed an alternate approach for selective functionalization of external and internal MCM-41 surfaces [108]. The first (external) grafting step was carried out with the as-synthesized mesoporous sieve whose pores were still filled with the surfactant template. Exposure of this support to a solution of trimethylsilyl chloride resulted in functionalization mainly of the external surface due to steric restrictions in the surfactant-filled mesochannels. The template was then extracted and the internal pore surfaces were functionalized with phenylpropyldimethylchlorosilane.

Aronson et al. [109], as well as Antochshuk and Jaroniec [110], demonstrated that one needs to be cautious in assuming that silylating agents are excluded from the channels of as-synthesized MCM-41, in particular when high concentrations of silylation reagents are used. Antochshuk and Jaroniec [110] carried out simultaneous grafting and extraction of template molecules by modification of uncalcined MCM-41 with trialkylchlorosilanes. As-synthesized MCM-41 was refluxed in the neat trialkylchlorosilane, first by itself, and then with added anhydrous pyridine, followed by multiple washing with different solvents, leading to surfactant-free mesoporous products. The loading of surface groups exceeded that on calcined supports that were otherwise treated in a similar way. Several advantages were noted for this procedure: more surface hydroxyl groups were present by eliminating the calcination step; the reduction in pore size was minimized by eliminating shrinkage during calcinations or during formation of smaller channels in a direct synthesis. This method was demonstrated for short and long alkyl groups (trimethyl- and octyl-dimethylchlorosilyl groups).

1.5.2.2. Coating Method

In the grafting processes noted above, silylation reagents were typically added under dry conditions to avoid hydrolysis and condensation away from the pore walls. Under anhydrous conditions the hydrophilic portion of the silica surface is preserved during silylation [111] and surface groups are relatively isolated. However, by employing just enough water in the process to form a monolayer on the pore surface, more continuous coats of organosilanes may be obtained, leading to a high concentration of organics in the product (Figure 1.3). Excess water must be avoided, because it can lead to uncontrolled polymerization of the silylation reagents within the channels or external to the mesoporous sieve.Water-controlled coating has been employed with mercaptopropyl functions on MCM-41 and HMS type structures [88, 112].

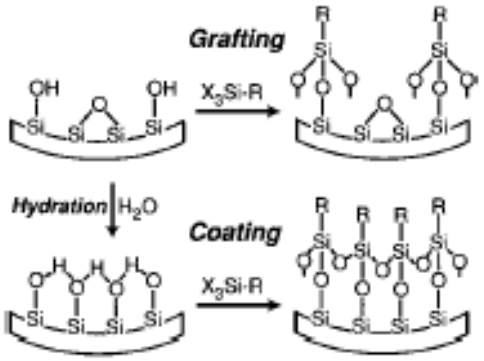

Figure 1.3. Comparison of coating and grafting process

Dai et al. recently described an interesting imprint coating method [113]. They coated the mesoporous surface of MCM-41 with complexes of ligands and target metal ions rather than just with the free ligands. When the metal ions were removed, the ligands were already positioned for complexation with metal ions of the same type. The selectivity to binding the original metal ion in competitive binding experiments was greater than in randomly functionalized mesoporous sieves. The material's performance remained high after repeated absorption and elution of metal ions. The effects of imprint coating on selectivities were observed only with mesoporous sieves as supports but not with amorphous silica gel. The different behavior was attributed to the curvature of the mesopores and the confinement of guest species.

1.5.2.3. Co-condensation Reactions

Co-condensation of a tetraalkoxysilane and one or more organoalkoxysilanes with Si–C bonds is an alternative method of producing inorganic–organic hybrid networks by sol–gel chemistry [114]. Such co-condensation reactions (also called "one-pot" syntheses) have also been applied to surfactant templated syntheses (Figure 1.4). Since the early work by the research groups of Mann [115,116], Macquarrie [117], Stucky [118] and Stein [96], co-condensation reactions have been used to prepare hybrid mesoporous silicates under a wide range of reaction conditions. Some common criteria in the choice of the co-condensation reaction system include the need to avoid phase separation of the precursors to obtain uniform distributions of functional groups and the need to avoid Si–C bond cleavage during the sol–gel reaction and during surfactant removal.

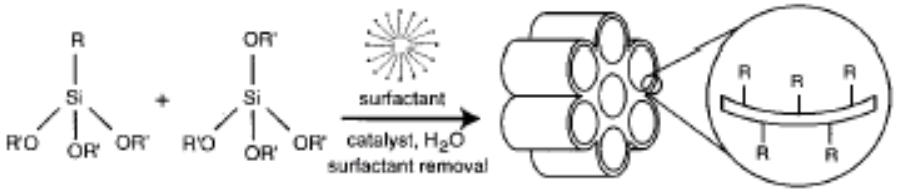

Figure 1.4. Preparation of hybrid mesoporous silicates by co-condensation

1.5.2.3.1. Co-condensation by an S^+I^- Pathway

The S^+I^- pathway is the method used to prepare the original MCM-41 and related structures. Here, S^+ refers to cationic surfactants, such as alkylammonium surfactants, and I^- to anionic silica precursors, which are obtained under basic reaction conditions. When organic groups are incorporated in the mesoporous sieve by this pathway, the surfactants are normally extracted with HCl/alcohol mixtures [95,119], although with phenyl surface groups the surfactant can be removed by calcination at 350 °C [120]. The first studies by Mann and co-workers involved mixtures of cetyltrimethylammonium bromide (CTAB) surfactants with tetraethylorthosilicate (TEOS) and organosilanes chosen from the following set: phenyltriethoxysilane (PTES), octyltriethoxysilane (OTES), allyltrimethoxysilane (ATMS), 3-mercaptopropyltrimethoxysilane (MPTMS), 3-aminopropyltriethoxysilane (APTES), 3-(2,3-epoxypropoxy) propyltrimethoxysilane, or 3-imidazolyltriethoxysilane [115,116,121]. In selected systems hexagonal order was obtained when up to 20 mol.-% of the

organoalkoxysilane was used [122]. Based on ^{29}Si magic angle spinning nuclear magnetic resonance (MAS-NMR) spectra, the distribution of organic groups in the silica network appeared to be uniform [122]. The upper limit of organoalkoxysilane incorporation into the hybrid mesostructured materials has been estimated to be less than 40 %, because some fully linked Q^4 silicate groups are necessary to form stable wall structures [115].

At about the same time, Stucky and coworkers investigated several long-chain alkoxysilanes as surfactant precursors in mesostructure syntheses [118]. MCM-41 and MCM-48 type structures were synthesized using n-tetradecyldimethyl(3-trimethoxysilylpropyl) ammonium chloride as a covalently bonded surfactant–silica source. They surmised that the surfactant was part of the inorganic framework of the product. Stein and co-workers prepared hybrid MCM-41 structures with reactive vinyl groups by co-condensation of vinyltriethoxysilane (VTES) with TEOS [96]. The highest hexagonal order was obtained with VTES/TEOS mole ratios below 1:4. The surfactant could be extracted without affecting the vinyl functionalities. A difficult question in many surface modifications of porous materials is whether the functional groups are located on the internal pore surface, the external particle surface, or within the walls.

Stein and co-workers employed a bromination reaction of vinyl- MCM-41 to probe the functional group location. During bromination in dichloromethane, a very slow reaction rate indicated that most vinyl groups were present within the mesopore channels. The bromination rate increased with increasing pore diameter. A strong dependence of the reaction rate on the presence and type of solvent molecules was observed. Gas-phase bromination was complete within 40 min. These results provide evidence for attachment of most vinyl groups to the accessible surface within the mesopore channels. This conclusion was corroborated by small angle neutron scattering experiments using contrast matching techniques [123].

Bein and co-workers co-condensed 3-methacrylpropyltrimethoxysilane and tetramethoxysilane (TMOS) in an MCM-41 type structure and also found that the C=C double bonds could be completely brominated [124].

Similarly, mercaptopropyl-functionalized porous silicates were synthesized by the co-condensation of 3-mercaptopropyltriethoxysilane (MPTES) and TMOS in the presence of a cationic surfactant under basic conditions [97]. Ordered hexagonal arrays of channels, similar

to those of MCM-41 mesoporous sieves but with smaller pore diameters, were obtained with MPTES/TMOS ratios as high as 1:2.5 and a thiol content up to 5 mmol S/g silica. The extracted solids were microporous, with an average pore diameter of ca. 14 Å. The thiol surface groups could be oxidized to sulfonic acid functionalities, creating a solid acid ion exchanger with the advantages of the ordered porous support, including high surface area, controlled pore size, mechanical stability, as well as reduced swelling or contraction upon ion exchange, compared to polymeric sulfonic acids [97] Similar mercaptopropyl-MCM-41 structures were prepared by Jacobs and co-workers [112] and Laha et al. [125]. A cubic phase, phenyl-MCM-48 was prepared by Mann and co-workers [126]. This phase could not be prepared with amino, thiol, or allyl groups.

In co-condensation reactions involving the S^+I^- pathways it is commonly observed that, as the concentration of organoalkoxysilane increases, both the d_{100}-spacings and the pore sizes of the channels are significantly reduced, even when the same surfactant is used [106,116]. At the same time, the apparent wall thickness increases, partly because organic groups extend into the channels. One possible reason for the shrinkage in cell dimensions may be a stronger interaction between nonpolar organic groups and the tails of the surfactant molecules, which draw the organic precursors further into the micelles.

The co-condensation reaction has now also been applied to incorporate covalently attached organic groups within zeolite cages [127,128]. The organic groups were incorporated directly during the synthesis of zeolite beta and other zeolites, using phenethyltrimethoxysilane as one of the precursors. The intrapore phenyl rings were subsequently sulfonated to produce sulfonic-acid sites within the zeolite cages. Shape-selective catalysis involving formation of a cyclic ketal was demonstrated.

1.5.2.3.2. Co-condensation by an $S^+X^-I^+$ Pathway

This mechanism involves cationic silicate precursors (I^+), which are obtained under acidic reaction conditions. The I^+ species interact with cationic surfactant molecules via anions (X^-) present. Under these conditions, Stucky and co-workers obtained a lamellar phase from an aqueous reaction mixture containing $C_{16}H_{33}Si(OEt)_3$, TEOS, and HCl. A lamellar phase was also formed with this surfactant in the absence of any other silica source [118].

Babonneau and co-workers studied co-condensation reactions of a series of hybrid mesoporous sieves under acidic conditions, incorporating methyl, ethyl, octyl, vinyl, and phenyl surface groups in the structure [129]. Hexagonally ordered structures were obtained only with the phenyl groups. Due to the weaker interactions between the surfactant and the silicate surface under acidic conditions, the surfactant could be extracted with ethanol, although some structural disordering was observed after this process. Calcination at 350 °C, on the other hand, preserved the ordered structure as well as the phenyl groups. Most other organic groups cleave or decompose during this heat treatment. A 2D hexagonal phase analogous to SBA-3 and a cubic phase analogous to SBA-1 [77,78,118] were prepared by co-condensation of a mixture of phenyltriethoxysilane and TEOS under acidic conditions templated by CTAB [129,130]. The hexagonal phase was obtained when the precursors were pre-hydrolyzed before addition of the surfactant, while the cubic phases resulted when the pre-hydrolysis step was left out. It is notable that the cubic phase also retained its structure after removal of the surfactant by calcinations at 350 °C and even after removal of the phenyl groups by calcination at 600 °C.

Compared to basic conditions, acid conditions are more amenable to the formation of mesostructured monoliths and films, which can be of interest, for example, in optical applications. Mann and co-workers prepared transparent yellow thin films and millimeter thick monoliths of silica mesostructures [131] by slow solvent evaporation from an aqueous precursor solution containing TEOS, 3-(2,4-dinitrophenylamino)-propyltriethoxysilane, and CTAB surfactant following the acid synthesis procedure of Brinker and co-workers [132,133]. In prior work carried out under basic conditions, the product was in powder form [134].

1.5.2.3.3. Co-condensation by an S^0I^0 Pathway

Uncharged silica precursors (I^0), such as TEOS, can also form mesostructures with neutral amine surfactant micelles (S^0), e.g., octylamine or dodecylamine. Because of the weak interaction between the neutral surfactants and the wall, removal and recovery of the surfactant is possible by extraction with ethanol. This approach was first used by Macquarrie for hybrid materials with 3-aminopropyl and 2-cyanoethyl groups [117] and was subsequently extended to other functional groups, including vinyl and chloropropyl groups

[135], 3-imidazole [121] and mercaptopropyl groups [112,136]. As with pure silica HMS structures [63] the products have disordered, worm-like channels with narrow pore size distributions. Corriu et al. included phosphorus centers in hybrid mesoporous solids by cocondensing TEOS and R´Si(OEt)$_3$ (R´ contains P atom) in the presence of n-hexadecylamine [137]. The resulting mesopore structure was maintained even after subsequent sulfuration or quaternization of the phosphorus centers.

A detailed investigation of co-condensation reactions involving the S^0I^0 assembly was carried out by Mercier and Pinnavaia who considered octyl-, butyl-, propyl-, mercaptopropyl and phenyl groups [138]. This study differentiated between template substitution pathways and direct addition pathways. Template substitution refers to partial replacement of the surfactant and TEOS by an equivalent amount of organoalkoxysilane whose organic component is comparable in length to the surfactant. With greater incorporations of the long-chain precursors the pore volume and surface area of the mesoporous products decreased systematically. The direct addition pathway was applied to organoalkoxysilanes with relatively short organic moieties, which replaced equivalent amounts of TEOS. Very short ethyl groups apparently became trapped in the walls, leading to reduced order and porosity of the products. In these processes the pore volumes and surface areas did not vary systematically with loading, but as in materials prepared by the S^+I^- pathway, smaller pore sizes were observed with increased loading of the organic component. This behaviour was also noted by Koya and Nakajima for HMS structures containing alkyl, alkenyl, and phenyl groups [139]. They also noted that the absorption capacity for water was less in the hybrid materials than in the pure silica samples, and it decreased with increasing alkyl chain length.

1.5.2.3.4. Co-condensation by an N^0I^0 Pathway

Mercier and co-workers investigated an N^0I^0 pathway, employing a non-ionic surfactant (N^0), such as alkylpoly(ethyleneoxide), Tergitol 15-S-12 [$CH_3(CH_2)_{14}(OCH_2CH_2)_{12}OH$] or Triton-X100 [$(CH_3)_3C(CH_3)_2CCH_2C_6H_4(OCH_2CH_2)_{10}$-OH]), as the structure-directing agent [140,141]. This synthesis was carried out at neutral pH and surfactant extraction was possible with ethanol. With TEOS and organotrialkoxysilanes, worm-like channel structures were obtained with lattice spacings that became smaller with

higher loadings of organics [140]. A product from co-condensation of TEOS with MPTMS exhibited a high capacity for the absorption of mercury ions (2.3 mmol/g) [141].

1.5.2.3.5. Multifunctional Surfaces

Incorporation of two or more functional groups in a one-pot synthesis is also possible, although the location of functional groups is not as controlled as by the grafting processes described earlier; the functional groups are randomly distributed in the product. Published examples include mixtures containing phenyl and aminopropyl, phenyl and mercaptopropyl, phenyl and allyl, and methyl and aminopropyl groups [126,142]. Typically an excess of TEOS (at least 80 mol.%) was used and loadings of the organic groups were in the range 1–5 mmol/g.

1.5.2.3.6. Co-condensation of Hybrid Mesoporous Silicates with Inorganic Heteroatoms

Incorporation of inorganic heteroatoms, such as titanium, is feasible during co-condensation reactions. Corma et al. prepared an active epoxidation catalyst, methyl-tethered-Ti-MCM-41, in an one step synthesis using mixtures of TMOS, methyltriethoxysilane, and titanium tetraethoxide as precursors with CTAB as the template (Ti/Si: 0.0075–0.0166) [143]. Bhaumik and Tatsumi synthesized a whole range of organically modified Ti-MCM-41 samples by co-condensation of TEOS, organo-triethoxysilane (methyl, vinyl, allyl, 3-chloropropyl, pentyl, phenyl), and titanium tetrabutoxide and tested the materials as epoxidation catalysts [144]. A higher Ti content could be obtained than in the absence of the organic groups. Unlike for organically modified silica MCM-41 samples, in the Ti-doped analogs the pore sizes and d-spacings increased slightly upon incorporation of C_1–C_3 groups. With pentyl and phenyl groups the pore sizes and *d*-spacings decreased. Enhanced selectivity for epoxide in epoxidation reactions compared to Ti-MCM-41 without organic surface groups was attributed to the greater hydrophobicity of the modified surface.

1.5.2.4. Hybrid Wall Components

A recent development in the field of hybrid materials has been the study of mesoporous materials with wall structures that consist of covalently bonded hybrid

inorganic–organic networks. The surfactant-templated syntheses of these materials use a precursor that has two trialkoxysilyl groups connected by an organic bridge. Such precursors have already been used in the production of hybrid materials [145,146], specifically the synthesis of bridged polysilsesquioxanes [147]. Shea and co-workers prepared hybrid polysilsesquioxane xerogels employing bis(triethoxysilyl)alkane, alkylene, and aryl derivatives either alone or with TEOS [147–149]. Even without surfactant templating, arylene bridged polysilsesquioxanes are porous and have high surface areas [147]. Alkylene-bridged polysilsesquioxanes with short, stiff alkylene bridges are also mesoporous; the pore size depending on the length of the alkylene chain [150].

The first report of these new materials was from Inagaki et al. who used 1,2-bis(trimethoxysilyl)ethane (BTME) as the framework precursor and octadecyltrimethylammonium chloride (ODTMA) surfactant [151]. Depending on reaction conditions, they obtained a highly ordered 2D hexagonal phase consisting of rod-like particles with hexagonal cross sections, or a 3D hexagonal mesophase consisting of spherical particles. The surfactant-extracted products contained accessible mesopores with pore sizes of 3.1 nm and 2.7 nm for the 2D and 3D materials, respectively. The bridging ethane components decomposed at 400–700 °C, temperatures higher than those required to decompose ethyl groups grafted onto a solid support. In hydrothermal stability tests, XRD patterns did not change significantly after boiling the materials in water for 8 h. The authors also describe a cubic hybrid mesophase, which forms decaoctahedral crystals [155].

Stein and co-workers used 1,2-bis(triethoxysilyl)ethane (BTSE) and CTAB to synthesize a mesoporous hybrid framework designated UOFMN-1 (unified organically functionalized mesoporous network) [152]. The precursor was prehydrolyzed with acid before the pH was raised by adding base. A material designated UOFMN-2 was made by a similar procedure using 1,2-bis(triethoxysilyl)ethylene (BTSEY) as the precursor. The products consisted of fine particles with no regular shape. They contained uniform pores (pore size: 2.2 nm for UOFMN-1, 2.4 nm for UOFMN-2). In contrast to Inagaki's structures, the channel systems of UOFMN-1 and UOFMN-2 were worm-like, lacking long-range order.

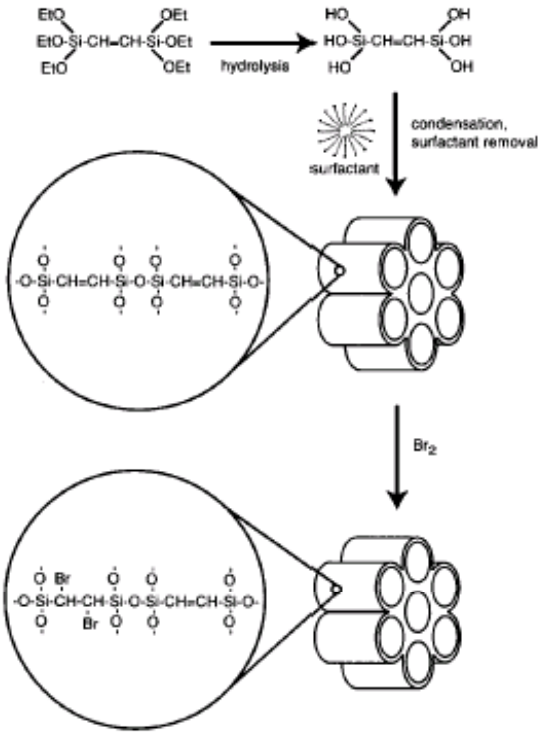

Figure 1.5. Preparation of mesoporous hybrid framework solids, showing an example with reactive ethene bridges (which can be bromine functionalized) in the walls [Ref. 152]

Ozin and co-workers also used BTSEY or mixtures of BTSEY with TEOS to synthesize hexagonal hybrid frameworks, which they labeled PMOs (periodic mesoporous organosilicas) [153,154]. The intensity of powder XRD reflections of the resulting products increased upon adding larger proportions of TEOS to the hybrid precursor. This effect could be due to greater product order as well as increased electron density in walls as the ratio of Si/C in the walls increased, demonstrating that organic groups were part of the framework. The pore diameter of the ordered product (3.94 nm) was significantly larger than those of UOFMN materials and of Inagaki's materials, which made use of a C_{18} chain surfactant. Like UOFMN-2, the ethene bridges in a PMO material made with BTSEY were proven to be reactive. The PMO sample was refluxed in CH_2Cl_2 with Br_2 for 8 days. All alkene groups were consumed according to ^{13}C cross polarization (CP) MAS-NMR. However, based on chemical analysis, it was estimated that only ca. 10% of the ethene groups were brominated and the others had reacted with solvent.

1.5.2.5. Catalytic Applications

During the last few years, hybrid mesoporous solids have been considered for a wide range of heterogeneous catalysis reactions [33,100]. Heterogenization of active centers can improve the overall efficiency of the catalytic processes because: 1) it is easier to retain the solid catalyst in the reactor or to separate it from the liquid process stream by filtration (compared to extraction or distillation requirements for homogeneous processes); 2) often the catalyst can be regenerated and recycled; and 3) confinement of the catalyst within mesopores provides a means of introducing size and/or shape selectivity and thus greater specificity to a reaction. In contrast to organic polymers, mesoporous silicates used in organic solvents do not swell or dissolve. If functional groups are covalently attached to the surface, leaching is minimized.

Typically, mesoporous supports are initially functionalized with relatively inexpensive organotrialkoxysilanes to incorporate surface amines, alkyl halides, alkenes, nitriles, or thiols. These moieties can be further modified by the methods mentioned earlier. Reactions that have been studied using functionalized mesoporous solids include acid catalysis [97,98,112,136], base catalysis [103,142,156–162], oxidations [163–166], reductions [167,168], enantioselective catalysis [111,169–171], stereospecific polymerizations [172] and other catalytic reactions that produce fine chemicals [101,157,173–175]. It has been noted that mesoporous catalysts differ significantly in many respects from their post-functionalized, amorphous silica counterparts [159]. In several investigations, confinement of the catalyst in the mesoporous solid improved the activity compared to attachment to amorphous or non-porous silica, either due to enhanced selectivity in a sterically homogeneous environment or due to higher catalyst turnover brought about by stabilization of the catalyst within the channels. In other instances the performance of the mesoporous catalyst was worse than for a catalyst attached to a non-porous support, due to limited accessibility of the active sites in the mesopores. In the latter studies, the pores were typically smaller than 4.0 nm, and improved performance would be expected with larger mesoporous hosts. For example, in an enantioselective reaction (asymmetric diethylzinc addition to benzaldehyde), using a proline-derived ligand attached to the surface of MCM-41 or SBA-15, the best performance was observed with SBA-15, which had larger pores (8.4 nm) than MCM-41 (2.3 nm), although both materials exhibited significantly better

performance than functionalized amorphous silica [170]. Other advantages exist; for example, mesoporous silicates with highly acidic surface groups are relatively safe to handle, since most of the acidic groups are confined within the channels.

1.6. HYDROCARBOXYLATION OF OLEFINS USING HETEROGENEOUS CATALYSTS

Catalytic hydrocarboxylation and hydroesterification of alkenes have attracted considerable interest during the last 20 years. In general, Co, Pd, Pt, Ni, Rh and Ru have been used as catalyst metals for hydrocarboxylation or carbonylation reactions [176]. For reasons working at milder reaction conditions (20–80°C, 1–10 bar CO pressure) Pd and Rh catalysts were applied most frequently to carry out the reactions [177].

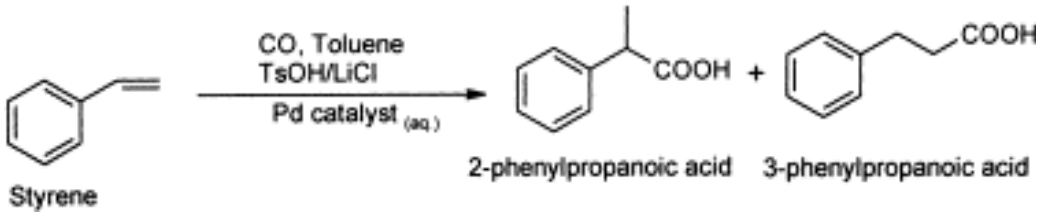

Figure 1.6. Hydrocarboxylation of styrene with homogeneous Pd-catalyst systems

Main synthetic interest focuses on the development of superior regioselective methods. A recent example employed Pd acetate immobilized on clay in presence of free triphenylphosphine (TPP) ligand and acid promoter for hydroesterification of aryl olefins [178]. The reaction is totally regiospecific for the branched isomer of aromatic olefins, while aliphatic olefins afforded branched chain esters with iso/ normal regioselective ratio of 3:1. Moreover, the regioselectivity of the hydroesterification of alkyl acrylates catalyzed by $PdCl_2L_2$ type complexes (L = phosphine ligand) could be largely controlled by variation and choosing the right ligands. TPP promotes preferential carboxylation to the branched isomer, whereas with bidentate phosphines (e.g. dppb; dppb = 1,4-bis(diphenylphosphino) butane) the linear product is produced. A classic example has been selective hydrocarboxylation to linear acid products with Pd acetate and dppb ligand in the presence of formic acid

[179,180]. A wide range of applications using the carbonylation or hydrocarboxylation reactions has been monumental for various processes, of which few are listed below:

(a) Synthesis of adipic acid from butadiene by carbonylation (BASF).
(b) Synthesis of acetic anhydride (Eastman Chemicals, 240,000 t/year in 1983).
(c) Synthesis of fluorinated acids, silylated esters and β-amino acids.
(d) Copolymerization of ethylene with CO to yield low-cost polyketones (Shell,AG, 20,000 t/year in 1996).
(e) Synthesis of cinnamic acid from styrene by oxidative addition (Montedison).
(f) Synthesis of diphenyl carbonate and dimethyl carbonate by oxidative addition (Enichem, 8,800 t/year in 1988).
(g) Synthesis of acrylic acid from alkynes (BASF, 100,000 t/year).
(h) Synthesis of cyclopentenones by *Pausand-Khand* reaction.
(i) Synthesis of Ibuprofen (Hoechst-Celanese Corp., 3,500 t/year in 1992).

Carbonylation or hydrocarboxylation of aryl olefins and alcohols provides a highly promising and eco-friendly route for the synthesis of aryl propanoic acids having applications as non-steroidal, anti-inflammatory drugs [181]. This is considered as one of the best examples of the role of catalysis in developing cleaner, environmentally benign routes replacing stoichiometric organic synthesis [182] as evidenced by the commercial success of the Hoechst-Celanese process for the synthesis of Ibuprofen [183], which involves mainly a Pd catalyst with 10% $HCl_{(aq)}$ as a promoter [184]. High regioselectivity for Ibuprofen (>95%) is achieved at high pressures (16–35 MPa), while the selectivity reduces to 67% with a TOF of 50–70 h^{-1} at lower pressures (6–7 MPa). In this reaction, the turn over frequency (TOF) was found to be only 50–150 h^{-1} even at high pressures (35 MPa) and separation of the catalyst and products is a tedious task involving the precipitation of the complex by adding non polar solvents. In recent reports [185], a significant enhancement in the catalytic activity (TOF = 800–2600 h^{-1}) and regioselectivity (99%) for Ibuprofen at lower pressures has been demonstrated with modified promoters, different phosphorus ligands and Pd-complexes [186,187]. These homogeneous catalysts often pose a serious threat in practical utility due to difficulties in catalyst-product separation and re-use. The widespread application of homogeneous catalysis in C–C bond formation reactions including carbonylation is attributed

to their high catalytic activity as well as high selectivity, which are, in many cases, difficult to achieve by heterogeneous catalysis. Despite these advantages, the industrial applications of many of these processes were not realized due to difficulties in separation and recycle of the precious catalysts. Hence, it has been a target of research during the last decade to heterogenize the homogeneous catalysts to incorporate the advantages of the homogeneous catalysis as well as the efficient catalyst–product separation.

Recently, Sheldon and co-workers [188], and Chaudhari and co-workers [189] have reported carbonylation of IBPE and styrene respectively using water-soluble palladium complexes in biphasic systems. These catalyst systems have the advantages of easy catalysts recovery, but the reaction rates as well as the selectivity in both the cases (TOF: ~ 40 h^{-1} and 244 h^{-1} and selectivity: 72% and 78% in the respective studies) were found to be lower compared to the homogeneous analogues.

Using supported Pd catalysts (Pd/C) for carbonylation of aryl halides [190] and *p*-isobutylphenylethanol (IBPE) [191], high activity (TOF = 1675–3375 h^{-1}) and selectivity (99%) for branched carboxylic acid derivatives was achieved for IBPE, however, in both the cases it was concluded that the catalytic activity was due to leached Pd in solution under reaction conditions.

Carbonylation of IBPE was reported [192] using a heterogeneous catalyst system consisting of supported Pd in the presence of phosphine ligands together with aqueous HCl as a promoter to give Ibuprofen with 23–77% selectivity at 4 MPa pressure and 398 K. The selectivity was increased up to 97% when silyl ligands were used together with the Pd-montmorillonite catalyst, but the catalytic activity was found to be very low (TOF: 3–10 h^{-1}).

In another report [193], Alper and co-workers have reported the carbonylation of olefins using a heterogeneous Pd-C catalyst in the presence of formic or oxalic acid and a bidentate phosphine ligand, dephenylphosphino propane (dppb) [193]. Though, total carboxylic acid yields achieved were in the range of 65–80%, the reaction rates were poor (10–17 h^{-1} at 423 K) with the regioselectivity towards the linear carboxylic acid in a range of 76–100%. In another study by the same group [194], the hydroesterification of styrene and derivatives was carried out using $Pd(OAc)_2$ immobilized on montmorillonite in the presence of PPh_3 as a ligand. Here, the regioselective formation of methyl esters of 2-arylpropanoic acids (~ 95%) was observed at 373 K at 4 MPa (TOF = 20 h^{-1}).

Very recently, Jacobs and coworkers [195] have reported a heterogeneous catalyst using MgAl layered double hydroxides as a support for oxidative carbonylation of phenol to diphenyl carbonate (DPC), which is an important precursor for polycarbonates. Though TOF of 387 h^{-1} could be achieved for a certain catalysts system in this reaction, yet Pd-leaching from the system is very high ca. 17%, hence, the catalyst cannot be called a truly heterogeneous catalyst system [195]. These reports reveal that a major drawback in most of these cases is the significantly lower reaction rates, often followed by leaching of the Pd metal during re-use. Therefore, the problem of developing a true heterogeneous Pd-catalyst for such carbonylation reactions remained an open challenge.

Heterogeneous catalysis has the obvious advantage of easy catalyst separation over the homogeneous catalysis; consequently, supported transition metal or metal complex catalysts have tremendous value in the development of efficient and industrially feasible processes. Several attempts have been made by different research groups to explore heterogeneous palladium catalysts for the carbonylation of olefins. A common observation was that, supported Pd does not catalyze the alkene hydrocarboxylation on its own; but was active in the presence of ligands or co-catalysts and promoters. For example, in the presence of bidentate phosphine ligands such as dppb, carbonylation of olefins were reported with a heterogeneous Pd-C catalyst along with formic or oxalic acid as promoters [193]. With styrene as the substrate this catalyst system provided 76 % selectivity to 3-phenyl propionic acid at 423 K and 0.68 MPa. In the absence of phosphines, Cu-salts such as $CuCl_2$ were found to effect carbonylation with Pd–C as the catalyst, but with very low catalytic activities (7–8 days of reaction for quantitative conversion). Palladium salts such $Pd(OAc)_2$ immobilized on solid supports such as montmorillonite is also active in the presence of phosphines such as PPh_3 as explained by Lee and Alper for the hydroesterification of styrene and other vinyl aromatics. Regioselective formation of methyl esters of 2-arylpropionic acids (up to 95%) was observed at 398 K at 4 MPa though with lower rates (TOF = 20 h^{-1}). In this case, acidic promoters were found to be necessary for significant catalytic activity and inorganic acids like HCl was more effective than organic acids such as *p*-toluenesulphonic acid. Bulky bidentate ligands such as dppp and dppb instead of PPh_3 were inactive in this case, unlike the case of Pd-C catalyst. The role of PPh_3 was explained as to promote the formation and stabilization of Pd (0) intermediate on the support.

Polymer supported palladium catalyst was also shown to be active for the alkoxycarbonylation of olefins. For example, polymer anchored palladium catalysts such as $PdCl_2(Resin\text{-}PPh_3)_2$ (resin is 1% polyvinyl benzene-polystyrene) gave high selectivity to linear ester of alkoxycarbonylation of 1-pentene [196]. A bimetallic catalyst consisting of palladium and nickel [197] anchored on PVP (poly(*N*-vinyl-2-pyrrolidone) along with PPh_3 was reported to produce arylpropanoic acid esters with high selectivity (~ 99%) with complete conversion at 80 °C and 2.1 MPa pressure using benzene as a solvent; but the rate of the reaction was very poor (TOF = 0.25 – 0.5h^{-1}).

1.7. HYDROFORMYLATION OF OLEFINS USING HETEROGENEOUS CATALYSTS

Hydroformylation or Oxo synthesis, as it is commonly known as, is one of the largest scale applications of homogeneous catalysis in industry with worldwide capacities of over 6.6×10^6 tonnes per annum [198]. This process involves a reaction of an olefin, carbon monoxide and hydrogen to produce linear or branched next higher aldehyde products (Figure 1.7).

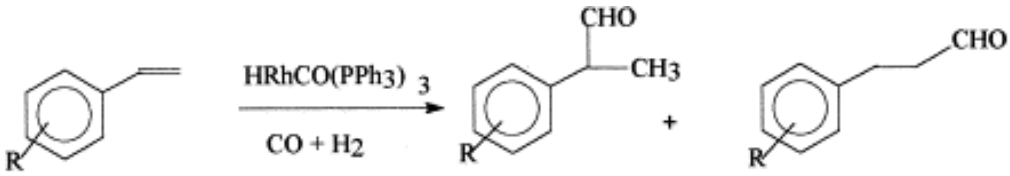

Figure 1.7. Hydroformylation of olefin (arene) with homogeneous $HRh(CO)(PPh_3)_3$ catalyst

The process was discovered in 1938 by Otto Roelen at Ruhrchemie, where it was first commercialized [199]. The most important olefin starting material is propene, which is mainly converted to 1-butanol and 2-ethylhexanol via the initial product butyraldehyde. The original catalyst was $[Co_2(CO)_8]$, which was modified with phosphines to increase the yield of the industrially more important linear aldehydes. A breakthrough was achieved in 1976 at Union Carbide with the introduction of rhodium catalysts such as $HRh(CO)(PPh_3)_3$. Almost

all the commercial processes employ homogeneous cobalt or rhodium complex catalysts, of which the process using the Wilkinson's catalyst $HRh(CO)(PPh_3)_3$ has been considered as a major breakthrough because of its high activity and selectivity at mild operating conditions (at 100 °C and 10–25 bar pressure) [198]. While, $HRh(CO)(PPh_3)_3$ catalyst has been commercialized for hydroformylation of propylene, wherein, the product can be easily separated from the catalyst due to its high volatility, its application for the higher olefinic substrates has been limited due to difficulties in catalyst – product separation [199,200]. Therefore, several attempts have been made to heterogenize the homogeneous catalysts, so that the advantages of the homogeneous and heterogeneous catalysts can be combined. In previous work, polymer anchored [201], supported liquid phase (SLP) [202], supported aqueous phase (SAP) [203], biphasic catalysts using water-soluble metal complexes [204], using sulfonated [205] or fluorinated phosphines [19] as ligands, ionic liquids as new solvents [21-27], as well as bimetallic catalysts [206] for hydroformylation have been proposed. In these reports, interesting concepts have emerged; however, with the exception of biphasic catalysis no other approach has been found to be commercially attractive. Even the biphasic catalysts for hydroformylation of *higher olefins* suffer from the disadvantages of the lower rates limited by the solubility of olefins in water [205-b].

Earlier, heterogenized catalysts were reported using Rh complex dendrimers on silica [207], water soluble Calix[4]arene ligands [208] for biphasic hydroformylation of water-insoluble olefins, silica immobilized with tripodal polyphosphine rhodium catalysts [209] to name a few. But in majority of the cases, they suffer from lower selectivity and activity, low recyclability, use expensive ligands, unsuitable for commercial applications.

Whereas the hydroformylation of alkenes preferably into *n*-aldehydes is one of the largest processes today running on Rh or Co catalysts, it still suffers from the usual drawbacks of homogeneous catalysis. As metal (and ligand) recovery and metal regeneration are energy and time consuming [210], attempts to heterogenize catalysts remain relevant. Literature only reports work on Rh-based catalysts. Apart from zeolites, clays have been frequently used as a support, both for liquid and gas-phase hydroformylation catalysis. There have been mixed success [211]; for instance, stable activity in a series of consecutive runs was claimed with a $Rh(PPh_3)_3^+$/montmorillonite catalyst in the liquid-phase hydroformylation of allyl alcohol [212], but in 1-hexene liquid phase hydroformylation, loss

of a neutral Rh-phosphine complex from the support was reported. Although the catalysts show acceptable activity and selectivity for aldehydes and moderate regioselectivity (*n*ormal/ iso-aldehydes), the available data do not allow one to evaluate whether clays are generally applicable as supports in Rh-catalyzed hydroformylations.

1.7.1. Phosphine-Free Rh Zeolites

It can be anticipated that using zeolites as polydentate ligands would allow one to stabilize specific catalytic species and induce stereochemical control of the regioselectivity for hydroformylation reaction. Among the procedures for preparation of Rh-zeolites, dilute aqueous exchange at room temperature with $RhCl_3$ or $Rh(NH_3)_5Cl_3$ is most popular [212]. In large-pore zeolites such as Y and mordenite, Rh can be uniformly distributed across the zeolites, while medium pore size zeolites (ZSM-34 and ZSM-11) show rhodium enrichment at the surface due to hydrolysis. In small pore zeolites (e.g., erionite, zeolite A, ZK-5) surface hydrolysis dominates, and most rhodium is found on the external surface [212]. Depending on the pretreatments of these zeolites, e.g., calcination, autoreduction, reduction at various temperatures, under H_2 or CO, various species can be formed, e.g., lattice-coordinated Rh^{3+}, RhO_2, or Rh_2O_3 particles, metallic Rh^0 clusters, or carbonyl complexes such as $Rh^I(CO)_2$ or $Rh_6(CO)_{16}$ [212]. These zeolites have been applied for gas and liquid-phase reactions [213,214]. As an example, gas-phase hydroformylation of 1-hexene was performed with a zeolite CaA synthesized in the presence of Rh [213h]. Enhanced selectivity for the *n*-aldehyde was observed in comparison with an exchanged zeolite, but loss of volatile Rh-carbonyls resulted in a gradually decreasing activity.

Liquid phase 1-hexene hydroformylation was investigated with $Rh(NH_3)_5Cl^{2+}$ exchanged NaY zeolite after carbonylation treatment. This material contains $Rh_6(CO)_{16}$ clusters associated with the zeolite crystals. This catalyst was characterized by a high hydroformylation selectivity and a lack of regioselectivity. This is very similar to the behavior of homogeneous rhodium carbonyls, which were found to be present in the reaction mixture [214a]. While for Rh^{III}-exchanged NaY and CaA the observed activity is caused by eluted rhodium [213h], experiments with poisons and additives allowed the speculation that *i.a.* NaX zeolites exchanged with $Rh(NH_3)_5(H_2O)Cl_3$ are a source of homogeneous as well as heterogeneous activity [214b,c,212h]. At high reaction temperatures, leaching from the

zeolite decreased, possibly due to the formation of larger Rh clusters that are difficult to be converted into soluble species [214b]. Unfortunately, under such conditions, the chemoselectivity is largely in favor of substrate isomerization, probably catalyzed by residual zeolite acidity.

1.7.2. Rhodium-Phosphine Complexes in Zeolites: The Ship-in-a-Bottle Approach

The bulky nature of the phosphine ligands makes entrapment of their rhodium complexes in zeolites cages a difficult task. A computational study revealed that phosphine ligands with more than one aromatic substituent are not able to diffuse into the pore system of zeolite Y [215-a]. Only a few examples of rhodium-phosphine complexes inside zeolites have been reported. Intrazeolitic rhodium carbonyl clusters are able to react with small phosphines such as dimethylphenylphosphine. When larger molecules such as triphenylphosphine and tris(2-cyanoethyl)phosphine are used, a species such as $Rh^{I}(CO)_2$ probably migrates to the outer surface to react with the phosphine [215-b].

Compared to $Rh_6(CO)_{16}$/Na-Y, zeolite Y entrapped Rh-dimethylphenylphosphine complexes in propene hydroformylation show a higher *n*/*i* ratio (2.00 vs 1.75). However, the catalyst is completely deactivated after 24 h [213c]. With other Rh-zeolite-phosphine complexes, similar increases of the *n*/*i* ratio have been observed [215c]. With triphenylphosphine ligands, selectivity to aldehydes improved, while the high regioselectivity was retained. However, a small loss of rhodium was detected [212c]. It is clear that only at the very low substrate conversions, no leaching of Rh into the reaction medium is encountered. Whereas the hydroformylation selectivity is acceptable, the regioselectivity is moderate. It further seems that activity and leaching are dependent on reaction conditions and nature of the phosphine ligand.

In recent work, it seems that truly heterogeneous hydroformylation with such zeolite-based catalysts is possible, though no specific evidence for the absence of leaching was offered [216a,b]. Stable hydrocarbonylation of unsaturated compounds seems possible at 120°C and 5 MPa. Generally speaking, a higher regioselectivity for linear products (*n*/*i*) was obtained compared to the homogeneous counterparts, though the use of zeolite supports resulted in a decreased activity.

Sulfur ligands more stable toward oxidation and degradation than P-ligands have been used for comparative purposes as well. However, the stability advantage is balanced by activity and selectivity loss. $Rh^{I}(CO)_2$-zeolites with faujasite and Beta topology were contacted with S-ligands via diffusion and via intrazeolite ligand synthesis. Although the regioselectivity was rather low, claims for good reusability and negative filtration tests were presented [216-b].

1.7.3. Zeolite Pore Mouth Adsorption of Rh-Phosphine Complexes

As Rh-phosphine complexes are sometimes too large to diffuse inside zeolites, they can at best interact with the external surface and the pore mouths of the crystals. An example of "pore mouth sorption" in the aqueous (bi)phase hydroformylation of propene, concerns a NaY immobilized 2.0 nm $Rh_{55}L_{12}Cl_6$ cluster (L = $P(tBu)_3$, x = 20; L = PPh_3). This cluster is adsorbed on NaY, blocking its micropores. The catalyst could be reused 27 times without deactivation, while turnover frequencies in the range 400-600 mol propene mol^{-1} Rh min^{-1} were possible with an *n*/*i* ratio of 1.0 (30.0 MPa CO/H_2 = 1, 120-130 °C) [216-c]. It is not clear at this moment whether the catalyst stability is the result of the interaction of the cluster with the zeolites pore mouths rather than of the biphasic reaction conditions.

1.7.4. Silica-Tethered Rh-Phosphine Complexes

Introduction of groups amenable to covalent linking on phosphines is difficult and explains why only a limited range of silica-anchored phosphines has been reported. Silylation is often accompanied by side reactions involving transformation of part of P^{III} into P^{V}, but this oxidation can be avoided in specific reaction conditions. The possibility of using rhodium on phosphinated silica as hydroformylation catalyst was already considered in the 1970s [216-e]. Silica anchored $RhH(CO)((Ph_2P(CH_2)_2Si(C_2H_5O)_3)_3$ in rhodium catalyzed hydroformylation of 1-hexene was claimed to show good activity and stability. Rhodium elution was only observed during the first hours.

More recently anchored bidentate phosphines have been used for hydroformylation reactions [216-f,-g]. Such heterogeneous catalysts could be used for 14 days without loss of activity [216-f]. The rigid backbone with large bite-angle seems responsible for the high *n*/*i* ratio of 32. Whereas such systems are more difficult to prepare, their performance by far

supersede that of all previously described systems. With the present knowledge on structured mesoporous silicas, this performance might still be susceptible to further major improvement.

But, the heterogenized catalysts suffered either from lower selectivity and activity or low recyclability and often followed by leaching of Rh metal in reaction conditions; hence, they were not considered for commercial applications. It is envisaged that the metal complexes encapsulated in zeolites and mesoporous supports lead to very high metal dispersion and stable catalysts. Similarly, the zeolite microstructure could prevent leaching of metal complexes in solution, a serious problem with most of the "heterogenized" catalysts.

1.8. SCOPE AND OBJECTIVES

In this context, encapsulation of metal complexes as a mean of "heterogenization" of homogeneous metal complex catalysts in porous insoluble supports has particular significance. In this approach, the organometallic complex is encapsulated or anchored inside the pores of the inorganic inert matrices, e.g. zeolites, M41S materials, clay etc. in such a way that the complex is tightly bound inside the pores [33]. The prime requirement is stability of the encapsulated complex, so that it does not leach out of the catalyst pores to the liquid phase in the course of reaction, while retaining high activity, selectivity and original configuration. It is envisaged that the metal complexes encapsulated in zeolites and mesoporous supports lead to very high metal dispersion and stable catalysts in addition to the possibility of tuning the selectivity. Similarly, the micro- and mesostructures could prevent leaching of metal complexes in solution, a serious problem with most of the "heterogenized" catalysts. Immobilized catalysts reported earlier, suffer either from lower selectivity and activity (TON, turn over number), or low recyclability, or use expensive ligands and hence, not suitable for practical applications. Therefore, there is ample opportunity to explore development of new methods of heterogenization, which will eliminate the limitations of the state of the art methods. Thus, from the separation and reusability point of view and maintaining good activity and selectivity, heterogenization of rhodium and palladium complex catalysts by anchoring or encapsulation techniques on porous supports may provide an alternative approach opening up new vistas for the industrial applications e.g. hydroformylation and hydrocarboxylation reactions in synthesis of speciality chemicals and fine chemicals. These catalysts could also have important applications in other homogeneous

or organic reactions, wherein selectivity, catalyst-product separation and use of eco-friendly technologies is still a challenging task. The aim of this thesis was to investigate the approach of encapsulation or anchoring for heterogenization of industrially significant catalysts used in hydroformylation and carbonylation reactions.

The thesis is also aimed at characterization of the heterogeneous catalysts and investigation of the catalytic performance in comparison to the homogeneous and previously known heterogeneous catalysts. The specific problems chosen are:

- Synthesis of zeolites and mesoporous materials by employing heteropolyacids and metal oxoanions of group VI (molybdenum and tungsten) as novel promoters.
- Novel heterogeneous catalysts containing encapsulated $HRh(CO)(PPh_3)_3$ in different porous supports for hydroformylation of olefins to aldehydes.
- Novel heterogeneous catalysts containing encapsulated Pd-pyca complex catalysts in different porous supports for hydrocarboxylation of olefins and alcohols to corresponding carboxylic acids.
- Metal complexes anchored on heteropolyacids tethered to zeolite and other supports for hydroformylation and hydrocarboxylation of alkenes.

REFERENCES:

[1] B. M. Trost, *Science* **1991**, *254*, 1471.

[2] Gates, B. C. *Catalytic Chemistry*, Wiley: New York, 1992.

[3] Bond, G. C. in *Heterogeneous Catalysis: Principles and Applications* Eds.: Atkins, P. W.; Holker, J. S. E.; Holliday, A. K.; Oxford Chemistry Series: Oxford, 1987.

[4] Bond, G. C. in *Principles of Catalysis*, The Chemical Society: London, 1972.

[5] Sinflet, J. H.; Cusumano, J. A. in *Advanced Materials in Catalysis*, Eds.: Burton, J. J.; Garten, R. L., Academic Press: London, 1977.

[6] (a) Cornils, B.; Herrmann, W. A. in *Applied Homogeneous Catalysis with Organometallic Compounds*, Volume 1, Wiley-VCH: Weinheim, 1996. (b) Hagen, J. *Industrial Catalysis: A Practical Approach*, Wiley-VCH: Weinheim, 1999.

[7] Parshall, G. W. *Homogeneous Catalysis*, John Wiley: New York, 1980.

[8] Sheldon, R. A. *Chem. Ind.* **1992**, 903.

[9] Frohling, C. D.; Kohlpaintner, C. W. in *Applied Homogeneous Catalysis with Organometallic Compounds*, Volume 1, Eds.: Cornils, B; Herrmann, W. A., Wiley-VCH: Weinheim, 1996, 27.

[10] Parshall, G.W.; Ittel, S. D. *Homogeneous Catalysis*; John Wiley: New York, 1992.

[11] *Handbook of Heterogeneous Catalysis*, Eds.: Ertl, G.; Knoezinger, H.; Weitkamp. J., Wiley-VCH: Weinheim, 1997, Volumes 1 and 3.

[12] *Applied Homogeneous Catalysis with Organometallic Compounds*; Cornils, B.; Herrmann, W. A., Eds.; VCH: Weinheim, 1996; Vols. 1 and 2.

[13] Neibecker, D.; Reau, R. *J. Mol. Catal. A: Chemical* **1989**, *57*, 153.

[14] Manassen, J. in *Catalysis, Progress in Research*, Eds.: Basolo, F; Burwell Jr., R. E., Plenum Press: New York, 1973, 177.

[15] Herrmann, W. A.; Cornils, B. *Angew. Chem. Intl. Ed.* **1997,** *36*, 1048.

[16] Cole-Hamilton, D. J. *Science* **2003**, *299*, 1702.

[17] Cornils, B. in *Applied Homogeneous Catalysis with Organometallic Compounds*, Eds.: Cornils, B.; Herrmann, W. A. Volume 1, Wiley-VCH: Weinheim, 1996, 245.

[18] Zheng, X. L.; Jiang, J. Y.; Liu, X. Z.; Jin, Z. L. *Catal. Today* **1998**, *44*, 175.

[19] (a) Horvarth, I. T.; Rabai, J. *Science* **1994**, *266*, 72. (b) Wende, M.; Meier, R.; Gladysz, J. A. *J. Am. Chem. Soc.*, **2001**, *123*, 11490.

[20] (a) Koch, D.; Leitner, W. *J. Am. Chem. Soc.* **1998**, *120*, 13398. (b) Dupont, J.; de Souza, R. F.; Suarez, P. A. Z. *Chem. Rev.* **2002**, *102*, 3667.

[21] Kainz, S.; Brinkman, A.; Leitner, W.; Pfaltz, A. *J. Am. Chem. Soc.* **1999**, *1211*, 6421.

[22] (a) Chauvin, Y.; Mussmann, L.; Olivier, H. *Angew. Chem. Int. Ed. Engl.* **1996**, *34*, 2698. (b) Brasse, C. C.; Englert, U.; Salzer, A.; Waffenschmidt, H.; Wasserscheid, P. *Organometallics* **2000**, *19*, 3818.

[23] Mehnert, C. P.; Cook, R. A.; Dispenziere, N. C.; Afeworki, M. *J. Am. Chem. Soc.* **2002**, *124*, 12932.

[24] Sellin, M. F.; Webb, P. B.; Cole-Hamilton, D. J. *Chem. Commun.* **2001**, 781.

[25] Blanchard, L. A.; Hancu, D.; Beckman, E. J.; Brennecke, J. F. *Nature* **1999**, *399*, 28.

[26] Reetz, M. T.; Wiesenhofer, W.; Francio, G.; Leitner, W. *Chem. Commun.* **2002**, 992.

[27] (a) McNamara, C. A.; Dixon, M. J.; Bradley, M. *Chem. Rev.* **2002**, *102*, 3275. (b) Dickerson, T. J.; Reed, N. N.; Janda, K. D. *ibid.*, 3325.

[28] Tupitsyn, S. B.; Imyanitov, N. S. *Pet. Chem.* **1996**, *36*, 249.

[29] Schwab, E.; Mecking, S. *Organometallics* **2001**, *20*, 5504.

[30] van Heerbeek, R.; Kamer, P. C. J.; van Leeuwen, P. W. N. M.; Reek, J. N. H. *Chem. Rev.* **2002**, *102*, 3717.

[31] Ropartz, L. et al. *J. Chem. Soc. Dalton Trans.* **2002**, 4323.

[32] Bourque, S. C.; Alper, H.; Manzer, L.; Arya, P. *J. Am. Chem. Soc.* **2000**, *122*, 956.

[33] De Vos, D. E.; Dams, M.; Sels, B. F.; Jacobs, P. A. *Chem. Rev.* **2002**, *102*, 3615.

[34] Corma, A. *Chem. Rev.* **1997**, *97*, 2373.

[35] Nowotny, M.; Maschmeyer, T.; Johnson, B. F. G.; Lahuerta, P.; Thomas, J. M.; Davies, J. E. *Angew. Chem. Int. Ed. Engl.* **2001**, *40*, 955.

[36] Sandee, A. J.; van der Veen, L. A.; Reek, J. N. H.; Kamer, P. C. J.; Lutz, M.; Spek, A. L.; van Leeuwen, P. W. N. M. *Angew. Chem. Int. Ed. Engl.* **1999**, *38*, 3231.

[37] Meehan, N. J.; Sandee, A. J.; Reek, J. N. H.; Kamer, P. C. J.; van Leeuwen, P. W. N. M.; Poliakoff, M. *Chem. Commun.* **2000**, 1497.

[38] (a) Bein, T. *Compr. Supramol. Chem.* **1996**, *7*, 579.

[39] (a) Davis, M. *Nature* **2002**, *417*, 813. (b) Herron, N.; *Inorg. Chem.* **1986**, *25*, 4741. (c) Gerrits, P. P. K.; De Vos, D. E.; Starzyk, F. T.; Jacobs, P. A. *Nature* **1994**, *369*, 543. (d) Eswaramoorthy, M.; Neeraj; Rao, C. N. R. *Chem. Commun.* **1998**, 615. (e) Chavan, S.;

Ratnasamy, P. *Chem. Commun.*, **2001**, 1124. (f) Corma, A.; Nemeth, L. T.; Renz, M.; Valencia, S. *Nature* **2001,** *412*, 423.

[40] Kowalak, S.; Weiss, R. C.; Balkus Jr., K. J. *J. Chem. Soc. Chem. Commun.* **1998**, 615.

[41] (a) Ogunwumi, S. B.; Bein, T. *Chem. Commun.* **1997**, 901. (b) Sabater, M. J.; Corma, A.; Domenech, A.; Fornes, V.; Garcia, H. *Chem. Commun.* **1997**, 1285.

[42] (a) Herron, N.; Tolman, C. A. *J. Am. Chem. Soc.* **1987**, *109*, 2837. (b) J. P. Collman, Gagne, R. R.; Halbert, T. R.; Marchon, J. C.; Reed, C. A. *J. Am. Chem. Soc.* **1973**, *95*, 7678. (b) Herron, N. *New. J. Chem.* **1989**, *13*, 761.

[43] (a) Zakharov, V. Y.; Romanovsky, B. V. *Sov. Mosc. Univ. Bull.* **1977**, *32*, 16. (b) Zakharov, V. Y.; Zakharova, O. M.; Romanovsky, B. V.; Mardaleishvili, R. E. *React. Kinet. Catal. Lett.* **1977**, *6*, 133.

[44] Ozin, G. A.; Gil, C. *Chem. Rev.* **1989**, *89*, 1749.

[45] (a) Huybrechts, D. R. C.; De Bruyker, L.; Jacobs, P. A. Nature, **1990**, *345*, 242. (b) Espeel, P. H.; Tielen, M.; Jacobs *J. Chem. Soc. Chem. Commun.*, **1991**, 669.

[46] Klier, K.; Ralek, M. *J. Phys. Chem. Solids* **1968**, *29*, 951.

[47] Mortier, W. J.; Schoonheydt, R. a. *Progr. Solid. State. Chem.* **1985**, *16*, 99.

[48] Kalyansundaram, K. *Coord. Chem. Rev.* **1982**, *46*, 159.

[49] Woltermann, G. M.; Durante, V. A. *Inorg. Chem.* **1983**, *22*, 1954.

[50] (a) Ichikawa, M.; Rao, L. F.; Fukuoka, A. *Catal. Sci. Tech.* **1991**, *1*, 111. (b) Iwamoto, M.; Nakamura, S. I.; Kusano, H.; Kagawa, S. *J. Phys. Chem.* **1986**, *90*, 5244. (c) Zhou, P. L.; Maloney, S. D.; Gates, B. C. *J. Catal.* **1991**, *129*, 315.

[51] Meyer, G.; Wohrle, D.; Mohl, D.; Ekloff, G. S. *Zeolites* **1984**, *4*, 30.

[52] (a) Balkus Jr.; K. J.; Welch, A. A.; Gnade, B. E. *Zeolites* **1990**, *10*, 722. (b) For an overview: De Vos, D. E.; Starzyk, F. T.; K-Gerrits, P. P.; Parton, R. F.; Jacobs, P. A. *Macromol. Symp.* **1994**, *80*, 157.

[53] Gaillon, L.; Sajot, N.; Bedioui, F.; Devynck, J.; Balkus Jr., K. J. *J. Electroanal. Chem. Interface. Electrochem.* **1993**, *345*, 157.

[54] (a) Balkus Jr., K. J.; Gabrielov, A. G.; Bedioui, F.; Devynck, J. *Inorg. Chem.* **1994**, *33*, 67. (b) Gabrielov, A. G.; Balkus Jr., K. J.; Bedioui, F.; Devynck, J. *Micropor. Mater.* **1994**, *2*, 119.

[55] Peigneur, P.; Lunsford, J. H.; De Wilde, W.; Schoonheydt, R. A. *J. Phys. Chem,* **1977**,

81, 1179.

[56] Schoonheydt, R. A.; Peigneur, P.; Uytterhoeven, J. B. *J. Chem. Soc. Faraday Trans.* **1978,** ***74***, 2550.

[57] (a) Augustine, R.; Tanielyan, S.; Anderson, S.; Yang, H. *Chem. Commun.*, 1999, 1257. (b) Tanielyan, S. K.; Augustine, R. *U. S. Patent* 6,025,295, **1999**. (c) Burk, M. J.; Gerlach, A.; Semmerji, D. *J. Org. Chem.* **2000**, *65*, 8933.

[58] Kresge, C. T.; Leonowicz, M. E.; Roth, W. J.; Vartuli, J. C.; Beck, J. S. *Nature* **1992**, *359*, 710.

[59] Beck, J. S., Vartuli, J. C.; Roth, W. J.; Leonowicz, M. E.; Kresge, C. T.; Schmitt, K. D.; Chu, C. T.-W.; Olson, D. H.; Sheppard, E. W.; McCullen, S. B.; Higgins, J. B.; Schlenker, J. L. *J. Am. Chem. Soc*. **1992**, *114*, 10 834.

[60] Yanagisawa, T.; Shimizu, T.; Kuroda, K.; Kato, C. *Bull. Chem. Soc. Jpn.* **1990**, *63*, 988.

[61] Inagaki, S.; Fukushima, Y.; Kuroda, K. *J. Chem. Soc., Chem. Commun.* **1993**, 680.

[62] Ryoo, R.; Jun, S. *J. Phys. Chem. B* **1997**, *101*, 317.

[63] Tanev, P. T.; Pinnavaia, T. J. *Science* **1995**, *267*, 865.

[64] Tanev, P. T.; Pinnavaia, T. J. *Chem. Mater.* **1996**, *8*, 2068.

[65] Bagshaw, S. A.; Prouzet, E.; Pinnavaia, T. J. *Science* **1995**, *269*, 1242.

[66] Prouzet, E.; Pinnavaia, T. J. *Angew. Chem. Int. Ed. Engl.* **1997**, *36*, 516.

[67] Kim, S. S.; Zhang, W.; Pinnavaia, T. J. *Science* **1998**, *282*, 1302.

[68] Huo, Q.; Leon, R.; Petroff, P. M.; Stucky, G. D. *Science* **1995**, *268*, 1324.

[69] Zhao, D.; Feng, J.; Huo, Q.; Melosh, N.; Fredrickson, G. H.; Chmelka, B. F.; Stucky, G. D. *Science* **1998**, *279*, 548.

[70] Zhao, D.; Yang, P.; Huo, Q.; Chmelka, B. F.; Stucky, G. D. *Curr. Opin. Solid State Mater. Sci.* **1998**, *3*, 111.

[71] Zhao, D.; Huo, Q.; Feng, J.; Chmelka, B. F.; Stucky, G. D. *J. Am. Chem. Soc.* **1998**, *120*, 6024.

[72] Schmidt-Winkel, P.; Lukens, W. W.; Zhao, D.; Yang, P.; Chmelka, B. F.; Stucky, G. D. *J. Am. Chem. Soc.* **1999**, *121*, 254.

[73] Schmidt-Winkel, P.; Lukens, W. W.; Yang, P.; Margolese, D. I.; Lettow, J. S.; Ying, J. Y.; Stucky, G. D. *Chem. Mater.* **2000**, *12*, 686.

[74] Sing, K. S. W.; Everett, D. H.; Haul, R. A. W.; Moscou, L.; Pierotti, R. A.; Rouquÿrol, J.; Siemieniewska, T. *Pure Appl. Chem.* **1985**, *57*, 603.

[75] Moller, K.; Bein, T. *Chem. Mater.* **1998**, *10*, 2950.

[76] Ozin, G. A.; Chomski, E.; Khushalani, D.; MacLachlan, M. J. *Curr. Opin. Colloid Interface Sci.* **1998**, *3*, 181.

[77] Huo, Q.; Margolese, D. I.; Ciesla, U.; Demuth, D. G.; Feng, P.; Gier, T. E.; Sieger, P.; Firouzi, A.; Chmelka, B. F.; Schuth, F.; Stucky, G. D. *Chem. Mater.* **1994**, *6*, 1176.

[78] Huo, Q.; Margolese, D. I.; Ciesla, U.; Feng, P.; Gier, T. E.; Sieger, P.; Leon, R.; Petroff, P. M.; Schuth, F.; Stucky, G. D. *Nature* **1994**, *368*, 317.

[79] Unger, K. K.; Porous Silica–Its Properties and Use as Support in Column Liquid Chromatography, Vol. 16, Elsevier, Amsterdam 1979.

[80] Price, P. M.; Clark, J. H.; Macquarrie, D. J. *J. Chem. Soc., Dalton Trans.* **2000**, 101.

[81] Moller, K.; Bein, T. *Stud. Surf. Sci. Catal.* **1998**, *117*, 53.

[82] Ishikawa, T.; Matsuda, M.; Yasukawa, A.; Kondori, K.; Inagaki, S.; Fukushima, T.; Kondo, S. *J. Chem. Soc., Faraday Trans.* **1996**, *92*, 1985.

[83] Kimura, T.; Kuroda, K.; Sugahara, Y.; Kuroda, K. *J. Porous Mater.* **1998**, *5*, 127.

[84] Anwander, R.; Palm, C.; Stelzer, J.; Groeger, O.; Engelhardt, G. *Stud. Surf. Sci. Catal.* **1998**, *117*, 135.

[85] Zhao, X. S.; Lu, G. Q. *J. Phys. Chem. B* **1998**, *102*, 1556.

[86] Liu, J.; Feng, X.; Fryxell, G. E.; Wang, L.-Q.; Kim, A. Y.; Gong, M. *Adv. Mater.* **1998**, *10*, 161.

[87] Feng, X.; Fryxell, G. E.; Wang, L.-Q.; Kim, A. Y.; Liu, J.; Kemner, K. M. *Science* **1997**, *276*, 923.

[88] Mercier, L.; Pinnavaia, T. J. *Environ. Sci. Technol.* **1998**, *32*, 2749.

[89] Liu, J.; Fryxell, G. E.; Mattigod, S.; Zemanian, T. S.; Shin, Y.; Wang, L.-Q. in Proc. Nanoporous Materials II, Banff, Canada, May 25-28, 2000.

[90] Beck, J. S.; Calabro, D. C.; McCullen, S. B.; Pelrine, B. P.; Schmitt, K. D.; Vartuli, J. C.; Method for Functionalizing Synthetic Mesoporous Crystalline Material, Mobil Oil Corp., USA 1992.

[91] Kimura, T.; Saeki, S.; Sugahara, Y.; Kuroda, K. *Langmuir* **1999**, *15*, 2794.

[92] Jaroniec, C. P.; Kruk, M.; Jaroniec, M.; Sayari, A. *J. Phys. Chem. B* **1998**, *102*, 5503.

[93] Antochshuk, V.; Jaroniec, M. *J. Phys. Chem. B* **1999**, *103*, 6252.

[94] Tatsumi, T.; Koyano, K. A.; Tanaka, Y.; Nakata, S. *Stud. Surf. Sci. Catal.* **1998**, *117*, 143.

[95] Anwander, R.; Nagl, I.; Widenmeyer, M.; Engelhardt, G.; Groeger, O.; Palm, C.; Roser, T. *J. Phys. Chem. B* **2000**, *104*, 3532.

[96] Lim, M. H.; Blanford, C. F.; Stein, A. *J. Am. Chem. Soc.* **1997**, *119*, 4090.

[97] Lim, M. H.; Blanford, C. F.; Stein, A. *Chem. Mater.* **1998**, *10*, 467.

[98] van Rhijn, W. M.; De Vos, D. E.; Sels, B. F.; Bosaert, W. D.; Jacobs, P. A. *Chem. Commun.* **1998**, 317.

[99] Lim, M. H.; Stein, A.; unpublished results.

[100] Clark, J. H.; Macquarrie, D. J. *Chem. Commun.* **1998**, 853.

[101] Brunel, D. *Microporous Mesoporous Mater.* **1999**, *27*, 329.

[102] Sutra, P.; Brunel, D. *Chem. Commun.* **1996**, 2485.

[103] Subba Rao, Y. V.; De Vos, D. E.; Jacobs, P. A. *Angew. Chem. Int. Ed. Engl.* **1997**, *36*, 2661.

[104] DÌaz, J. F.; Balkus, K. J. Jr.; Bedioui, F.; Kurshev, V.; Kevan, L. *Chem. Mater.* **1997**, *9*, 61.

[105] Anwander, R.; Gorlitzer, H. W.; Gerstberger, G.; Palm, C.; Runte, O.; Spiegler, M. *J. Chem. Soc., Dalton Trans.* **1999**, 3611.

[106] Lim, M. H.; Stein, A. *Chem. Mater.* **1999**, *11*, 3285.

[107] Shephard, D. S.; Zhou, W.; Maschmeyer, T.; Matters, J. M.; Roper, C. L.; Parsons, S.; Johnson, B. F. G.; Duer, M. J. *Angew. Chem. Int. Ed. Engl.* **1998**, *37*, 2719.

[108] De Juan, F.; Ruiz-Hitzky, E. *Adv. Mater.* **2000**, *12*, 430.

[109] Aronson, B. J.; Blanford, C. F.; Stein, A. *Chem. Mater.* **1997**, *9*, 2842.

[110] Antochshuk, V.; Jaroniec, M. *Chem. Commun.* **1999**, 2373.

[111] Bellocq, N.; Abramson, S.; Laspÿras, M.; Brunel, D.; Moreau, P. *Tetrahedron: Asymmetry* **1999**, *10*, 3229.

[112] van Rhijn, W.; De Vos, D.; Bossaert, W.; Bullen, J.; Wouters, B.; Grobet, P.; Jacobs, P. *Stud. Surf. Sci. Catal.* **1998**, *117*, 183.

[113] Dai, S.; Burleigh, M. C.; Shin, Y.; Morrow, C. C.; Barnes, C. E.; Xue, Z. *Angew. Chem. Int. Ed. Engl.* **1999**, *38*, 1235.

[114] Sanchez, C.; Ribot, F. *New J. Chem.* **1994**, *18*, 1007.

[115] Burkett, S. L.; Sims, S. D.; Mann, S. *Chem. Commun.* **1996**, 1367.

[116] Sims, S. D.; Burkett, S. L.; Mann, S. *Mater. Res. Soc. Symp. Proc.* **1996**, *431*, 77.

[117] Macquarrie, D. J. *Chem. Commun.* **1996**, 1961.

[118] Huo, Q.; Margolese, D. I.; Stucky, G. D. *Chem. Mater.* **1996**, *8*, 1147.

[119] Chen, C.-Y.; Burkett, S. L.; Li, H.-X.; Davis, M. E. *Microporous Mater.* **1993**, *2*, 27.

[120] Goletto, V.; Imperor, M.; Babonneau, F. in Proc. Nanoporous Materials II, Banff, Canada, May 25-28, 2000.

[121] Fowler, C. E.; Burkett, S. L.; Mann, S. *Chem. Commun.* **1997**, 1769.

[122] Mann, S.; Burkett, S. L.; Davis, S. A.; Fowler, C. E.; Mendelson, N. H.; Sims, S. D.; Walsh, D.; Whilton, N. T. *Chem. Mater.* **1997**, *9*, 2300.

[123] Lim, M. H.; Stein, A. *Mater. Res. Soc. Symp. Proc.* **1998**, *519*, 89.

[124] Moller, K.; Bein, T.; Fischer, R. X. *Chem. Mater.* **1999**, *11*, 665.

[125] Laha, S. C.; Mukherjee, P.; Kumar, R. *Bull. Mater. Sci.* **1999**, *22*, 623.

[126] Hall, S. R.; Fowler, C. E.; Lebeau, B.; Mann, S. *Chem. Commun.* **1999**, 201.

[127] Jones, C. W.; Tsuji, K.; Davis, M. E. *Nature* **1998**, *393*, 52.

[128] Tsuji, K.; Jones, C. W.; Davis, M. E. *Microporous Mesoporous Mater.* **1999**, *29*, 339.

[129] Babonneau, F.; Leite, L.; Fontlupt, S. *J. Mater. Chem.* **1999**, *9*, 175.

[130] Goletto, V.; Dagry, V.; Babonneau, F. *Mater. Res. Soc. Symp. Proc.* **1999**, *576*, 229.

[131] Lebeau, B.; Fowler, C. E.; Hall, S. R.; Mann, S. *J. Mater. Chem.* **1999**, *9*, 2279.

[132] Lu, Y.; Ganguli, R.; Drewien, C. A.; Anderson, M. T.; Brinker, C. J.; Gong, W.; Guo, Y.; Soyez, H.; Dunn, B.; Huang, M. H.; Zink, J. I. *Nature* **1997**, *389*, 364.

[133] Brinker, C. J.; Lu, Y.; Sellinger, A.; Fan, H. *Adv. Mater.* **1999**, *11*, 579.

[134] Fowler, C. E.; Lebeau, B.; Mann, S. *Chem. Commun.* **1998**, 1825.

[135] Macquarrie, D. J.; Jackson, D. B.; Mdoe, J. E. G.; Clark, J. H. *New J. Chem.* **1999**, *23*, 539.

[136] Bossaert, W. D.; De Vos, D. E.; Van Rhijn, W. M.; Bullen, J.; Grobet, P. J.; Jacobs, P. A. *J. Catal.* **1999**, *182*, 156.

[137] Corriu, R. J. P.; Mehdi, A.; Reyÿ, C.; *C. R. Acad. Sci. Paris* **1999**, *t2*, 35.

[138] Mercier, L.; Pinnavaia, T. J. *Chem. Mater.* **2000**, *12*, 188.

[139] Koya, M.; Nakajima, H. *Stud. Surf. Sci. Catal.* **1998**, *117*, 243.

[140] Richer, R.; Mercier, L. *Chem. Commun.* **1998**, 1775.

[141] Brown, J.; Richer, R.; Mercier, L. *Microporous Mesoporous Mater.* **2000**, *37*, 41.

[142] Macquarrie, D. J. *Green Chem.* **1999**, 195.

[143] Corma, A.; Jorda, J. L.; Navarro, M. T.; Rey, F. *Chem. Commun.* **1998**, 1899.

[144] Bhaumik, A.; Tatsumi, T. *J. Catal*. **2000**, *189*, 31.

[145] Wen, J.; Wilkes, G. L. *Chem. Mater.* **1996**, *8*, 1667.

[146] Schmidt, H. *J. Non-Cryst. Solids* **1985**, *73*, 681.

[147] Loy, D. A.; Shea, K. J. *Chem. Rev.* **1995**, *95*, 1431.

[148] Loy, D. A.; Jamison, G. M.; Baugher, B. M.; Myers, S. A.; Assink, R. A.; Shea, K. J. *Chem. Mater.* **1996**, *8*, 656.

[149] Shea, K. J.; Loy, D. A.; Webster, O. *J. Am. Chem. Soc.* **1992**, *114*, 6700.

[150] Loy, D. A.; Jamison, G. M.; Baugher, B. M.; Russick, E. M.; Assink, R. A.; Prabakar, S.; Shea, K. J. *J. Non-Cryst. Solids* **1995**, *186*, 44.

[151] Inagaki, S.; Guan, S.; Fukushima, Y.; Ohsuma, T.; Terasaki, O. *J. Am. Chem. Soc.* **1999**, *121*, 9611.

[152] Melde, B. J.; Holland, B. T.; Blanford, C. F.; Stein, A. *Chem. Mater.* **1999**, *11*, 3302.

[153] Asefa, T.; MacLachlan, M. J.; Coombs, N.; Ozin, G. A. *Nature* **1999**, *402*, 867.

[154] Yoshina-Ishii, C.; Asefa, T.; Coombs, N.; MacLachlan, M. J.; Ozin, G. A. *Chem. Commun*. **1999**, 2539.

[155] Guan, S.; Inagaki, S.; Ohsuna, T.; Terasaki, O. *J. Am. Chem. Soc.* **2000**, *122*, 5660.

[156] Macquarrie, D. J. *Philos. Trans. R. Soc. London A* **2000**, *358*, 419.

[157] Cauvel, A.; Renard, G.; Brunel, D. *J. Org. Chem.* **1997**, *62*, 749.

[158] Macquarrie, D. J.; Clark, J. H.; Lambert, A.; Mdoe, J. E. G.; Priest, A. *React. Polym.* **1997**, *35*, 153.

[159] Macquarrie, D. J.; Jackson, D. B. *Chem. Commun.* **1997**, 1781.

[160] Sheldon, R. A.; Downing, R. S. *Appl. Catal. A: General* **1999**, *189*, 163.

[161] Mdoe, J. E. G.; Clark, J. H.; Macquarrie, D. J. *Synlett* **1998**, 625.

[162] Kantam, M. K.; Sreekanth, P. *Catal. Lett.* **1999**, *57*, 227.

[163] Liu, C. J.; Li, S. G.; Pang, W. Q.; Che, C. M. *Chem. Commun.* **1997**, 65.

[164] Holland, B. T.; Walkup, C.; Stein, A. *J. Phys. Chem. B* **1998**, *102*, 4301.

[165] Knops-Gerrits, P.-P.; Verberckmoes, A.; Schoonheydt, R.; Ichikawa, M.; Jacobs, P. A. *Microporous Mesoporous Mater.* **1998**, *21*, 475.

[166] Maschmeyer, T.; Oldroyd, R. D.; Sankar, G.; Thomas, J. M.; Shannon, I. J.; Klepetko, J. A.; Masters, A. F.; Beattie, J. K.; Catlow, C. R. A. *Angew. Chem. Int. Ed. Engl.* **1997**, *36*, 1639.

[167] Anwander, R.; Palm, C.; Gerstberger, G.; Groeger, O.; Engelhardt, G. *Chem. Commun.* **1998**, 1811.

[168] Shyu, S.-G.; Cheng, S.-W.; Tzou, D.-L. *Chem. Commun.* **1999**, 2337.

[169] Laspÿras, M.; Bellocq, N.; Brunel, D.; Moreau, P. *Tetrahedron: Asymmetry* **1998**, *9*, 3053.

[170] Bae, S. J.; Kim, S.-W.; Hyeon, T.; Kim, B. M. *Chem. Commun.* **2000**, 31.

[171] Johnson, B. F. G.; Raynor, S. A.; Shephard, D. S.; Mashmeyer, T.; Thomas, J. M.; Sankar, G.; Bromley, S.; Oldroyd, R.; Gladden, L.; Mantle, M. D. *Chem. Commun.* **1999**, 1167.

[172] Tudor, J.; O'Hare, D. *Chem. Commun.* **1997**, 603.

[173] Lin, X.; Chuah, G. K.; Jaenicke, S. *J. Mol. Catal. A: Chem.* **1999**, *150*, 287.

[174] Gerstberger, G.; Palm, C.; Anwander, R. *Chem. Eur. J.* **1999**, *5*, 997.

[175] van Looveren, L. K.; Geysen, D. F.; Vercruysse, K. A.; Wouters, B. H.; Grobet, P. J.; Jacobs, P. A. *Angew. Chem. Int. Ed. Engl.* **1998**, *37*, 517.

[176] (a) Colquhoun, H. M.; Thompson, D. J.; Twigg, M. V. *Carbonylation: Direct Synthesis of Organic Compounds*; Plenum: New York, 1991. (b) Beller, M.; Cornils, B.; Frohning, C. D.; Kohlpaintner, C. W. *J. Mol. Catal. A: Chemical* **1995**, *104*, 17. (c) Rieu, J. P.; Boucherle, A.; Cousse, H.; Mouzin, G. *Tetrahedron* **1986**, *42*, 4095.

[177] (a) Chenal, T.; Cipres, I.; Jenck, J.; Kalck, P.; Peres, Y. *J. Mol. Catal.* **1993**, *78*, 351. (b) Garlaschelli, L.; Marchionna, M.; Iapalucci, M. C.; Longoni, G. *J. Organomet. Chem.* **1989**, *378*, 457. (c) Miekuz, D.; Joo, F.; Alper, H. *Organometallics* **1987**, *6*, 1591. (d) Alper, H.; Woell, J. B.; Despeyroux, B.; Smith, D. J. H. *J. Chem. Soc., Chem. Commun.* **1983**, 1270.

[178] Lee, C. W.; Alper, H. *J. Org. Chem.* **1995**, *60*, 250.

[179] (a) El Ali, B.; Alper, H. *J. Org. Chem.* **1993**, *58*, 3595. (b) El Ali, B.; Alper, H. *J. Mol. Catal. A: Chemical* **1992**, *77*, 7.

[180] El Ali, B.; Alper, H. *J. Mol. Catal. A: Chemical* **1993**, *80*, 377. (b) El Ali, B.; Vasapollo, G.; Alper, H. *J. Org. Chem.* **1993**, *58*, 4739.

[181] (a) Beller, M.; Bolm, C. *Transition Metals for Organic* Synthesis, Wiley-VCH, Weinheim, 1998. (b) Wu, G. G.; Wong, Y; Poirier, M. *Org. Lett.* **1999**, *1*, 745. (c) Beller, M.; Eckert, M.; Geissler, H., Napierski, B.; Rebenstock, H. P; Holla, E. W. *Chem. Eur. J.* **1998**, *4*, 935. (d) Imada, Y.; Alper, H. *J. Org. Chem.* **1996**, *61*, 6766. (e) Pisano, C.; Consiglio, G.; Sironi, A.; Moret, M. *J. Chem. Soc. Chem. Commun.* **1991**, 421.

[182] (a) *Applied Homogeneous Catalysis with Organometallic Compounds*; Cornils, B.; Herrmann, W. A., Eds.; VCH: Weinheim, 1996; Vols. 1 and 2. (b) Sheldon, R. A. *Chem. Ind.* **1992**, 903.

[183] Armor, J. N. *Appl. Catal.* **1991**, *78*, 141.

[184] Elango, V.; Davenport, K. G.; Murphy, M. A.; Mott, G. N.; Zey, E.G.; Smith, B. L.; Moss, G. L. Eur. Pat. 400892, **1990**.

[185] (a) Jayasree, S.; Seayad, A.; Chaudhari, R. V. *Org. Lett.* **2000**, *2*, 203. (b) Chaudhari, R. V.; Jayasree, S.; Seayad, A. M. U. S. Patent 6,093,847, **2000**.

[186] (a) Seayad, A.; Kelkar, A. A.; Chaudhari, R. V. S*tud. Surf. Sci. Catal.* **1998**, *113*, 883. (b) Seayad, A.; Jayasree, S.; Chaudhari, R. V. *Catal. Lett.* **1999**, *61*, 99.

[187] del Rio, I.; Ruiz, N.; Claver, C.; van der Veen, L. A.; van Leeuwen, P. W. N. M. *J. Mol. Catal. A: Chem*. **2000**, *161*, 39.

[188] (a) Sheldon, R. A.; Maat, L.; Papadogianakis, G. (Hoechst Celanese Corp.) US Patent 5,536,874, **1996**. (b) Papadogianakis, G.; Maat, L.; Sheldon, R. A. *J. Chem. Tech. Biotech.* **1997**, *70*, 83.

[189] Jayasree, S.; Seayad, A.; Chaudhari, R. V. *Chem. Commun.* **2000**, 1239.

[190] Davies, I. W.; Matty, L.; Hughes, D. L.; Reider, P. J. *J. Am. Chem. Soc.* **2001**, *123*, 10139.

[191] Jayasree, S.; Seayad, A.; Chaudhari, R. V. *Chem. Commun.* **1999**, 1067.

[192] Jang, E. J.; Lee, K. H.; Lee, J. S.; Kim, Y. G. *J. Mol. Catal. A: Chem.* **1999**, *144*, 431.

[193] El Ali B.; Alper, H. *J. Org. Chem.* **1993**, *60*, 4731.

[194] Lee, C. W.; Alper, H. *J. Org. Chem.* **1995**, *60*, 250.

[195] Linsen, K. J. L.; Libens, J.; Jacobs, P. A. *Chem. Commun.* **2002**, 2728.

[196] Charles, U. P.; Tuscaloosa, A.; Quock, Y.; Lake, E. M. US Patent 4,258,206 **1981**.

[197] Wan, B. S.; Liao, S. J.; Xu, Y.; Yu, D. R. *J. Mol. Catal. A.: Chem.* **1998**, *136*, 263.

[198] (a) Cornils, B.; Hermann, W. A.; Eds. *Applied Homogeneous Catalysis with Organometallic Compounds*; VCH, **1996**, Volumes 1 and 2. (b) Beller, M.; Bolm, C.; Eds. *Transition Metals for Organic Synthesis*; Wiley-VCH: Weinheim, **1998**; Vol. 2, Chapters 1 & 2.

[199] Cornils, B.; Hermann, W. A.; Kohlpainter, C. W. *Nachr. Chem. Tech. Lab.* **1993**, *41*, 544.

[200] Hartley, F. R. *Supported Metal Complexes*; Reidel: Dordrecht, 1985.

[201] (a) Pittmann Jr., C. U.; Smith, L. R. *J. Am. Chem. Soc*. **1975**, *97*, 1742. (b) Mecking, S. Thomann, R. *Adv. Mater.* **2000**, *12*, 953.

[202] (a) Rony, P. R. *J. Catal.* **1969**, *14*, 142. (b) Kuntz, E. *CHEMTECH* **1987**, *17*, 570.

[203] Arhancet, J. P.; Davis, M. E.; Merola, J. S.; Hanson, B. E. *Nature* **1989**, *339*, 554.

[204] Herrmann, W. A.; Cornils, B. *Angew. Chem. Intl. Ed.* **1997,** *36*, 1048.

[205] (a) Hermann, W. A.; Albanese, G. P.; Manetsberger, R. B.; Lappe, P.; Bahrmann, H. *Angew. Chem. Intl. Ed. Engl.* **1995**, *34*, 811. (b) Chaudhari, R. V., Bhanage, B. M., Deshpande, R. M., Delmas, H. *Nature* **1995**, *373*, 501.

[206] Broussard, M. E.; Juma, B.; Train, S. G.; Peng, W-J.; Laneman, S. A.; Stanley, G. G. *Science* **1993**, *260*, 1784.

[207] Bourque, S. C.; Alper, H. *J. Am. Chem. Soc.* **2000**, *122*, 956.

[208] Shimizu, S.; Shirakawa, S.; Sasaki, Y.; Hirai, C. *Angew. Chem. Int. Ed. Engl.* **2000**, *39*, 1256.

[209] Bianchini, C.; Burnaby, D. G.; Evans, J.; Frediani, P.; Meli, A.; Oberhauser, W.; Psaro, R.; Sordelli, L.; Vizza, F. *J. Am. Chem. Soc.* **1999**, *121*, 5961.

[210] Dickson, R. S., *Homogeneous Catalysis with Compounds of Rhodium and Iridium*, *Series*: *Catalysis by Metal Complexes*, D. Reidel Publishing Company: Dordrecht, 1985.

[211] (a) Bath, K. N.; Halligudi, S. B. *J. Mol. Catal*. **1994**, *91*, 187. (b) Lee, B.; Alper, H. *J. Mol. Catal. A* **1996**, *111*, 17. (c) Lenarda, M.; Ganzerla, R.; Storaro, L.; Trovarelli, A.; Zanoni, R.; Kaspar, J. *J. Mol. Catal.* **1992**, *72*, 75.

[212] (a) Schlegel, L.; Miessner, H.; Gutschick, D. *Catal. Lett.* **1994**, *23*, 215. (b) Weitkamp, J.; Ernst, S.; Bock, T.; Kiss, A.; Kleinschmit, P. *Stud. Surf. Sci Catal.* **1995**, *94*, 278. (c) Davis, M. E.; Saldarriaga, C.; Rossin, J. A. *J. Catal.* **1987**, *103*, 520. (d) Rossin, J. A.; Davis, M. E. *JCS Chem. Commun*. **1986**, 234. (e) Shannon; Vedrine, J. C.; Naccache, C.; Lefebvre, F. *J. Catal.* **1984**, *88*, 431. (f) Tomczak, D. C.; Lei, G. D.; Schunemann, V.; Trevino, H.; Sachtler, W. M. H. *Microporous Mater.* **1996**, *5*, 263. (g) Homeyer, S. T.; Sachtler, W. M. H. *J. Catal.* **1989**, *117*, 91. (h) Rode, E. J.; Davis, M. E.; Hanson, B. E. *J. Catal.* **1985**, *96*, 563. (i) Rode, E. J.; Davis, M. E.; Hanson, B. E. *J. Catal.* **1985**, *96*, 574. (j) Goellner, J. F.; Gates, B. C.; Vayssilov, G. N.; Rösch, N. *J. Am. Chem. Soc.* **2000**, *122*, 8056. (k) Rao, L. F.; Fukuoka, A.; Kosugi, N.; Kuroda, H.; Ichikawa, M. *J. Phys. Chem.* **1990**, *94*, 5317.

[213] (a) Weber, W. A.; Gates, B. C. *J. Phys. Chem. B* **1997**, *101*, 10423. (b) Rao, L. F.; Fukuoka, A.; Kosugi, N.; Kuroda, H.; Ichikawa, M. *J. Phys. Chem.* **1990**, *94*, 5317. (c) Rao, L. F.; Pruski, M.; King, T. S. *J. Phys. Chem. B* **1997**, *101*, 5717. (d) Rode, E. J.; Davis, M. E.; Hanson, B. E. *J. Catal.* **1985**, *96*, 563. (e) Rode, E. J.; Davis, M. E.; Hanson, B. E. *J. Catal.* **1985**, *96*, 574. (f) Takahashi, N.; Mijin, A.; Suematsu, H.; Shinohara, S.; Matsuoka, H. *J. Catal.* **1989**, *117*, 348. (g) Davis, M. E.; Rode, E. J.; Taylor, D.; Hanson, B. E. *J. Catal.* **1984**, *86*, 67. (h) Davis, R. J.; Rossin, J. A.; Davis, M. E. *J. Catal.* **1986**, *98*, 477.

[214] (a) Mantovani, E.; Palladino, N.; Zanobi, A. *J. Mol. Catal*. **1978**, *3*, 285. (b) Davis, M. E.; Butler, P. M.; Rossin, J. A.; Hanson, B. E. *J. Mol. Catal.* **1985**, *31*, 385.

[215] (a) Janssen, A.; Niederer, J. P. M.; Hölderich, W. F. *Catal. Lett.* **1997**, *48*, 165. (b) Hanson, B. E.; Davis, M. E.; Taylor, D.; Rode, E. *Inorg. Chem*. **1984**, *23*, 52. (c) Andersen, J. A. M.; Currie, A. W. S. *Chem. Commun.* **1996**, 1543.

[216] (a) Andersen, J. M. *Platinum Met. Rev.* **1997**, *41*, 132. (b) Andersen, J. M.; Karodia, N. *Catal. Lett*. **2000**, *66*, 49. (c) Taylor, D. F.; Hanson, B. E.; Davis, M. E. *Inorg. Chim. Acta* **1987**, *128*, 55. (d) Smith, R. T.; Ungar, R. K.; Baird, M. C. *Trans. Met. Chem.* **1982**, *7*, 288. (e) Blümel, J. *Inorg. Chem.* **1994**, *33*, 5050. (f) Allum, K. G.; Hancock, R. D.; Howell, I. V.; Pitkethly, R. C.; Robinson, P. J. *J. Catal.* **1976**, *43*, 322. (g) Sandee, A. J.; van der Veen, L. A.; Reek, J. N. H.; Kamer, P. C. J.; Lutz, M.;

Spek, A. L.; van Leeuwen, P. W. N. M. *Angew. Chem.*, *Int. Ed. Engl.* **1999**, *38*, 3231.
(h) Hardee, J. R.; Tunney, S. E.; Frye, J.; Stille, J. K. *J. Polym. Sci. A* **1990**, *28*, 3669.

CHAPTER 2

PROMOTER MEDIATED SYNTHESES OF MICROPOROUS AND MESOPOROUS MATERIALS

2.1. INTRODUCTION

The discovery of ordered porous materials and an explosive research in this area have opened new vistas in materials science. These materials have been used for applications in chemistry, catalysis, electronics, separation science, biochemistry and nanotechnology [1,2]. The fact that these materials can be made use of incorporating polymeric, organic, inorganic and organometallic 'guests' in the porous 'hosts' has served numerous important chemical applications [3]. Microporous (e.g. zeolites) and mesoporous materials serve as the two major categories of the porous inorganic matrices. Zeolites are crystalline microporous materials and are being used widely as industrial catalysts [4]. Of the microporous materials used for industrial purposes, zeolites ZSM-5 (MFI) and Na-Y (Faujasite, FAU) are the two most important members of the zeolite family, possessing medium and large pores in their respective frameworks.

Surfactant-templated mesostructures have played a prominent role in materials chemistry during the last decade [5]. The excitement began with the discovery of hexagonally ordered mesoporous silicate structures by Mobil Corporation (M41S materials) [6] and by Kuroda, Inagaki and coworkers (FSM-16 materials) [7]. These materials initially appeared to be the Holy Grail sought after by zeolite chemists of the time. They possessed extremely high surface areas and easily accessible, uniform pore sizes. Most importantly the pore sizes exceeded those attainable in zeolites and they could be tuned in the nanometer range by choosing an appropriate surfactant templating system, sometimes with co-solvent or swelling agent. However, the original mesoporous silicates and aluminosilicates exhibited a number of limitations, including lower hydrothermal stability and lower reactivity than zeolites with comparable compositions. These mesoporous materials possessed thin walls, which prevented incorporation of secondary pores within the walls, and they only formed fine particles. Yet, the ability to manipulate structures of the porous solids on a nanometer scale in a controlled way proved to be so important to the research community, that many of these limitations have been addressed and overcome in the last few years. For example, the hydrothermal stability of the mesoporous silicates has been improved by adding inorganic salts to the synthesis mixtures [8], or by producing materials with thicker pore walls [9,10]. Structures with uniform pore sizes can now be formed throughout most of the mesopore size

range, which encompasses 2–50 nm by International Union of Pure and Applied Chemistry (IUPAC) nomenclature [11].

The two most important members of the mesoporous family are MCM-41 and MCM-48 comprising an array of hexagonal '*honeycomb*' and cubic '*gyroid*' structures respectively [5,6]. Though synthesis of MCM-41 is facile, that of MCM-48 is intricate because of the '*swinging*' presence of its cubic phase lying amidst hexagonal and lamellar ones; hence, not many reports on reliable, low template content, cost effective synthesis of MCM-48 have been accounted for [12-15].

Synthesis of molecular sieve zeolites and mesoporous materials is carried out in concentrated aluminosilicate (or silicate) solutions that contain amorphous gel phases. During the growth process, an amorphous gel can serve as a reservoir for the components that are eventually deposited at the surface of the growing crystals. A great deal of work has sought a better understanding of the mechanisms for nucleation and crystal growth of zeolites and mesoporous materials from the gels. Although, the nature of surface and acid catalytic properties of zeolites and mesoporous molecular sieves is relatively better understood, there are not much reports available on nucleation and growth processes for mesoporous materials [16]. The chemistry governing their hydrothermal syntheses at autogenous pressure (crystallization temperature = 353 – 473 K, time = few hours to few days) continues to be intriguing and challenging. Inui, has suggested various drawbacks to long crystallization process [17], which causes (i) extensive labor coupled with delays and expenses, (ii) poor reproducibility and (iii) formation of larger crystals with inhomogeneous particle size distribution (mainly owing to secondary crystallization), hence, lower surface area. An approach to reduce synthesis time of zeolites [12] and M41S type molecular sieves [13] using simple inorganic anions as promoter has been reported earlier. Recently, it has been found that Keggin anions or heteropolyacids (HPA) can efficiently be used as a new class of promoters in the synthesis of such mesoporous solids [18]. This prompted to endeavor using these heteropolyacid promoters for the synthesis of microporous materials, e.g. Na-Y (Faujasite, FAU), Silicalite-1 (MFI) and Ferrierite (FER), and mesoporous MCM-41 and MCM-48 materials.

In the following section, a general and brief overview of the syntheses and nucleation/ formation of microporous and mesoporous materials as postulated till date has been

presented before the syntheses strategy and results for promoter mediated syntheses of microporous and mesoporous materials presented in this chapter is being discussed.

2.2. SYNTHESES AND MECHANISM OF FORMATION OF MICROPOROUS MATERIALS

The perspective taken in this work, based on research results from the literature, has been that molecular sieve zeolite crystals are formed from the species dissolved in the caustic solution medium, and that formation of zeolites by solid-solid transformations does not occur. As such, classical treatments of crystallization systems should adequately describe molecular sieve zeolite crystallization processes. Growth of molecular sieve zeolites in hydrothermal systems has been shown to occur from sub-micron sizes to macroscopic sizes in a continuous fashion. Assimilation of material from the solution phase has been speculated to involve "secondary building units", that is myriad aluminosilicate oligomers known to exist in solution. It is more likely that the growth units are monomers, dimers, or other small aluminosilicate units, which are known to persist in the basic environments. It is quite common for the original mixture comprising of caustic aluminate and caustic silicate solutions, to become viscous shortly after mixing, due to the formation of an amorphous phase, i.e., amorphous aluminosilicate gel suspended in the basic medium. As the synthesis proceeds at elevated temperatures, zeolite crystals are formed by a nucleation step, and these zeolite nuclei then grow larger by assimilation of aluminosilicate materials from the solution phase. During the synthesis, the amorphous gel has a thermodynamic tendency to dissolve, while the thermodynamic driving force is toward formation of the crystalline zeolite phase. The first phase in this transformation usually involves the formation of the smallest entity having the identity of the new crystalline phase, the crystal nucleus. The event is normally followed by the subsequent assimilation of mass from the solution and its reorientation into ordered crystalline material via crystal growth.

2.2.1. SYNTHESIS

Zeolites are crystalline, porous aluminosilicate molecular sieves composed of three dimensional networks formed by sharing of oxygen atoms of $[SiO_4]^{4-}$ and $[AlO_4]^{5-}$ tetrahedra

in such a way that two Al tetrahedra are never adjacent to each other. The crystallographic unit cell of zeolites may be represented as:

$$M_{x/n}[(SiO_2)_x . (AlO_2)_y]. zH_2O$$

where, M is a charge compensating cation with valency '***n***', generally selected from metal ions of group I or II or may be an organic cation and the ratio x/y can be varied from one to infinity. Since, Al^{3+} does not occupy adjacent tetrahedral sites, the Si/Al molar ratio corresponds the density of the acid sites in the zeolites. The number of water molecules, which can be reversibly adsorbed and desorbed in the zeolite pores, is represented by '***z***'. Usually, the pore size diameter of zeolites is of molecular dimensions ranging from 0.5 nm to 1.0 nm. Zeolites are synthesized essentially from a silica source and an aluminium source in aqueous medium, often followed with template source (organic) or seed solutions, in either acidic or basic medium.

2.2.2. NUCLEATION

Crystallization is usually believed to proceed through two primary steps: (a) nucleation of discrete particles of the new phase, and (b) subsequent growth of those entities. The first, and most intriguing, process can be broken down further in the following way.

Primary Nucleation:

Primary nucleation mechanisms occur in the absence of the desired crystalline phase, i.e., they are solution-driven mechanisms. This can be further classified into two categories.

Homogeneous Nucleation: In the case of homogeneous nucleation, the mechanism is purely solution driven.

Heterogeneous Nucleation: In case of heterogeneous nucleation, the presence of extraneous surface to facilitate a solution-driven is a probable cause for the nucleation.

Secondary Nucleation:

Secondary nucleation mechanisms require the desired crystalline phase to be present to catalyze a nucleation step. This can be further subdivided into three categories.

Initial Breeding: This phenomenon stems from microcrystalline "dust" being washed off the surface of seed crystals into growth medium, thereby providing nuclei directly to the solution.

Micro-attrition: Nuclei formation sometimes can be promoted by micro-attrition by agitation in the absence of seed crystals added to the solution. This causes microcrystalline fragments to be broken off of existing growing crystals in the medium. These fragments arise from crystal contacts with the stirrer, other crystals, or the walls of the container, and may become growing entities in a supersaturated solution.

Fluid Shear-Induced Nucleation: It has been speculated that nuclei can be created by fluid passing by the surface of a growing crystal with sufficient velocity to seep away quasi-crystalline entities (clusters or embryos) adjacent to the surface, which were about to become incorporated in the crystalline surface. If these clusters are swept away into a sufficiently supersaturated environment, they will have the thermodynamic tendency to become grow and become viable crystals. Thus, in the event that high shear fields in the neighborhood of growing crystal surfaces exist, nucleation can sometimes be promoted.

A more detailed review of these mechanisms, and their relevance to zeolite crystallizations may be found elsewhere. However, it is not expected that fluid shear-induced nucleation will be relevant to zeolite synthesis, due to the viscosity of the solutions, and because it is not believed to be important except at quite high agitation rates, or quite high fluid velocities relative to crystals in the medium [22]. Whereas many zeolite syntheses are carried out with no agitation, or very mild agitation, micro-attrition breeding also may be viewed as not universally important in zeolite crystallizations (systems using intense agitation being the exception).

One should understand the differences between secondary nucleation and seeding, i.e., the common strategy of promoting the "rate of crystallization" by adding crystals of the desired phase to a precipitating system. Secondary nucleation is, strictly speaking, the promotion of crystal nucleation due to the physical presence of the crystals of the desired phase, while seed crystals may promote crystallization by providing additional surface area for dissolved material to grow onto. However, a seed crystal sample may contain sub-micron-sized fragments, which eventually grow to macroscopic sizes, in some cases it may

appear that a newly formed population was created, when, in fact, it was the result of growth on very small seed crystal pieces.

Subotic and his coworkers have proposed and studied a so-called autocatalytic nucleation mechanism [25]. According to their concept, suggested by the proposal of Zhdanov somewhat earlier [26], there are three possible sources of nuclei: *homogeneous* nuclei formed by a classical mechanism, *heterogeneous* nuclei formed in conjunction with foreign particulate matter and *autocatalytic* nuclei formed within the amorphous gel phase. According to the conceptual model, the autocatalytic nuclei lie dormant in the amorphous gel phase until they are released into the solution by dissolution of the gel phase and become active growing crystals. As the cumulative zeolite crystal surface area increases due to crystal growth, the rate of solute consumption increases, which, in turn, increases the rate of gel dissolution, finally resulting in increased rate of dormant nuclei activation. Hence, it is clear why the mechanism was labeled autocatalytic.

There have been few recent reports, which shed new light on the possible structure precursors to zeolite nucleation and crystal growth:

Davis et al. reported ^{1}H-^{29}Si and ^{1}H-^{13}C cross-polarization MAS-NMR observations of a pure silica ZSM-5 synthesis mixture containing 0.5 TPA_2O: 3 Na_2O: 10 SiO_2: 2.5 D_2SO_4: 380 D_2O at 383 K [27]. The results of their study revealed that TPA-silicalite structures form prior to the formation of observable long-range crystalline structure, and have short-range interactions on the order of 3.3 Å, indicative of van der Waals interactions. The authors argued that the observed layered intergrowth behaviour noted in several high silica zeolite systems (e.g., ZSM-5, ZSM-11, beta etc.) supported the hypothesized model of nucleation and growth by the TPA-silicalite species suggested by their results. Their findings strongly support the clathration hypothesis of zeolite formation, where the silicate polyanions (mainly the Q^4 species) clathrate the organic structure directing agent (TPA in Si-ZSM-5 system). They have proposed that these clathrated TPA-silicalite hydrophobic hydration spheres come nearer and overlap one another, thus forming the composite species leading to crystal growth.

Another recent work by van Santen et al. used the in situ combined small-angle X-ray scattering/ wide-angle X-ray scattering (SAXS/ WAXS) monitoring of an all-silica ZSM-5 crystallization. The combined technique allowed to simultaneously observing particles in the

system, to determine their fractal dimension, and to determine the level of crystallinity within the particles, and the crystalline phase(s) present. In essence, the authors suggested that primary silica particles formed quite early in the process, perhaps of the nature described by Davis et al.

With the advent of scanning electron microscopy (SEM) and atomic force microscopy (AFM), a very powerful technique for imaging non-conducting solid surfaces, various zeolites like zeolite A, mordenite , Y (faujasite) and EMT polymorphs have revealed crystal growth terraces with a constant step height of the known structures, orientations, positions, and geometries concurrent with a layer growth mechanism [29]. For example, crystal growth for zeolite A has been shown to occur via a process akin to a terrace – ledge – kink (TLK) layer mechanism.

Very recently, Lee et al. [29g] reported synthesis of uniformly aligned 2D and 3D arrays of Silicalite-1 crystals using polyurethane films as templates. The authors have proposed that supramolecularly organized organic-inorganic composites, which consists of the hydrolyzed organic products and the seed crystals to be responsible for the orientations of the Silicalite-1 crystals those are controlled by the nature of polymers.

2.3. Syntheses and Mechanism of Formation of Mesoporous Materials

The M41S family of mesoporous materials contains several unique structures [5,6,8,10,14–18]: those that can be indexed to an hexagonal unit cell, MCM-41 (2D, *p6m*), SBA-2 (3D, $p6_3/mmc$), and SBA-3 (2D, *p6m* similar to MCM-41 but synthesized in acidic media); cubic structures including MCM-48 (*Ia3d*) and SBA-1 (*Pm3n*); and lamellar structures including MCM-50 that is post-stabilized lamellar material. Using a silica source and varied organic structure directing agents e.g. cationic surfactants containing long alkyl chain quaternary ammonium compound containing 10 – 20 carbons, often followed with addition of co-surfactants, M41S family of mesoporous materials are synthesized. Vartuli et al. studied the effect of the surfactant/silica molar ratio in a ternary synthesis system containing tetraethylorthosilicate (TEOS, silica source), water and C_{16}TMA cations (surfactant) at 100 °C [30]. As the surfactant/silica molar ratio was increased, the products obtained could be grouped into four categories:

Surfactant/silica	< 1.0	Hexagonal phase (MCM-41)
	= 1.0 – 1.5	Cubic phase (MCM-48)
	= 1.2 – 2.0	Thermally unstable materials
	= 2.0	Cubic octamer $[(CTMA)SiO_{2.5}]_8$

Different synthesis mechanisms have been proposed in the literature to rationalize the formation of mesoporous nanostructures and to allow for the rational design of new surfactant-templated materials. A brief account of the postulates for the mechanism of formation of mesoporous materials will be discussed below.

2.3.1. Molecular – Packing Model (Conventional Surfactant-Water Systems)

Surfactants are large, organic molecules with a hydrophilic head and a long hydrophobic alkyl tail of variable length. The synthesis of mesoporous materials is based on the ability of surfactant molecules to form spherical or cylindrical micelles or even higher-order phases in aqueous solution [31]. In aqueous solution, these species aggregate their hydrophobic tails together and expose their polar head to the solution in order to reach the minimum energy configuration. The micelles, thus formed, are in dynamic equilibrium with soluble surfactant molecules. The first critical micelle concentration (cmc1) is defined as the lowest concentration at which spherical micelle formation may be observed and the second critical micelle concentration (cmc2) is the concentration at which the transformation from spherical to rod-like micelles takes place. This transformation is strongly dependant on temperature, anion degree of dissociation and on the length of the surfactant alkyl chain. The packing of surfactant molecules is determined by the equilibrium among three forces: (1) the tendency of alkyl chains to minimize their contact with water and maximize their organic interactions, (2) the Coulombic interactions between charged head groups, and (3) the solvation energies. A local effective surfactant packing parameter, $\boldsymbol{g}$, which accounts for the first two kinds of interaction, is used to describe amphiphilic liquid-crystal phases. It is defined as $\boldsymbol{g} = \mathbf{V}/\boldsymbol{a}_0\boldsymbol{l}$, where $\mathbf{V}$ is the total volume of the surfactant chains plus any cosolvent organic molecules between the chains, $\boldsymbol{a}_0$ is the effective head group area at the surface of the micelle, and $\boldsymbol{l}$ is the kinetic surfactant tail length or the curvature elastic energy. If the value of $\boldsymbol{g}$ increases, phase transitions are expected to occur in the order indicated in Table 2.1. These transitions reflect a decrease in surface curvature with increasing $\boldsymbol{g}$.

Table 2.1. Phase Transition versus Local Effectiveness Surfactant Packing Parameter, '***g***'

g	Mesophase
1/3	Cubic (*Pm3n*)
1/2	Hexagonal (*p6m*)
1/2 – 1/3	Cubic (*Ia3d*)
1	Lamellar

(Source: Huo, Q.; Margolese, D. I.; Stucky, G. D. *Chem. Mater.* **1996**, *8*, 1147.)

2.3.2. MECHANISMS POSTULATED FOR THE SYNTHESIS OF M41S MESOSTRUCTURES

2.3.2.1. The Mobil Hypotheses:

Researchers at Mobil proposed two synthesis mechanisms to explain the formation of MCM-41 materials [6a,b].

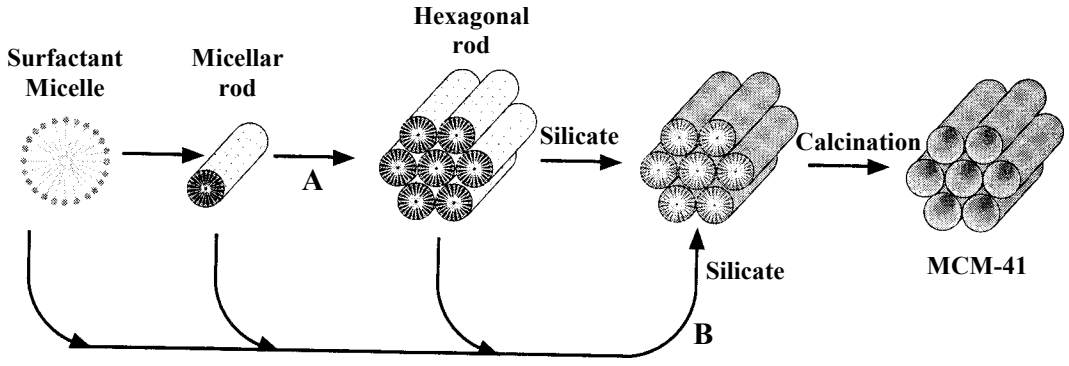

Scheme 2.1. Liquid crystal templating mechanism proposed for the formation of MCM-41: (A) liquid crystal phase initiated and (B) silicate anion initiated [Ref. 6, 33].

In the first route, the surfactant hexagonal liquid-crystal phase forms first and directs the growth of the inorganic materials. The $C_nH_{2n+1}(CH_3)_3N^+$ surfactant micelles aggregate into hexagonal array of rods and the silicate or aluminate anions present in the reaction mixture interact with the surfactant cationic head groups. Condensation of the silicate species leads to the formation of an inorganic polymer. Upon calcinations, the organic template is

burnt off, leaving the inorganic hollow cylinders in a hexagonal arrangement. However, this synthesis pathway did not meet much support in the literature, as was pointed out by Cheng et al. [32]. Since MCM-41 may be formed at low surfactant concentrations (1 wt.%) with respect to water content, in situ ^{15}N-NMR spectra revealed that the hexagonal liquid-crystalline phase CTMA (H_1) was not present at anytime during MCM-41 formation [33], thus, the synthesis scheme proposed by Beck et al. was abandoned.

In the second approach proposed by the same group, the presence of silicate species in the reaction mixture initiates the hexagonal ordering [6]. This second route is widely accepted in the literature. Chen et al. [33], explained that randomly distributed rod-like surfactant micelles form initially and interact with silicate oligomers to generate randomly oriented surfactant micelles surrounded by two or three monolayers of silica. The isotropic ^{14}N-NMR resonance was found to be consistent with the presence of rod-like micelles in solution [33]. A base catalyzed condensation between silicate species on adjacent rods occurs with further heating, which initiates the long-range hexagonal ordering that corresponds to the minimum energy configuration for the packing of the rods, illustrated in Scheme 2.2.

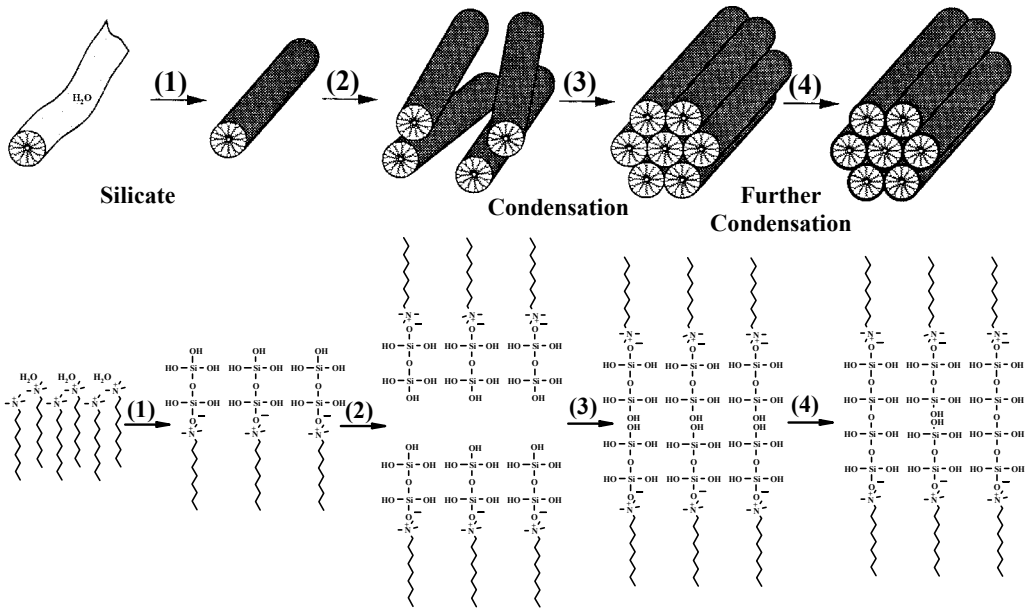

Scheme 2.2. Silicate rod assembly proposed for the formation of MCM-41: (1) and (2) involve the random ordering of rod-like micelles and interaction with silicate species; (3) represents the spontaneous packing of the rods and (4) is the remaining condensation of silicate species upon final heating of the organic/inorganic composites [Ref. 33].

2.3.2.2. Layered Intermediates:

Monnier et al. [14a] observed, in addition to amorphous silica, the presence of a layered material with a primary *d*-spacing of 3.1 nm in the synthesis mixture after reaction times in the order of 1 min. At longer crystallization times, the lamellar intermediate disappeared and the diffraction pattern of the hexagonal structure was detected in the solid product. The transition from the lamellar to the hexagonal phase was confirmed by ^{2}H-NMR spectra of the surfactant molecules deuterated at the α-carbon. In order to account for the presence of a layered intermediate, Stucky's group proposed a synthesis mechanism supported by thermodynamic analysis [34], which basically stated that the synthesis of silica-based mesophases may be regarded as the formation of lyotropic liquid crystals from a system in which inorganic species are attached to surfactants. Schematically, the formation of nanostructures proceeds through three steps that are not necessarily sequential; see Scheme 2.3 (A). The three steps are as follows:

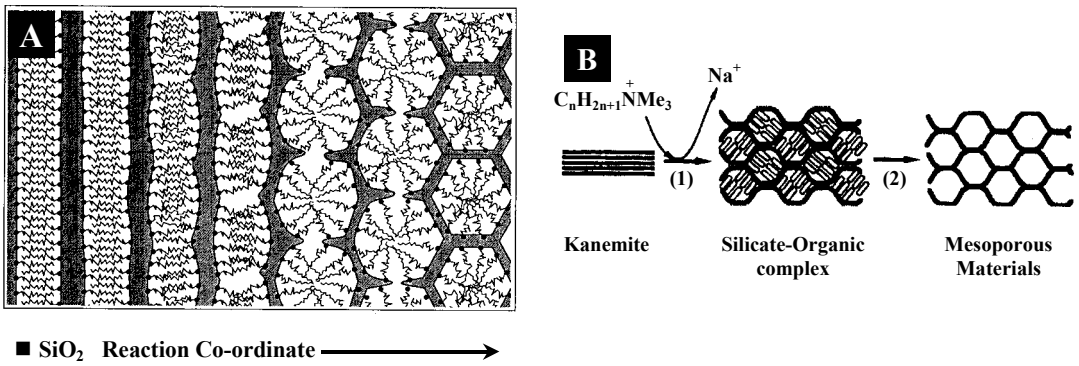

Scheme 2.3. Mechanisms proposed for the transformation of surfactant-silicate systems from lamellar to hexagonal mesophases [Ref. 34]. (A) Hexagonal mesophase obtained by charge density matching and (B) folding of kanemite silicate sheets around intercalated surfactant molecules formed the hexagonal mesostructure [Ref. 7].

Small silica oligomers compete for the access to the cationic heads of the surfactant. The type of silica species present in the reaction mixture depend on the pH; at high pH (pH > 9.5), large silicate oligomers are completely ionized and bind preferentially to charged surfactant molecules as envisaged by ^{29}Si-NMR by Firouzi et al. [35]. Charged silica species then coordinate electrostatically with the surfactant molecules, which may originate from loosely structured micelles. Unlike the synthesis scheme proposed by Chen et al. [33], this

synthesis mechanism does not require the existence of rod-like micelles; instead the interface consists of tightly held silicate oligomers that act as multidentate ligands for surfactant head groups. This step is highly favoured thermodynamically, leading to precipitation of mesophase from solution; this is probably the main reason for forming silicate mesostructures at room temperature.

The above-mentioned process is then followed by silicate polymerization within the surfactant-silicate interface. It is favoured for two reasons: (i) the concentration of silica near the interface is high and (ii) the negative charge is partially screened by the surfactant. The second step is slow and the rate limiting step. Silica polymerization leads to a strong and extended framework with thermal, mechanical and hydrolytic strengths and condensation between inorganic species proceeds according to the following schemes:

$$\equiv Si{-}O^{-} + HO{-}Si\equiv \rightarrow \equiv Si{-}O{-}Si\equiv + OH^{-}$$

$$\equiv Si{-}OR + HO{-}Si\equiv \rightarrow \equiv Si{-}O{-}Si\equiv + ROH$$

As polymerization proceeds, the charge density within the inorganic wall decreases resulting in a decrease in the number of surfactant cations required for charge compensation. Charge density matching at the organic-inorganic interface may then drive the rearrangement of the organic molecules, leading to a phase transformation.

In the early stages of the reaction, the presence of highly charged silica oligomers favours small surfactant head groups and a surfactant surface with a minimal curvature. This is readily accomplished by a lamellar structure. As polymerization proceeds, the density of anionic silanol groups and the number of necessary charge compensating cations decrease. The optimal value of the surfactant head group (A_0) therefore, increases and the system finds it minimal energy by adopting hexagonal structure in case of MCM-41. If the silicate wall is poorly condensed, it is flexible enough to allow the transition from a lamellar to a hexagonal phase. Although the silica-initiated synthesis mechanism has been widely accepted, the presence of an intermediate lamellar species has been disputed.

2.3.2.3. Crystal – growth mechanism:

Cheng et al. [32] advanced a crystal-growth mechanism supporting the viability of the silica-initiated crystallization reaction, but they discounted the existence of the lamellar intermediate. They proposed that when all the faces of a nucleus grow at the same rate, the

resulting crystal has a perfect hexagonal morphology. However, the composite micellar rod is a large molecular group surrounded by a highly concentrated and inhomogeneous gel and faces at nucleus may grow at different rates if they are confined to different environments. Thus, both hexagonal crystals and crystals irregular in shape and size may be observed and formation of an intermediate layered material is unlikely to occur.

2.3.2.4. Heterogeneous Nucleation mechanism:

Liu et al. [36] studied the effect of colloidal particles on MCM-41 crystallization, where they used TEM micrographs to show that colloidal silica and titania promoted the formation of a MCM-41 phase. In contrast, no ordered structure formed when TEOS was used instead of Ludox as the silica source in the same hydrogel. Based on these results, the authors proposed the existence of a heterogeneous nucleation mechanism at their particular reaction conditions.

2.3.2.5. Surfactant Control of Silica-based Mesophases:

The nanostructured assembly can be regarded as a special case of a water surfactant system, in which surfactants are bound to inorganic species through either Coulombic, covalent, or hydrogen bonds. Stucky's group has conducted systematic investigation of the effect (surfactant organization in liquid – crystal arrays) of the surfactant packing parameter '***g***' on the structure of siliceous mesophases [37].

Gemini surfactants, of general formula $C_nH_{2n+1}N^+(CH_3)_2(CH_2)_s(CH_3)_2N^+C_mH_{2m+1}$ (designated as $C_{n–s–m}$) having two quaternary ammonium head groups separated by methylene chain of variable length proved especially useful in generating amphiphiles with tunable head groups. By tuning the head-group area of gemini surfactants through presence of spacer '***s***' one can attain either MCM-50 (s = 2 or 3) or MCM-41 (s = 5 or 6). It has been observed that $C_{12\ -12\ -\ 12}$ gives MCM-41 whereas, $C_{16\ -12\ -\ 16}$ yields MCM-48 at room temperature. The presence of the hydroxyls decreases the hydrophobicity of the head group and, thereby, the effective head-group area. This, in turn, favours the formation of structures with low surface curvature.

There is a two-fold role of pH, which is very influential in the synthesis of mesophases; it controls the type of oligomeric silicate species present in solution and it

controls the electrolyte concentration and, therefore, the ionic environment surrounding the surfactant head groups (see Table 2.1). As '***g***' is increased, phase changes occur in a sequence controlled by the solution pH. In acidic hydrogels, the sequence is cubic (*Pm3n*, SBA-1) → 3*d* hexagonal (*$P6_3/mmc$*, SBA-2) → 2*d* hexagonal (*P6m*, SBA-3) → lamellar (MCM-50). In contrast, for basic hydrogels, the sequence was 3*d* hexagonal (*$P6_3/mmc$*, SBA-2) → 2*d* hexagonal (*P6m*, MCM-41) → cubic (*Ia3d*, MCM-48) → lamellar (MCM-50) [37]. Stucky and coworkers concluded that the molecular-packing model could be extended to mesoporous silicate structures.

2.3.3. SYNTHESIS OF KANEMITE-DERIVED MESOSTRUCTURES

2.3.3.1. Folded - Sheet Mechanism:

Inagaki et al. [7] proposed a folded-sheet mechanism to explain the formation of kanemite-derived nanostructures; see Scheme 2.3 (B). Time-resolved X-ray diffraction results show the presence of intercalated silicate phases in the synthesis medium of the reaction products. The flexible silicate layers of kanemite then fold around the ion-exchanged surfactant cations, cross-linking of the interlayer occur by condensation of silanol groups on adjacent silicate sheets. This folding and cross-linking process is facilitated by the flexibility of the single-layered kanemite sheets. When pH is increased, the amount of occluded alkyltrimethylammonium cations in kanemite increases as well and as a result the interlayers of kanemite expand and form a regular hexagonal structure with high adsorption capacity called FSM-16. The undissolved portion of kanemite converts to more FSM-16, whereas the dissolve species yields amorphous silica.

2.3.3.2. Dissolution mechanism:

Chen et al. [38] refined the folded-sheet mechanism of Inagaki et al. [7] and proposed dissolution mechanism. According to Chen et al., the kanemite layers are first intercalated with surfactant cations, and then at high pH, silica dissolves into synthesis medium, decomposing the kanemite layers. The loss the kanemite structural integrity, with the ability of the surfactant molecules to form micellar aggregates, drives organization of the composite

material to completion. Condensation of adjacent silanol groups around the organic micelles results in the formation of a periodic mesoporous silicate isomorphous to MCM-41.

2.3.4. GENERALIZED LIQUID CRYSTAL TEMPLATING MECHANISM

2.3.4.1. Ionic Route (Electrostatic Interaction):

Huo and coworkers [39] postulated a generalized mechanism for the formation of mesostructured materials based on the specific type of electrostatic interaction between a given inorganic precursor (**I**) and surfactant head group (**S**) with a view that the new inorganic species should be capable of forming flexible polyionic species that can undergo extensive polymerisation and charge density matching between the surfactant and the inorganic species should be possible. Based on this concept, four different strategies were proposed to synthesize transition metal oxide mesostructures [39]. The first two routes involve the charge density matching between cationic surfactants and anionic inorganic species ($\mathbf{S^+I^-}$) and the charge-reversed situation ($\mathbf{S^-I^+}$). The third and fourth routes are counteranion-mediated pathways that allow the assembly of cationic and anionic species via halide ($\mathbf{S^-X^+I^-}$) or alkali metal ($\mathbf{S^+X^-I^+}$) ions respectively. These synthesis approaches allowed for the formation of a wide variety of lamellar, hexagonal or cubic surfactants/inorganics mesophases, but a common problem faced was the instability of the inorganic framework, which very often, collapsed upon removal of the organic template.

2.3.4.2. Neutral Templating Route (Hydrogen Bonding Interaction):

Tanev and Pinnavaia [9a,b] proposed a fifth route to synthesize hexagonal mesoporous silicas (HMS) that have thicker pore walls, high thermal stability and smaller crystallite size but, have higher amounts of interparticle mesoporosity and lower degree of long-range ordering of pores than MCM-41 materials. This route is essentially based on hydrogen bonding between neutral primary amines (S°) and neutral inorganic precursors (I°), wherein hydrolysis of TEOS in an aqueous solution of dodecylamine yields neutral inorganic precursor. Using the same approach, lamellar silicas with vesicular particle morphology (MSU-V) have been synthesized [9c] with the help of bola – amphiphile surfactants having two polar head groups linked by a hydrophobic alkyl chain.

Bagshaw et al. [9d] used nonionic polyethylene oxide surfactants (PEO) to prepare nanostructures (MSU) with pore sizes in the range of 2 – 6 nm range, with an added advantage of facile recovery of the template besides using low-cost, nontoxic and biodegradable surfactants.

Recently, Prouzet and Pinnavaia [9e] reported a new synthesis procedure that allows tuning the mesopore size by controlling the synthesis temperature (e.g. an increase in temperature from 25 °C to 65 °C shows and increase in d_{100}-spacing from 4.5 to 5.8 nm), wherein, the mesostructure assembly was initiated by adding NaF salt to an aqueous suspension of TEOS in the surfactant.

2.3.4.3. Ligand-Assisted Templating Route (Covalent Interactions):

Antonelli and Ying [40] have proposed a novel ligand-assisted templating mechanism for the synthesis of hexagonally packed mesoporous metal oxide materials (e.g. niobium oxide) that are completely stable to surfactant removal. This route is novel in that ^{15}N MAS-NMR results suggest that the surfactant is covalently bonded to the metal atom in the Nb precursor. In a typical synthesis, the surfactant (tetradecylamine) was dissolved in the metal alkoxides precursor (niobium ethoxide) before addition of water to form metal-ligated surfactants by nitrogen-metal bond formation between the surfactant head group and the metal alkoxide precursor. Subsequent addition of ethanol and water resulted in the formation of white solid having a surface area between 400 – 600 $m^2 g^{-1}$. Highly sensitive liquid crystal structures formed in surfactant solutions may also interact with the silicate species directly which results in the ordering of the subsequent silicate-enclatherated surfactant micelles to form MCM-41 structure.

2.4. PROMOTER MEDIATED SYNTHESIS: STRATEGY

An approach to reduce synthesis time of porous materials using inorganic cations as promoters have been reported earlier [12,13], but synthesis of mesoporous materials and zeolites using catalytic amount of promoter and maintaining the ordered structures is a daunting task. It is in this context, use of HPAs as new class of promoters for the synthesis of microporous and mesoporous materials have been endeavored [21]. Finally, the effect of

HPAs on structure and growth patterns of the mesoporous and the microporous crystals will be looked into.

In this chapter, a novel, convenient and rapid synthesis route for microporous (zeolites Na-Y, Ferrierite and Silicalite-1) and mesoporous materials (MCM-41 and MCM-48) using catalytic amount of Keggin anions ($H_3PMo_{12}O_{40}.24H_2O$, $H_3PW_{12}O_{40}.24H_2O$ and the their corresponding oxoanions $Na_2MoO_4.\ 2H_2O$, $Na_2WO_4.2H_2O$, $NaH_2PO_4.2H_2O$) as promoters will be presented. This has been supported by vital characterizations based on NMR and powder XRD and a plausible reason for the cause of rapid synthesis has been put forth based on the hard and soft acid base (HSAB) theory. The main emphasis will be laid on the synthesis, characterization and results on mesoporous MCM-41 and MCM-48 materials and extended further, with additional details, to microporous materials e.g. Na-Y, Silicalite-1 and Ferrierite.

The main features when the oxoanions of molybdenum (MoO_4^{2-}), tungsten (WO_4^{2-}) and phosphorus (PO_4^{3-}) together are used as catalysts here are: (i) the rapid synthesis of the zeolites and mesoporous materials by using catalytic amounts of these promoters, (ii) the formation of smaller and uniform crystal sizes of the zeolites compared to either Gr. V or Gr. VII oxoanions or in the absence of any promoter, (iii) the stability of zeolite Na-Y for at least 6 hours before the formation of zeolite-P (GIS) starts (instead of conventional 1 hour), which is a remarkable improvement for stability of faujasite, (iv) synthesis of sub-micron sized crystals of Na-Y and Silicalite-1 using these promoters, (v) synthesis of high surface area and more ordered mesoporous MCM-41 and MCM-48, and (vi) higher stability regime of the MCM-48 materials using these promoters.

2.5. HPA–MEDIATED SYNTHESIS OF MESOPOROUS MATERIALS

HPAs (heteropolyacids) of molybdenum and tungsten, when used in catalytic amounts in the syntheses gels, reduce the nucleation time for microporous zeolites and mesoporous materials, by many folds [21]. The presence of catalytic amounts of the promoters (vis-à-vis in its absence) in the synthesis of these inorganic materials may be carried at lower temperature in all the cases. Zeolite structures containing small pore (FER, 5 Å), medium pore (MFI, 8 Å), large pore (FAU, 13 Å) and mesoporous materials such as hexagonal MCM-41 and cubic MCM-48 having mesopores (~ 30 Å) have been chosen as

illustrative examples for novel and rapid syntheses of these porous materials using HPAs as promoters. Further, it is demonstrated for the first time that in the synthesis of MCM-48, presence of Keggin anions does not need the addition of any co-surfactant or mineral acid [15, 17]; and additionally, very low template concentration (Si/template ≈ 5) was required in the promoter-assisted synthesis of MCM-48.

2.5.1. Materials

The silica source used was fumed silica (Aldrich) in case of MCM-41 and MCM-48 syntheses. Cetyltrimethylammonium bromide (CTMABr, Aldrich) was used as template for the syntheses of the mesoporous materials. The heteropolyacids (phosphotungstic acid, phosphomolybdic acid), sodium molybdate, sodium tungstate and sodium dihydrogen phosphate were obtained from s. d. Fine Chem, India. Other chemicals required for synthesis like sodium aluminate ($NaAlO_2$), sodium hydroxide (NaOH), were all procured from s. d. Fine Chem, India.

2.5.2. Synthesis of Si-MCM-41

In a typical synthesis of MCM-41, 3 g of fumed silica (Aldrich) was added to a solution of 0.64 g NaOH in 25 mL H_2O and stirred for 45 min. To this, a solution of 3.64 g CTABr in 50 mL H_2O was added drop wise and stirred another 45 min. Finally a solution of required amount of promoter in 37 mL of H_2O was added to the synthesis mixture and stirred for another 30 min. For the synthesis without promoter, only 37 mL of H_2O was added to the gel. The final gel composition was SiO_2: 0.32 NaOH: 0.2 CTABr: 125 H_2O: 0.0033 P (P = promoter used). The materials were autoclaved at 100 °C, washed with copious amounts of water and calcined at 540 °C.

2.5.3. Synthesis of Si-MCM-48

In a typical synthesis of MCM-48, 3 g of fumed silica (Aldrich) was added to a solution of 0.8 g NaOH in 25 mL H_2O and stirred for 1 h. A solution of 3.82 g of CTABr in 50 mL H_2O was added to the gel drop wise and stirred for another 1 h. Finally a solution of necessary amount of promoter in 33 mL of H_2O was added to the synthesis mixture and

stirred for another 30 min. For the synthesis without promoter, only 33 mL of H_2O was added finally. The final gel composition was SiO_2: 0.4 NaOH: 0.21 CTABr: 120 H_2O: 0.0033 P. The materials were autoclaved at 150 °C and calcined materials obtained by the procedure as mentioned earlier. The hydrothermal syntheses in both the cases were carried out for different time intervals by taking out in batches to study the effect of promoters.

2.6. HPA-MEDIATED SYNTHESIS OF MICROPOROUS MATERIALS

2.6.1. Materials

The silica source was sodium silicate (Loba, India) in zeolite Y and Ferrierite synthesis and tetraethyl orthosilicate (TEOS, Aldrich) in case of silicalite-1 synthesis. Templates for Silicalite-1 synthesis, tetrapropylammonium hydroxide (TPAOH), and Ferrierite synthesis, pyrrolidine were obtained from Aldrich. The heteropolyacids (phosphotungstic acid, phosphomolybdic acid), sodium molybdate, sodium tungstate and sodium dihydrogen phosphate were obtained from s. d. Fine Chem, India. Sodium aluminate ($NaAlO_2$), sodium hydroxide (NaOH), aluminium sulfate hexadecahydrate ($Al_2(SO_4)_3.16H_2O$) were all procured from s. d. Fine Chem, India.

2.6.2. Synthesis of zeolite NaY (FAU)

Zeolite Na-Y has been synthesised based on the procedure reported earlier [41]. In a typical synthesis of zeolite Na-Y (faujasite), seed crystals of zeolite NaY were prepared separately from an aqueous mixture of Na_2SiO_3 (95 mmol, 28% SiO_2), $NaAlO_2$ (9.76 mmol, 43% Al_2O_3, 39% Na_2O), NaOH (70 mmol) and H_2O (0.55 mmol) by stirring for 1 h and keeping it to rest for 18 h. Before mixing the starting materials, the aqueous solution of $NaAlO_2$ was filtered through a membrane filter with pore size of 0.2 μm to remove impurities, e.g. $Fe(OH)_3$. The seed crystals of zeolite NaY thus prepared were then added to the aqueous solution of Na_2SiO_3 (355 mmol). Subsequent addition of $NaAlO_2$ (34.2 mmol), NaOH (92.5 mmol), $Al_2(SO_4)_3.16H_2O$ (6.02 mmol) and H_2O (1.94 mmol) were followed under constant stirring for 2 h. Aqueous solutions of promoters (0.315 mmol), $H_3PMo_{12}O_{40}.24H_2O$, $H_3PW_{12}O_{40}.24H_2O$, $Na_2WO_4.2H_2O$, $Na_2MoO_4.2H_2O$ and $NaH_2PO_4.H_2O$ with molar ratio of SiO_2: promoter as 400:1 were made separately in 5 ml de-ionised water. These solutions were finally added to the respective gel mixtures, with an

additional stirring of 1 h; final pH of the gel is 13.1. The final molar composition of the reaction mixture was 400 SiO_2: 85 Al_2O_3: 280 Na_2O: 7575 H_2O: P (P = promoter used). The reaction mixtures for zeolite were then sealed in polypropylene bottles and kept in an oven at 358 K at different time intervals from 3 h to 12 h under autogenous pressure. The as-synthesized samples were filtered and washed several times with deionised water, dried at 353 K and then calcined at 813 K for 12 h.

2.6.3. Synthesis of Ferrierite (FER)

Ferrierite was synthesized implementing a published procedure [12c], with an aid of these promoters. In a typical synthesis of ferrierite, to a stirred solution of Na_2SiO_3 (430 mmol), Pyrrolidine (0.12 mmol) and then $Al_2(SO_4)_3.16H_2O$ (3.8 mmol) is added and further stirred for 1 h. Aqueous solutions of the above-mentioned promoters (0.3 mmol) with the same molar ratio were made in de-ionised H_2O (2.2 mmol) and added slowly while stirring for another 1 h. The final pH was kept at 12. The final molar composition of the reaction mixture is 400 SiO_2: 120 Na_2O: 6 Al_2O_3: 222 Pyrrolidine: 7710 H_2O: P (P = promoter used). The reaction mixtures for ferrierite were then sealed in stainless steel autoclaves and kept in oven at 423 K at time intervals ranging from 15 to 60 h, and then were filtered and washed several times with de-ionised water, dried at 373K and then calcined at 813 K for 12 h.

2.6.4. Synthesis of Silicalite-1 (Si – MFI)

In a typical synthesis of Silicalite-1 [12b], TPAOH (166 mmol; 20% aq. solution) was added to a stirred solution of TEOS (100 mmol; 98%), and further stirred for 2 h. To this, aqueous solutions of the above-mentioned promoters (0.25 mmol) with same molar ratio were made in de-ionised H_2O (1 mmol) and added slowly while stirring for another 3 h. The final pH was 10.7. The final molar composition of the reaction mixture is 4 SiO_2: 1.34 TPAOH: 100 H_2O: 0.01P (P = promoter used). The reaction mixtures for silicalite-1 were then sealed in polypropylene bottles and kept in oven at 358 K for a period ranging from 8 to 48 h, followed by filtration and washing several times with de-ionised water, drying at 353K and then calcining at 813 K for 12 h.

2.7. CHARACTERIZATION

Powder X-ray diffraction (XRD) was obtained on Rigaku D MAX III VC diffractometer using Ni-filtered Cu K_α radiation of wavelength 1.5404 Å, a scan rate of 1° per minute at room temperature. The crystallinity of the samples was determined by integrating the area of the powder XRD patterns in the 2 θ ranges from 1.5° to 10°. Scanning electron microscopy (SEM) was obtained on a JEOL, JSM 5200 machine operated at 20 kV. Samples for investigations were prepared by suspending the crystalline materials in isopropanol, then casting on gold plated discs and subsequent drying under vacuum. For transmission electron microscopy (TEM) of the mesoporous materials, the samples were dispersed by isopropanol on Holey carbon grids and TEM images were scanned on a Jeol Model 1200 EX instrument operated at an accelerating voltage of 100 kV. ^{29}Si solid-state MAS NMR spectra of the solid materials were obtained on a Bruker MSL 300 NMR spectrometer at 59.664 MHz using 7 mm CP-MAS probe at 7.01 Tesla. The chemical shifts were referred to TMS at 0 ppm and the spectra were collected at a spectral width of 20 kHz, with a flip angle of 45^o, 6000 real data points and 5 s relaxation delay.

2.8. RESULTS AND DISCUSSION

In this work, $H_3PMo_{12}O_{40}.24H_2O$, $H_3PW_{12}O_{40}.24H_2O$ and their oxoanions $Na_2MoO_4.2H_2O$, $Na_2WO_4.2H_2O$, $NaH_2PO_4.2H_2O$, have been used to study the catalytic effect in the synthesis of MCM-41 and MCM-48. It is well known that these polyoxometalates break up into their respective oxoanions in alkaline medium. Hence, we have performed separate synthesis experiments where, the oxoanions (phosphate and molybdate or tungstate) have been added separately to the gel mixtures of each mesoporous materials, to study the effect of addition of various anions in the syntheses of these mesoporous materials.

2.8.1. Effect of various promoters in the syntheses

In this work, sodium molybdate ($Na_2MoO_4.2H_2O$), sodium tungstate ($Na_2WO_4.2H_2O$), sodium dihydrogen phosphate ($NaH_2PO_4.2H_2O$), phosphomolybdic acid ($H_3PMo_{12}O_{40}.24H_2O$) and phosphotungstic acid ($H_3PW_{12}O_{40}.24H_2O$) have been used to study

the overall catalytic effects in the synthesis of (a) mesoporous materials such as MCM-41 and MCM-48 and (b) microporous materials such as Faujasite (Na-Y), Silicalite-1 (Si-MFI) and Ferrierite (FER). It is known that these polyoxometalates dissolve and break up into their respective oxometalates or oxoanions in alkaline medium (pH ≥ 10). In order to understand the effect of promoters, a separate synthesis experiment for MCM-41 material (as a typical example) have been performed, where the oxoanions (phosphate, molybdate or tungstate) and their polyoxometalate (phosphomolybdate or phosphotungstate) anions are added separately in the same molar ratio (Si: P = 300:1) to gel mixtures of MCM-41.

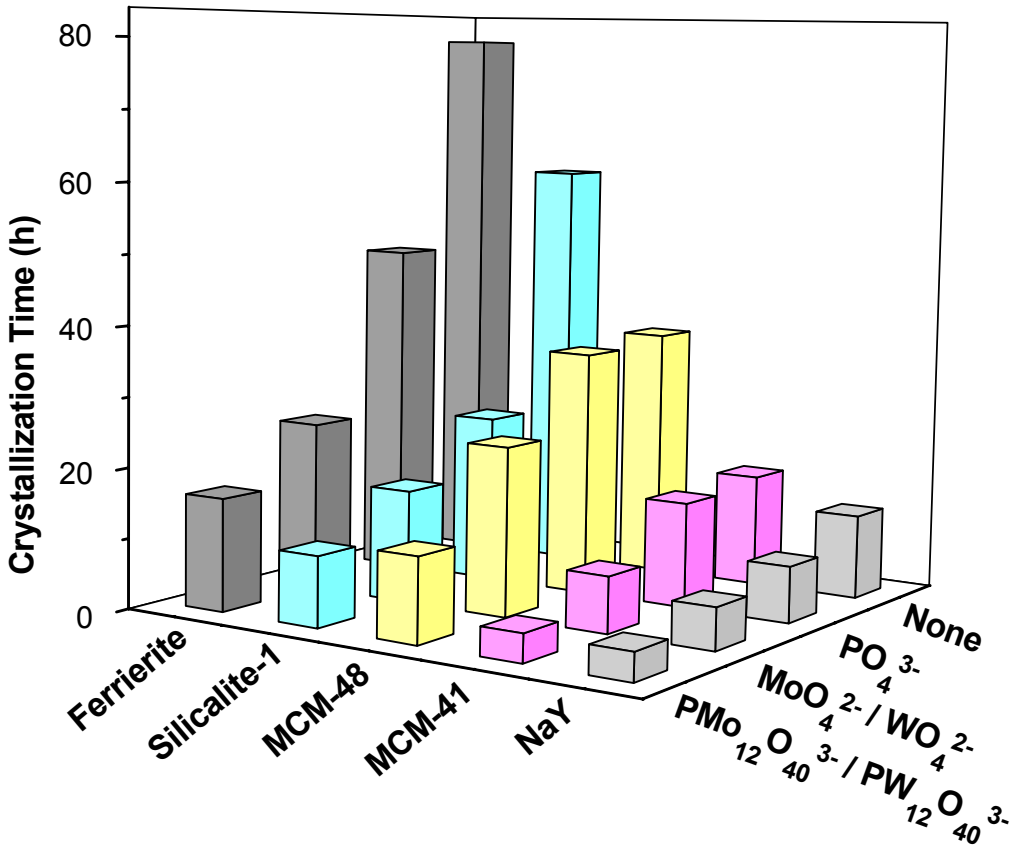

Figure 2.1. Effect of addition of different promoters for crystallization of zeolites and mesoporous materials (Si : Promoter = 300).

The effect of various promoters (with equivalent promoter concentrations) in the synthesis of mesoporous MCM-41 has been shown in Figure 2.2 (A) with respect to the powder XRD patterns of the synthesized MCM-41 materials using the promoters. It is observed that synthesis of MCM-41 is very rapid in the presence of heteropolyacids e.g. phosphomolybdate or phosphotungstate anions compared to other oxoanions e.g. phosphate, molybdate or tungstate and ofcourse in the absence of any promoters. The degree of orderedness of the MCM-41 and MCM-48 materials in presence or absence of promoters has been adjudicated by ^{29}Si MAS NMR of the materials, thus synthesized (see section 2.8.4.3). On the whole, it is distinctly observed that phosphotungstate or phosphomolybdate anions render rapid nucleation than compared to other oxoanions. A typical synthesis time data for the synthesis of these materials has been presented in Table 2.2.

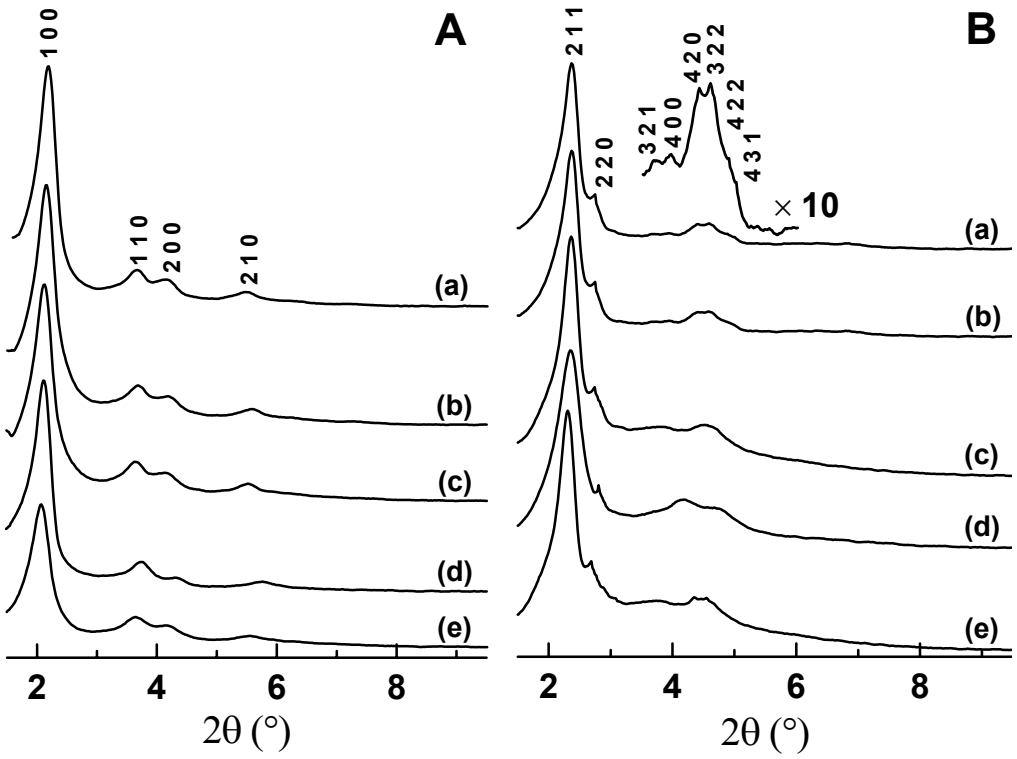

Figure 2.2. Powder XRD patterns of **(A)** calcined MCM-41 samples synthesized at 100°C using promoters (a) $H_3PW_{12}O_{40}$ (3 h), (b) $H_3PMo_{12}O_{40}$ (3 h), (c) Na_2WO_4 (6 h), (d) Na_2MoO_4 (6 h) and (e) without promoter (16 h); **(B)** calcined MCM-48 samples synthesized at 140°C using $H_3PW_{12}O_{40}$ as promoter for different times, (a) 9 h, (b) 12 h, (c) 18 h, (d) 24 h, and (e) without promoter for 36 h.

The same trend has also been observed in the synthesis of microporous materials. In a typical experiment for synthesis of zeolite Na-Y using the above mentioned promoters, percentage crystallization was determined using powder XRD intensity patterns (I) at {111}, that corresponds to the principal Bragg's reflection index for zeolite Y. Powder XRD of a standard zeolite Na-Y sample was performed and the peak intensity at {111} is termed as I_0 (see Table 2.2). The various intensities, which are obtained at different time intervals with different promoters were compiled and the ratio $(I)_{111}/ (I_0)_{111}$ of these data presents a qualitative insight of the zeolite Y crystallization patterns for different promoters (see Figure 2.3). The crystallization kinetics using this qualitative approach show how the rapidity and the ease of formation for zeolite Y vary by choosing the promoter anions in the respective order in the synthesis gel: $PW_{12}O_{40}^{3-} \approx PMo_{12}O_{40}^{3-} \ll WO_4^{2-} \approx MoO_4^{2-} < PO_4^{3-} \ll$ no promoter.

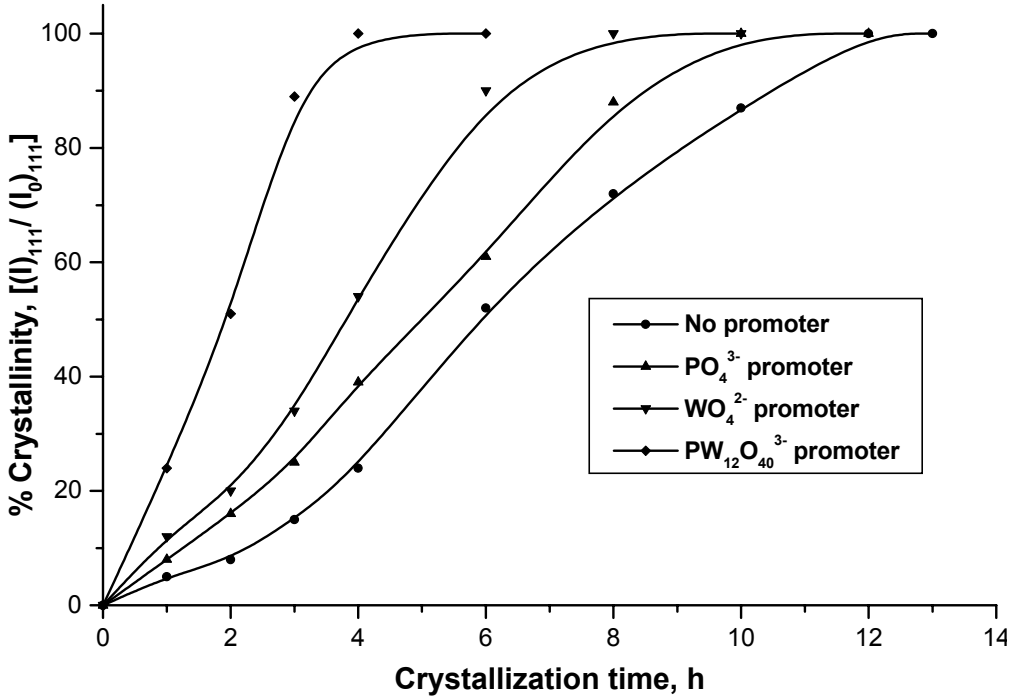

Figure 2.3. Crystallization kinetics of zeolite Na-Y using various promoters (see inset).

As an illustration, in absence of promoters, the average particle size of zeolite Na-Y crystal is around 900 – 1000 nm. Using various promoters in the respective synthesis gels of zeolite Y, crystallite sizes differed markedly; 550 – 600 nm and 270 – 300 nm for WO_4^{2-} and $PW_{12}O_{40}^{3-}$ anions respectively, with enhanced surface area (Table 2.2.). Hence, using promoters in the synthesis of microporous or mesoporous materials not only reduced the synthesis time and enhanced the crystallinity, but also incurred uniform and nanosized crystallites of the materials that exhibited a gradual increase in the surface of the materials.

2.8.2. Effect of time in the promoter aided syntheses

Claims regarding obtaining of hexagonal mesostructure diffraction patterns was reported in 1 h [14a,33], but, long-range ordering and thermal stability was poor and they were attained only after several hours of synthesis. The concept of using promoters has been basically been used for rapid synthesis (hence, lesser time) of porous materials with long-range ordering and high thermal stability. In an experiment to examine the thermal stability of the materials, 1 g of Si-MCM-41 was suspended in 50 mL of double distilled water and allowed to reflux for 30 h. The solid powder was separated from the filtrate by filtration and the Si-MCM-41 thus recovered was scanned by powder XRD analysis. The powder XRD pattern showed that there was almost no change in the hexagonal mesostructure patterns of the MCM-41 sample, but there was a slight decrease in the {100} peak intensity. We resolved the extent of orderedness of MCM-41 or MCM-48 materials using powder XRD (Figure 2.2 (B)) and ^{29}Si MAS NMR spectra (to be discussed later) of the materials to study the effect of time in the synthesis of well ordered MCM-41 and MCM-48 materials using phosphotungstate anions as promoters.

2.8.3. Effect of promoter concentration in the syntheses

Concentration of the promoters in obtaining well-ordered porous materials, e.g. mesoporous MCM-41 and MCM-48, and microporous Na-Y, Silicalite-1 or Ferrierite materials, through rapid synthesis is an important parameter for determining the optimum Si: P (P = Promoter) molar ratio to be maintained. As a typical example, the effect of promoter concentration has been studied in the synthesis of MCM-41 employing variable Si:P molar ratios (SiO_2:Promoter) ranging from 25 to 600 in the synthesis gel for a constant time of 4 h

(Figure 2.4 A). The best-ordered patterns of MCM-41, as obtained from powder XRD, is obtained at the lowest Si:P molar ratio of 300. This molar ratio (Si:P = 300) has been chosen as the standard for synthesis of mesoporous MCM-48 or other zeolitic materials (Na-Y, Ferrierite and Silicalite-1) through out this work.

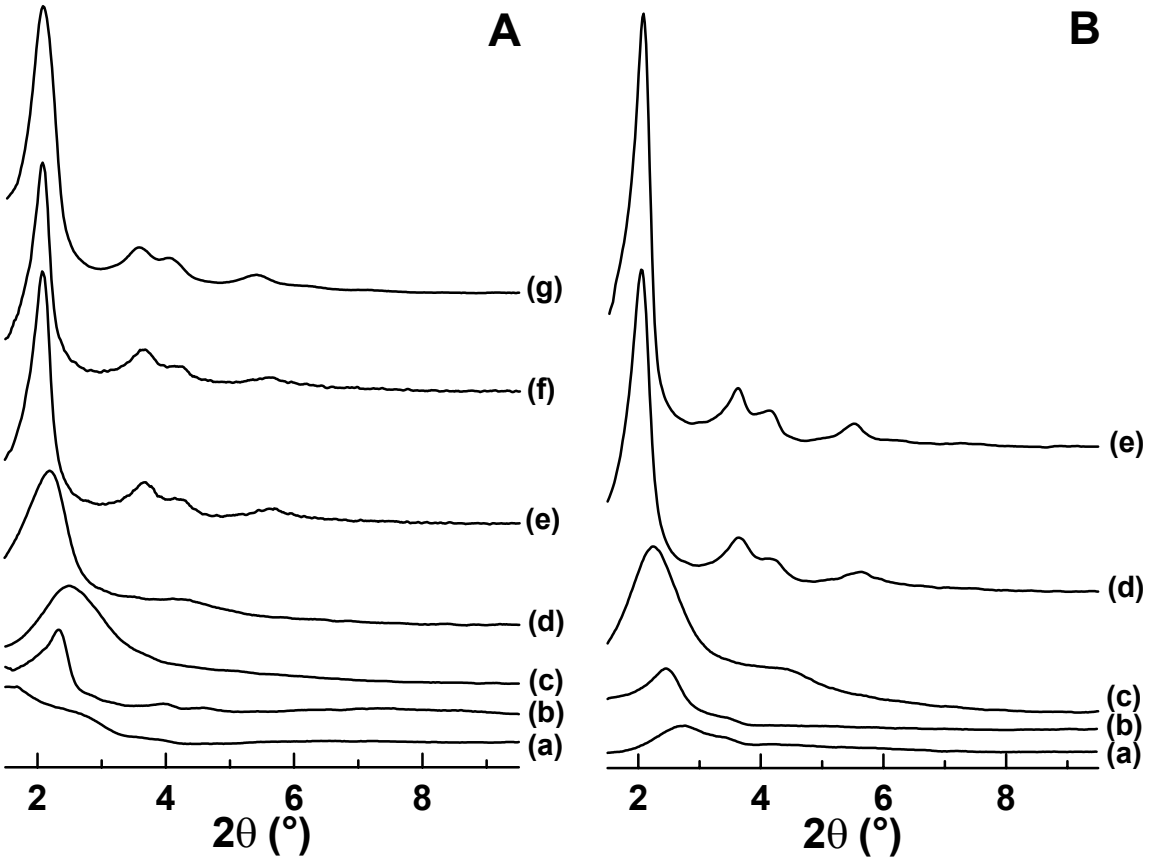

Figure 2.4. (A) Powder XRD patterns of calcined MCM-41 samples synthesized at 100 °C for 4 h using $PW_{12}O_{40}^{3-}$ as promoter and following Si/promoter ratios, (a) 25, (b) 50, (c) 600, (d) 400, (e) 300, (f) 200, and (g) 100. **(B)** Powder XRD patterns of calcined MCM-41 samples synthesized at 100 °C for 4 h by simultaneous addition of PO_4^{3-} and WO_4^{2-} keeping Si: PO_4^{3-} = 300 and following WO_4^{2-}: PO_4^{3-} ratios, (a) 1, (b) 3, (c) 6, (d) 12, and (e) 15.

2.8.4 PHYSICAL CHARACTERIZATIONS

2.8.4.1. Powder XRD and Atomic Absorption Spectra of the materials

Atomic Absorption Spectroscopic (AAS) analyses of the samples, dissolved in HF, reveal absence of P, Mo or W hence, they do not get incorporated in the mesoporous or microporous zeolite materials. The powder X-ray diffraction (XRD) patterns of the calcined Na-Y, Silicalite-1 and Ferrierite, and MCM-41 and MCM-48 samples using $H_3PW_{12}O_{40}$ as promoter show excellent crystallinity and are presented in Figure 2.5 (A) and (B).

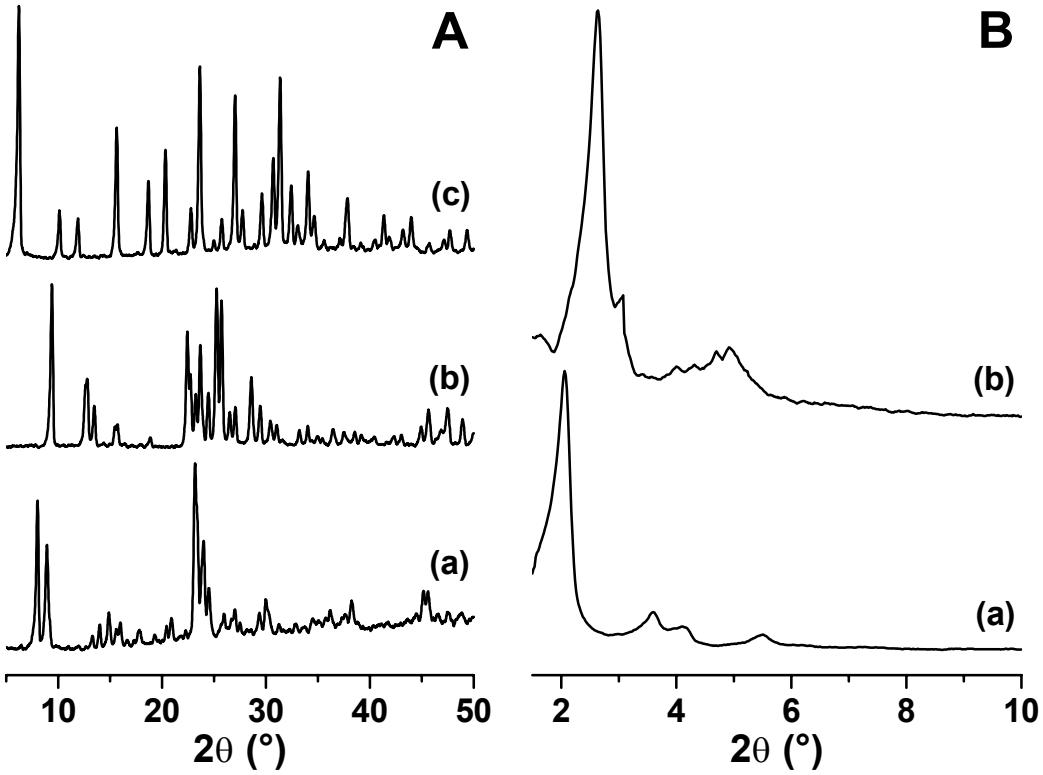

Figure 2.5. Powder XRD patterns: (A) (a) Silicalite-1, (b) Ferrierite, (c) Na-Y; and (B) (a) MCM-41, (b) MCM-48, synthesized using PTA as promoter.

The calcined powders show excellent well-resolved XRD patterns in the 2θ region of 1.5 to 6°, which are indexed to the {100}, {110}, {200} and {210} diffraction peaks of MCM-41 and the {211}, {220}, {321}, {400}, {420}, {322}, {422} and {431} diffraction peaks of MCM-48. Using $PMo_{12}O_{40}^{3-}$ or $PW_{12}O_{40}^{3-}$ ions as promoters, though the 100 peak of MCM-41 can clearly be observed for the sample obtained after 1 h, the best result was observed with the sample taken out after 3 h with its distinct peaks and a surface area of 1322

$m^2 g^{-1}$. Similarly, MCM-48 with high degree of orderedness was obtained after 12 h using HPAs as promoters with its distinct peaks and a surface area of 1932 $m^2 g^{-1}$. MCM-41 and MCM-48 were synthesized respectively at 6 h and 24 h when MoO_4^{2-}/ WO_4^{2-} ions were used as promoters, and at 16 h and 36 h without using promoters. In comparison to the samples synthesized using other oxoanions, e.g., MoO_4^{2-} or WO_4^{2-} or without adding promoters, the mesoporous samples synthesized using HPAs were far better in terms of respective mesostructural patterns. Similar trend of very good crystallinity (see Figure 2.5 A) has been observed for zeolites Na-Y, Ferrierite and Silicalite-1 microporous samples; as an example, an increase in surface area for zeolite Na-Y from 512 $m^2 g^{-1}$ to 750 $m^2 g^{-1}$ is observed when PTA-mediated synthesis is performed.

As an additional experiment to explore the effects of different oxoanions, we added PO_4^{3-} and WO_4^{2-} anions separately in the synthesis gel of MCM-41 at various molar ratios (P: W varied from 1 to 15, where W = WO_4^{2-} and P = PO_4^{3-} anions) and taken out at after 3 h. From the powder XRD patterns (see Figure 2.4 B) we observe that at lower W: P molar ratio of 1 to 6, poor mesophases of MCM-41 are obtained. At P: W ratio of 1:12, which is exactly similar to that of P: W in $PW_{12}O_{40}^{3-}$ anion added in the synthesis gel, excellent and distinct hexagonal mesophases are obtained, while reversing the ratios give amorphous phases. This proves conclusively that WO_4^{2-} or MO_4^{2-} anions infact are better promoters in comparison to PO_4^{3-} and both the oxoanions play crucial roles in increasing the crystallization rates of the mesoporous materials when HPAs are used. We could not obtain crystalline materials by using phosphate promoter in the molar ratio of 300:1 (Si: P), hence, we had to perform experiments with higher molar ratio of 30:1 (Si: P), as reported earlier [12], to get a good comparison with the other promoters used in the MCM-41 or MCM-48 synthesis.

Table 2.2. Physical Characteristics of the materials synthesized (SiO_2 : Promoter mole ratio = 300 : 1)

Material	Promoter[(a)]	Synthesis time (h)	d_{hkl} (Å)	a_o[(b)] (Å)	Particle Size[(c)] (μm)	Surface area ($m^2\ g^{-1}$)	PV[(d)] cm^3g^{-1}	PD[(e)] (Å)	FWT[(f)] (Å)	(Q^3/Q^4)[(g)]
MCM-41	none	16	42.37 (100)	48.92	10.0 × 2.00	1260	1.186	29.93	18.99	1.22 (0.32)
	MA/WA	8	41.73 (100)	48.18	4.00 × 1.00	1271	n. d.	n. d.	n. d.	n.d.
	PMA/PTA	4	41.16 (100)	47.52	0.60 × 0.40	1322	1.233	26.68	20.84	0.49 (0.16)
MCM-48	none	36	38.08 (211)	93.28	3.00 × 2.00	1701	1.137	22.69	18.82	0.79 (0.18)
	MA/WA	24	37.55 (211)	91.98	2.00 × 1.00	1827	n. d.	n. d.	n. d.	n.d.
	PMA/PTA	12	37.11 (211)	90.90	0.50 × 0.40	1932	1.399	20.40	19.20	0.47 (0.15)
Na-Y	none	12	14.29 (111)	24.75	1.00 × 0.90	512				
	MA/WA	6	13.91 (111)	24.09	0.65 × 0.55	630	n. d.	n. d.	n. d.	n. d.
	PMA/PTA	4	13.60 (111)	23.56	0.30 × 0.27	750				
Silicalite-1	none	60	3.85 (051)	19.63	2.20 × 2.00					
	MA/WA	16	3.80 (051)	19.38	0.10 × 0.08	n. d.	n. d.	n. d.	n. d.	n. d.
	PMA/PTA	10	3.76 (051)	19.17	0.05 × 0.04					
Ferrierite	none	80	9.61 (200)	19.22	12.0 × 3.00					
	MA/WA	24	9.52 (200)	19.04	6.00 × 1.00	n. d.	n. d.	n. d.	n. d.	n. d.
	PMA/PTA	16	9.41 (200)	18.82	3.00 × 0.50					

[a] PMA ($PMo_{12}O_{40}^{3-}$), PTA ($PW_{12}O_{40}^{3-}$), MA (MoO_4^{2-}), WA (WO_4^{2-}); [b] $a_0 = 2d_{100}/\sqrt{3}$ (MCM-41); $a_0 = d_{211}\times\sqrt{6}$ (MCM-48); $a_0 = d_{111}\times\sqrt{3}$ (Na-Y); $a_0 = d_{051}\times\sqrt{26}$ (Sil-1); $a_0 = d_{200}\times 2$ (Fer); [c] Particle size (diameter versus width), determined from SEM; [d] PV = Pore Volume; [e] PD = Pore Dimension; [f] FWT = Frame Wall Thickness, $FWT_{MCM\text{-}41} = a_0 - PD$, $FWT_{MCM\text{-}48} = a_0/3.092 - PD/2$ [Ref. [44]: Schumacher *et al.*, Langmuir 2000, 16, 4648.]; [g] as-synthesized samples, values in parentheses are for calcined samples. n. d. = not determined.

2.8.4.2. TEM and SEM studies

Transmission electron microscopic (TEM) images and the diffraction patterns of MCM-41 and MCM-48 were well consistent with the hexagonal and cubic mesophases respectively (Figures 2.6 A and B). Especially, the TEM images of MCM-48 resembled plate-like morphology and were completely devoid of any intra-particle defects, which usually account for secondary mesoporosity [17]. Scanning electron micrographs (SEM) of the samples revealed well distributed hexagonal (also spheroidal) and cuboidal structures [21] of MCM-41 and MCM-48 respectively (Figures 2.6 C and D), further supporting the XRD and TEM results. The average crystal-size, as observed by scanning electron microscopy (SEM) of the calcined Na-Y samples obtained using different promoters along with a standard Na-Y sample prepared in absence of promoter is shown in Figure 2.7, while Figure 2.8 presents SEM images of Silicalite-1 and Ferrierite. The patterns clearly indicate that smaller crystals are formed with more uniform particle size distribution, when promoter assisted synthesis of zeolites is performed (Table 2.2).

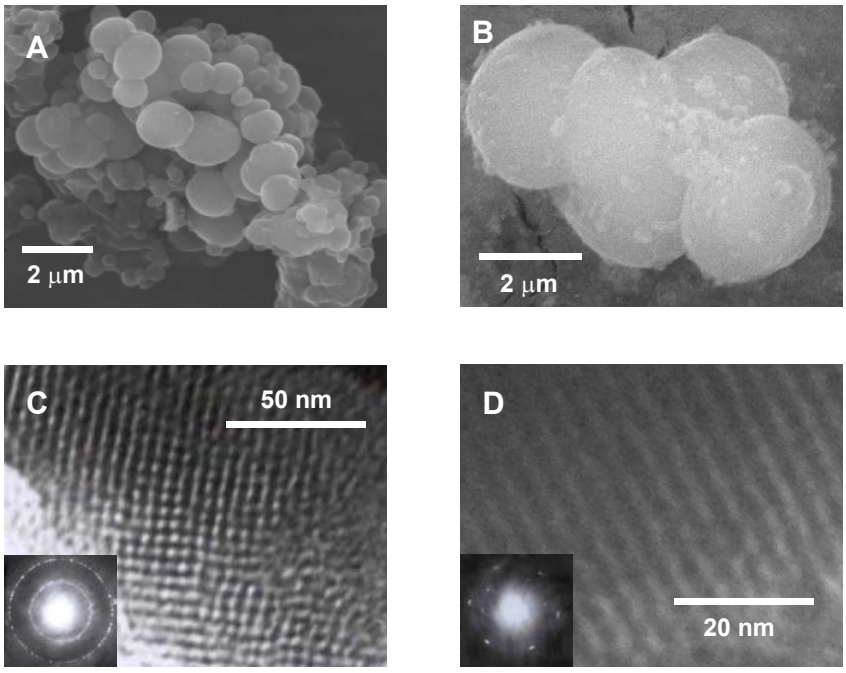

Figure 2.6. (A) TEM image of calcined MCM-41 sample synthesized using $H_3PW_{12}O_{40}$ for 3 h, (B) TEM image of calcined MCM-48 sample synthesized using $H_3PW_{12}O_{40}$ for 12 h (insets show the respective electron diffraction patterns), (C) SEM image of the calcined MCM-41 sample synthesized using $H_3PW_{12}O_{40}$ for 3 h, and (D) SEM image of calcined MCM-48 sample synthesized using $H_3PW_{12}O_{40}$ for 12 h.

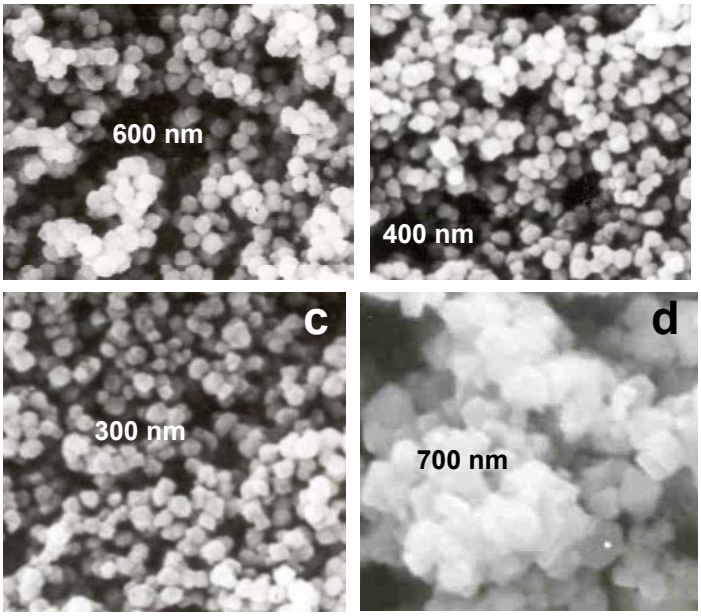

Figure 2.7. SEM of zeolite Na-Y crystals using: (a) PO_4^{3-}, 6h; (b) WO_4^{2-}, 5h; (c) $PW_{12}O_{40}^{3-}$ 3h; (d) no promoter, 12h (images at magnification = 5 K; 1 mm measurements denote average crystal diameter).

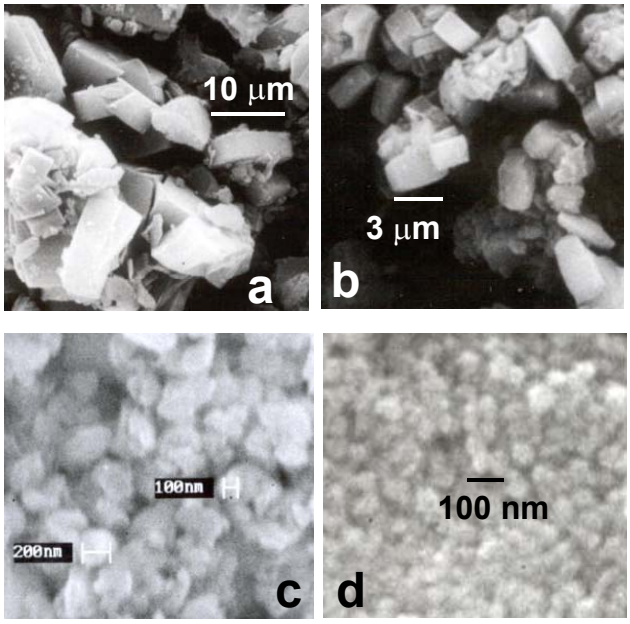

Figure 2.8. SEM of (a) Ferrierite using PO_4^{3-}, 45h (magnification = 2 K); (b) Ferrierite using $PMo_{12}O_{40}^{3-}$, 16h (magnification = 5 K); (c) Silicalite-1 using PO_4^{3-}, 24h; (d) Silicalite-1 using $PMo_{12}O_{40}^{3-}$, 10h (both images at magnification = 20 K).

2.8.4.3. ^{29}Si Magic Angle Spinning (MAS) NMR studies

In a typical experiment, ^{29}Si MAS NMR studies of MCM-41 synthesis were carried out using $H_3PW_{12}O_{40}$ as promoter at different time intervals of 1 h, 2 h, 2.5 h and 3 h (see Figure 2.9). This was performed to determine the degree of polymerization and concentration of silanol groups usually measured by the ratios of Q^3 and Q^4, the two major peaks. Q^3 and Q^4 measures the number of ^{29}Si of the type $(SiO)_3{\equiv}Si{-}OH$ and $(SiO)_3{\equiv}Si{-}O{-}Si{\equiv}$ respectively. Using $PW_{12}O_{40}^{3-}$ ions (PTA) as promoters, hexagonal phases of MCM-41 similar to type A and B were observed as reported earlier [16,39,42], from 0 h to 2.5 h and at 3 h respectively. It was observed that the % Q^4 species increases with time at the expense of Q^3 and Q^2, which in comparison to the spectra obtained without using promoter, concludes that the more condensed and ordered hexagonal array of MCM-41 and cubic arrays of MCM-48 are obtained at 3 h and 12 h respectively, as observed by the Q^3/Q^4 ratio. The Q^3/Q^4 ratio for the PTA mediated synthesis of MCM-41 as well as MCM-48 is always lower then the samples prepared without using PTA promoter (see Figure 2.9). From the ^{29}Si MAS NMR spectral patterns, a substantial condensation of Q^3 to Q^4 species was observed during calcinations of the as-synthesized MCM-41 and MCM-48 samples (see Table 2.2). A typical Q^3/Q^4 ratio for MCM-41 sample, prepared in absence of promoter shows a value of 1.22 and 0.32 before and after calcinations, while for PTA mediated MCM-41 sample, the respective values are 0.49 and 0.16 before and after calcinations (Figure 2.9). The results thus imply the effect of PTA (or HPAs) in rapid nucleation, that with advancement of time produce a very high degree of silanol condensation and orderedness of the MCM-41 and MCM-48 materials.

The Si/Al ratio of 2.35 for Na-Y, calculated from solid-state ^{29}Si MAS NMR [43], is well in accordance with the ratio of 2.37 obtained by elemental analysis (by AAS). The solid-state ^{29}Si-MAS-NMR spectrum of zeolite Na-Y synthesized using various promoters, is in excellent match with that of standard Na-Y zeolite (Figure 2.10).

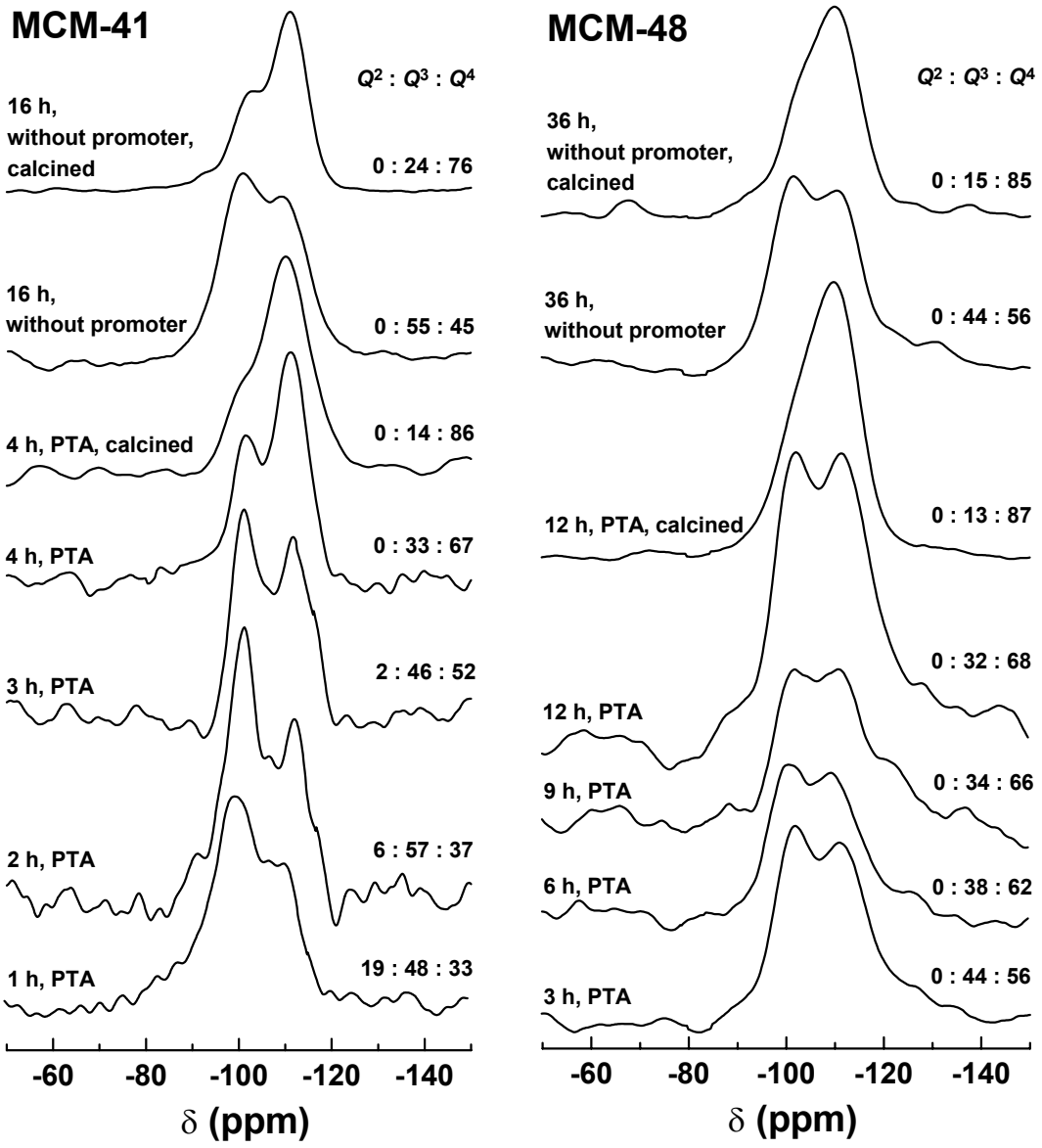

Figure 2.9. ^{29}Si MAS NMR spectra of as-synthesized MCM-41 and MCM-48 at different time intervals. The NMR experiments were performed on a Bruker MSL 300 spectrometer, in a 7 mm zirconia rotor at 4.0 kHz and 11.7 Tesla. Chemical shifts were measured with respect to tetraethyl orthosilicate (TEOS) as the reference compound. The Q^2: Q^3: Q^4 ratios were calculated using Jandel Scientific PeakFit deconvolution program.

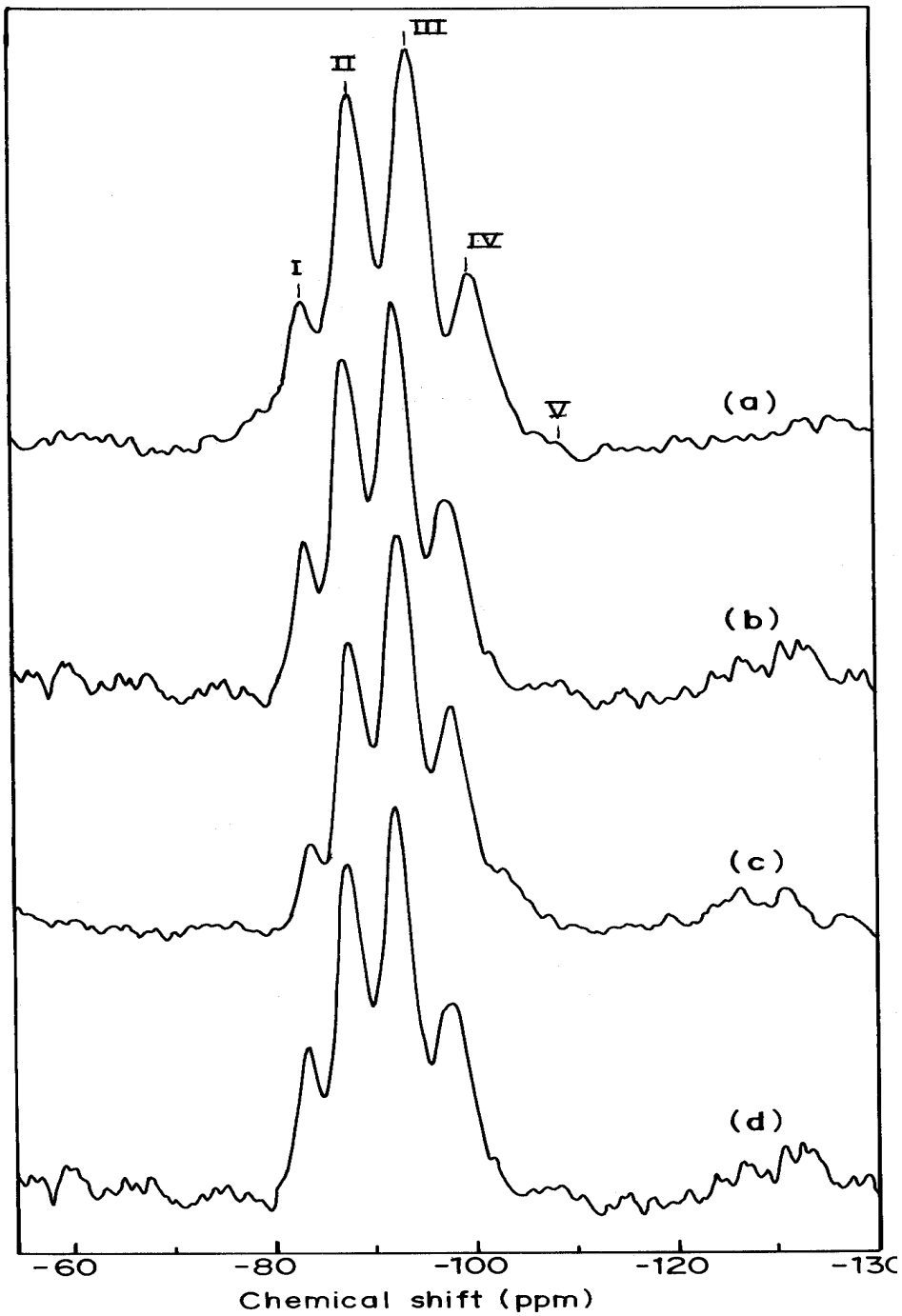

Figure 2.10. ^{29}Si solid-state MAS NMR of zeolite Na-Y using promoters (a) molybdate, (b) phosphomolybdate, (c) phosphate and (d) standard Na-Y sample, where **I**: Q^0, Si (4Al, 0Si); **II:** Q^1, Si (3Al, 1Si); **III:** Q^2, Si (2Al, 2Si); **IV:** Q^3, Si (1Al, 3Si); **V:** Q^4, Si (0Al, 4Si)

2.8.4.4. Surface Area and Pore Size Distribution of MCM-41 and MCM-48

The BET surface area increases when PTA promoter is added in the synthesis gels of the materials. Typical N_2 adsorption isotherm along with the pore size distribution of the promoter mediated (PTA) synthesis of MCM-41 and MCM-48 materials has been presented in Figures 2.11 and 2.12, respectively. For PTA-mediated synthesis of MCM-41 material, the inflection in the N_2 isotherm around $P/P_0 = 0.25 – 0.40$ (Figure 2.11) becomes sharper indicating narrower and uniform pore size distribution. In general, the BET surface areas of the promoter mediated MCM-41 samples are higher than the MCM-41 material synthesized in absence of promoters. The results w.r.t surface area, pore diameter and frame wall thickness as have been acquired from the N_2 adsorption isotherm data is also presented in Table 2.2. PTA-mediated MCM-41 sample shows a surface area of 1322 m^2g^{-1}, pore diameter of 26.68 Å and a frame wall thickness of 20.84 Å (frame wall thickness calculated based on Ref. 44) in comparison promoter-absent MCM-41 material having surface area of 1260 m^2g^{-1}, pore diameter of 29.93 Å and a frame wall thickness of 18.99 Å. Similarly, for PTA-mediated MCM-48 sample, N_2 adsorption isotherm with a sharp nitrogen condensation step at $P/P_0 = 0.25 – 0.35$ (Figure 2.12) and extremely narrow pore size distribution with a maximum at ca. 22.46 Å clearly indicate that the material has a high order pore system. Especially, the PTA-mediated MCM-48 material shows a pore volume of 1.399 cm^2g^{-1}, which is very high compared to that of other similar mesoporous systems [45]. PTA-mediated MCM-48 sample shows a very high surface area of 1932 m^2g^{-1}, pore diameter of 20.40 Å and a frame wall thickness of 19.20 Å [44] in comparison promoter-absent MCM-48 material having surface area of 1701 m^2g^{-1}, pore diameter of 22.69 Å and a frame wall thickness of 18.82 Å. The PTA-mediated MCM-41 and MCM-48 samples when suspended and stirred for 30 h in boiling water, the samples still retained their respective hexagonal and cubic structures. On the basis of the above-mentioned data and in reference to the TEM images, it can be further conjectured that the wall thickness of the promoter-mediated samples are uniform and very dense. Infact, to our knowledge, we obtained the highest framework density MCM-48 material using PTA as a promoter [45].

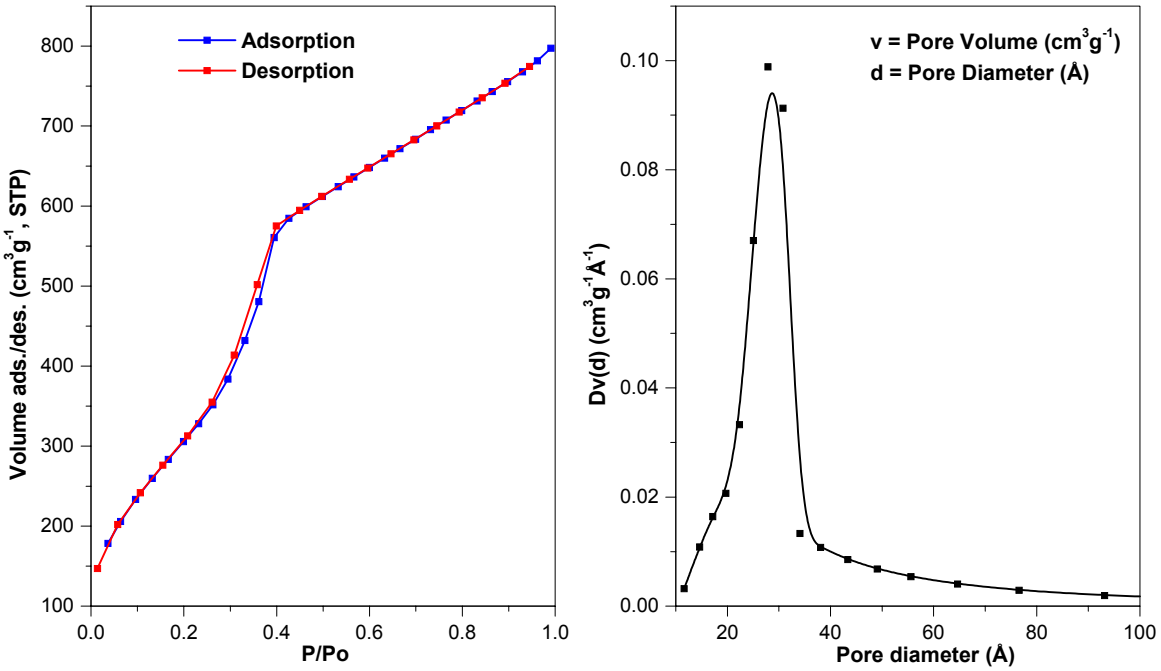

Figure 2.11. N_2 adsorption-desorption (BET) isotherm (left) and BJH pore size distribution (right) for Si-MCM-41 (using PTA as promoter; molar ratio of SiO_2 : PTA = 300).

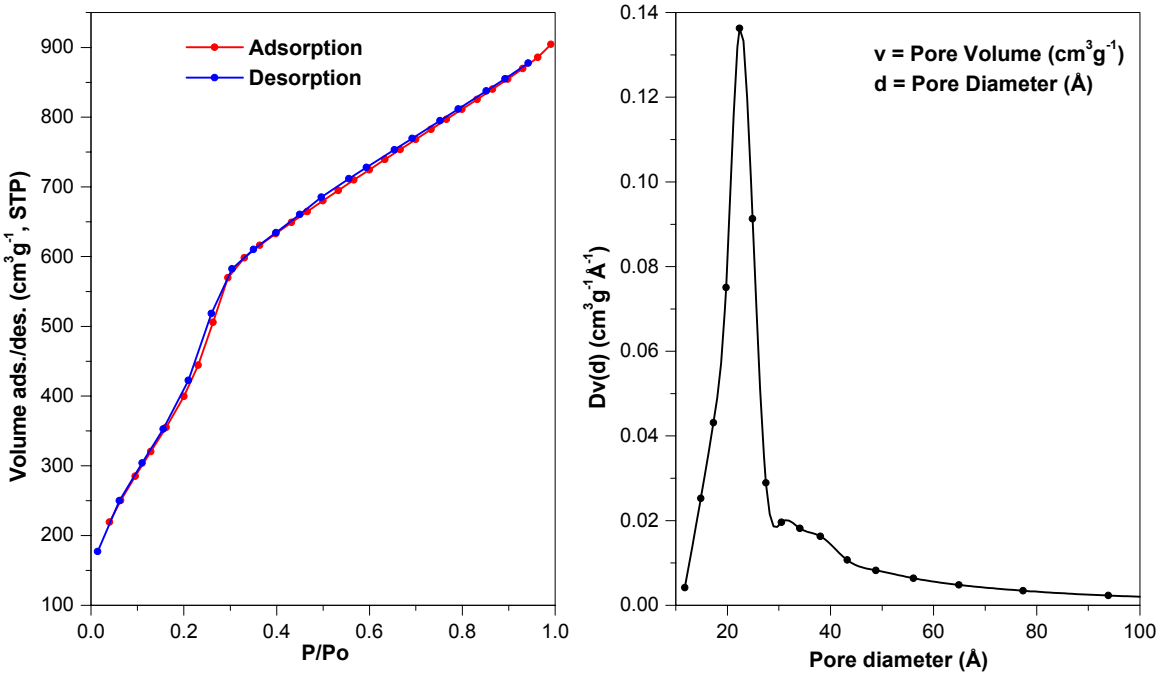

Figure 2.12. N_2 adsorption-desorption (BET) isotherm (left) and BJH pore size distribution (right) for Si-MCM-48 (using PTA as promoter; molar ratio of SiO_2 : PTA = 300.

2.9. POSTULATE FOR RAPID NUCLEATION: HSAB THEORY

It has been demonstrated that classical nucleation theory can predict nucleation rates during colloidal crystallization [22,46]. Crystal formation and growth are governed by particle gradient diffusivity [47]. We too consider here that the zeolite crystals are formed from the colloidal phase of the zeolite precursor, usually known as 'gel'. Once the crystals start forming from the colloidal phase the subsequent synthesis of the zeolite is thus made very facile, as the formation of crystal nucleus depletes the suspension of colloidal particles in the immediate vicinity of the crystal surface of the zeolite formed. A concentration gradient from the bulk suspension to the crystal surface is therefore established. Particles diffuse down this concentration gradient and are incorporated onto the crystal surface during nucleation and growth. Furthermore, the growth of crystalline regions depends on a competition between a decrease in surface energy favouring growth, and an increase in surface energy, which favours shrinkage [48]. Growth becomes favourable when the crystallites reach a critical size, called the critical nuclei, wherein the primary or secondary nucleation plays a crucial role to further enhance the crystallization rate of the zeolites and form the crystals. Promoters like HPAs play a crucial role by bringing down the surface energy (free energy of the crystal-liquid interface) and dissipating the surrounding aqueous layer that hinders the formation of the critical nuclei.

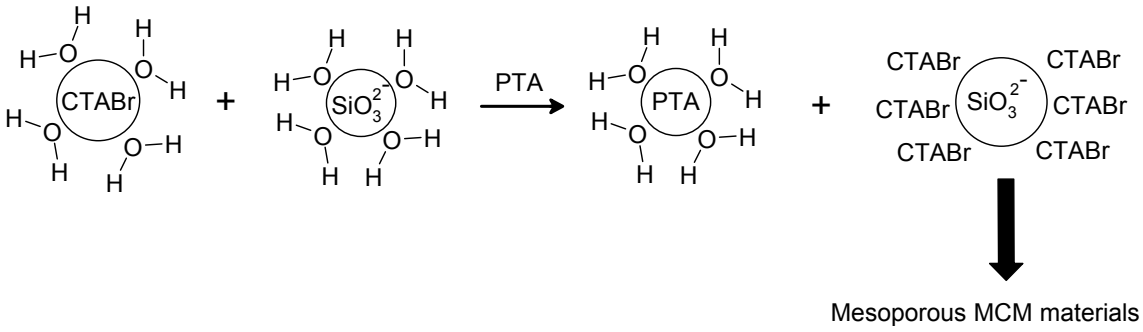

Scheme 2.4. HSAB concept for promoter mediated nucleation of MCM type materials

Based on the HSAB (Hard and Soft Acid Base) theory [49], we surmise that rapid crystallization of mesoporous materials primarily occurs owing to hard-hard interaction of hydration sphere of water molecules and the HPA anions used (see Scheme 2.4). The water molecules thus, surrounding the crystallization region is extracted out, leaving the silicates and organic template (CTABr) to have a soft-soft interaction in between them for the formation of mesoporous matrices. It is this factor (water extraction), which plays a crucial role in bringing down the crystallization time of the mesoporous materials, that otherwise, takes a much longer time by conventional synthesis procedure without promoters. In zeolite Na-Y, aluminium ions are condensed onto monomer (Q^0), dimer (Q^1), trimer and tetramer species having terminal [$Si(OH)_3$] groups [50]. Presumably, aluminium (Al 3(Si) and Al 4(Si)) incorporation to form the aluminosilicate species is very fast owing to this condensation process. The uptake of Al from the gel to the solid using these promoters was quantitative leading to a comparable molar ratio in the solid crystalline product in Na-Y and FER zeolites, as present in the synthesis mixture. Hence, crystallization occurs very fast with these promoters, than phosphates or oxometalates for syntheses of MCM-41 and MCM-48, as well as microporous Na-Y, Silicalite-1 and Ferrierite.

2.10. CONCLUSION

Thus, a rapid and convenient route using low amount of template (CTABr) for the syntheses of highly ordered mesoporous MCM-41 and MCM-48, and zeolites (large pore FAU, medium pore Si-MFI and small pore FER) using heteropolyacids as promoters is reported here for the first time. A very interesting aspect by using these promoters was observed while comparing the crystal size in zeolites and mesoporous materials. The similarities in shape and size of the zeolite crystals obtained using WO_4^{2-} (WA) and MoO_4^{2-} (MA), $PW_{12}O_{40}^{3-}$ (PTA) and $PMo_{12}O_{40}^{3-}$ (PMA) is observed presumably, owing to the same size of these pair of promoters. Fully crystalline sub-micron sized zeolites have been obtained by the promoter catalyzed synthesis of microporous zeolites and mesoporous materials those are reflected in the high surface areas and enhanced crystallinity of the materials. The materials thus prepared are very stable e.g., MCM-41 and MCM-48 possess high frame wall thickness when promoters are used in the synthesis gels.

REFERENCES

[1] (a) Davis, M. E. *Nature* **2002**, *417*, 813. (b) Schüth, F.; Schmidt, W. *Adv. Mater.* **2002**, *14*, 629.

[2] (a) Bein, T. *Chem. Mater.* **1996**, *8*, 1636. (b) Bein, T. *Compr. Supramol. Chem.* **1996**, *7*, 579.

[3] (a) Stein, A. *Adv. Mater.* **2003**, *15*, 763. (b) Stein, A.; Melde, B. J.; Schroden, R. C. *Adv. Mater.* **2000**, *12*, 1403.

[4] (a) Corma, A. *Chem. Rev.* **1995**, *95*, 559. (b) Breck, D.W. *Zeolite Molecular Sieves: Structure, Chemistry and Uses*, Wiley: New York, 1974. (c) Karge, H. G.; Weitkamp, J., Eds.; *Zeolites as Catalysis, Sorbents and Detergent Builders: Applications and Innovations*, Elsevier: Amsterdam, 1989. (d) Barrer, R. M. *Hydrothermal Chemistry of Zeolites*, Academic Press: New York, 1982.

[5] Corma, A. *Chem. Rev.* **1997**, *97*, 2373.

[6] (a) Kresge, C. T.; Leonowicz, M. E.; Roth, W. J.; Vertulli, J. C.; Beck, J. S. *Nature* **1992**, *359*, 710. (b) Beck, J. S.; Vertulli, J. C.; Roth, W. J.; Leonowicz, M. E.; Kresge, C. T.; Schmitt, K. D.; Chu, C. T.-W.; Olson, D. H.; Sheppard, E. W.; McCullen, S. B.; Higgins, J. B.; Schlenker, J. L. *J. Am. Chem. Soc.* **1992, *114*,** 10834.

[7] (a) Yanagisawa, T.; Shimizu, T.; Kuroda, K. *Bull. Chem. Soc. Jpn.* **1990**, *63*, 988. (b) Yanagisawa, T.; Shimizu, T.; Kuroda, K.; Kato, C. *ibid.*, 1535. (c) Inagaki, S.; Fukushima, Y.; Kuroda, K. *J. Chem. Soc. Chem. Commun.* **1993**, 680.

[8] Ryoo, R.; Jun, S. *J. Phys. Chem. B* **1997**, *101*, 317.

[9] (a) Tanev, P. T.; Pinnavaia, T. J. *Science* **1995**, *267*, 865. (b) Tanev, P. T.; Pinnavaia, T. J. *Chem. Mater.* **1996**, *8*, 2068. (c) Tanev, P. T.; Pinnavaia, T. J. *Science* **1996**, *271*, 1267. (d) Bagshaw, S. A.; Prouzet, E.; Pinnavaia, T. J. *Science* **1995**, *269*, 1242. (e) Prouzet, E.; Pinnavaia, T. J. *Angew. Chem. Int. Ed. Engl.* **1997**, *36*, 516. (f) Kim, S. S.; Zhang, W.; Pinnavaia, T. J. *Science* **1998**, *282*, 1302.

[10] (a) Huo, Q.; Leon, R.; Petroff, P. M.; Stucky, G. D. *Science* **1995**, *268*, 1324. (b) Zhao, D.; Feng, J.; Huo, Q.; Melosh, N.; Fredrickson, G. H.; Chmelka, B. F.; Stucky, G. D. *Science* **1998**, *279*, 548. (c) Zhao, D.; Yang, P.; Huo, Q.; Chmelka, B. F.; Stucky, G. D. *Curr. Opin. Solid State Mater. Sci.* **1998**, *3*, 111. (d) Zhao, D.; Huo, Q.; Feng, J.; Chmelka, B. F.; Stucky, G. D. *J. Am. Chem. Soc.* **1998**, *120*, 6024. (e) Winkel, P. S.;

Lukens, W. W.; Zhao, D.; Yang, P.; Chmelka, B. F.; Stucky, G. D. *J. Am. Chem. Soc.* **1999**, *121*, 254. (f) Winkel, P. S.; Lukens, W. W.; Yang, P.; Margolese, D. I.; Lettow, J. S.; Ying, J. Y.; Stucky, G. D. *Chem. Mater.* **2000**, *12*, 686.

[11] Sing, K. S. W.; Everett, D. H.; Haul, R. A. W.; Moscou, L.; Pierotti, R. A.; Rouquÿrol, J.; Siemieniewska, T. *Pure Appl. Chem.* **1985**, *57*, 603.

[12] (a) Kumar, R.; Bhaumik, A.; Ahedi, R. K.; Ganapathy, S. *Nature* **1996**, *381*, 298. (b) Kumar, R.; Mukherjee, P.; Pandey, R. K.; Rajmohanan, P.; Bhaumik, A. *Microporous Mesoporous Mater.* **1998**, *22*, 23. (c) Ahedi, R. K.; Kotasthane, A. N. *J. Porous Mater.* **1997**, *4*, 171.

[13] Laha, S. C.; Kumar, R. *Microporous Mesoporous Mater.* **2002**, *53*, 163.

[14] (a) Monnier, A.; Schüth, F.; Huo, Q.; Kumar, D.; Margolese, D.; Maxwell, R. S.; Stucky, G. D.; Krishnamurthy, M.; Petroff, P.; Firouzi, A.; Janicke M.; Chmelka, B. F. *Science* **1993**, *261*, 1299. (b) Anderson, M. W. Zeolites **1997**, *19*, 220.

[15] Ryoo, R.; Joo S. H.; Kim, J. M. *J. Phys. Chem. B* **1999**, *103*, 7435.

[16] Xu, J.; Luan, Z.; He, H.; Zhou W.; Kevan, L. *Chem. Mater.* **1998**, *10*, 3690.

[17] Liu, Y.; Karkamkar, A.; Pinnavaia, T. J. *Chem. Commun.*, **2001**, 1822.

[18] Zhao, W.; Li, Q. *Chem. Mater.* **2003**, *15*, 4160.

[19] (a) Chao, K. J.; Tasi, T. C.; Chen, M. S.; *J. Chem. Soc., Faraday Trans.* **1981**, *77*, 547. (b) Anderson, M.W.; Agger, J. R.; Thornton, J. T.; Forsyth, N. *Angew. Chem. Int. Ed. Engl.* **1996**, *35*, 1210. (c) Agger, J. R.; Pervaiz, N.; Cheetham, A. K.; Anderson, M. W. J. *J. Amer. Chem. Soc.* **1998**, *120*, 10754. (d) Francis, R. J.; Hare, D. O' *J. Chem. Soc., Dalton Trans.* **1998**, 3133. (e) Mintova, S.; Olson, N. H.; Bein, T. *Angew. Chem. Int. Ed. Engl.* **1999**, *38*, 3201. (f) Mintova, S.; Olson, N. H.; Valtchev, V.; Bein, T. *Science* **1999**, *283*, 958. (g) Li, Q.; Creaser, D.; Sterte, J. in *Porous Materials in Environmentally Processes*: *Stud. Surf. Sci. Catal.* **1999**, *125*, 133. (g) Thompson, R. W. *Molecular Sieves Science and Technology (Synthesis)*, Eds.: Karge, H. G.; Weitkamp, J., Springer: **2000**, *1*, pp. 1 - 33 and references therein. (h) Li, Q.; Creaser, D.; Sterte, J. *Chem. Mater.* **2002**, *14*, 1319.

[20] Inui, T. in *Zeolite Synthesis* (Eds.: Occelli, M. L.; Robson, H. E.); ACS Symp. Ser., Am. Chem. Soc.: Washington D. C., **1989**, *398*, 479.

[21] Mukhopadhyay, K.; Ghosh, A.; Kumar, R. *Chem. Commun.* **2002**, 2404.

[22] Randolph, A. D.; Larson, M. A. *Introduction to the Theory of Crystallization Processes, 2nd Edition*; Academic Press: London, 1988.

[23] (a) Cundy, C. S.; Lowe, B. M.; Sinclair, D. M. *Crstl. Gr.* **1990**, *100*, 189. (b) Knight, C. T. G. *Zeolites* **1990**, *10*, 140. (c) Cundy, C. S.; Lowe, B. M.; Sinclair, D. M. *Fara. Discuss.* **1993**, *95*, 235. (d) Twomey, T. A. M.; Mackay, M.; Kuipers, H. P. C. E.; Thompson, R. W. *Zeolites* **1994**, *14*, 162.

[24] Sung, C. Y.; Estrin, J.; Youngquist, G. R. *AIChE J* **1973**, *19*, 957.

[25] (a) Golemme, G.; Nastro, A.; B-Nagy, J.; Subotic, B.; Crea, F.; Aiello, R. *Zeolites* **1991**, *11*, 776. (b) Subotic, B. in *Zeolite Synthesis* (Eds.: Occelli, M. L.; Robson, H. E.); American Chemical Society: Washington D. C., 1989, 124. (c) Katovic, A.; Subotic, B.; Smit, I.; Despotovic, L. jA.; Curic, M. *ibid.*, 124.

[26] Zhdanov, S. P. *Adv. Chem. Ser.* (Eds.: Flanigen, E. M.; Sand, L. B.) **1971**, *101*, 20.

[27] Burkett, S. L.; Davis, M. E. *J. Phys. Chem.* **1994**, *98*, 4647.

[28] Doktor, W. H.; van Garderen, H. F.; Beelen, T. P. M.; van Santen, R. A.; Bras, W. *Angew. Chem. Int. Ed. Engl.* **1995**, *22*, 259.

[29] (a) Anderson, M.W.; Agger, J. R.; Thornton, J. T.; Forsyth, N. *Angew. Chem. Int. Ed. Engl.* **1996**, *35*, 1210. (b) Agger, J. R.; Pervaiz, N.; Cheetham, A. K.; Anderson, M. W. J. *J. Amer. Chem. Soc.* **1998**, *120*, 10754. (c) Mintova, S.; Olson, N. H.; Bein, T. *Angew. Chem. Int. Ed. Engl.* **1999**, *38*, 3201. (d) Mintova, S.; Olson, N. H.; Valtchev, V.; Bein, T. *Science* **1999**, *283*, 958. (e) Feng, S.; Bein, T. *Nature* **1994**, *368*, 834. (f) Feng, S.; Bein, T. *Science* **1994**, *265*, 1839. (g) Lee, J. S.; Lee, Y-J.; Tae, E. L.; Park, Y. S.; Yoon, K. B. *Science* **2003**, *301*, 818. (h) Sadasivan, S.; Fowler, C. E.; Khusalani, D.; Mann, S. *Angew. Chem., Int. Ed. Engl.* **2002**, *41*, 2151.

[30] Vartuli, J. C.; Schmitt, K. D.; Kresge, C. T. *Chem. Mater.* **1994**, *6*, 2317.

[31] (a) Israelachvili, J. *Colloids Surf. A: Physicochem. Eng. Aspects* **1994**, *91*, 1. (b) Davis, H. T. *ibid.*, 9.

[32] Cheng, C. F.; He, H.; Zhou, W.; Klinowski, J. *Chem. Phys. Lett.* **1995**, *244*, 117.

[33] Chen, C-Y.; Burkett, S. L.; Li, H-X.; Davis, M. E. *Microporous Mater.* **1993**, *2*, 27.

[34] Stucky, G. D.; Monnier, A.; Scüth, F.; Huo, Q.; Margolese, D. I.; Kumar, D.; Krishnamurty, M.; Petroff, P.; Firouzi, A.; Janicke, M.; Chmelka, B. F. *Mol. Cryst. Liq. Cryst.* **1994**, *240*, 187.

[35] Firouzi, A.; Kumar, D.; Bull, L. M.; Besier, T.; Sieger, P.; Huo, Q.; Walker, S. A.; Zasadzinski, J. A.; Glinka, C.; Nicol, J.; Margolese, D. I.; Stucky, G. D.; Chmelka, B. F. *Science* **1995**, *267*, 1138.

[36] Liu, J.; Kim, A. Y.; Virden, J. W.; Bunker, B. C. *Langmuir* **1995**, *11*, 689.

[37] Huo, Q.; Margolese, D. I.; Stucky, G. D. *Chem. Mater.* **1996**, *8*, 1147.

[38] Chen, C-Y.; Xiao, S-Q.; Davis, M. E. *Microporous Mater.* **1995**, *4*, 1.

[39] Huo, Q.; Margolese, D. I.; Ciesla, U.; Feng, P.; Gier, T. E.; Sieger, P.; Leon, R.; Petroff, P. M.; Schüth, F.; Stucky, G. D. *Nature* **1994**, *368*, 317.

[40] Antonelli, D. M.; Ying, J. Y. *Angew. Chem. Int. Ed. Engl.* **1996**, *35*, 426.

[41] Mukhopadhyay, K.; Mandale, A. B.; Chaudhari, R. V. *Chem. Mater.* **2003**, *15*, 1766.

[42] Steel, A.; Carr, S. A.; Anderson, M. W. *Chem. Mater.* **1995**, *7*, 1829.

[43] (a) Engelhardt, G.; Michel, D. *High-Resolution Solid-State NMR of Silicates and Zeolites*; John Wiley & Sons Inc.: New York, 1987, pp. 150 – 228. (b) Fyfe, C. A.; Thomas, J. M.; Klinowski, J.; Gobbi, G. C. *Angew. Chem. Int. Ed. Engl.* **1983**, *22*, 259. The Si/Al ratio in the tetrahedral alumonosilicate framework was calculated after deconvolution (using Jandel Scientific Peakfit program) from the equation:

$$(Si/Al)_{NMR} = \sum_{n=0}^{4} I_{Si(nAl)} \Big/ \sum_{n=0}^{4} 0.25 n I_{Si(nAl)}$$

[44] Schumacher, K.; Ravikovitch, P. I.; Du Chesne, A.; Neimark, A. V.; Unger, K. K. *Langmuir* **2000**, *16*, 4648.

[45] Zhao, W.; Li, Q. *Chem. Mater.* **2003**, *15*, 4160.

[46] ten Wolde, P. R.; Frenkel, D. *Science* **1997**, *277*, 1975.

[47] Schatzel, K.; Ackerson, B. J. *Phys. Rev. E* **1993**, *48*, 3766.

[48] Gasser, U.; Weeks, E. R.; Schoefield, A.; Pusey, P. N.; Weitz, D. A. *Science* **2001**, *292*, 258.

[49] Pearson, R. G. *J. Am. Chem. Soc.* **1963**, *85*, 3533.

[50] Thangaraj, A.; Kumar, R. *Zeolites* **1990**, *10*, 117.

[51] Cotton, F. A.; Wilkinson, G. *Advanced Inorganic Chemistry, 5th Edition*; Wiley: New York. 1988, 811.

CHAPTER 3

ENCAPSULATION OF $HRh(CO)(PPh_3)_3$ IN MICROPOROUS AND MESOPOROUS MATERIALS: NOVEL HETEROGENEOUS CATALYSTS FOR HYDROFORMYLATION

3.1. INTRODUCTION

Hydroformylation is one of the largest scale applications of homogeneous catalysis in industry [1–3]. This process involves a reaction of an olefin, carbon monoxide and hydrogen to produce linear or branched aldehyde products. The commercial processes employ homogeneous cobalt or rhodium complex catalysts, of which the process using the Wilkinson's catalyst $HRh(CO)(PPh_3)_3$ has been considered as a major breakthrough because of its high activity and selectivity at mild operating conditions [4]. While, $HRh(CO)(PPh_3)_3$ catalyst has been commercialized for hydroformylation of propylene, wherein, the product can be easily separated from the catalyst due to its high volatility, its application for the higher olefinic substrates has been limited due to difficulties in catalyst – product separation [5, 6]. Therefore, several attempts have been made to heterogenize the homogeneous catalysts, so that the advantages of the homogeneous and heterogeneous catalysts can be combined. In previous work, polymer anchored [7], supported liquid phase (SLP) [8], supported aqueous phase (SAP) [9], biphasic catalysts using water-soluble metal complexes [10], using sulfonated [11] or fluorinated phosphines [12] as ligands, ionic liquids as new solvents [13], as well as bimetallic catalysts [14] for hydroformylation have been proposed. In these reports, interesting concepts have emerged; however, with the exception of biphasic catalysis no other approach has been found to be commercially attractive. Even the biphasic catalysts for hydroformylation of *higher olefins* suffer from the disadvantages of the lower rates limited by the solubility of olefins in water [15].

Earlier, heterogenized catalysts were reported using Rh complex dendrimers on silica [16], water soluble Calix[4]arene ligands [17] for biphasic hydroformylation of water-insoluble olefins, silica immobilized with tripodal polyphosphine rhodium catalysts [18] to name a few. But in majority of the cases, they suffer from lower selectivity and activity, low recyclability, use expensive ligands, unsuitable for commercial applications.

In this context, encapsulation of metal complexes as a mean of "heterogenization" in porous matrices like zeolites and mesoporous materials has particular significance. Zeolites and zeotypes (molecular sieves) owing to their varied intrinsic properties (e.g. acidity, basicity, redox behaviour etc.), channel sizes, high surface areas, thermal and chemical stabilities and channel structures (shape selectivities) have been extensively used in oil refining, petrochemical and fine chemical industries for the past couple of decades, for

producing bulk chemicals, fine chemicals and speciality chemicals [19]. However, with the limitation of micro-pore sizes (less than 13 Å) [20], synthesis of complex organic molecules is inefficient, demanding a search for new materials with larger pore sizes. The discovery of a novel family of M41S mesoporous materials has opened new opportunities in catalytic applications in this context [21, 22]. The M41S family has been generally classified into three different categories: MCM–41 (hexagonal), MCM–48 (cubic) and MCM–50 (lamellar). The properties of the mesoporous materials such as larger surface areas (> 700 m^2g^{-1}), well-defined pore sizes (20–100 Å) and tenability to change the pore sizes have made them the most sought after materials of the last decade. The syntheses of these materials with the aid of host-guest chemistry have expanded the applications of solid catalysts for developing new processes for fine and bulk chemicals. In immobilization approach, the organometallic complex is encapsulated or anchored inside the pores of the inorganic inert matrices, e.g. zeolites, M41S materials, clay etc. in such a way that the complex is tightly bound inside the pores [23]. The prime requirement is stability of the encapsulated complex, so that it does not leach out of the catalyst pores to the liquid phase in the course of a reaction, while retaining high activity, selectivity and original configuration. In several reports, heterogeneous catalysis by encapsulated materials has been addressed for oxidation [24], hydrogenation [25], epoxidation [26] and Heck reactions [27]. But, attempts to heterogenize hydroformylation catalysts with true heterogeneity, high activity and selectivity, high reusability and easy preparative approaches for commercial utilization in industry taking care of catalyst product separation and leaching problems is one of the burning issues.

In previous reports for hydroformylation of various olefins and alcohols, supported Rh based catalysts on clays [28], supported Rh complexes on zeolites [29], encapsulated Rh complexes using 'ship-in-a-bottle' approach [30], adsorbed Rh complexes on zeolite pore-mouth [31], tethered Rh complexes to silica matrices [32] and anchored Rh complex in MCM-41 materials have been proposed [33] (details have already been discussed in Chapter 1). But, the heterogenized catalysts suffered either from lower selectivity and activity or low recyclability, often followed by leaching of Rh metal under reaction conditions; hence, they were not considered for commercial applications.

Herein, we report syntheses of novel and true heterogeneous catalysts consisting of $HRh(CO)((PPh_3)_3$ complex encapsulated in zeolite Na-Y and mesoporous M41S materials

(MCM-41 and MCM-48) and their performance as catalysts for hydroformylation of various olefins [34], as shown in Scheme 3.1. A detailed investigation of the characterization of these catalysts using powder-XRD, CP-MAS NMR (^{29}Si, ^{31}P and ^{27}Al), TEM, XPS, FTIR, ICP analyses has also been reported.

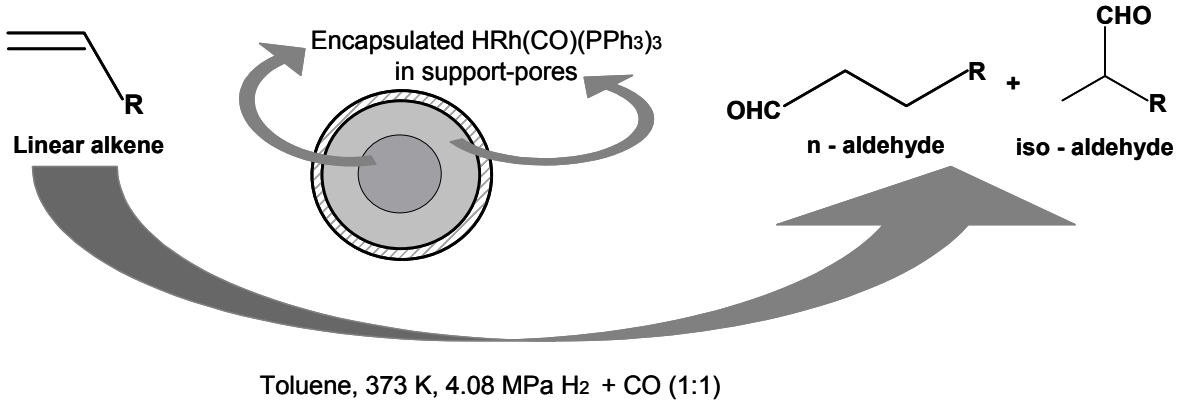

Scheme 3.1. Hydroformylation of olefins using $HRh(CO)(PPh_3)_3$ encapsulated supports

It is expected that the metal complexes encapsulated in zeolites and mesoporous supports lead to very high metal dispersion and stable catalysts [19]. Similarly, the zeolite microstructure could prevent leaching of metal complexes in solution, a serious problem with most of the "heterogenized" catalysts. The performance of the catalysts with respect to these issues has been discussed.

3.2. EXPERIMENTAL SECTION

3.2.1. MATERIALS

The materials required for zeolite Na–Y preparation were: Sodium silicate (Loba, India) as silica source, sodium aluminate ($NaAlO_2$), aluminium sulfate ($Al_2(SO_4)_3.16H_2O$) as aluminium sources and sodium hydroxide (all procured from S. D. Fine Chem, India). In the syntheses of MCM-41 and MCM-48 materials, fumed SiO_2 (380 m^2g^{-1}, Aldrich) as a silica source, cetyl trimethyl ammonium bromide (CTABr, Aldrich), as a templates and dodecaphosphotungstic acid (PTA, Aldrich) as a promoter to accelerate the syntheses, were used. De-ionized water was used throughout the syntheses of zeolite Na-Y and mesoporous

materials. Rhodium Chloride ($RhCl_3$. $3H_2O$, 40% Rh, Aldrich), sodium borohydride ($NaBH_4$, s. d. Fine Chem), triphenyl phosphine (PPh_3, Aldrich), ethanol (EtOH, 99.9%, BDH, UK) and formaldehyde solution (37% HCHO, S. D. Fine Chem) were used for the synthesis of $HRh(CO)(PPh_3)_3$ complex. Hydrogen and nitrogen gases supplied by Indian Oxygen Ltd. Bombay, and carbon monoxide (> 99.8% pure, Matheson Gas Co., U.S.A.) were used directly from cylinders. The syngas mixture (with 1:1 ratio of H_2 + CO) was prepared by mixing H_2 and CO in a reservoir.

3.2.2. SYNTHESES

Syntheses of zeolite Na-Y, mesoporous MCM-41 and MCM-48 materials, $HRh(CO)(PPh_3)_3$ complex, as well as supported, encapsulated and anchored $HRh(CO)(PPh_3)_3$ complex in zeolite Na-Y, MCM-41 and MCM-48 materials have been discussed in the following sections.

3.2.2.1. Zeolite Na–Y and encapsulated Wilkinson's complex $HRh(CO)(PPh_3)_3$ in Na–Y

In a typical synthesis of zeolite Na-Y [34], seed crystals of zeolite Na–Y were prepared separately from an aqueous mixture of Na_2SiO_3 (95 mmol, 28% SiO_2 and 8.4% Na_2O), $NaAlO_2$ (9.76 mmol, 43% Al_2O_3, 39% Na_2O), NaOH (70 mmol) and 10 mL H_2O by stirring for 1 h and keeping it to rest for 18 h. The seed crystals of zeolite Na–Y thus prepared were then added to aqueous solution of Na_2SiO_3 (355 mmol). Subsequent addition of $NaAlO_2$ (34.2 mmol), NaOH (92.5 mmol), $Al_2(SO_4)_3.16H_2O$ (6.02 mmol) and 35 mL H_2O was followed under constant stirring for 2 h. The overall initial gel composition of the zeolite Na-Y was 5.05 SiO_2: Al_2O_3: 5.46 Na_2O: 111.58 H_2O. $HRh(CO)(PPh_3)_3$, prepared as reported earlier by Evans *et al*.,[11] (~ 0.135 mmol) was then dissolved in 30 mL EtOH and the solution finally added to the zeolite Na–Y gel under stirring for 1 h; pH of the final gel was 13.1. The choice of *ethanol* as the solvent was made considering the complete miscibility with water and hence, also with the ethanolic solution of the Rh-complex in the aqueous gel of the zeolite. The mixture of $HRh(CO)(PPh_3)_3$ – zeolite gel was then sealed in a polypropylene bottle and kept in an oven at 373 K for 12 h under autogenous pressure. The samples were then filtered and washed several times with de-ionised water, dried at 353 K and soxhlet

washed twice with dry toluene to ensure that no free complex was adhered to the encapsulated zeolite (*labeled as **Wk–Y***).

*Henceforth, we have labelled all the encapsulated catalysts by the term '**Wk**' as an abbreviation for the Wilkinson's catalyst/complex, $HRh(CO(PPh_3)_3$.*

3.2.2.2. Supported $HRh(CO)(PPh_3)_3$ on zeolite Na–Y (by impregnation)

Supported $HRh(CO)(PPh_3)_3$ on zeolite Na–Y was prepared by suspending 3 g of Na–Y in ethanolic solution containing 0.135 moles of the complex and refluxing it at 363 K for 18 h. The light yellow solid was filtered and dried at 353 K and used as such (*labeled as **Wk–Y–S***) for analysis by ^{31}P CP–MAS NMR spectra and hydroformylation reactions.

3.2.2.3. Synthesis of Si–MCM–41 and Si–MCM–48

Following a procedure reported earlier [35], Si–MCM–41 and Si–MCM–48 were synthesized having initial gel compositions of SiO_2–0.32NaOH–0.2CTABr–125H_2O–0.0033PTA and SiO_2–0.4NaOH–0.21CTABr–120H_2O–0.0033PTA respectively (PTA = phosphotungstic acid). In a typical synthesis of MCM-41, 50 mmol of fumed SiO_2 was added to a solution of 16 mmol NaOH in 25 mL H_2O and stirred for 1 h. To this mixture, 10 mmol of CTABr was added drop-wise followed by an addition of 0.165 mmol of PTA (as a promter) in 37 mL of H_2O. The final gel was stirred for another 1.5 h and then autoclaved in polypropylene bottle at 373 K for 4 h. The as-synthesized sample was then filtered, washed repeatedly with de-ionizedwater and air calcined at 813 K to obatin calcined Si–MCM–41.

In the synthesis of MCM-48, 50 mmol of fumed silica was added to a solution of 20 mmol NaOH in 25 mL H_2O and stirred for 1 h. To this mixture, 10.5 mmol of CTABr was added drop-wise followed by an addition of 0.165 mmol of PTA (as a promoter) in 33 mL of H_2O. The final gel was stirred for another 1.5 h and then autoclaved in a teflon-lined stainless steel autoclave at 423 K for 12 h. The as-synthesized sample was then filtered, washed repeatedly with de-ionized water and air calcined at 813 K to obtain calcined Si–MCM–48.

3.2.2.4. Synthesis of $HRh(CO)((PPh_3)_3$ complex

$HRh(CO)((PPh_3)_3$ complex was prepared according to the method described by Ahmad et. al. [36]. To a refluxing solution of triphenylphosphine (13.1 g) in 100 ml distilled

ethanol, was added in rapid succession a solution of rhodium trichloride trihydrate (1.15 g) in 100 ml ethanol, 50 ml of aqueous formaldehyde (40% w/v) and then a solution of potassium hydroxide (3 g) in 100 ml hot ethanol. The mixture was refluxed for 15 minutes and allowed to cool to room temperature. The yellow crystals obtained were filtered, washed with ethanol, water and hexane, in succession and finally dried under vacuum. Yield was 3.8 g. The product thus obtained, was characterized by FT-IR and ^{31}P CP-MAS NMR spectra.

3.2.2.5. Functionalization of Si–MCM–41, Si–MCM–48 by APTS and anchoring of $HRh(CO)(PPh_3)_3$ complex inside the mesopores.

Functionalization of Si–MCM–41 and Si–MCM–48 was done by a procedure reported earlier by Mukhopadhyay et al. [37]. 1.0 g of Si–MCM–41 or Si–MCM–48 was suspended in 30 ml of dry dichloromethane (DCM) and to this 0.142 mmol of dichlorodiphenylsilane (Ph_2SiCl_2, Fluka) was added and the mixture stirred for 1 h. The contents were then cooled to 195 K and 5.73 mmol of 3-aminopropyltrimethoxysilane (APTS, Aldrich) was added drop wise to this slurry, stirred for further 24 h at 313 K. The contents were filtered, washed repeatedly with dry DCM and dried in vacuum to get functionalized MCM–41 and MCM–48 supports.

To prepare the anchored $HRh(CO)(PPh_3)_3$ catalysts in MCM–41 and MCM–48, 1.0 g of the functionalized support (MCM–41 or MCM–48) was added to a solution containing the Rh-complex (~ 0.108 mmol) in 100 ml of dry, distilled ethanol and stirred for 16 h at room temperature. The light yellow solid powder was then washed several times with dry ethanol, soxhlet-extracted once with EtOH to remove any Rh-complex adhered to the support walls, then dried and stored under vacuum. The catalysts thus prepared (*labeled as* ***Wk–M41*** *and* ***Wk–M48***), were used as such for hydroformylation reactions. Some important physical characteristics of all the three encapsulated catalysts are presented in Table 3.1.

In a similar fashion, we also prepared $HRh(CO)(PPh_3)_3$ tethered to the external surfaces of APTS grafted MCM-41 and MCM-48 without Ph_2SiCl_2 treatment (labeled as ***Wk–M41–S*** *and* ***Wk–M48–S***). These materials were used for comparison of the TEM images and hydroformylation reaction data (especially to compare the TEM patterns for Rh-complex grafted on/in the supports and Rh-leaching in the reaction mixture using ***Wk–M48–S***) with those of the encapsulated catalysts (Wk–M41 and Wk–M48). The comparison has been

discussed in detail in later section of this chapter (see Section 3.3.1.6). *For the sake of simplicity, the word '**encapsulated**' has been used through out the text in case of $HRh(CO)(PPh_3)_3$ anchored to the amine functionalized mesoporous supports*.

This unique approach of passivation of the external-surface silanol groups (Si–OH) of the mesoporous materials by reacting with controlled amount of Ph_2SiCl_2 and subsequent treatment with APTS for selective functionalization of the inner-surface Si–OH groups of the mesoporous matrices was reported earlier by Shephard et al. [38]. The silylation reaction between Ph_2SiCl_2 and the external-surface Si–OH groups deactivated the silanol groups. Thus, the treatment of Ph_2SiCl_2 with the mesoporous materials compelled anchoring of APTS as well as Rh-complex selectively inside the mesopore channels.

3.2.3. HYDROFORMYLATION REACTION SET-UP

All the hydroformylation reactions were carried out in a 50 ml capacity micro-reactor, supplied by Parr Instrument Company, USA. The reactor was provided with arrangements for sampling of liquid and gaseous contents, automatic temperature control and variable agitation speeds. The reactor was designed for a working pressure of 3000 psi and temperature up to 523 K. A safety rupture disk was also fitted to the reactor. The consumption of CO and H_2 at a constant pressure was monitored by observation of the pressure drop in the gas reservoir, from which (CO + H_2) mixture was supplied through a constant pressure regulator at 1:1 ratio. The pressure in the reservoir was recorded using a pressure transducer to follow the consumption of (CO + H_2) as a function of time. The schematic diagram of the experimental set up is shown in Scheme 3.2.

3.2.4. HYDROFORMYLATION EXPERIMENTAL PROCEDURE

In a typical experiment, known amount of olefin with degassed toluene (as a solvent) and heterogenized catalyst were charged into the reactor and the contents flushed with nitrogen and then with a mixture of 1:1 CO and H_2. The contents of the reactor were heated to a desired temperature, and then a mixture of CO and H_2 (1:1) was introduced slowly into the autoclave up to a desired pressure. A sample of the liquid phase mixture was withdrawn and the reaction started by switching the stirrer on. The reaction was then continued at a constant pressure of CO and H_2 by supplying CO/H_2 mixture as per consumption, from the

reservoir vessel using a constant pressure regulator. *Hydroformylation experiments should be performed with utmost care and precautions as it involves use of CO and H_2 at high pressures.*

1. Reactor 2. Stirrer shaft 3. Impeller 4. Cooling water 5. Sampling valve 6. Magnetic stirrer 7. Electric furnace

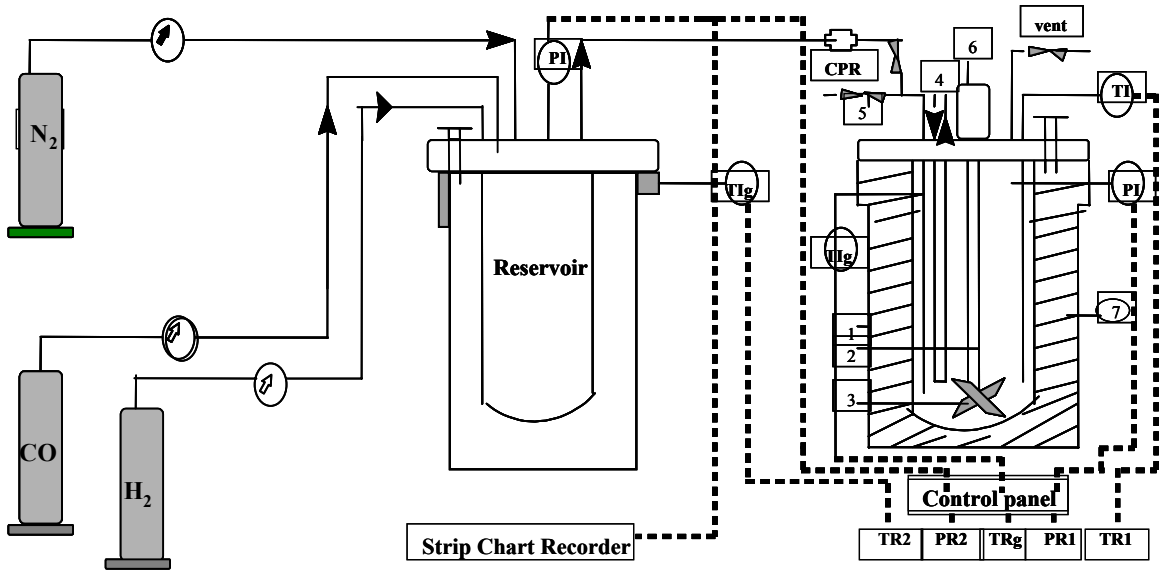

TI: Thermocouple PI: Pressure transducer TIg: Thermocouple for gas N_2:Nitrogen cylinder H_2:Hydrogen cylinder CO: Carbon monoxide cylinder PR: Pressure regulator CPR: Constant pressure regulator TRg: Gas temperature indicator PR2: Reservoir pressure indicator TR2: Reservoir temperature indicator TR1: Reactor temperature indicator PR1: Reactor pressure indicator

Scheme 3.2. A schematic of the hydroformylation reactor set-up

3.2.5. CATALYST LEACHING AND RECYCLE EXPERIMENTS

Catalyst leaching experiments were performed by hot filtration of the reaction mixture at 373 K and subsequently testing the catalytic activity of the filtrates for hydroformylation without addition of fresh catalyst. These solutions and the catalysts thus recovered were also analysed for determination of Rh-content by ICP–AES (inductively coupled plasma with atomic emission spectra) analyses. In a typical catalyst recycle experiment, the heterogeneous catalyst was allowed to settle down and the clear supernatant liquid was decanted slowly. The residual solid catalyst was re-used with fresh charge of

solvent and reactants for further recycle runs maintaining the same reaction conditions. In the recycle studies, the rhodium content of the catalyst and subsequent hydroformylation reaction mixtures were analysed for metal content as well as metal leaching.

3.3. RESULTS AND DISCUSSIONS

3.3.1. CHARACTERIZATION OF CATALYSTS

The porous supports and the heterogeneous catalysts Na–Y, MCM–41, MCM–48, Wk–Y, Wk–Y–S, Wk–M41 and Wk–M48 thus prepared were characterized using ^{31}P CP–MAS NMR, Fourier Transform Infrared (FT-IR) Spectroscopy, X-ray Photoelectron Spectroscopy (XPS) measurements and Powder X-ray Diffraction (XRD). For Scanning electron microscopy (SEM), the crystalline supports were suspended in isopropanol, casted on gold plated discs followed by drying under vacuum and then were imaged on a Philips XL 30 instrument. Specific surface area of the catalyst was determined by the BET method using N_2 adsorption measured on an Omnisorb CX–100 Coulter instrument. Prior to adsorption, the catalyst was activated at 423 K for 6 h at 10^{-4} Torr pressure. Inductively coupled plasma with atomic emission spectra (ICP-AES) analyses of the heterogenized catalysts (before and after reactions) as well as reaction mixtures after hydroformylation reaction were performed in a Perkin Elmer 1200 instrument for determination of metal content. Gas chromatography (GC) of the reactants and products was performed in a HP 5890 instrument fitted with a FFAP capillary column.

3.3.1.1. ^{31}P CP–MAS NMR SPECTRA OF $HRh(CO)(PPh_3)_3$ COMPLEX

^{31}P CP–MAS (cross-polarized, magic angle spinning) NMR spectra of $HRh(CO)(PPh_3)_3$ complex and the Rh-complex inside the pores of Na-Y, MCM-41 and MCM-48 materials (shown in Figure 3.1) were obtained on a Bruker DRX 500 FT-NMR spectrometer at 202.64 MHz and 11.7 Tesla using 3 mm CP-MAS probe. The chemical shifts were referred to H_3PO_4 at 0 ppm and the spectra were collected at a spectral width of 20 kHz, with a flip angle of 45^o, 6000 real data points and 5 s relaxation delay.

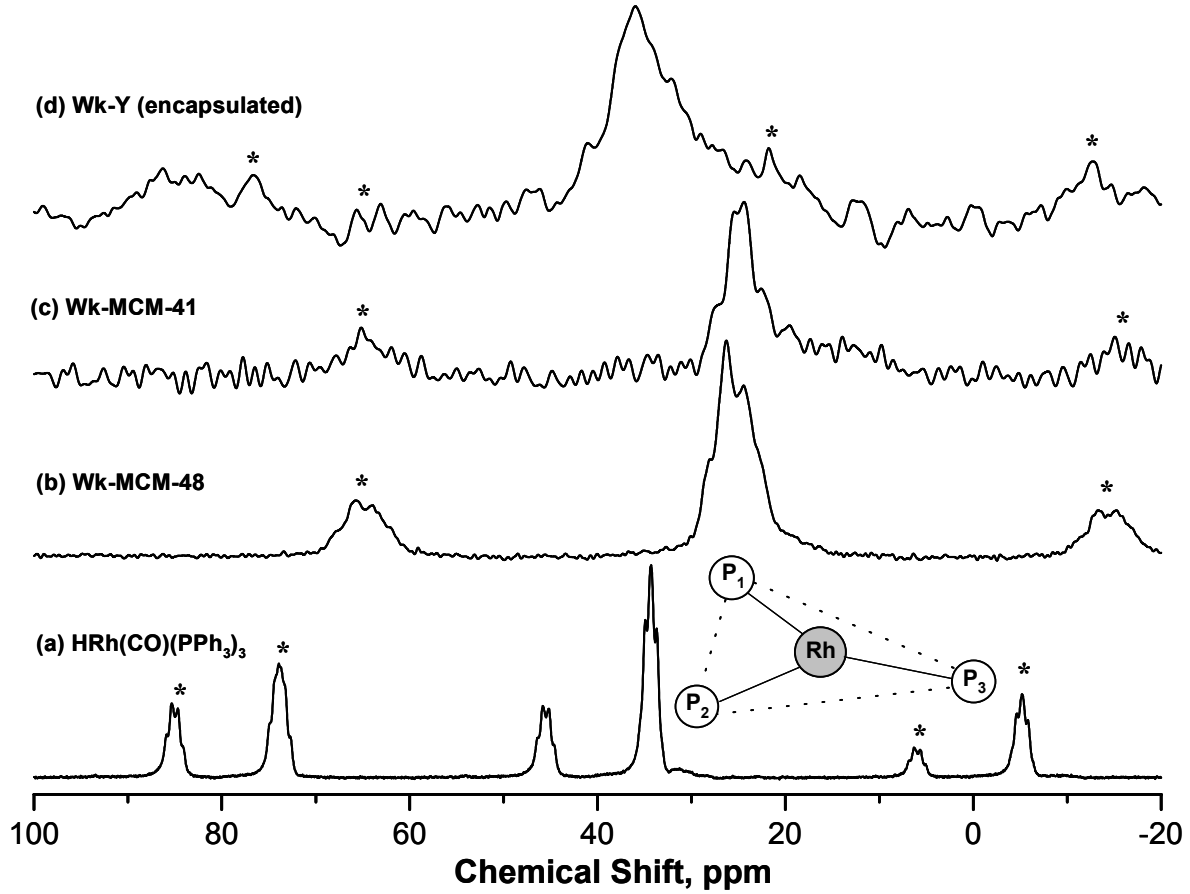

Figure 3.1. ^{31}P CP–MAS NMR spectra of different catalysts; inset of (a): trigonal plane of $HRh(CO)(PPh_3)_3$ comprising three phosphorus atoms (designated as P_1, P_2 and P_3) bonded to Rh atom, atoms are not to scale; * in NMR patterns denote sidebands at 8 KHz.

A coupled ^{1}H–^{31}P CP–MAS NMR spectra of the pure $HRh(CO)(PPh_3)_3$ complex shows two major ^{31}P peaks (δ_{iso}= 34.4, 45.4 ppm), each split by J-coupling to other ^{31}P and ^{103}Rh (n = 100%) nuclei (see Figure 3.1 (a)). Since, dipolar and anisotropic part of the J couplings are averaged to zero by magic angle spinning, the observed multiplet structure arises due to the isotropic P-P and P-Rh scalar couplings [39]. We observed that the chemical shift difference for the two major signals (δ_{iso}= 34.4, 45.4 ppm) is larger than the P-P scalar couplings and the integrated intensity for these major signals is in the ratio of 2:1. The three phosphorus atoms in $HRh(CO)(PPh_3)_3$ complex may be grouped into one distinct (P_3) and two equivalent (P_1 and P_2) environments (see '*inset*' of Figure 3.1 (a)). For the distinct P_3-atom, the coupling to two equivalent phosphorus (P_1 and P_2) nuclei by P-P coupling ($J_{P\text{-}P}$ =

127.5 Hz) and to rhodium by P-Rh coupling ($J_{P\text{-}Rh}$ = 142.3 and 140.6 Hz) causes the observed multiplet in the intensity ratio of 1:3:3:1. Similarly, the equivalent P_1- P_2 atoms are split into a doublet by the distant P_3-atom, further split by coupling to rhodium to give a doublet of a doublet. However, since $| J_{P\text{-}P} - J_{P\text{-}Rh}| < \Delta\nu$ ($\Delta\nu$ is the MAS line width), we observe only a triplet. Based on the observed $J_{P\text{-}P}$ values, the three phosphorus atoms are expected to be in a plane with P-Rh-P angle ~ 120°, which lead to a structure with least strain from the three bulky PPh_3 groups. Due to random orientations of the nine-phenyl groups in the Rh-complex, all the atoms in the molecule become crystallographically non-equivalent, as also noticed by the X-ray crystal structure [40, 41].

Assignments for the three phosphorus atoms (P_1, P_2, P_3) can be made based on the P-Rh-CO bond angle [40, 42], which shows a larger difference compared to the P-Rh bond distances. Compared to the P_1 and P_2 atoms, the P_3 atom has a larger bond angle that results in a better overlap of the bonding orbital hence, the electronegative effect of CO would be felt more on the P_3 atom to cause a downfield shift, which we indeed observe. Thus, the P_3 atom can be assigned to the low-field multiplet and P_1 and P_2 atoms as the high-field triplets in our observed spectra. The ^{31}P CP-MAS results clearly show that $HRh(CO)(PPh_3)_3$ complex has a *distorted* trigonal bipyramidal (TBP) structure (local symmetry tends towards C_s instead of C_{3v}) in which the three phosphorus atoms lie in the basal plane (this is in perfect agreement with the spectral analysis [39] and crystal structure [40, 41] reported earlier).

3.3.1.2. ^{31}P CP–MAS NMR AND FTIR SPECTRAL ANALYSIS

To validate that $HRh(CO)(PPh_3)_3$ complex was encapsulated in zeolite Na–Y, mesoporous MCM-41 and MCM-48 materials, *solid-state* ^{31}P CP–MAS NMR spectra of the encapsulated catalysts (Wk–Y, Wk–M41 and Wk–M48) were recorded and compared with the spectra obtained for pure $HRh(CO)(PPh_3)_3$ complex.

The ^{31}P CP-MAS spectra of Wk-M41 and Wk-M48 samples (see Figures 3.1-b and 3.1-c) showed a marked difference in chemical shifts when compared with the pure Rh-complex. The upfield shifts for Wk-M41 (δ_{iso}= 25.4 ppm) and Wk-M48 (δ_{iso}= 26.0 ppm) in comparison to the Rh-complex (δ_{iso}= 34.4, 45.4 ppm) suggests that there is a definite coordination between N_{APTS} and Rh-atom. APTS (anchored inside the mesopores walls of MCM-41 and MCM-48) when bound with the Rh-complex, donates the electron pair from

N_{APTS} to the Rh-atom (see Figure 3.7), which in turn increases the electron density on the P_{PPh3} atoms (of the complex) by a $(d\pi)_P - (d\pi)_{Rh}$ bonding, a fact that we observed earlier for anchored Pd-phosphine complex in mesoporous systems [37]. It was indiscernible to classify the ^{31}P splitting for Wk-M48 or Wk-M41 based on J-coupling since, the splitting as well as the line broadening were much larger than the J_{P-P} or J_{P-Rh} observed for the Rh-complex. This may be either due to: (1) the change in geometry from the *distorted* TBP (trigonal bipyramidal) of $HRh(CO)(PPh_3)_3$ molecule to an octahedral one due to coordination of the N_{APTS} and Rh atoms, or (2) loss of a PPh_3 atom from the complex while anchoring in the mesopores walls. Possibility of having two resonances in 1:2 ratio similar to the neat Rh-complex is unlikely even if there are three PPh_3 groups attached to the Rh-atom, since, crystallographic non-equivalence and retention of the original structure of Rh-complex anchored inside the mesopores-walls is no longer viable [43]. The fact we did not observe any spectral line for free PPh_3 ligand in the filtrate-solutions after filtration of the solid catalysts (δ_{iso} = –3.5 ppm by ^{31}P-$CDCl_3$ spectra) indicates that coordination of the Rh-complex with the APTS tethered MCM-materials does not proceed through cleavage of a PPh_3 ligand from the Rh-complex (a fact well known for the dissociation of the Rh-complex in solution during hydroformylation reactions). This further strengthens our presumption based on the change in the TBP geometry due to N_{APTS}–Rh-complex coordination. In case of subsequent loss of one PPh_3 atom and addition of N_{APTS} atom to Rh, we would have obtained spectra similar to bis(triphenylphosphine) rhodium complex [43, 44]. In contrast, we see quite different spectra for the encapsulated Wk–M41 and Wk–M48 catalysts wherein, the broad spectral line appears at one place with a complex splitting pattern. In this context, we refer to a report by Lindner *et al.* [45] wherein, it has been shown that ^{31}P CP-MAS spectra of the Rh-triphosphanyl complex bound to a polysiloxane matrix gives rise to a broad spectral line with complex patterns, similar to the spectral patterns observed in this work (see Figure 3.1). The Rh-phosphanyl complex attached inside the polymer-matrix has an octahedral geometry, which is similar to the Rh-complex bound to Wk–M41 and Wk–M48 catalysts.

Thus, on the basis of the inferences obtained herein, a plausible reason for the absence of the Rh-complex multiplet peak in the $HRh(CO)(PPh_3)_3$ complex anchored inside the mesopores of MCM-41 and MCM-48 samples, ushers a change in geometry from TBP to

octahedral.

Interestingly, the $^{1}H–^{31}P$ CP–MAS NMR spectrum of catalyst Wk–Y (see Figure 3.1-d) showed a different pattern in chemical shift (δ_{iso}= 36.1, 47.1 ppm; signal to noise ratio was poor for this sample, hence weak spectral line is observed at 47.1 ppm). The changes in signal positions indicate a geometrical constraint in Wk–Y. To further ensure that the Rh-complex is encapsulated inside the faujasite (Na-Y) supercage in case of Wk–Y, a ^{31}P MAS experiment was performed for the Wk–Y–S sample. ^{31}P MAS spectrum of Wk–Y–S was taken in the Bloch decay mode with proton decoupling, since no $^{1}H–^{31}P$ cross-polarization MAS spectrum for this sample was feasible, presumably due to high surface mobility of the physisorbed or chemisorbed species. Despite the somewhat poor spectra/noise for Wk–Y–S sample, a comparison of ^{31}P CP-MAS spectra of samples $HRh(CO)(PPh_3)_3$ and Wk–Y–S (spectra not shown) clearly show that the two major ^{31}P signals (δ_{iso}= 34.4, 45.8 ppm) are observed at nearly the same chemical shifts. A mere surface adsorption, rather than encapsulation, is envisaged in case of Wk–Y–S catalyst that consists of $HRh(CO)(PPh_3)_3$ impregnated on zeolite Na–Y. Both these observations suggest that in case of Wk–Y, a possible encapsulation of $HRh(CO)(PPh_3)_3$ in the supercage of Na–Y zeolite has occurred (see Figure 3.8).

FTIR (transmittance-mode) spectra were performed on a Bio-Rad instrument for detecting the Rh–CO and Rh–P bands [42] of the Rh-complex and the encapsulated catalysts (see Figure 3.2 and Table 3.2). FTIR spectra of the Rh-complex (1922 cm^{-1} for symmetric CO band and 1995 $cm^{-}1$, 2030 cm^{-1} for asymmetric CO bands, 514 cm^{-1} for metal phosphorus band) and Wk–Y catalyst (1930 cm^{-1}, 513 cm^{-1}; spectra not shown here) revealed almost similar $\nu_{Rh–CO}$ and $\nu_{Rh–P}$ respectively. In contrast, a typical FTIR spectra of Wk–M41 catalyst showed distinguishable $\nu_{Rh–CO}$ bands at 1965 cm^{-1}, 1984 cm^{-1} and $\nu_{Rh–P}$ band at 518 cm^{-1} respectively; an increase in electron density on the Rh–CO and Rh–P due to N_{APTS}–Rh coordination might be a plausible reason for these changes. Broad bands at 3430 cm^{-1} were also observed in the IR spectra of the Wk–M41 catalyst, which probably is due to $\nu_{Rh–NH2}$ frequency, ofcourse, an overlap of this band with that of the un-tethered surface-silanol groups (ν_{OH}) lying in the same frequency range is also not over-ruled.

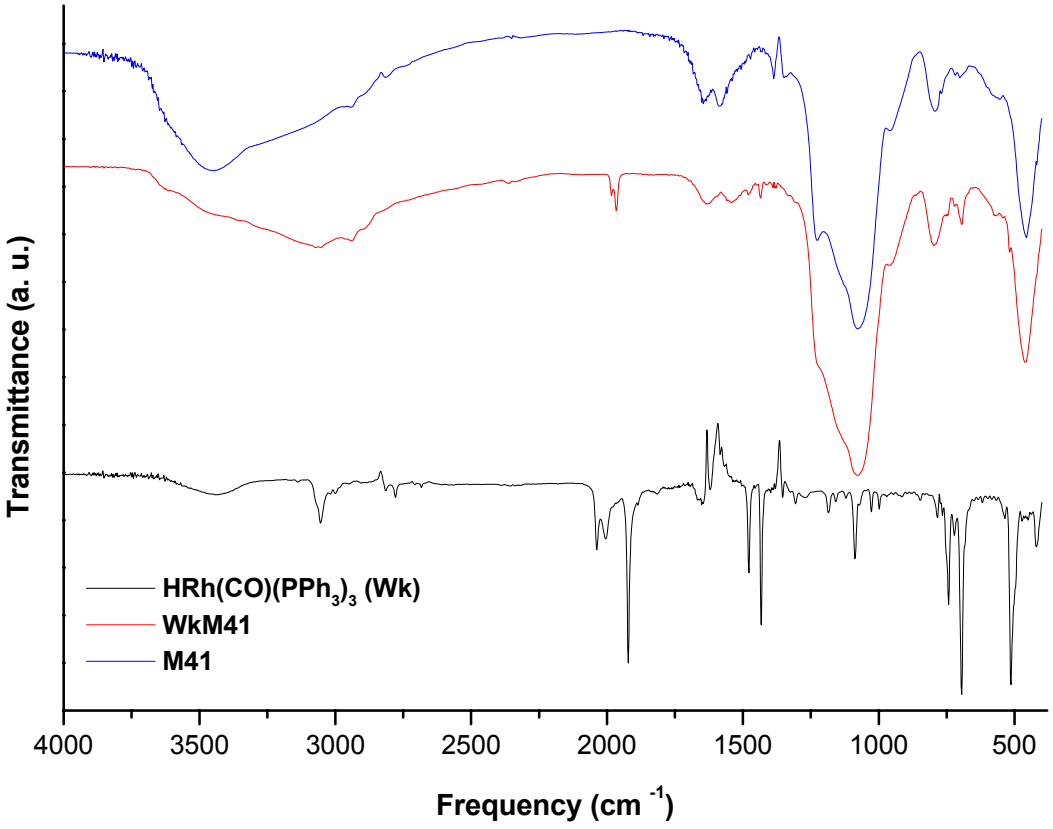

Figure 3.2. FTIR spectra of $HRh(CO)(PPh_3)_3$, Wk-M41 and MCM-41 catalyst supports

3.3.1.3. ^{29}Si AND ^{27}Al MAS NMR SPECTRAL ANALYSIS

^{29}Si and ^{27}Al MAS NMR spectra (at 99.44 MHz and 130.42 MHz respectively at 11.7 Tesla) of Wk–Y confirmed that the framework Si/Al ratio [46, 47] remained the same (2.37) as that of zeolite Na–Y used here thus, showing that the framework structure is intact after encapsulation (see Figure 3.3). In the ^{29}Si MAS NMR spectra of Wk–Y, Q^4 (nAl wherein n = 0, 1, 2, 3) environments were detected in Na–Y as well as Wk–Y, further suggesting that the Al site distributions and population remain unaltered. The ^{27}Al MAS NMR in case of Wk–Y confirms that all Al or most of the Al atoms were in the tetrahedral framework environment [47] and not replaced by Rh atoms (see Figure 3.3).

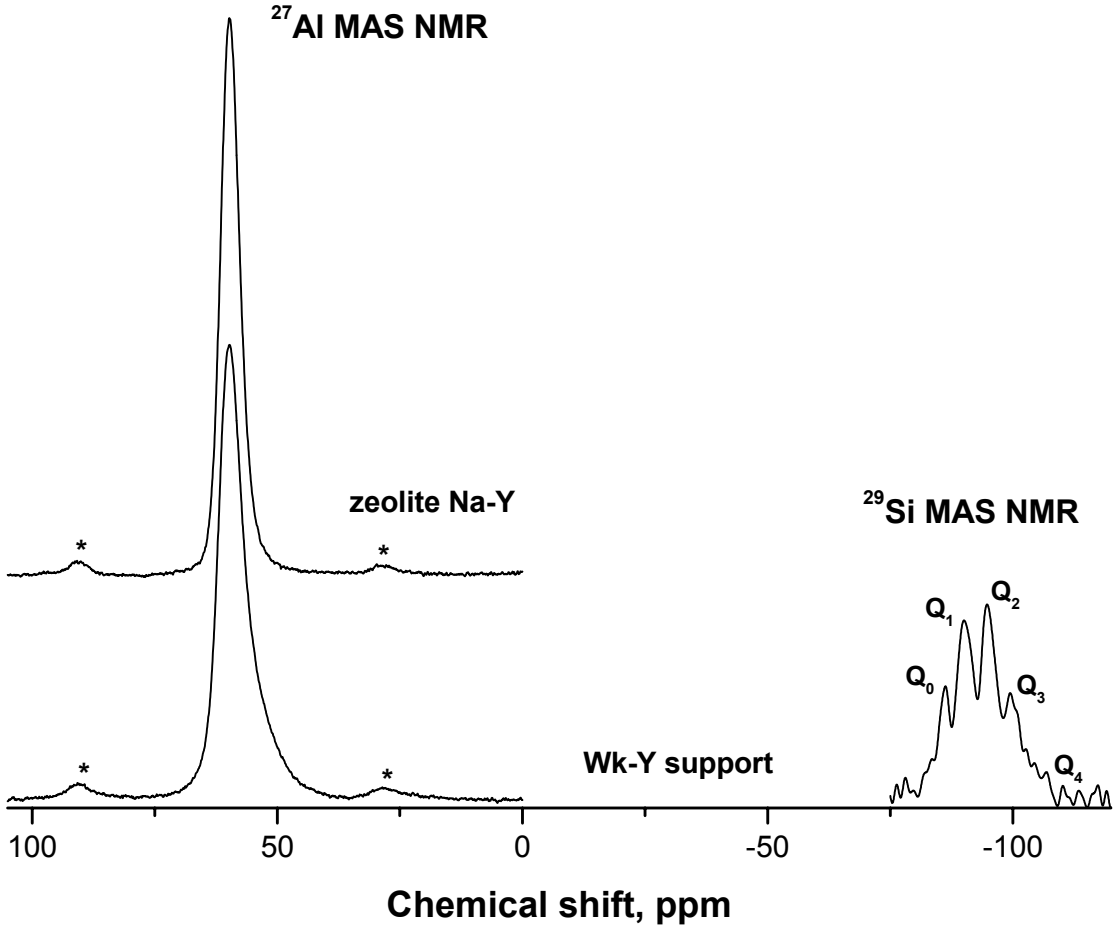

Figure 3.3. ^{27}Al and ^{29}Si MAS NMR spectra of zeolite Na–Y and Wk–Y supports (* in NMR patterns denote sidebands at 4 KHz)

^{29}Si MAS NMR spectra of Wk–M41 and Wk–M48 (spectra not shown) revealed almost no variations in the Q^3 ($(SiO)_3{\equiv}Si–OH$) and Q^4 ($(SiO)_3{\equiv}Si–O–Si{\equiv}$) chemical shifts [35] ($\delta$ = –100 ppm and –110 ppm respectively) although, there was a substantial change observed in the Q^3/Q^4 ratio (see Table 3.1). A possible reason for the lower Q^3/Q^4 values might be the decrease in population of the free silanol groups of the Q^3 species due to the linkage arising from anchoring of APTS with the silanol groups (of the Q^3 species) present in the mesoporous materials. This further confirmed that the meso-structures of Wk–M41 and Wk–M48 were intact even after encapsulation of the Rh-complex in the mesoporous materials.

3.3.1.4. X–RAY PHOTOELECTRON SPECTRA (XPS) ANALYSIS

XPS of the samples were recorded in VG Microtech-ESCA 3000 spectrometer, applying vacuum at 10^{-10} torr, pass energy of 50 eV and using un-monochromatized Mg–K_α as the radiation source (photon energy of 1253.6 eV). Surface analyses by XPS spectra was carried out quantitatively in terms of the binding energy (B. E.) values of various elements present in the catalyst supports after necessary C 1s correction, especially taking into consideration of the Rh $3d_{5/2}$ and $3d_{3/2}$ B. E. values for the catalysts Wk–Y, Wk–M41 and Wk–M48 (see Figure 3.4).

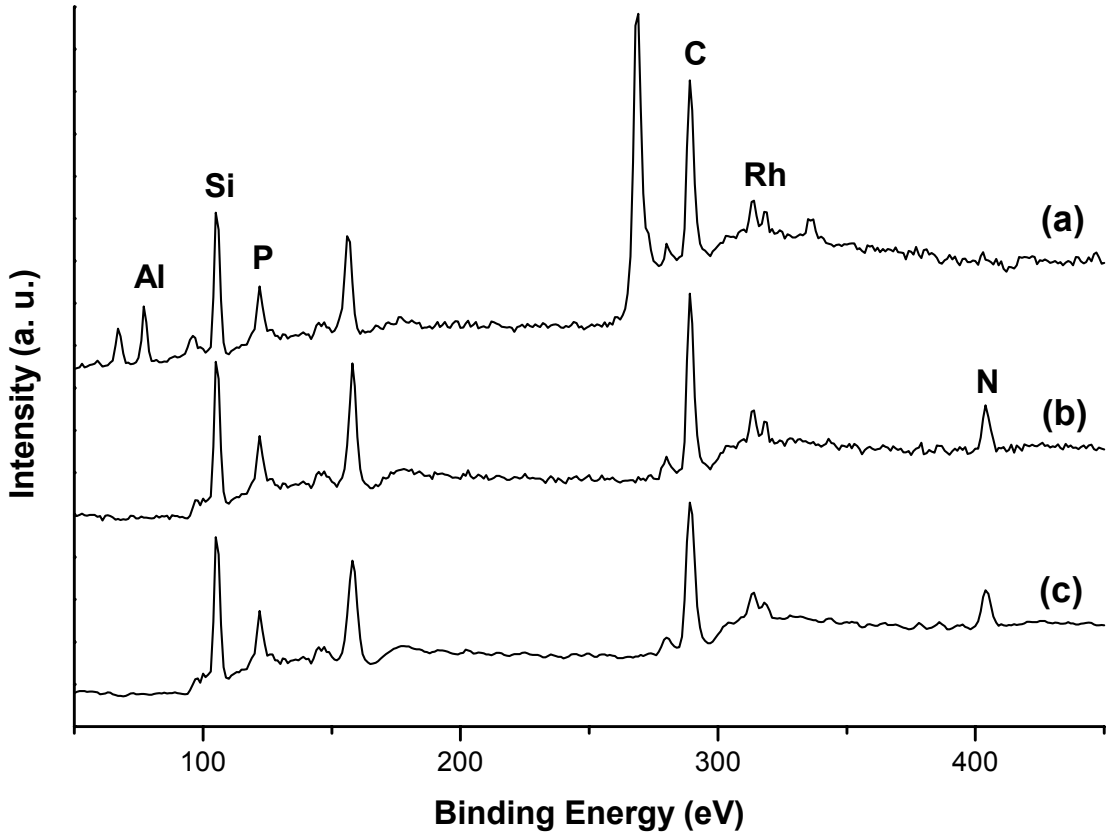

Figure 3.4. X-ray photoelectron spectra of (a) Wk–Y, (b) Wk–M41 and (c) Wk–M48 supports

XPS of these catalysts were also performed after hydroformylation reactions in order to record any change observed in the oxidation states or B. E. values of the elements present in the supports during the reaction and these were found to be in compliance with the

literature values [48]. The B. E. values of the supports before and after hydroformylation reactions were almost similar, which proves essentially that all rhodium was present as Rh (I) in the encapsulated materials and the oxidation state remained unaltered even after the reactions (Table 3.1).

Table 3.1. XPS binding energy values[§] for different elements present in various encapsulated catalysts before (B) and after (A) hydroformylation of styrene

Elements / Supports	Al	Si	P	Rh ($3d_{5/2}$, $3d_{3/2}$)	N
Wk–Y–B	74.8	102.7	126.9	310.2, 314.8	–
Wk–Y–A	74.7	102.8	127.0	310.3, 314.8	–
Wk–M41–B	–	103.3	127.2	309.3, 313.8	400.2
Wk–M41–A	–	103.3	127.3	309.6, 314.0	400.1
Wk–M48–B	–	103.3	127.1	309.5, 314.1	400.1
Wk–M48–A	–	103.3	127.2	309.7, 314.2	400.1

[§]All the values were corrected to C 1s with binding energy of 285 eV using adventitious carbon.

The silicon, phosphorus, rhodium (I), aluminium (incase of Wk–Y, Figure 3.4 (a)) and nitrogen (incase of Wk–M41 and Wk–M48, Figures 3.4 (b) and (c)) present in various supports showed no change in their B. E. values. A slight decrease in B. E. values of rhodium (I) (by 1 eV) was observed for Wk–Y in contrast to Wk–M41 or Wk–M48. This might be due to the different immobilization procedures used for $HRh(CO)(PPh_3)_3$ encapsulation inside the pores of zeolite Na–Y and mesoporous MCM-41 and MCM-48 materials. During the synthesis of catalyst Wk–Y, the encapsulation of $HRh(CO)(PPh_3)_3$ might have caused removal of some of the sodium cations from the zeolitic sites to accommodate the Rh complex in the supercage by a *ship-in-a-bottle* fashion. In the case of Wk–M41 and Wk–M48 catalysts, the Rh-complex was anchored inside the mesopore walls by tethering to amino group bonded to the silica matrices. In the latter case (the mesoporous systems), we presume that an ionic interaction rather than a covalent one accounted for the decrease in rhodium (I) binding energy values (B. E. values of Rh $3d_{5/2}$: 310.2, 309.3 and 309.5 for Wk–

Y, Wk–M41 and Wk–M48 respectively). This further showed that the integrity of the $HRh(CO)(PPh_3)_3$ complex was retained when encapsulated in the supports and that all the rhodium was present as Rh(I) with no beam damage suffered by the encapsulated supports.

3.3.1.5. POWDER X–RAY DIFFRACTION (XRD) ANALYSIS

Powder XRD of the encapsulated catalysts and supports were obtained at room temperature on Rigaku D MAX III VC diffractometer using Ni-filtered Cu K_α radiation, λ = 1.5404 Å. In case of MCM–41, MCM–48, Wk–M41 and Wk–M48, observable 2 θ ranges were from 1.5° and 10° at a scan rate of 1°/min and for zeolite Na-Y and Wk-Y, observable 2 θ ranges were from 5° and 50° at a scan rate of 8°/min. A comparison of the bare supports (Na–Y, MCM–41 and MCM–48) and $HRh(CO)(PPh_3)_3$ encapsulated catalysts (Wk–Y, Wk–M41 and Wk–M48) by powder XRD has been presented in Table 3.2 and Figure 3.5.

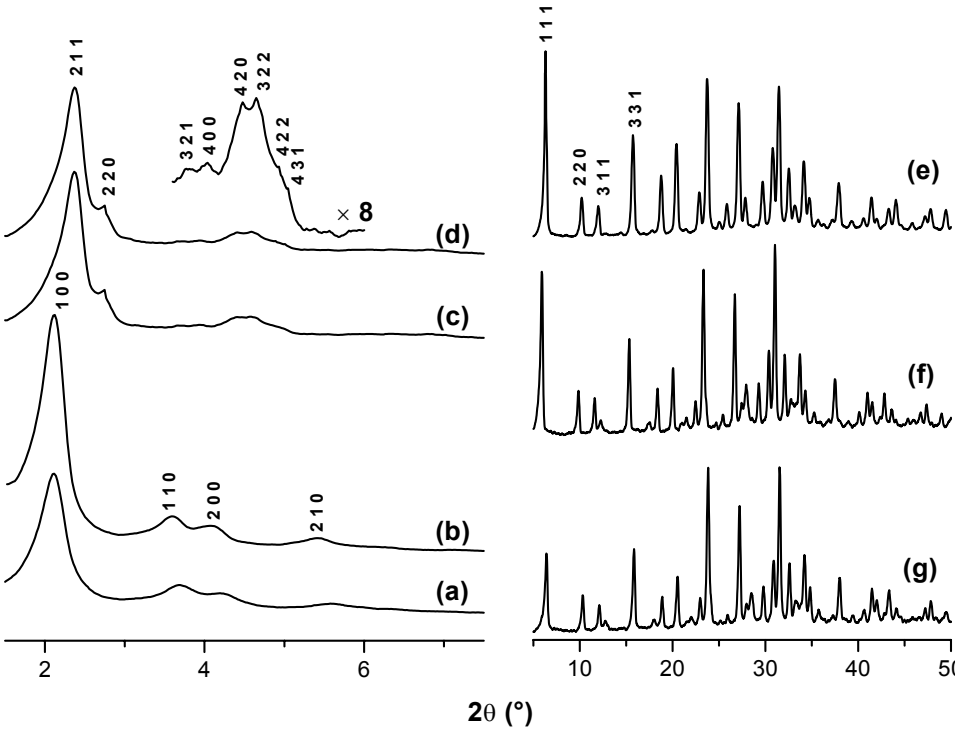

Figure 3.5. Powder X-ray diffraction patterns of (a) Wk–M41, (b) MCM–41, (c) Wk–M48, (d) MCM–48, (e) Na–Y; (f) Wk–Y–S and (g) Wk–Y.

This showed that the respective cubic (*Ia*3*d*) and hexagonal (*p6mm*) mesoporous phases [35] of MCM–41, Wk–M41, MCM–48 and Wk–M48 remain unaltered in peak

positions. The changes in respective intensities have been observed perhaps due to pore fillings of the $HRh(CO)(PPh_3)_3$ complex inside mesopores. Distinct Bragg reflections at {100}, {110}, {200} and {210} for MCM–41 and Wk–M41 (Figures 3.5 (a) and (b)) and at {211}, {220}, {321}, {400}, {420}, {332}, {422} and {431} for MCM-48 and Wk-M48 (Figures 3.5 (c) and (d)), further confirmed the restoration of the respective ordered patterns of the bare and the Rh-complex encapsulated mesoporous matrices without any breakdown of the meso-structures. In case of zeolite Na–Y and its impregnated and encapsulated analogues (Wk–Y–S and Wk–Y respectively), retention of the microporous phase zeolite Y was confirmed, though differences in the peak intensities were observed in case of Wk–Y sample (Figures 3.5 (e), (f) and (g)).

Table 3.2. Physical characteristics of the supports and the encapsulated catalysts

Materials	Rh (w/w %)	d_{hkl} (Å)[a]	a_o (Å)[b]	Surface area ($m^2\ g^{-1}$)	ν (cm^{-1})[c]	(Q^3/Q^4)[d]
Na–Y	–	14.29 (111)	24.75	735	–	–
Wk–Y–S	0.567	14.43 (111)	24.99	n. d.	n. d.	–
Wk–Y	1.130	14.48 (111)	25.08	n. d.	1930, 513	–
MCM–41	–	41.63 (100)	48.07	964	–	1.2 (0.32)
Wk–M41	0.747	41.83 (100)	48.30	n. d.	1965, 517	0.05
MCM–48	–	36.93 (211)	90.46	1210	–	0.8 (0.18)
Wk–M48	0.690	37.09 (211)	90.85	n. d.	1966, 518	0.05
$HRh(CO)(PPh_3)_3$	11.21	–	–	–	1922, 514	–

[a] calculated from powder XRD spectra ($n\lambda = 2d\sin\theta$; n = 1, λ = 1.5404 Å), values in '()' are respective principal Miller indices; [b] determined by: $a_o = d_{111} \times \sqrt{3}$ (zeolite Y supports); $a_o = d_{100} \times 2/\sqrt{3}$ (MCM-41 supports); $a_o = d_{211} \times \sqrt{6}$ (MCM-48 supports); [c] determined by FT–IR spectra; [d] as-synthesized samples, values in parentheses are for calcined samples (values determined from ^{29}Si MAS NMR spectra); deconvolution of Q^3 and Q^4 peaks were done using Jandel Scientific Peakfit program; n. d. = not determined

Earlier, with the aid of powder XRD, Quayle *et al.* [49] reported an empirically derived relationship as a possible explanation for the encapsulation of Fe (II) and Ru (II) complexes inside zeolite Na-Y by a term $I_{331} > I_{311} > I_{220}$ (where, '*I*' represents intensity). In our case however, we have not observed any such patterns, probably due to differences in the

encapsulation procedures (of the complex to be entrapped inside zeolite Na-Y). In contrast, we observed a marked decrease in the intensity of {111} diffraction pattern of Wk–Y as compared to Na–Y or Wk–Y–S (Figures 3.5 (e), (f) and (g)), which showed almost no difference in the peak intensities owing to random distribution of cations (due to impregnation) within the zeolite lattice (wherein, $I_{331} > I_{220} > I_{311}$). We presume that the noticeable decrease in the {111} intensity of the Wk–Y sample might have occurred due to possible incorporation of $HRh(CO)(PPh_3)_3$ complex inside the framework of zeolite Na-Y. But, it was confirmed by XRD that the porous framework of encapsulated supports (microporous as well as mesoporous) was not affected or damaged during the Rh-complex entrapment.

3.3.1.6. TRANSMISSION ELECTRON MICROSCOPY (TEM) ANALYSIS

TEM has been used extensively for structural elucidation of zeolites and mesoporous materials [23-25, 50]. Recently, to envisage three-dimensional structures of micro- and mesoporous solids, imaging nanoparticle catalysts inside mesoporous hosts and determine their occluded structure-directing organic species, high-resolution TEM was used as a convincing tool [37, 51]. In order to direct the location of the anchored Rh-complex inside the pores, we imaged the mesoporous MCM-41 and MCM-48, Ph_2SiCl_2–untreated Wk-M41-S and Wk-M48-S, microporous Na–Y and their encapsulated analogues (Wk–M41, Wk–M48 and Wk–Y) by TEM (Figure 3.6). The samples were dispersed in isopropanol, placed on holey carbon grids and a Jeol Model 1200 EX instrument operated at an accelerating voltage of 100 kV was used for imaging the samples. The TEM images of bare MCM–41 and MCM–48 were well consistent with the regular hexagonal and cubic mesophases respectively (Figure 3.6 (a) and (c); insets) with homogeneity in patterns throughout.

TEM images of Wk-M41-S and Wk-M48-S (Figure 3.6 (a) and (c)) indicate the presence of Rh-complex tethered by APTS (by a host-guest interaction) at the external surfaces of MCM-41 and MCM-48. In contrast, startling differences in the TEM images were observed when these images were compared with the Wk–M41 and Wk–M48 samples (Figure 3.6 (b) and (d)), wherein the Rh-complex has been encapsulated exclusively inside the mesopores by treating with Ph_2SiCl_2. A comparison of the images of Wk–M41–S and Wk–M48–S (see Figures 3.6 (a) and (c)) with those of Wk–M41 and Wk–M48 (Figure 3.6

(b) and (d)) showed 'clean' exterior surfaces of the latter ones with retention of strong image contrasts of the grafted Rh-complex inside the mesopores. The encapsulated samples prepared by treating with Ph_2SiCl_2 and further tethered with APTS, established that the Rh-complex is immobilized totally inside the mesopores and the distribution of the complex entrapped inside was very much uniform, unlike Wk–M41–S and Wk–M48–S materials (untreated with Ph_2SiCl_2, Rh-complex bound to the external mesopores-walls); a similar fact was observed by Shephard *et al.* [37] earlier. Thus, by TEM we could not only image the hexagonal and cubic patterns of the mesoporous materials, but also distinctly distinguish the internally bound Rh-complex to that of the externally grafted ones.

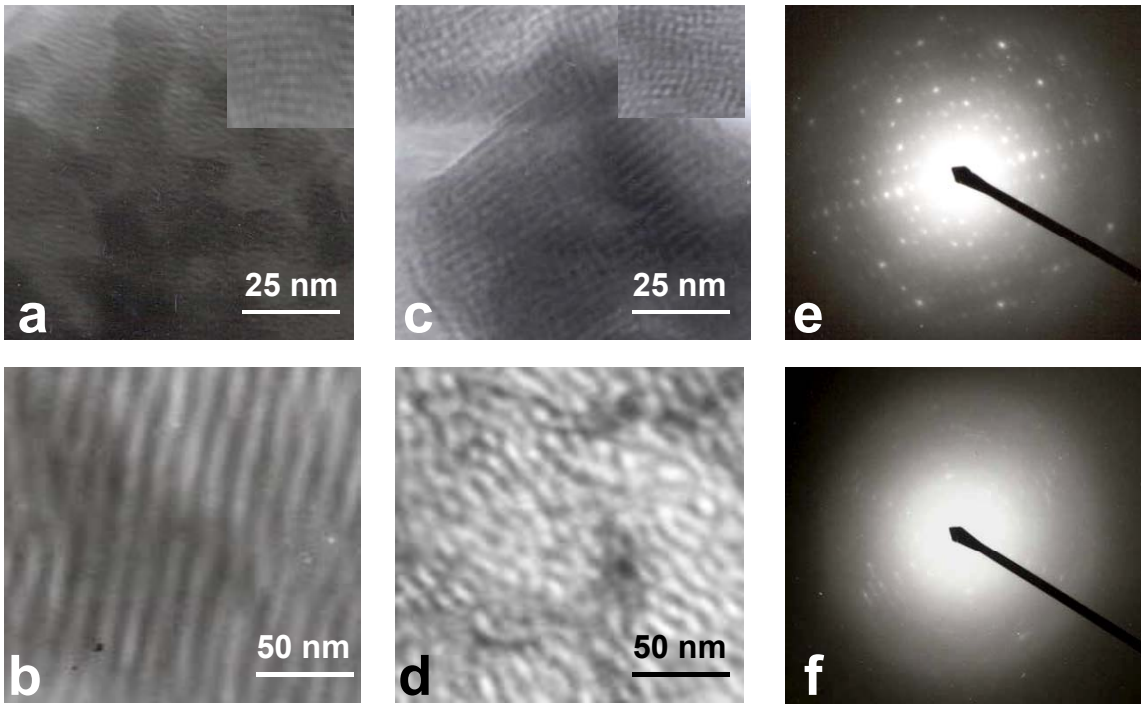

Figure 3.6. TEM images of (a) Wk–M41–S (untreated with Ph_2SiCl_2), inset: Si-MCM-41; (b) Wk–M41 (treated with Ph_2SiCl_2), inset: Si-MCM-48; (c) Wk–M48–S (untreated with Ph_2SiCl_2) (d) Wk–M48 (untreated with Ph_2SiCl_2); (e) diffraction patterns of Na–Y and (f) diffraction patterns of Wk–Y.

In another survey, TEM was used to image the diffraction patterns of zeolite Na–Y and Wk–Y (Figure 3.6 (e) and (f)). We could observe another distinction between the bare and the encapsulated samples, wherein the '*neat*' zeolite Y showed well-resolved cubic diffraction patterns, whereas Wk–Y showed a '*foggy*' image. In Wk–Y, the encapsulated Rh-

complex occupying the faujasite (Na-Y) supercage obscures the zeolite pores, hence, the '*foggy*' diffraction pattern is observed. This might be a possible reason for obtaining decreased {111}-diffraction intensity in the XRD patterns of Wk–Y as we had observed earlier (see Figure 3.5 (g)).

These characterizations supported the absence of the complex at the solid surface with no noticeable Rh-clusters and restoration of the uniformity of the catalysts. For a better understanding, we investigated for the clue to an obvious question: whether the Rh-complex with three bulky PPh_3 groups is able to sit inside the supercage of zeolite Y without any conformation change or bond breakage. An insight into the crystal structure of $HRh(CO)(PPh_3)_3$ [38, 39] reveals that the dimension of the complex is close to 10.8 × 10.7 × 10.8 $(Å)^3$. This reflects that entrapment of $HRh(CO)(PPh_3)_3$ inside the zeolite Y supercage (12–13 Å) is very much feasible (since, we prepare Wk–Y by a *ship-in-a-bottle* approach [23]), while there are no doubts for ~ 30 Å–mesopores of MCM-41 and MCM-48 to accommodate the Rh-complex inside.

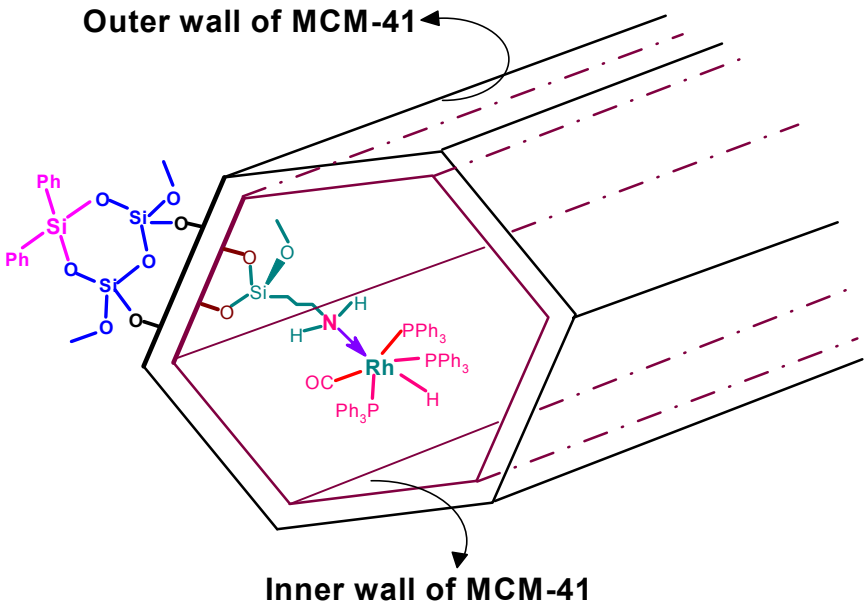

Figure 3.7. A model of $HRh(CO)(PPh_3)_3$ complex anchored inside the inner wall of MCM–41 channel by APTS, outer wall of the MCM-41 channel derivatized by dichlorodiphenylsilane

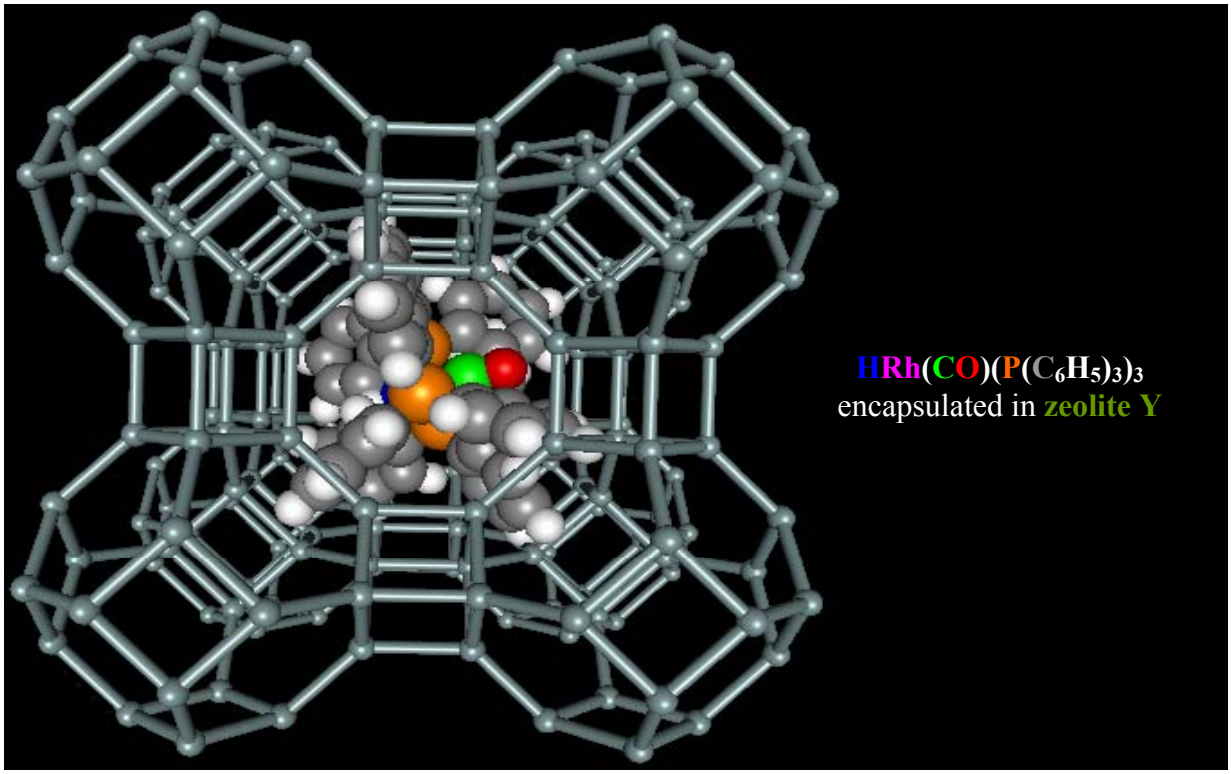

Figure 3.8. Molecular model representation of Wk–Y (structure generated in a *Indigo II* machine using *Insight II* software)
Colour code for atoms: **blue** (*hydride*), **green** (*carbonyl carbon*), **red** (*carbonyl oxygen*), **orange** (*phosphorus*), **grey** (*phenyl carbon*), white (*phenyl hydrogen*), ***rhodium*** is not seen here as it sits amidst green, blue and orange spheres and **moss-green** (*faujasite* structure)

A molecular model representation for the encapsulated $HRh(CO)(PPh_3)_3$ inside the mesoporous matrices (Figure 3.7) and the supercage of zeolite Y (Figure 3.8) have been proposed based on the characterization reported in this work. Thus, we can conclude that $HRh(CO)(PPh_3)_3$ is encapsulated in the MCM-41 and MCM-48 mesopores and zeolite Na-Y supercage (see Figures 3.7 and 3.8) and not merely impregnated/adhered on the porous surface.

3.3.2. CATALYST PERFORMANCE FOR HYDROFORMYLATION OF OLEFINS

3.3.2.1. Activity and selectivity behaviour of the encapsulated catalysts for hydroformylation of olefins

The catalysts Wk–Y, Wk–M41 and Wk–M48 were evaluated for their activity and selectivity behaviour for hydroformylation of 1-octene (see Table 3.3, entries 10–12) and styrene (see Table 3.4). Particularly, it is shown that these encapsulated rhodium complex catalysts are highly stable, can be recycled several times (each catalyst was recycled ten times) without loosing activity or selectivity and do not require presence of free PPh_3 as a ligand [34]. These catalysts (see Table 3.3, entries 10–12) when compared to other previously reported heterogeneous catalysts for hydroformylation exhibit superior activity, recyclability and selectivity. For the Rh-SiO_2 immobilized catalysts (Table 3.3, entries 7–9), though the n/iso ratio for *n*-nonaldehyde is significantly higher compared to our catalysts (Table 3.3, entries 10–12), TOF values are lower and in one case metal leaching (> 50%) was observed (Table 3.3, entry 9), which is undesirable for a true heterogeneous catalyst. With all the three encapsulated catalyst systems, high conversion (> 97%) and selectivity towards aldehydes (> 98%) were obtained (see Table 3.4). The selectivity towards the desirable products was found to be comparable for styrene and 1-hexene, but lower for higher olefinic substrates (1-octene, 1-decene, 1-dodecene) in almost all the cases. A plausible reason might be due to the geometric constraints of the substrates accessing the complex-site inside the pores. The enhanced activity for Wk-M41 and Wk-M48 is due to larger pore dimensions in these catalysts (~ 30 Å) that give better access for the substrates to the catalytic sites present inside the mesopores of MCM–48, in comparison to that of confined micropores of zeolite Y having 12 Å supercage and 8 Å window.

In a typical experiment using Wk–M48–S catalyst (Rh-content 0.63 wt./ wt. %) for hydroformylation of styrene, we observed ~ 6% overall Rh-leaching, compared to < 0.05% overall Rh-leaching using Wk–M48 catalyst (Rh-content 0.69 wt./wt. %) after 6 recycles. Therefore, this method (Ph_2SiCl_2 treatment with the mesoporous materials) coupled with anchoring of APTS and Rh-complex inside the mesopores provides a distinct advantage over the conventional anchoring method with APTS (no Ph_2SiCl_2 treatment) in avoiding Rh-

leaching in the course of reaction due to prolong use. Using impregnated Rh-complex on zeolite Y (Wk–Y–S) showed higher activity due to appreciable leaching of Rh metal from the support (~ 27% Rh loss in a single run, see Table 3.4). Hence, true heterogeneity in case of encapsulated catalysts (Wk–Y, Wk–M41 and Wk–M48) could be established in comparison to the impregnated Wk–Y–S or untreated Ph_2SiCl_2 catalysts (Wk–M41–S and Wk–M48–S). Since, Wk–M48 showed the best activity and selectivity for styrene hydroformylation among the heterogeneous catalysts used (see Table 3.4), it was selected for further work on comparison of its activity and selectivity with homogeneous $HRh(CO)(PPh_3)_3$ catalyst for hydroformylation of olefins (see Table 3.5). Though the TONs and TOFs for the heterogeneous catalysts were lower compared to the homogeneous $HRh(CO)(PPh_3)_3$ catalyst, the encapsulated catalysts could be easily separated from the reaction mixtures and recycled several times, an obvious advantage over the homogeneous catalyst.

Table 3.3. Comparison activity and selectivity of few selected heterogeneous catalysts used in hydroformylation of various olefins

Entry	Substrate	S : Rh[a]	Conv.[b] (%)	n/iso	TON	TOF (h^{-1})	Rh-leaching, %	Catalyst used[c]	Reference
1	1-hexene	100	37.0	2.3	37.0	1.7	trace	Rh–Y	29 (a)
2	1-hexene	100	88.5	0.6	88.5	29.5	n. d.	Rh–SiO_2	18
3	1-pentene	106	97.1	2.7	103.0	22.9	appreciable	Rh–polymer	7 (a)
4	1-decene	200	81.0	1.5	162.0	40.5	appreciable	Rh_2–MCM-41	33
5[d]	Oleyl alcohol	500	96.6	n. d.	483.0	87.8	untraced	Rh–SAPC	9
6	1-octene	250	75.0	2.6	187.5	7.8	untraced	Rh–calix[4]arene	17
7[e]	1-octene	4255	9.4	32.0	400.0	87.0	untraced	Rh–$ScCO_2$	32 (b)
8	1-octene	637	69.0	32.0	440.0	35.0	< 1	Rh–SiO_2	32 (a)
9[f]	1-octene	637	64.0	1.6	408.0	175.0	> 50	Rh–SiO_2	32 (a)
10[g]	1-octene	581	97.2	1.5	565.0	141.0	< 0.01	Rh–Y	Wk–Y
11[g]	1-octene	879	98.2	1.7	863.0	216.0	< 0.01	Rh–MCM-41	Wk–M41
12[g]	1-octene	951	99.4	1.7	945.0	270.0	< 0.01	Rh–MCM-48	Wk–M48

[a] S:Rh = substrate:rhodium; [b] conversion to aldehydes; [c] The term 'Rh' has been used for various Rh-complexes used as catalysts; [d] supported aqueous phase catalyst; [e] supercritical conditions, 180 bar CO_2, reaction temperature 353 K; [f] without addition of free ligand; [g] Rh-leached (%) after single run, see Table 4 for reaction conditions; TON = kmol of olefins converted to aldehydes × (kmol of Rh)$^{-1}$; TOF = TON × h^{-1}; n. d. = not determined

Table 3.4. Activity and selectivity of hydroformylation of styrene using various catalysts

Entry	Catalyst	Conversion (%)	Selectivity ald. (%)	n/iso	Rh-content (wt./wt. %)	% Rh-leaching [a]	TON	TOF (h^{-1})	Time (h)
1	Wk–Y	100	98.1	0.67	1.130	0.053 [b]	780	173	4.5
2	Wk–Y–S	99	98.5	0.44	0.567	~ 27.0	1700	567	3.0
3	Wk–M41	100	99.1	0.43	0.747	0.054 [b]	1200	279	4.3
4	Wk–M48	100	99.1	0.43	0.690	0.043 [b]	1300	325	4.0
5	Wk–M48–S	99	99.0	0.41	0.630	~ 6.0 [b]	1750	583	3.0
6	$HRh(CO)(PPh_3)_3$	98	98.9	0.33	11.21	–	2675	2876	0.93

Reaction conditions: catalyst: 8 kg m^{-3} for entries 1–5 and 0.96 kg m^{-3} for entry 6; substrate: 0.698 kmol m^{-3} for entries 1–5 and 3.49 kmol m^{-3} for entry 6; P_{CO}, P_{H2}: 2.04 MPa; agitation speed: 16.67 Hz; temperature: 373 K; solvent: toluene; total volume: 2.5×10^{-5} m^3; TON = kmol of styrene converted to aldehydes × (kmol of Rh)$^{-1}$; TOF = TON × h^{-1}; [a] Rh-leaching (%) = ppm of Rh-leached × 100/ ppm of Rh-content (evaluated from Rh-content wt./wt. %); [b] overall Rh-leached after 6 recycles, otherwise, for single run.

Table 3.5. Comparison of activity and selectivity of hydroformylation of linear olefins using $HRh(CO)(PPh_3)_3$ and Wk–M48 catalysts

Entry	Catalysts	Substrate	Substrate (kmol m^{-3})	Conversion (%)	Selectivity ald. (%)	n/iso	TON	TOF (h^{-1})	Time (h)
1	$HRh(CO)(PPh_3)_3$	1-Hexene	3.198	98.8	98.8	2.55	2450	2467	1.05
2	Wk–M48	1-Hexene	0.639	100.0	99.5	2.33	1182	338	3.50
3	$HRh(CO)(PPh_3)_3$	1-Octene	2.548	98.8	98.2	2.42	1850	1391	1.33
4	Wk–M48	1-Octene	0.509	100.0	99.4	1.67	945	270	3.50
5	$HRh(CO)(PPh_3)_3$	1-Decene	2.113	98.2	92.2	1.36	1518	961	1.58
6	Wk–M48	1-Decene	0.423	99.0	99.2	1.50	383	109	3.50
7	$HRh(CO)(PPh_3)_3$	1-Dodecene	1.801	97.4	89.1	0.79	1210	630	1.92
8	Wk–M48	1-Dodecene	0.360	99.0	98.6	1.00	326	88	3.70

Reaction conditions: catalyst: 0.96 kg m^{-3} $HRh(CO)(PPh_3)_3$ and 8 kg m^{-3} Wk–M48 (0.69 wt./wt. % Rh); P_{CO}, P_{H2}: 2.04 MPa; agitation speed: 16.67 Hz; temperature: 373 K; solvent: toluene; total volume: 2.5×10^{-5} m^3; TON = kmol of olefin converted to aldehydes × $(\text{kmol of Rh})^{-1}$; TOF = TON × h^{-1}

3.3.2.2. Leaching and recycle experiments with the encapsulated catalysts

Catalyst leaching experiments have been performed by hot filtration of the reaction mixture at 373 K and subsequently testing the catalytic activity of the filtrate for hydroformylation without addition of a catalyst. This solution and the catalyst thus recovered (dissolved in conc. HNO_3) were also analyzed for determination of Rhodium content by ICP–AES analyses. Leaching experiments were performed for each catalyst in all the hydroformylation reactions. For catalyst recycle experiments, the encapsulated catalysts were allowed to settle down and the clear supernatant liquid was decanted slowly. The residual solid catalyst was re-used with fresh charge of solvent and reactants for the recycle run maintaining the same reaction conditions. In the recycle studies, the rhodium content of the catalysts and subsequent hydroformylation reaction mixtures were analyzed for Rh content.

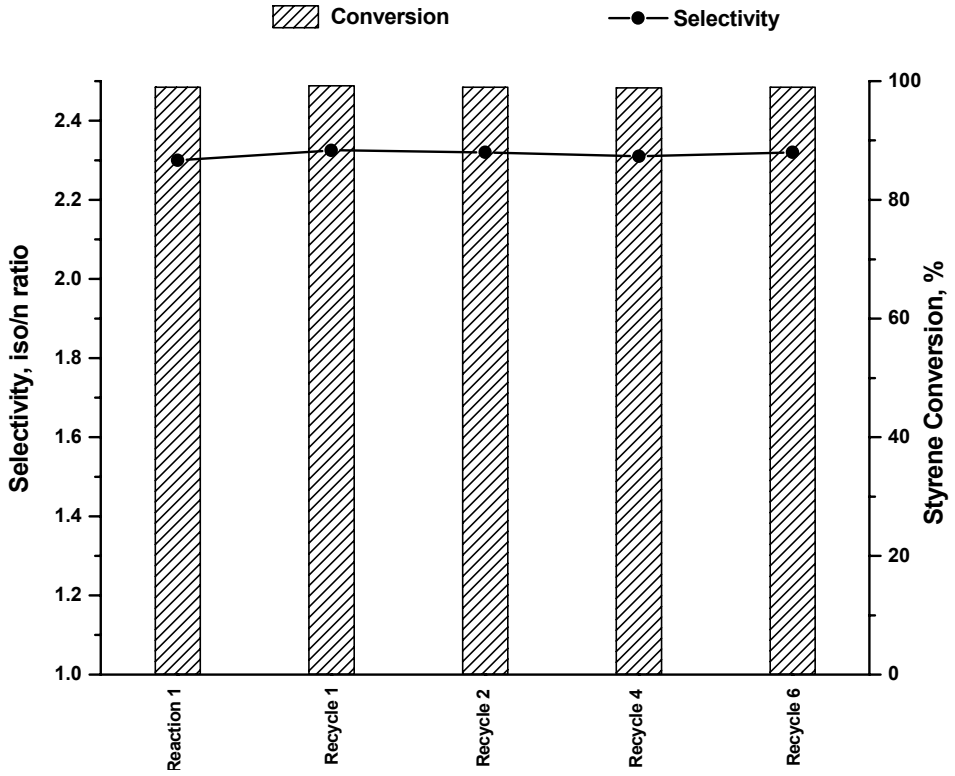

Figure 3.9. Recycle studies using Wk–M48 catalyst for hydroformylation of styrene

Reaction conditions: catalyst: 8 kg m^{-3} (0.69 wt./wt. % Rh); styrene: 0.698 kmol m^{-3}; P_{CO}, P_{H2}: 2.04 MPa; agitation speed: 16.67 Hz; temperature: 373 K; solvent: toluene; total volume: 2.5×10^{-5} m^3.

A typical recycle experiment with Wk–M48 catalyst for hydroformylation of styrene showed that the catalyst is truly stable even after 6 recycles without loosing activity or selectivity (Figure 3.9). Elemental analysis for Rh in these encapsulated catalysts, as well as the reaction mixtures before and after the reaction by ICP showed < 0.05% overall Rh loss after the 6^{th} recycle, thus, ensuring negligible leaching of rhodium from the catalyst. The reaction mixture, after separation of the solid catalyst, was also tested for hydroformylation activity (after catalyst removal from the 5^{th} recycle), which showed no catalytic activity (Rh-content was below detection limit of the ICP–AES instrument, 0.01 ppm), further supporting that the leaching of Rh from the catalyst was negligible.

3.4. CONCLUSION

Novel heterogeneous catalysts consisting of encapsulated $HRh(CO)(PPh_3)_3$ in the pores of microporous Na–Y and cubic and hexagonal mesophases of MCM–48 and MCM–41 respectively have been reported, for hydroformylation of olefins *without catalyst leaching and use of free ligands*, for the first time. The use of such air-stable catalysts showed high activity, recyclability and easy catalyst-product separation from the liquid phase, though the n/iso ratio was lower compared to the homogeneous catalyst, $HRh(CO)(PPh_3)_3$. Though, the reaction rates are lower compared to the homogeneous system, the cumulative turn over numbers for the encapsulated catalysts were significantly higher considering recycle experiments with complete conversion of styrene in each batch cycle. These encapsulated catalysts can open up new vistas for the industrial applications in synthesis of high boiling specialty aldehydes. This approach can also be extended to encapsulate Rh-complexes with other ligands to tailor the desired n/iso selectivity in specific cases. A detailed characterization of the catalysts specially using CP MAS NMR, TEM and XPS (before and after use) analyses, led to important conclusions like true encapsulation of the Rh-complex inside the support-pores.

REFERENCES

[1] Parshall, G.W.; Ittel, S. D. *Homogeneous Catalysis*; John Wiley & Sons: New York, **1992**.

[2] Falbe, J. *Carbon Monoxide in Organic Synthesis*, Springer-Verlag. Berlin, Heidelberg, **1970**.

[3] (a) Cornils, B.; Hermann, W. A.; Eds. *Applied Homogeneous Catalysis with Organometallic Compounds*; VCH, **1996**, Volumes 1 and 2. (b) Beller, M.; Bolm, C.; Eds. *Transition Metals for Organic Synthesis*; Wiley-VCH: Weinheim, **1998**; Vol. 2, Chapters 1 & 2.

[4] van Leeuwen, P. W. N. M.; Claver, C.; Eds. *Rhodium Catalyzed Hydroformylation*; Kluwer Academic: Dordrecht, **2000**.

[5] Hartley, F. R. *Supported Metal Complexes*; Reidel: Dordrecht, 1985.

[6] Bailey, D. C.; Langer, S. H. *Chem. Rev.* **1981**, *81*, 109.

[7] (a) Pittmann Jr., C. U.; Smith, L. R. *J. Am. Chem. Soc*. **1975**, *97*, 1742. (b) Mecking, S. Thomann, R. *Adv. Mater.* **2000**, *12*, 953.

[8] (a) Rony, P. R. *J. Catal.* **1969**, *14*, 142. (b) Kuntz, E. *CHEMTECH* **1987**, *17*, 570.

[9] Arhancet, J. P.; Davis, M. E.; Merola, J. S.; Hanson, B. E. *Nature* **1989**, *339*, 554.

[10] Herrmann, W. A.; Cornils, B. *Angew. Chem. Intl. Ed.* **1997,** *36*, 1048.

[11] Hermann, W. A.; Albanese, G. P.; Manetsberger, R. B.; Lappe, P.; Bahrmann, H. *Angew. Chem. Intl. Ed. Engl.* **1995**, *34*, 811.

[12] (a) Horvarth, I. T.; Rabai, J. *Science* **1994**, *266*, 72. (b) Wende, M.; Meier, R.; Gladysz, J. A. *J. Am. Chem. Soc.*, **2001**, *123*, 11490.

[13] (a) Chauvin, Y; Mussmann, L; Olivier, H. *Angew. Chem. Int. Ed. Engl.* **1995**, *34*, 2698. (b) Welton, T. *Chem. Rev.* **1999**, *99*, 2071. (c) Mehnert, C. P.; Cook, R. A.; Dispenziere, N. C.; Afeworki, M. *J. Am. Chem. Soc.* **2002**, *124*, 12932.

[14] Broussard, M. E.; Juma, B.; Train, S. G.; Peng, W-J.; Laneman, S. A.; Stanley, G. G. *Science* **1993**, *260*, 1784.

[15] Chaudhari, R. V., Bhanage, B. M., Deshpande, R. M., Delmas, H. *Nature* **1995**, *373*, 501.

[16] Bourque, S. C.; Alper, H. *J. Am. Chem. Soc.* **2000**, *122*, 956.

[17] Shimizu, S.; Shirakawa, S.; Sasaki, Y.; Hirai, C. *Angew. Chem. Int. Ed. Engl.* **2000**, *39*, 1256.

[18] Bianchini, C.; Burnaby, D. G.; Evans, J.; Frediani, P.; Meli, A.; Oberhauser, W.; Psaro, R.; Sordelli, L.; Vizza, F. *J. Am. Chem. Soc.* **1999**, *121*, 5961.

[19] De Vos, D. E.; Dams, M.; Sels, B. F.; Jacobs, P. A. *Chem. Rev.* **2002,** *102*, 3615.

[20] (a) Breck, D.W. *Zeolite Molecular Sieves: Structure, Chemistry and Uses*; Wiley, New York, **1974**. (b) Corma, A. *Chem. Rev.* **1995,** *95*, 559.

[21] (a) Kresge, C. T.; Leonowicz, M. E.; Roth, W. J.; Vertulli, J. C.; Beck, J. S. *Nature* **1992**, *359*, 710. (b) Beck, J. S.; Vertulli, J. C.; Roth, W. J.; Leonowicz, M. E.; Kresge, C. T.; Schmitt, K. D.; Chu, C. T.-W.; Olson, D. H.; Sheppard, E. W.; McCullen, S. B.; Higgins, J. B.; Schlenker, J. L. *J. Am. Chem. Soc.* **1992,** ***114*****,** 10834.

[22] (a) Monnier, A.; Schuth. F.; Huo, Q.; Kumar, D.; Margolese, D.; Maxwell, R. S.; Stucky, G. D.; Krishnamurthy, M.; Petroff, P.; Firouzi, A.; Janicke, M.; Chmelka, B. F. *Science* **1993,** *261*, 1299. (b) Corma, A. *Chem. Rev.* **1997,** *97*, 2373.

[23] (a) Herron, N. *CHEMTECH* **1989**, *19*, 542. (b) De Vos, D. E.; Thibault-Starzyk, F.; Knops-Gerrits, P. P.; Parton, R. F.; Jacobs, P. A. *Macromol. Symp.* **1994**, *80*, 157. (c) Bein, T. *Compr. Supramol. Chem.* **1996,** *7*, 579. (d) Ertl, G.; Knoezinger, H.; Weitkamp, J.; Eds. *Handbook of Heterogeneous Catalysis*; Wiley-VCH: Weinheim, **1997**.

[24] (a) Herron, N.; *Inorg. Chem.* **1986**, *25*, 4741. (b) Gerrits, P. P. K.; De Vos, D. E.; Starzyk, F. T.; Jacobs, P. A. *Nature* **1994**, *369*, 543. (c) Raja, R.; Ratnasamy, P. *J. Mol. Catal.*, **1995**, *100*, 93. (d) Corma, A.; Nemeth, L. T.; Renz, M.; Valencia, S. *Nature* **2001,** *412*, 423.

[25] Kowalak, S.; Weiss, R. C.; Balkus Jr., K. J. *J. Chem. Soc. Chem. Comm.* **1991**, 57.

[26] Ogunwumi, S. B.; Bein, T. *Chem. Comm.* **1997**, 901.

[27] (a) Mehnert, C. P.; Weaver, D. W.; Ying, J. Y. *J. Am. Chem. Soc.* **1998,** *120*, 12289. (b) Djakovitch, L; Koehler, K. *J. Am. Chem. Soc.* **2001,** *123*, 5990.

[28] (a) Bath, K. N.; Halligudi, S. B. *J. Mol. Catal.* **1994**, *91*, 187. (b) Lee, B.; Alper, H. *J. Mol. Catal. A* **1996**, *111*, 17. (c) Lenarda, M.; Ganzerla, R.; Storaro, L.; Trovarelli, A.; Zanoni, R; Kaspar, J. *J. Mol. Catal.* **1992**, *72*, 75.

[29] (a) Davis, M. E.; Butler, P. M.; Rossin, J. A. *J. Mol. Catal.* **1985**, *31*, 385. (b) Andersen, J. M.; Currie, A.W. S. *Chem. Commun.* **1996**, 1543.

[30] (a) Mukhopadhyay, K.; Nair V. S.; Chaudhari, R. V. *Stud. Surf. Sci. Catal.* **2000**, *130*, 2999. (b) Andersen, J. M.; Karodia, N. *Catal. Lett.* **2000**, *66*, 49. (c) Andersen, J. M. *Platinum Met. Rev.* **1997**, *41*, 132.

[31] Taylor, D. F.; Hanson, B. E.; Davis, M. E. *Inorg. Chim. Acta* **1987**, *128*, 55.

[32] (a) Sandee, A. J.; van der Veen, L. A.; Reek, J. N. H.; Kamer, P. C. J.; Lutz, M.; Spek, A. L.; van Leeuwen, P. W. N. M. *Angew. Chem. Int. Ed. Engl.* **1999**, *38*, 3231. (b) Meehan, N. J.; Sandee, A. J.; Reek, J. N. H.; Kamer, P. C. J.; van Leeuwen, P. W. N. M.; Poliakoff, M. *Chem. Commun.* **2000**, 1497.

[33] Nowotny, M.; Maschmeyer, T.; Johnson, B. F. G.; Lahuerta, P.; Thomas, J. M.; Davies, J. E. *Angew. Chem. Int. Ed. Engl.* **2001**, *40*, 955.

[34] Mukhopadhyay, K.; Mandale, A. B.; Chaudhari, R. V. *Chem. Mater.* **2003**, *in press*.

[35] Mukhopadhyay, K.; Ghosh, A.; Kumar, R. *Chem. Commun.* **2002**, 2404.

[36] Evans, D.; Osborn, J. A.; Wilkinson, G. J. *J. Chem. Soc. A.* **1968**, 3133.

[37] Mukhopadhyay, K.; Sarkar, B. R.; Chaudhari, R. V. *J. Am. Chem. Soc.* **2002**, *124*, 9692.

[38] Shephard, D. S.; Zhou, W.; Maschmeyer, T.; Matters, J. W.; Roper, C. L.; Parsons, S.; Johnson, B. F. G.; Duer, M. J. *Angew. Chem. Int. Ed.* **1998**, *37*, 2719.

[39] Wu, G.; Wasylishen, R. E.; Curtis, R. D. *Can. J. Chem.* **1992**, *70*, 863.

[40] La Placa, S. J.; Ibers, J. A. *J. Am. Chem. Soc.* **1963**, *85*, 3501.

[41] La Placa, S. J.; Ibers, J. A. *Acta Crystallogr.* **1965**, *18*, 511.

[42] Bath, S. S.; Vaska, L. *J. Am. Chem. Soc.* **1963**, *85*, 3500.

[43] (a) Diesveld, J. W.; Menger, E. M.; Edzes, H. T.; Veeman, W. S. *J. Am. Chem. Soc.* **1980**, *102*, 7936. (b) Scott, S. L.; Szpakowicz, M.; Mills, A.; Santini, C. C. *J. Am. Chem. Soc.* **1998**, *120*, 1883.

[44] Wu, G.; Wasylishen, R. E. *Organometallics* **1992**, *11*, 3242.

[45] Lindner, E.; Schneller, F.; Auer, F.; Mayer, H. A. *Angew. Chem. Int. Ed. Engl.* **1999**, *38*, 2154, and the references therein.

[46] Engelhardt, G; Michel, D. *High-Resolution Solid-State NMR of silicates and Zeolites*, Wiley, New York, 1987, 150 – 228.

[47] Fyfe, C. A.; Thomas, J. M.; Klinowski, J.; Gobbi, G. C. *Angew. Chem. Int. Ed. Engl.* **1983**, *22*, 259. The Si/Al ratio in the tetrahedral alumonosilicate framework was calculated after deconvolution (using Jandel Scientific Peakfit program) from the equation:

$$(Si/Al)_{NMR} = \sum_{n=0}^{4} I_{Si(nAl)} \Big/ \sum_{n=0}^{4} 0.25 n I_{Si(nAl)}$$

[48] (a) Quayle, W. H.; Lunsford, J. H. *Inorg. Chem.* **1982**, *21*, 97. (b) Quayle, W. H.; Peeters, G; De Roy, G. L.; Vansant, E. F.; Lunsford, J. H. *Inorg. Chem.* **1982**, *21*, 2226.

[49] Bursill, L. A.; Lodge, E. A.; Thomas, J. M. *Nature* **1980**, *286*, 111.

[50] (a) Thomas, J. M.; Terasaki, O.; Gai, P. L.; Zhou, W. Z.; Gonzalez–Calbet, J. *Acc. Chem. Res.* **2001**, *34*, 583. (b) Ozkaya, D.; Zhou, W. Z., Thomas, J. M.; Midgley, P. A.; Keast, V. J.; Hermans, S. *Catal. Lett.* **1999**, *60*, 113.

CHAPTER 4

ANCHORED Pd COMPLEX IN MESOPOROUS SUPPORTS: NOVEL HETEROGENEOUS CATALYSTS FOR HYDROCARBOXYLATION OF ARYL OLEFINS AND ALCOHOLS

4.1. INTRODUCTION

Carbonylation or hydrocarboxylation of aryl olefins and alcohols provides a highly promising and eco-friendly route for the synthesis of aryl propanoic acids having applications as non-steroidal, anti-inflammatory drugs [1]. This is considered as one of the best examples of the role of catalysis in developing cleaner, environmentally benign routes replacing stoichiometric organic synthesis [2] as evidenced by the commercial success of the Hoechst-Celanese process for the synthesis of Ibuprofen [3], which involves mainly a Pd catalyst with 10% $HCl_{(aq)}$ as a promoter [4]. High regioselectivity for Ibuprofen (>95%) is achieved at high pressures (16–35 MPa), while the selectivity reduces to 67% (ref) with a TOF of 50–70 h^{-1} at lower pressures (6–7 MPa). In this reaction, the turn over frequency (TOF) was found to be only 50–150 h^{-1} even at high pressures (35 MPa) and separation of the catalyst and products is a tedious task involving the precipitation of the complex by adding non polar solvents. In recent reports [5], a significant enhancement in the catalytic activity (TOF = 800–2600 h^{-1}) and regioselectivity (99%) for Ibuprofen at lower pressures has been demonstrated with modified promoters, different phosphorus ligands and Pd-complexes [6, 7]. These homogeneous catalysts often pose a serious threat in practical utility due to difficulties in catalyst-product separation and reuse. The widespread application of homogeneous catalysis in C–C bond formation reactions including carbonylation is attributed to their high catalytic activity as well as high selectivity, which are, in many cases, difficult to achieve by heterogeneous catalysis. Despite these advantages, the industrial applications of many of these processes were not realized due to difficulties in separation and recycle of the precious catalysts. Hence, it has been a target of research during the last decade to heterogenize the homogeneous catalysts to incorporate the advantages of the homogeneous catalysis as well as the efficient catalyst–product separation.

Recently, Sheldon and co-workers [8], and Chaudhari and co-workers [9] have reported carbonylation of IBPE and styrene respectively using water-soluble palladium complexes in biphasic systems. These catalyst systems have the advantages of easy catalysts recovery, but the reaction rates as well as the selectivity in both the cases (TOF: ~ 40 h^{-1} and 244 h^{-1} and selectivity: 72% and 78% in the respective studies) were found to be lower compared to the homogeneous analogues.

Using supported Pd catalysts (Pd/C) for carbonylation of aryl halides [10] and *p*-isobutylphenylethanol (IBPE) [11], high activity (TOF = 1675–3375 h^{-1}) and selectivity (99%) for branched carboxylic acid derivatives was achieved for IBPE, however, in both the cases it was concluded that the catalytic activity was due to leached Pd in solution under reaction conditions.

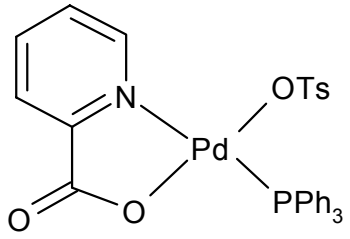

Figure 4.1. Pd(pyca)(PPh_3)(OTs) catalyst used for hydrocarboxylation reaction [Ref. 6, 7]

Carbonylation of IBPE was reported [12] using a heterogeneous catalyst system consisting of supported Pd in the presence of phosphine ligands together with aqueous HCl as a promoter to give Ibuprofen with 23–77% selectivity at 4 MPa pressure and 398 K. The selectivity was increased up to 97% when silyl ligands were used together with the Pd-montmorillonite catalyst, but the catalytic activity was found to be very low (TOF: 3–10 h^{-1}).

In another report [13], Alper and co-workers have reported the carbonylation of olefins using a heterogeneous Pd-C catalyst in the presence of formic or oxalic acid and a bidentate phosphine ligand, dephenylphosphino propane (dppb) [13]. Though, total carboxylic acid yields achieved were in the range of 65–80%, the reaction rates were poor (10–17 h^{-1} at 423 K) with the regioselectivity towards the linear carboxylic acid in a range of 76–100%. In another study by the same group [14], the hydroesterification of styrene and derivatives was carried out using $Pd(OAc)_2$ immobilized on montmorillonite in the presence of PPh_3 as a ligand. Here, the regioselective formation of methyl esters of 2-arylpropanoic acids (~ 95%) was observed at 373 K at 4 MPa (TOF = 20 h^{-1}).

Very recently, Jacobs and coworkers [15] have reported a heterogeneous catalyst using MgAl layered double hydroxides as a support for oxidative carbonylation of phenol to diphenyl carbonate (DPC), which is an important precursor for polycarbonates. Though TOF of 387 h^{-1} could be achieved for a certain catalysts system in this reaction, yet Pd-leaching

from the system is very high ca. 17%, hence, the catalyst cannot be called a truly heterogeneous catalyst system [15]. These reports reveal that a major drawback in most of these cases is the significantly lower reaction rates, often followed by leaching of the Pd metal during re-use. Therefore, the problem of developing a true heterogeneous Pd-catalyst for such carbonylation reactions remained an open challenge.

It is in this context that Pd-complex anchored to inorganic matrices e.g. mesoporous supports [16] like Si-MCM-41 and Si-MCM-48 were investigated as heterogeneous catalysts for hydrocarboxylation reaction [17]. Unlike silica gel support, Si-MCM-41 and Si-MCM-48 are highly ordered mesoporous silica possessing high surface areas, well-defined porous structures, high porosity and controllable narrow pore-size distribution [18]. For this purpose, hydrocarboxylation of olefins and alcohols using Pd-(Pyca)(PPh_3)(OTs) catalyst has been chosen as a reaction system, since with this catalyst, highest activity (e.g. TOF = 2600 h^{-1} for styrene hydrocarboxylation) and regioselectivity (> 99 %) for arylpropanoic acid has been achieved at lower pressure (5.04 MPa) so far [7].

In the following sections, the syntheses and characterization of these novel heterogeneous catalysts (Pd-pyca anchored on mesoporous supports) have been described along with their catalytic efficiency for hydrocarboxylation of aryl olefins and alcohols. For a comparison, the Pd-pyca complex has also been supported to other inorganic matrices like silica gel and microporous zeolite Na-Y and the resulting activity, regioselectivity and stability of the catalysts for hydrocarboxylation reactions have been compared with that of the Pd-pyca anchored to mesoporous supports. The regioselectivity and recyclability of the catalysts without leaching of Pd complex/metal from these supports have also been discussed. The stoichiometric reactions involved in hydrocarboxylation of aryl olefins and alcohols are presented in Scheme 4.1.

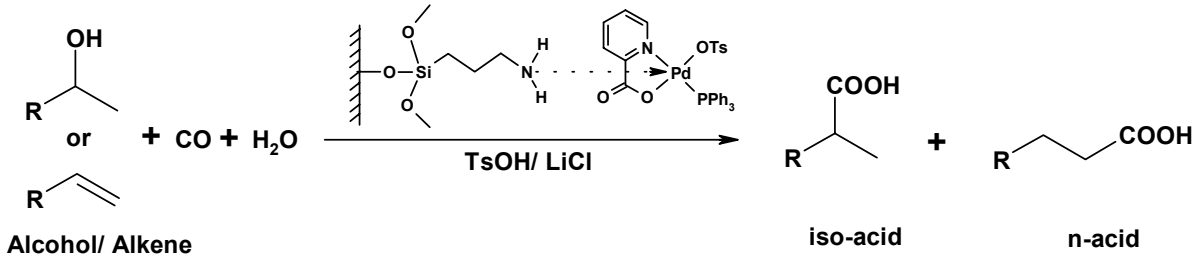

Scheme 4.1. Hydrocarboxylation of alkenes or alcohols to acids with heterogeneous catalysts

4.2. EXPERIMENTAL SECTION

4.2.1. MATERIALS

Styrene, substituted styrenes, *p*-toluenesulphonic acid monohydrate (TsOH), triphenyl phosphine (PPh_3), fumed silica (380 m^2g^{-1}), 3-aminopropyltrimethoxysilane (APTS), dichlorodiphenylsilane (Ph_2SiCl_2), cetyltrimethylammonium bromide, (CTABr) (Aldrich, USA), LiCl, NaOH (S.d. Fine-chem., India) and CO gas (Matheson, USA, 99.9% purity) were used as received. All solvents were freshly distilled using known procedures and degassed by argon before use.

4.2.2. SYNTHESES

4.2.2.1. Synthesis of Si-MCM-41

Following a procedure reported earlier [35], Si–MCM–41 and Si–MCM–48 were synthesized having initial molar gel ratio of SiO_2–0.32NaOH–0.2CTABr–125H_2O–0.0033PTA and SiO_2–0.4NaOH–0.21CTABr–120H_2O–0.0033PTA respectively (PTA = phosphotungstic acid). In a typical synthesis of MCM-41, 50 mmol of fumed SiO_2 was added to a solution of 16 mmol NaOH in 25 mL H_2O and stirred for 1 h. To this mixture, 10 mmol of CTABr is added drop-wise followed by an addition of 0.165 mmol of PTA (as a promoter) in 37 mL of H_2O. The final gel was stirred for another 1.5 h and then autoclaved in polypropylene bottle at 373 K for 4 h. The as-synthesized sample was then filtered, washed repeatedly with de-ionized water and air calcined at 813 K to obatin calcined Si–MCM–41.

4.2.2.2. Synthesis of Si-MCM-48

In the synthesis of MCM-48, 50 mmol of fumed silica was added to a solution of 20 mmol NaOH in 25 mL H_2O and stirred for 1 h. To this mixture, 10.5 mmol of CTABr was added drop-wise followed by an addition of 0.165 mmol of PTA (as a promoter) in 33 mL of H_2O. The final gel was stirred for another 1.5 h and then autoclaved in a teflon-lined stainless steel autoclave at 423 K for 12 h. The as-synthesized sample was then filtered, washed repeatedly with de-ionized water and air calcined at 813 K to obtain calcined Si–MCM–48.

A summary of the physical characteristics of Si-MCM-41 and Si-MCM-48 materials has been presented in Table 4.2.

4.2.2.3. Synthesis of Pd(Pyca)(PPh_3)(OTs) complex

$Pd(OAc)_2$ (0.89 mmol), pyridine-2-carboxylic acid (pycaH, 1 mmol), *p*-toluenesulphonic acid (TsOH, 1.78 mmol) and triphenylphosphine (PPh_3, 1.78 mmol) in chloroform were vigorously stirred or shaken under room temperature for a few minutes until all the components were completely dissolved and the solution turned yellow. The oily product was washed several times with *n*-hexane and diethyl ether and was kept under vacuum forming a yellow fluffy solid [6, 7]. For elemental and spectroscopic analysis, the complex was purified by re-precipitation from chloroform several times. Elemental analyses data for the Pd-pyca complex was found to be satisfactory with the given formulation, $C_{31}H_{26}NO_5PPdS.H_2O$. Theoretical values: C – 54.76, H – 4.15, N – 2.06, P – 4.56, S – 4.71 and Experimental values: C – 55.21, H – 4.18, N – 1.96, P – 4.08, S – 4.45; Yield: 88 %.

4.2.2.4. Synthesis of Pd(pyca)(PPh_3)(OTs) complex supported on zeolite Na-Y

Zeolite Y was synthesized according to the procedure reported in section *3.2.2.1* in chapter 3 of this thesis. Supported Pd(pyca)(PPh_3)(OTs) on zeolite Na–Y was prepared by suspending 3 g of Na–Y in ethanolic solution containing 0.135 moles of the complex and refluxing it at 363 K for 18 h. The light yellow solid was filtered and dried at 353 K and used as such (*labeled as* ***Pd–Y–S***) for hydrocarboxylation reactions.

Pd-content: 0.81% w/w, average particle size of catalyst: 600 nm, surface area: 374 m^2g^{-1}.

4.2.2.5. Functionalization of MCM-41, MCM-48 and anchoring of Pd(pyca)(PPh_3)(OTs) complex by APTS inside the mesopores

To ensure that the complex is accommodated inside the support mesopores and not grafted externally on the mesopore-walls, MCM-41 and MCM-48 were functionalized using APTS by a procedure described earlier [17, 20]. On treatment of these functionalized supports with Pd(pyca)(PPh_3)(OTs) complex (catalyst A) [5 d], stable heterogeneous catalysts are obtained. Following this approach, Pd-pyca-MCM-41 (catalyst B) and Pd-pyca-MCM-48 (catalyst C) were prepared.

In two different syntheses, 1.0 g of Si-MCM-41 or Si-MCM-48 was suspended on 30 mL of dry dichloromethane (DCM) and to this 0.03 ml of Ph_2SiCl_2 was added and stirred for 1 hour. The contents were then cooled to 195 K and 5.73 mmol of APTS was added drop

wise to this slurry, stirred for further 24 hours at 313 K, washed several times with dry DCM and dried in vacuum to get functionalized MCM-41 (M41-F) and MCM-48 (M48-F) supports.

To prepare anchored Pd(pyca)(PPh_3)(OTs) catalysts in MCM-41 and MCM-48, 1.0 g of the functionalized support (M41-F or M48-F) was added to a solution containing 330 mg of the complex in 100 ml of dry, distilled methanol and stirred for 16 hours at room temperature. The light yellow solid powder was then washed several times with dry methanol, soxhlet-extracted once with MeOH to remove any Pd-complex adhered to the support walls, then dried and stored under vacuum. The catalysts thus prepared (*labeled as* ***Pd–M41*** *and Pd–****M48***), were used as such for hydrocarboxylation reactions. Physical specifications of the anchored Pd-pyca complex in MCM-41 and MCM-48 supports have been presented in Table 4.2.

4.2.2.6. Preparation of 1(-4-isobutylphenyl)ethanol [IBPE]

IBPE was prepared [7] from isobutyl benzene by a two-step synthesis procedure, which involved acylation of isobutylbenzene to *p*-isobutylacetophenone followed by reduction. For the acylation step, isobutylbenzene was slowly added to a solution of acetyl chloride and anhydrous $AlCl_3$ in dichloromethane at 273–278 K under vigorous stirring. After 4–5 h of stirring at 273–278 K, the reaction was quenched by pouring the reaction mixture into excess of crushed ice. The organic layer was separated from the aqueous layer. The aqueous layer was then re-extracted with dichloromethane and the combined organic layer was washed with saturated brine and then with saturated sodium bicarbonate. The washed dichloromethane layer was then dried over anhydrous sodium sulfate, concentrated and distilled under reduced pressure to get *p*-isobutylacetophenone.

The reduction of *p*-isobutylacetophenone was carried out using sodium borohydride. Sodium borohydride was added to a solution of *p*-isobutylacetophenone in methanol under ice-bath. After 1 h of continuous stirring at 273–283 K, the reaction was treated with dilute HCl and extracted with dichloromethane. The dichloromethane layer was washed with brine and then with saturated $NaHCO_3$, dried over anhydrous sodium sulfate, concentrated and distilled under vacuum to yield pure *p*-isobutylphenylethanol (IBPE). Yield: 92 %.

4.2.3. HYDROCARBOXYLATION REACTION SET-UP AND PROCEDURE

The reactions were carried out in a 50 mL Parr Autoclave made of Hastelloy C – 276 having facilities for gas inlet and outlet, rupture disc as a safety measure in case of excessive pressure build up, intermediate sampling, temperature-controlled heating and variable agitation speed. For a typical hydrocarboxylation reaction using a heterogeneous catalyst, the autoclave was charged with required amount of catalyst (prepared as per above procedures) in 6 mL of water after making the total volume 25 mL with substrate in methylethylketone (MEK) as a solvent, along with promoters (TsOH, PPh_3 and LiCl). The contents were flushed few times with nitrogen followed by carbon monoxide and heated to the desired temperature (under low stirring, 10–20 rpm). After attaining the temperature, the autoclave was pressurized with CO to the desired level and the reaction started by starting agitation (1100 rpm). To maintain a constant pressure in the reactor, CO was fed through a constant-pressure regulator from a reservoir vessel (100 mL). Pressure drop in the reservoir vessel was recorded by means of a pressure transducer as a function of time. Intermediate samples were also taken at regular intervals of time and were subjected to analysis to determine the concentration of the reactants and products. From these data, the conversion, selectivity turnover frequency (TOF) and selectivity at any given time were calculated.

After the reaction was over, the reactor was kept at rest to settle the solid catalyst and the organic phase was decanted slowly to get the supernatant liquid phase separated from the remaining solid catalyst. For recycle studies, a fresh charge of reactants was continued and the reaction was progressed in the same manner as described above. The organic layer thus obtained, was subjected to gas chromatographic and ICP-AES analysis for conversion-selectivity and metal content respectively (to test metal leaching) in the reaction mixture. The hydrocarboxylation products were isolated by evaporation of the solvent and purified further by acid-base extraction to further confirm by NMR and FT-IR analysis. The final conversion, selectivity and TOF were calculated at the end of the reaction.

1. Reactor 2. Stirrer shaft 3. Impeller 4. Cooling water 5. Sampling valve 6. Magnetic stirrer 7. Electric furnace

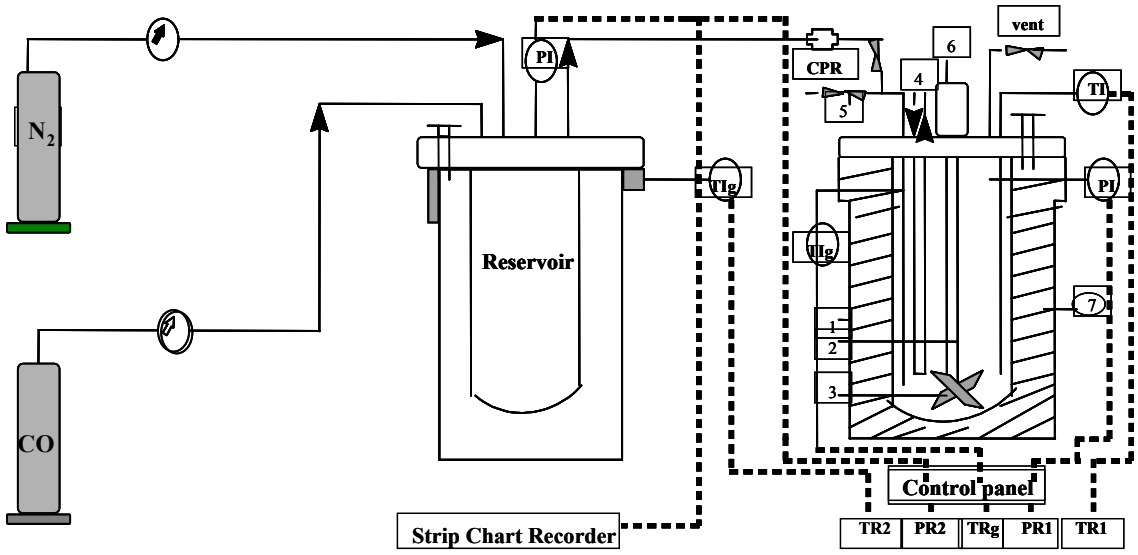

TI: Thermocouple PI: Pressure transducer TIg: Thermocouple for gas N_2:Nitrogen cylinder

CO: Carbon monoxide cylinder PR: Pressure regulator CPR: Constant pressure regulator

TRg: Gas temperature indicator PR2: Reservoir pressure indicator TR2: Reservoir temperature indicator

TR1: Reactor temperature indicator PR1: Reactor pressure indicator

Scheme 4.2. A schematic of the hydrocarboxylation reaction set-up

4.2.4. CATALYST LEACHING AND RECYCLE EXPERIMENTS

Catalyst leaching experiments were performed by hot filtration of the reaction mixture at 373 K and subsequently testing the catalytic activity of the filtrates for hydrocarboxylation without addition of the fresh heterogeneous catalyst. These solutions and the catalysts thus recovered were also analysed for Pd-content by ICP–AES (inductively coupled plasma with atomic emission spectra) analyses. In a typical catalyst recycle experiment, the heterogeneous catalyst was allowed to settle down and the clear supernatant liquid was decanted slowly. The residual solid catalyst was re-used with fresh charge of solvent and reactants for further recycle runs maintaining the same reaction conditions. In the recycle studies, the palladium content of the catalyst and subsequent hydrocarboxylation reaction mixtures were analysed for metal content as well as metal leaching.

4.3. RESULTS AND DISCUSSION

In this work, the solid-state characterization of the anchored Pd-complex catalysts (Pd-M41 and Pd-M48) and their catalytic performance for hydrocarboxylation of aryl olefins and IBPE was investigated. The results are discussed in the following sections.

4.3.1. CHARACTERIZATION OF THE CATALYSTS

^{31}P CP–MAS NMR spectra of Pd-pyca–MCM-41 and Pd-pyca–MCM-48 were obtained on a Bruker DRX 500 FT-NMR spectrometer at 202.64 MHz and 11.7 Tesla using 3 mm CP-MAS probe. The chemical shifts were referred to H_3PO_4 at 0 ppm and the spectra were collected at a spectral width of 20 kHz, with a flip angle of 45^o, 6000 real data points and 5 s relaxation delay. X-ray Photoelectron Spectroscopy (XPS) measurements of the porous catalysts were recorded in VG Microtech ESCA 3000 instrument, pressure at 10^{-10} Torr, pass energy of 50 eV and using un-monochromatized Mg–K_α (photon energy – 1253.6 eV) as the radiation. Powder X-ray Diffraction (XRD) of zeolite Pd-pyca–Y, Pd-pyca–MCM-41 and Pd-pyca–MCM-41 were obtained at room temperature on Rigaku D MAX III VC diffractometer using Ni-filtered Cu K_α radiation, λ = 1.5404 Å, where 2 θ ranges were from 5° and 50° at a scan rate of 8°/min for Pd-pyca supported zeolite-Y catalyst and, 1.5° and 10° at a scan rate of 1°/min for Pd-pyca–MCM-41 and Pd-pyca–MCM-48 catalysts. For Scanning electron microscopy (SEM) of the materials, the supports were suspended in isopropanol, casted on gold plated discs followed by drying under vacuum and then were imaged on a Philips XL 30 instrument. Specific surface area of the catalyst was determined by the BET method using N_2 adsorption measured on an Omnisorb CX–100 Coulter instrument. Prior to adsorption, the catalysts were activated at 423 K for 6 h at 10^{-4} Torr pressure. Gas chromatography (GC) of the reactants and products was performed in a HP 5890 instrument fitted with a FFAP capillary column.

4.3.1.1. POWDER X-RAY DIFFRACTION (XRD) ANALYSES

Powder-XRD patterns of the mesoporous supports (MCM-41 and MCM-48) and the encapsulated catalysts inside the mesoporous supports (Pd-pyca–M41 and Pd-pyca–M48) were obtained at room temperature on a Rigaku D MAX III VC diffractometer using Ni-

filtered Cu K_α radiation, λ = 1.5404 Å. In case of mesoporous supports and the encapsulated mesoporous catalysts, the observable 2 θ ranges were from 1.5° and 10° at a scan rate of 1°/min and for zeolite Na-Y and Pd-pyca–Y, observable 2 θ ranges were from 5° and 50° at a scan rate of 8°/min. Pd-pyca–M41 and Pd-pyca–M48 showed (Figure 4.2, a-d) the typical hexagonal phase (*p6mm*) of MCM-41 with the main {100} and other {110, 200 and 210} Bragg reflections and cubic phase (*Ia*3*d*) of MCM-48 with distinct {211} and {220} reflections along with {321, 400, 420, 332, 422 and 431} reflections indicating high degree of ordered mesoporosity even when the Pd-complex catalyst was encapsulated inside the mesopores. There was, ofcourse, a slight decrease in the peak intensities of the encapsulated catalysts, which might be due to the binding of the Pd-complex inside the APTS-functionalized mesoporous matrices. Pd-M41 and Pd-M48 catalysts showed no changes in the porous structures after functionalization and incorporation of Pd-pyca complex inside the mesopores and retention of the respective mesoporous structures.

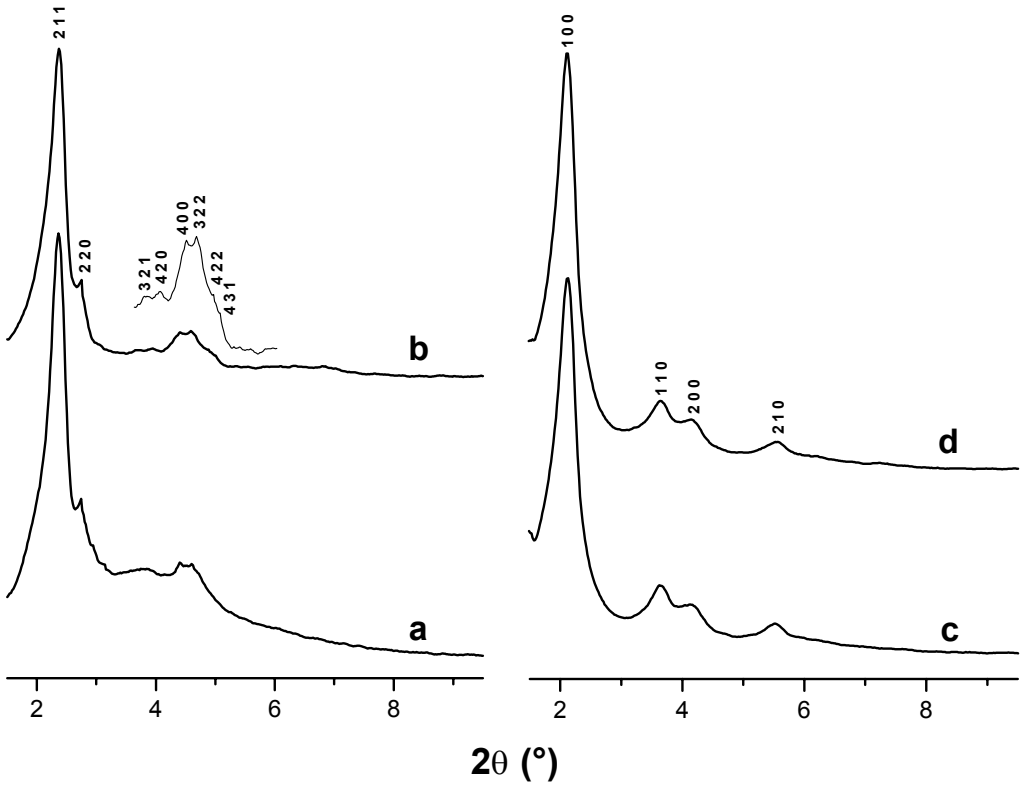

Figure 4.2. Powder XRD patterns of **(a)** MCM-48, **(b)** Pd-M48, **(c)** MCM-41 and **(d)** Pd-M41 (numbers on the patterns are the respective Bragg's reflections)

4.3.1.2. TRANSMISSION ELECTRON MICROSCOPE (TEM) ANALYSES

TEM has been used as an indispensable tool for structural elucidation of microporous as well as mesoporous supports [21,22]. Moreover, TEM has also been used extensively to envisage 3-D structures of the microporous and mesoporous solids, imaging metal nanoparticle catalysts inside mesoporous hosts and determine the occluded structure-directing organic species. In compliance to a recent report (by Sheppard *et al*. Ref. [21]) regarding imaging of metal complex catalysts specifically inside the mesoporous channels of MCM-41, we imaged parent MCM-41 and MCM-48 materials and Pd-anchored materials by TEM to direct the location of the anchored Pd-pyca complex inside the mesopores. The samples were dispersed in isopropanol, placed on holey carbon grids and a Jeol Model 1200 EX instrument operated at an accelerating voltage of 100 kV was used for imaging the samples. The TEM images of bare MCM–41 and MCM–48 were consistent with the regular hexagonal and cubic mesophases respectively (Figure 4.3 A-E) with homogeneity in patterns throughout. We could observe a striking difference among the images of the ***bare***, ***Ph_2SiCl_2 treated*** Pd-pyca anchored and ***Ph_2SiCl_2 untreated*** Pd-pyca anchored mesoporous (MCM-41 and MCM-48) materials. The exterior surface of Ph_2SiCl_2–treated–Pd-pyca–anchored mesoporous materials (Pd-M41 and Pd-M48) retains strong image contrast, probably due to Pd-pyca complex anchored inside the mesopores (treated with Ph_2SiCl_2), in comparison to the complex anchored (without Ph_2SiCl_2 treatment) both on the interior as well as exterior walls of MCM-41 (see Figure 4.3 -B and -C). In the previous chapter (*section 3.3.1.5*), TEM images have been portrayed to distinguish among bare, supported and encapsulated metal complex on/in porous supports.

Herein, MCM–41, Pd-pyca–M41 and Pd-pyca–M41-S (Figure 4.3 A–C) supports were chosen as a typical example to indicate the distinguishing features of the Pd-complex tethered by APTS (by a host-guest interaction) at the external or internal surfaces of MCM-41. In a similar fashion, as has been observed in case of Rh-complex anchored in/on the mesoporous MCM–41 supports (see Figure 3.5 of *section 3.3.1.5*), startling differences in the TEM images were observed when these images were compared with the Pd-pyca–M41 supports (Figure 2 (A–C)), wherein the Pd-complex has been encapsulated exclusively inside the mesopores by treating with Ph_2SiCl_2. A comparison of the images of Pd-pyca–M41–S with those of Pd-pyca–M41 (Figure 4.3 -B, -C) showed ‘clean’ exterior surfaces of the latter

case with retention of strong image contrasts of the grafted Pd-complex inside the mesopores. The encapsulated samples prepared treating with Ph_2SiCl_2 and further tethered with APTS, established that the Pd-complex is immobilized totally inside the mesopores and a uniform distribution of the complex entrapped inside has occurred, unlike Wk–M41–S materials (untreated with Ph_2SiCl_2, Rh-complex bound to the external mesopores-walls); a similar observation was reported earlier by Shephard *et al.* [20]. Similar distinguishable image patterns were also observed in case of the MCM–48 support. Thus, by TEM we could not only image the hexagonal and cubic patterns of the mesoporous materials, but also distinctly distinguish the internally bound Pd-complex to that of the externally grafted ones.

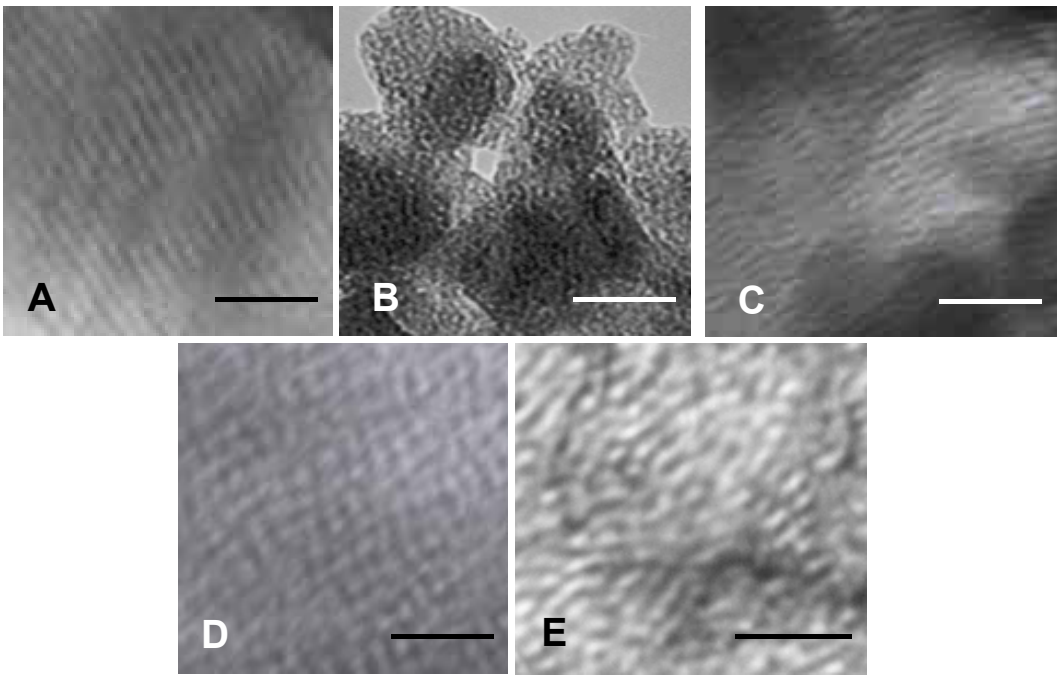

Figure 4.3. TEM images: **(A)** MCM-41, **(B)** Pd-pyca-MCM-41 (no Ph_2SiCl_2 treatment), **(C)** Pd-pyca-MCM-41 (treated with Ph_2SiCl_2), **(D)** MCM-48, **(E)** Pd-pyca-MCM-48 (treated with Ph_2SiCl_2); Scale Bar represents 50 nm.

4.3.1.3. X-RAY PHOTOELECTRON SPECTRA (XPS) ANALYSES

XPS of the encapsulated Pd-Y, Pd-pyca–M41 and Pd-pyca–M48 were recorded in VG Microtech-ESCA 3000 spectrometer, applying vacuum at 10^{-10} torr, pass energy of 50 eV and using un-monochromatized Mg–K_α as the radiation source (photon energy of 1253.6 eV). Surface analyses by XPS spectra were carried out quantitatively in terms of the binding

energy (B. E.) values of various elements present in the catalyst supports after necessary C 1s correction, especially taking into consideration the Pd $3d_{5/2}$ and $3d_{3/2}$ B. E. values [22] for the catalysts Pd-pyca–M48 as a typical example (see Figure 3). Pd-pyca–M41 and Pd-pyca–M48 catalysts showed typical Pd (II) oxidation state (Pd $3d_{5/2}$ = 337.0 eV, Pd $3d_{3/2}$ = 343.0 eV) and no cluster formation of Pd metal (respective B. E. values for Pd (0) species are 335.1 eV and 340.8 eV) in the catalyst (see Figure 4.4 and Table 4.1). Thus, Pd (II) species do not reduce to Pd (0) species after hydrocarboxylation reaction or even after reuse, a fact that posed hindrance in developing a stable Pd heterogeneous catalyst for the reaction.

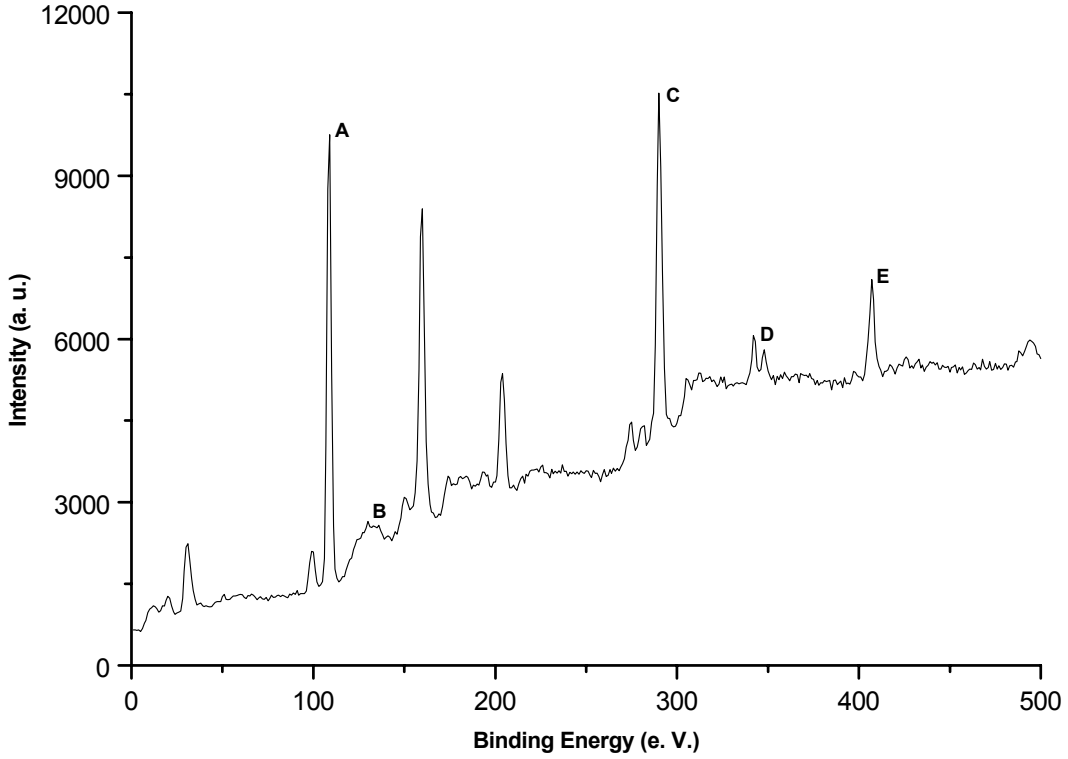

Figure 4.4. A typical X-ray photoelectron spectra (XPS) of Pd-pyca–MCM-48 catalyst (**A**: Si $2p_{3/2}$; **B**: P $2p_{3/2}$; **C**: C $1s_{1/2}$; **D**: Pd $3d_{5/2}$, $3d_{3/2}$; **E**: N $2p_{3/2}$)

XPS of these catalysts were also performed after hydrocarboxylation reactions in order to record any change observed in the oxidation states or B. E. values of the elements present in the supports during the reaction and these were found to be in compliance with the literature values [23(a)]. The silicon, phosphorus, palladium (II) and nitrogen present in the mesoporous supports showed no change in their B. E. values. This further showed that the

integrity of the Pd-pyca complex was retained on anchoring in the supports and that all the palladium was present as Pd (II) species with no beam damage suffered by the encapsulated supports. The B. E. values of the mesoporous supports before and after hydrocarboxylation reactions were almost similar, which proves essentially that all palladium was present as Pd (II) species in the encapsulated materials and the oxidation state remained unaltered even after the reactions (Table 4.1). B. E. values of Pd-pyca catalyst supported on zeolite Y (Pd–Y–S) before and after the reaction showed some differences in Pd B. E. values, which shows that after the reaction oxidation state of Pd shifts slightly towards Pd (0) from Pd (II) species. This might occur due to after-reaction catalyst decomposition of the impregnated Pd-pyca catalyst supported on zeolite Y. Besides the above-mentioned elements, B. E. values of P_{PPh3} (133.2 eV), O (534.1 eV) and S (169.2 eV) were also detected by XPS.

Table 4.1. Binding Energy (B. E.) values[§] from XPS for different elements present in the anchored catalysts

Elements / Supports	Al	Si	P	Pd ($3d_{5/2}$, $3d_{3/2}$)	N
Pd–Y–S–B[¶]	75.0	102.8	128.9	337.1, 343.1	–
Pd–Y–S–A[¶]	74.8	102.8	129.1	335.3, 340.8	–
Pd–M41–B	–	103.8	130.2	337.1, 343.2	402.2
Pd–M41–A	–	103.7	130.0	337.3, 343.3	401.9
Pd–M48–B	–	103.6	130.1	337.0, 343.0	401.7
Pd–M48–A	–	103.7	129.9	337.1, 343.2	401.8

[¶] B: before reaction, A: after reaction; [§] Corrected to C 1s with binding energy of 285 eV using adventitious carbon.

4.3.1.4. FOURIER TRANSFORM INFRARED SPECTROSCOPY (FTIR) ANALYSES

FT-IR of Pd-pyca and Pd-pyca–M41 catalysts with the parent support, MCM-41 are presented in Figure 4.5 as a typical example to elucidate the interaction of the Pd-pyca catalyst to the MCM-41 support. The representative FT-IR spectra of the MCM-41 framework shows characteristic bands at 962 cm^{-1} and 1090 cm^{-1}, which is attributed to ν(Si-OH) and ν_{asym}(Si-O-Si) vibrations respectively. Even after the Pd-pyca complex is encapsulated inside the mesopores' channels, these characteristic FT-IR bands of the Si-

MCM-41 are retained in Pd-M41 sample. Besides these bands, the encapsulated catalyst Pd-M41 showed the stretching vibrations at 1329 cm^{-1} ($\nu_{O=C-O}$), 1605 cm^{-1} ($\nu_{C=C}$, very weak band) and 1669 cm^{-1} ($\nu_{C=O}$), similar to those of Pd-pyca complex at 1330 cm^{-1}, 1604 cm^{-1} and 1668 cm^{-1} respectively [7].

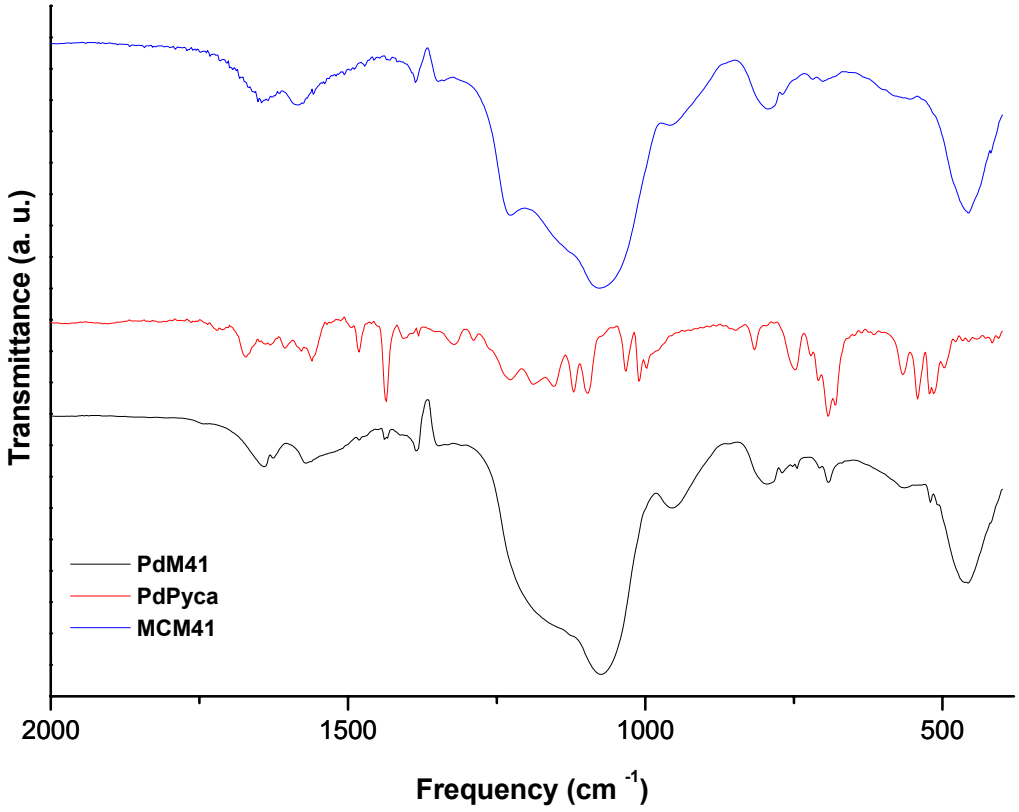

Figure 4.5. FTIR spectra of the homogeneous and heterogeneous Pd-catalysts

This shows that the Pd-pyca complex is well retained inside the MCM-41 channels without any bond breakage of its structure. But, there was a slight deviation observed in the Pd-N stretching frequencies of the Pd-M41 catalyst at 563 cm^{-1} (ν_{Pd-N}) from that of the Pd-pyca complex (ν_{Pd-N} = 569 cm^{-1}) [7]. The shift of this band to a lower wave number in case of the encapsulated Pd-pyca complex in MCM-41 mesopores reflects a possible coordination between N_{APTS} and Pd-atom bound through APTS. Thus, by FT-IR spectroscopy it was possible to elucidate the bonding interactions present as well as the typical spectral vibrations for the complex and the supports, while the complex was entrapped inside the mesopores.

Table 4.2. Summary of selected physical characterizations of the catalysts

Material	d_{hkl}	Unit Cell, Å	^{31}P CP-MAS δ_{iso}, ppm	Stretching frequency, cm^{-1}
Si–MCM-41	41.25 (100)	47.63	–	962, 1090[a]
Pd-M41	41.79 (100)	48.26	17.968	1329, 1669, 563[b]
Pd-M41–3	41.80 (100)	48.27	17.966	1329, 1669, 563
Si–MCM-48	37.43 (211)	93.56	–	963, 1090
Pd-M48	36.81 (211)	92.02	n. d.	1329, 1668, 563
Pd-pyca	–	–	33.13	1330, 1668, 569

Values in '()' are the Miller indices; n. d. = not determined; Pd-pyca–M41–3: Pd-pyca–M41 after 3rd recycle; values in respective order of (a) ν_{Si-OH}, $\nu_{Si-O-Si}$ & (b) $\nu_{o=c=o}$, $\nu_{c=o}$, ν_{Pd-N}

4.3.1.5. ^{31}P CP MAS NMR SPECTRA

^{31}P CP MAS (cross-polarized, magic angle spinning) NMR spectra of Pd-pyca complex and the Pd-complex inside the pores of MCM-41 and MCM-48 materials were obtained on a Bruker DRX 500 FT-NMR spectrometer at 202.64 MHz and 11.7 Tesla using 3 mm CP-MAS probe. The chemical shifts were referred to H_3PO_4 at 0 ppm and the spectra were collected at a spectral width of 20 kHz, with a flip angle of 45^o, 6000 real data points and 5 s relaxation delay.

A coupled ^{1}H–^{31}P CP MAS NMR spectra of the pure Pd-pyca complex shows a single ^{31}P peak (δ_{iso}= 33.13 ppm) as shown in Figure 4.6-a. In a typical ^{31}P CP MAS NMR of Pd-pyca complex encapsulated in MCM-41 material, only one ^{31}P signal (δ_{iso} = 17.968 ppm) as shown in Figure 4.6-b was observed. This sharp ^{31}P spectrum is pertinent to the single PPh_3 group of the Pd-pyca complex that is anchored inside the MCM-41 mesopore channel.

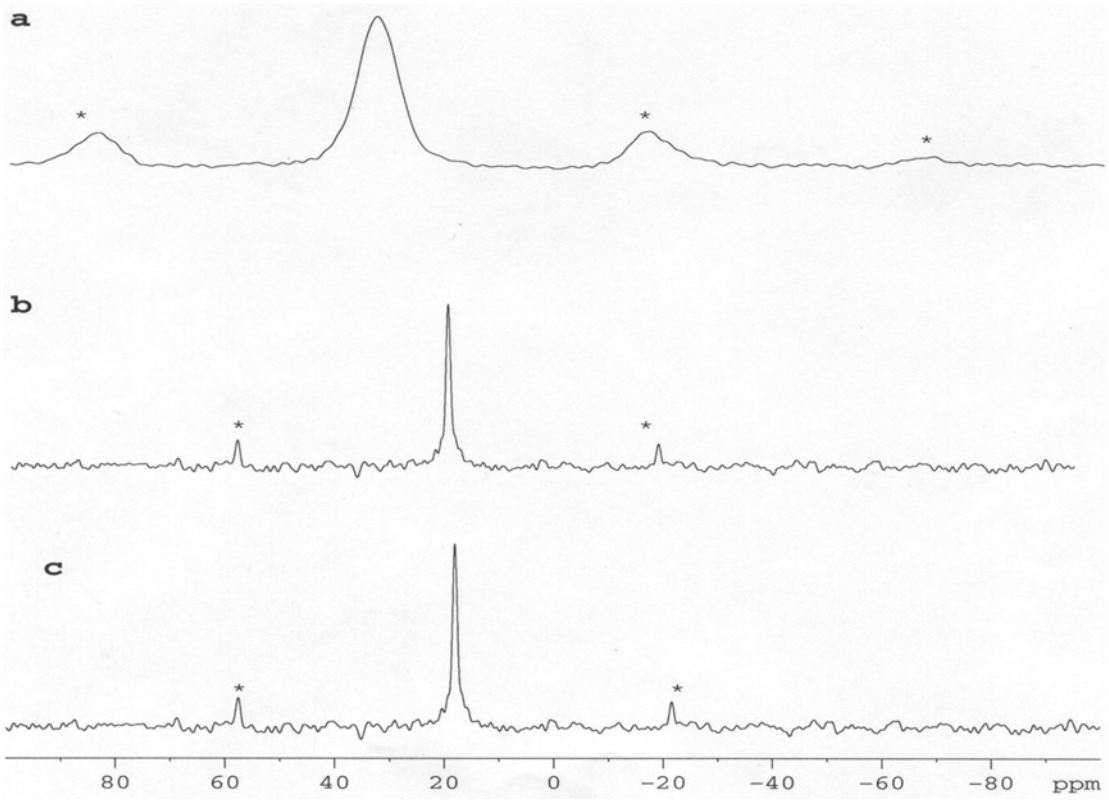

Figure 4.6. ^{31}P CP-MAS NMR of (a) Pd-pyca, (b) Pd-M41 and (c) Pd-M41-3

To ensure that the Pd-pyca complex was anchored inside the mesoporous channels, *solid-state* ^{31}P CP–MAS NMR spectra of a typical encapsulated catalyst (Pd-M41) was recorded and compared with the spectra obtained for neat Pd-pyca complex. The noticeable upfield shifts for Pd-M41 (δ_{iso}= 17.968 ppm, Figure 4.6-b) in comparison to the Pd-pyca complex observed (δ_{iso}= 33.13 ppm, Figure 4.6-a) suggests that there is a definite coordination between N_{APTS} and the Pd-atom. APTS (anchored inside the mesopores walls of MCM-41) when bound with the Pd-complex, donates the electron pair from N_{APTS} to the Pd-atom (see Figure 4.7), which in turn increases the electron density on the P_{PPh3} atoms (of the complex) by a dπ (P) $\leftrightarrow$ dπ (Pd) bonding, a fact that we observed earlier for anchored Rh-phosphine complex in mesoporous systems (*section 3.3.1.2*). This change in the NMR shift is consistent with the results of FT-IR spectral analysis obtained for these heterogeneous Pd catalysts (Scheme 4.1), which shows coordination between the N_{APTS} and Pd-atom of the Pd-pyca complex.

To validate that there was no leaching of Pd from the encapsulated catalyst (Pd-M41), ^{31}P CP-MAS NMR of the recycled Pd-M41-3 (Pd-M41 catalyst after the 3rd recycle) was recorded at same spectral frequency, width and accumulating 6000 real data points as that applied for the Pd-M41 catalyst. The spectra as presented in Figure 4.6 (-b, -c) show that the ^{31}P signal of Pd-M41-3 catalyst (17.966 ppm) lying in the equivalent position as that of Pd-M41 (17.968 ppm) with almost the same intensity. This is a conclusive proof that leaching of Pd metal has not occurred from the Pd-M41 catalyst system even after 3 recycles, which, otherwise, would have shown a completely different ^{31}P signal due to bond breakage of the Pd-pyca complex residing inside the mesopores. Thus, ^{31}P CP-MAS NMR of the encapsulated Pd-pyca catalyst not only determines the geometry or structure inside the mesopores, but also gives an evidence for no Pd-leaching from the support.

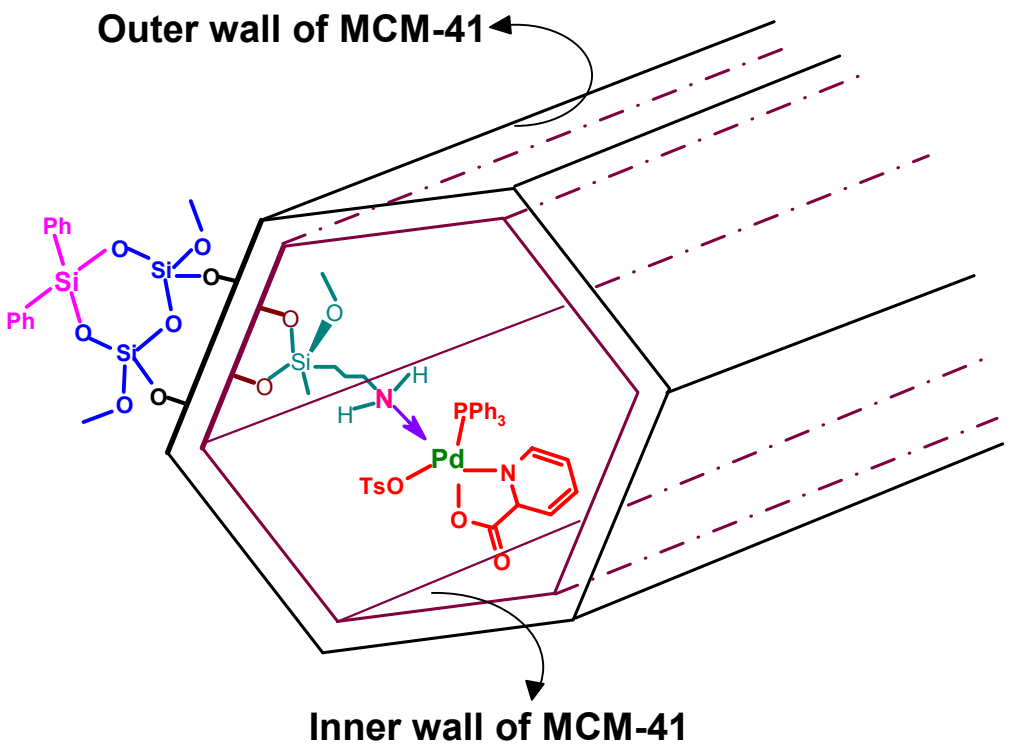

Figure 4.7. A schematic presentation of Pd-pyca–M41 catalyst

4.3.2. PERFORMANCE OF THE ENCAPSULATED CATALYSTS

The hydrocarboxylation experiments were carried out using catalysts Pd-pyca, Pd-M41 and Pd-M48 in a stirred high-pressure reactor, the details of the reaction set-up and procedure have already been presented in *section 4.2.3* of this chapter. Hydrocarboxylation (carbonylation) reactions are very hazardous because of handling of CO gas at high pressures and temperatures hence, extreme precautions and proper guidance while performing these reactions are suggested. The reaction mixtures and products were analyzed by gas chromatography (GC) to determine the conversion, selectivity and turnover frequency (TOF). The results on hydrocarboxylation of styrene, substituted styrenes as well as *p*-isobutylphenylethanol (IBPE) using these catalysts are presented in Table 4.3. The results showed almost complete conversion (> 95%) of all the substrates with a regioselectivity > 98% for the desired 2-arylpropanoic acids. The TOF values for hydrocarboxylation reaction using the anchored catalysts were in the range of 415 h^{-1} to 465 h^{-1} for styrene and 435 h^{-1} to 450 h^{-1} for IBPE as substrates [7]. Catalysts **Pd-M41** and **Pd-M48** show almost similar TOFs, which may be due to similar rate of interaction of the substrate molecules and the Pd atom residing inside the mesoporous matrices. Though, the TOF values are lower for anchored catalysts compared to the homogeneous **Pd-pyca** complex catalyst (TOF = 800 to 2600 h^{-1}), these heterogeneous catalysts are easier to separate and reuse in practice without affecting the activity or selectivity of the acid products formed in the reaction. The main concern, while using Pd-based catalyst systems for carbonylation or hydrocarboxylation reactions, has either been leaching of the Pd-metal in the course of reaction, or deactivation of the catalyst. In all the reactions carried out in this work using Pd-M41 or Pd-M48 catalysts, catalyst deactivation or formation of Pd (0) species in the encapsulated catalysts have never been observed (XPS and ^{31}P CP-MAS of the catalysts have proved this conclusively as presented in *sections 4.3.3* and *4.3.5* respectively).

Table 4.3. Comparison of activity and selectivity of various catalyst systems for hydrocarboxylation

Catalyst	Substrate	Conversion (%)	Selectivity (%)		TOF (h^{-1})	Time (h)
			iso	n		
Pd-pyca	Styrene	97.00	99.01	0.98	2600	0.18
Pd-M41	Styrene	98.12	99.31	0.68	463	12.0
Pd-M48	Styrene	98.37	99.03	0.96	417	12.0
Pd-pyca	4-Methyl-Styrene	95.06	99.12	0.81	1173	0.83
Pd-M41	4-Methyl-Styrene	97.80	98.60	1.38	406	12.0
Pd-M48	4-Methyl-Styrene	98.11	99.10	0.88	367	12.0
Pd-pyca	4-^{t}Butyl-Styrene	95.00	99.00	0.98	1313	0.35
Pd-M41	4-^{t}Butyl-Styrene	93.40	99.31	0.67	286	12.0
Pd-M48	4-^{t}Butyl-Styrene	95.10	99.23	0.75	262	12.0
Pd-pyca	IBPE[a]	99.00	99.00	0.99	804	0.60
Pd-M41	IBPE	95.60	97.50	2.45	450	12.0
Pd-M48	IBPE	95.00	97.90	1.98	439	11.0

Catalyst: 2 kg m^{-3} (0.5 kg m^{-3} Pd-Pyca); substrate: 9.6 mmol (14.04 mmol for Pd-Pyca); LiCl: 0.5 mmol (5.6 mmol for Pd-Pyca); TsOH: 0.5 mmol (5.6 mmol for Pd-Pyca); PPh_3: 0.095 mmol (0.19 mmol for Pd-Pyca); H_2O: 0.01 mmol (67 mmol for Pd-Pyca); solvent: MEK; P_{CO}: 5.4 MPa; agitation speed: 18.34 Hz; temperature: 388 K; total liquid volume: 2.5×10^{-5} m^3; Pd-content: 0.18 wt% in Pd-M41 and 0.20 wt% in Pd- M48; TOF = turn over frequency; [a] Isobutylphenylethanol

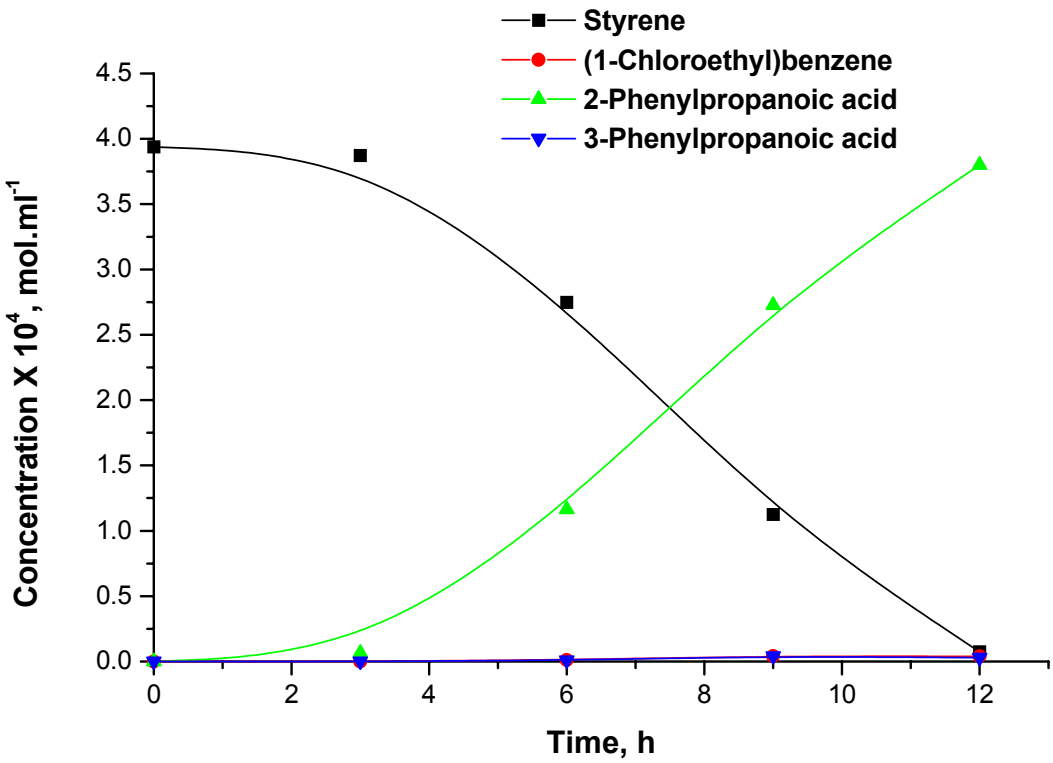

Figure 4.8. Concentration time profile for styrene hydrocarboxylation reaction using Pd-M41

Reaction conditions: catalyst: 2 kg m^{-3}; styrene: 9.6 mmol; LiCl: 0.5 mmol; TsOH: 0.5 mmol; PPh_3: 0.095 mmol; H_2O: 0.01 mmol; solvent: methylethylketone; P_{CO}: 5.4 MPa; agitation speed: 18.34 Hz; temperature: 388 K; total liquid volume: 2.5x10 $^{-5}$ m^3; Pd-content: 0.18 wt% in Pd-M41

The concentration-time profile (Figure 4.8) for hydrocarboxylation of styrene using Pd-M41/PPh_3/TsOH/LiCl as a catalyst system, revealed the formation of (1-Chloroethyl) benzene, though in very low concentrations. The C-T (concentration-time) profile elucidates that the concentration of 1-(Chloroethyl) benzene passes through a maximum, which is indicative of its formation as well as consumption during the reaction course. The olefin or halo-derivative or both can be activated by Pd-catalyst for carbonylation under the present set conditions. A strong effect of halide promoters on the carbonylation rate as well as selectivity for 2-Phenylpropanoic acid suggests that the chloro-derivative is the active substrate for carbonylation. The chloro-derivative is formed by the acid catalyzed addition of H^+ and Cl^- across the double bond (Scheme 4.3). Hence, sufficient concentration of H^+ and Cl^- are required for the enhanced formation of 1-haloderivative.

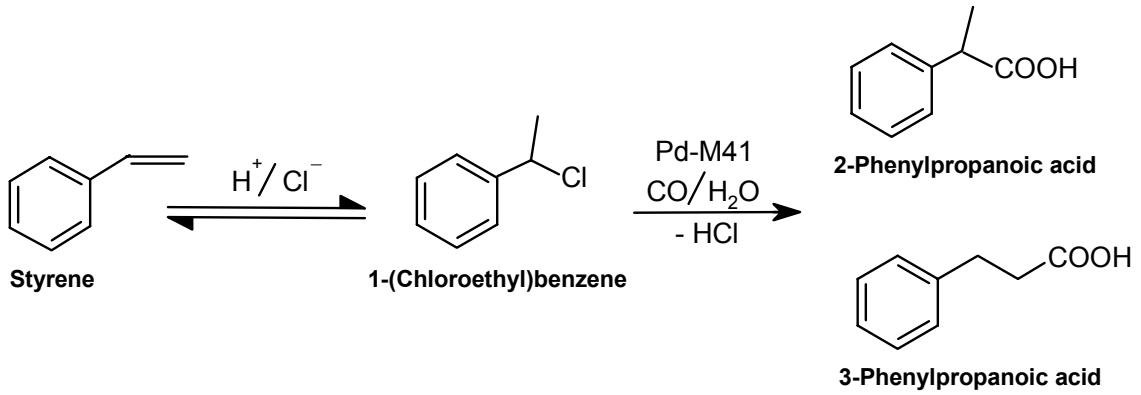

Scheme 4.3. Reaction pathway for hydrocarboxylation of styrene using Pd-M41 catalyst

4.3.2.1. ROLE OF PROMOTERS

Earlier Jayasree et al. [7, 23] reported the effect of promoters (LiCl and TsOH) in the hydrocarboxylation of styrene using homogeneous, biphasic as well as supported Pd/C catalysts. It was shown that catalytic activity varied significantly with the nature of counter ions of the acidic and halide promoters. The activity decreased in the reverse order of coordination ability for $TsO^- > CH_3SO_3^- > Cl^-$ ions, whereas, activity decreased in case of different cationic chloride promoters in the order, $Li^+ > H^+ > Bu_4N^+$. Chloride ions were found to exhibit higher activity as well as selectivity in comparison to other halide ions e.g. Br^-, F^- or I^-. Infact, bromide or iodide promoters were found to inhibit the hydrocarboxylation reaction when used instead of LiCl promoter. Thus, it was conclusive that use of optimum ratio TsOH and LiCl is a must for attaining high regioselectivity and activity for styrene conversion to respective iso- and normal-acids using Pd-pyca catalyst. Herein, the effect of TsOH and LiCl has been studied in varied proportions in the hydrocarboxylation of styrene (Table 4.4) and it was observed that the same trend was followed as in the homogeneous reaction medium. In order to understand the effect of halide ions in the hydrocarboxylation activity, a concentration-time profile experiment for styrene hydrocarboxylation using Pd-M41 catalyst was performed (see Figure 4.8). The analyses of the intermediate samples of the reaction using Pd-M41/TsOH/LiCl as a catalyst precursor system confirmed the presence of (1-Chloroethyl)benzene in lower concentrations. The strong effect of LiCl on the hydrocarboxylation rate as well as 2-Phenylpropanoic acid (yield of 2-Phenylpropanoic acid was of very low concentration and hence, could not be included in

the figure 4.8) suggests that the chloro-derivative is the active substrate for hydrocarboxylation, as observed earlier by Jayasree and coworkers [23]. A study on the effect of various promoters revealed a strong influence of the concentration of TsOH/LiCl ratio on the catalytic activity using Pd-M41 catalyst for styrene hydrocarboxylation to iso- and normal-acids. In absence of either TsOH or LiCl, the reaction yielded in very TOF (30 h^{-1}), whereas, keeping a ratio of 1:1 showed a quantum jump in the TOF (463 h^{-1}).

Table 4.4. Role of promoters on hydrocarboxylation of styrene with Pd-pyca and Pd-M41

Entry	Catalyst	TsOH/LiCl ratio	Time (h)	Conversion (%)	Selectivity iso : n	TOF (h^{-1})
1	Pd-pyca	5.6 : 5.6	0.468	99.00	98.42 : 1.58	2121
2	Pd-M41	0.5 : 0.5	12.0	98.12	99.31 : 0.68	463
3	Pd-pyca	5.6 : 2.8	0.8	97.00	98.43 : 1.57	1216
4	Pd-M41	0.5 : 0.25	20.0	97.19	99.25 : 0.73	280
5	Pd-pyca	2.3 : 5.6	0.417	98.00	98.21 : 1.78	2359
6	Pd-M41	0.25 : 0.5	15.0	98.01	99.19 : 0.80	370

Reaction conditions: catalyst: 2 kg m^{-3}; styrene: 9.6 mmol; PPh_3: 0.095 mmol; H_2O: 0.01 mmol; solvent: methylethylketone; P_{CO}: 5.4 MPa; agitation speed: 18.34 Hz; temperature: 388 K; total liquid volume: 2.5×10^{-5} m^3; Pd-content: 0.18 wt% in Pd-M41

4.3.2.2. ROLE OF ADDITION OF FREE PPh_3 LIGAND

In our laboratory, reports on carbonylation of aryl olefins and alcohols using Pd (II) complexes [5(b), 24, 25] showed that the catalytic activity as well as desired regioselectivity was substantially enhanced when a combination of TsOH and LiCl was used as promoters under homogeneous conditions. In order to have a heterogeneous Pd-catalyst for the carbonylation of styrene, a reaction was carried out using Pd-M41 in the presence of TsOH and LiCl as promoters that showed almost no carbonylation occurs (~ 3% conversion to 2-Phenylpropanoic acid (2-PPA) after 12 h, see Figure 4.9) under these conditions. The reaction was then repeated in the presence of 11 – 44 equivalents of PPh_3 to Pd (0.09 mg Pd present in 50 mg Pd-M41; PPh_3 varied from 1 mg – 4 mg) with only 15% conversion of

styrene to 2-PPA. After few trials for setting up an optimum concentration of PPh_3 for the reaction system, it was observed that above a minimum concentration of PPh_3 i.e., 1.2216×10^{-3} kmol/m^3 in solution (i.e., 8 mg PPh_3), the carbonylation occurred smoothly and the TOF increased steadily with the PPh_3 concentration till 3.8175×10^{-3} kmol/m^3 (25 mg PPh_3, see Figure 4.9). Similar observations indicating strong effect of PPh_3 concentration on catalytic activity of supported Pd-catalysts has been reported earlier for a few other reactions. Thus, a heterogeneous catalytic system consisting of Pd-M41/PPh_3/TsOH/LiCl showed a high TOF (463 h^{-1}) and regioselectivity (97.5 %) for 2-PPA at relatively lower CO pressure (5.4 MPa) and 388 K temperature.

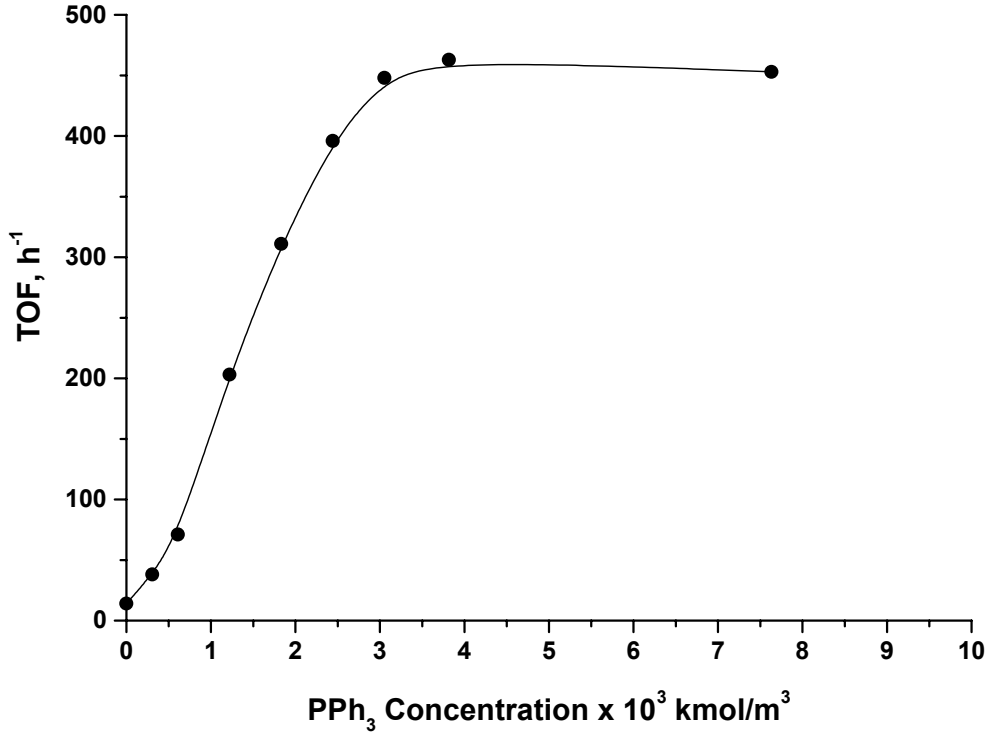

Figure 4.9. Effect of PPh_3 concentration on hydrocarboxylation of styrene using Pd-M41

Reaction conditions: catalyst: 2 kg m^{-3}; styrene: 9.6 mmol; LiCl: 0.5 mmol; TsOH: 0.5 mmol; H_2O: 0.01 mmol; solvent: methylethylketone; P_{CO}: 5.4 MPa; agitation speed: 18.34 Hz; temperature: 388 K; total liquid volume: 2.5×10^{-5} m^3; Pd-content: 0.18 wt% in Pd-M41

4.3.3. LEACHING EXPERIMENTS

To prove the stability of these catalysts, hot reaction-mixture filtrates were analyzed for Pd-content by ICP-AES, which showed almost no leaching of Pd metal from catalysts **Pd-M41** and **Pd-M48** in the liquid phase during reactions (for 50mg Pd-M41 catalyst: Pd-content: 900 ppm, total Pd leached after 3 recycles: 0.5 ppm). The filtrates showed no hydrocarboxylation activity, when tested without any addition of fresh catalysts. The catalysts were found to be very stable, restoring high activity and selectivity even after three recycles, as has been presented in Figure 4.10 for hydrocarboxylation of styrene with catalysts **Pd-M41** and **Pd-M48**. Comparison of catalysts **Pd-M41** and **Pd-M41-3** (recycle 3 with catalyst **Pd-M41**) analyzed by ^{31}P CP MAS NMR (see Figure 4.6-c), showed no change in δ_{iso} values. Thus, the geometry of the Pd-pyca anchored inside the MCM-41 remains intact even after 3rd recycle. This observation provides evidence that **Pd-pyca** complex is encapsulated inside the mesopores and does not leach out under reaction conditions. In contrast to this, the catalyst prepared by anchoring the **Pd-pyca** complex on zeolite Y as a support (**Pd-Y-S**) showed considerable amount of leaching of Pd metal (~ 19%) during reaction. A similar trend for leaching was observed by Fraile et al. for epoxidation reactions with silica supports [26]. Moreover, XPS of the used **Pd-Y-S** catalyst (see Table 4.1 of this chapter) showed a change in binding energy values [22] from Pd (II) species (337.1 eV and 343.1 eV) to Pd (0) species (335.3 eV and 340.8 eV). Infact, the first recycle suing Pd-Y-S catalyst for hydrocarboxylation of styrene showed a severe drop in conversion (as well as activity) from 92.3% to 37.1% with a consistent regioselectivity (> 98%), probably due to deactivation of the catalytic species and formation of Pd (0) metal owing to leaching from the zeolite support. XPS of the catalyst showed the B. E. values of $Pd_{5/2}$ and $Pd_{3/2}$ at 335.1 eV and 340.9 eV respectively that is consistent with the B. E. values of Pd (0) species.

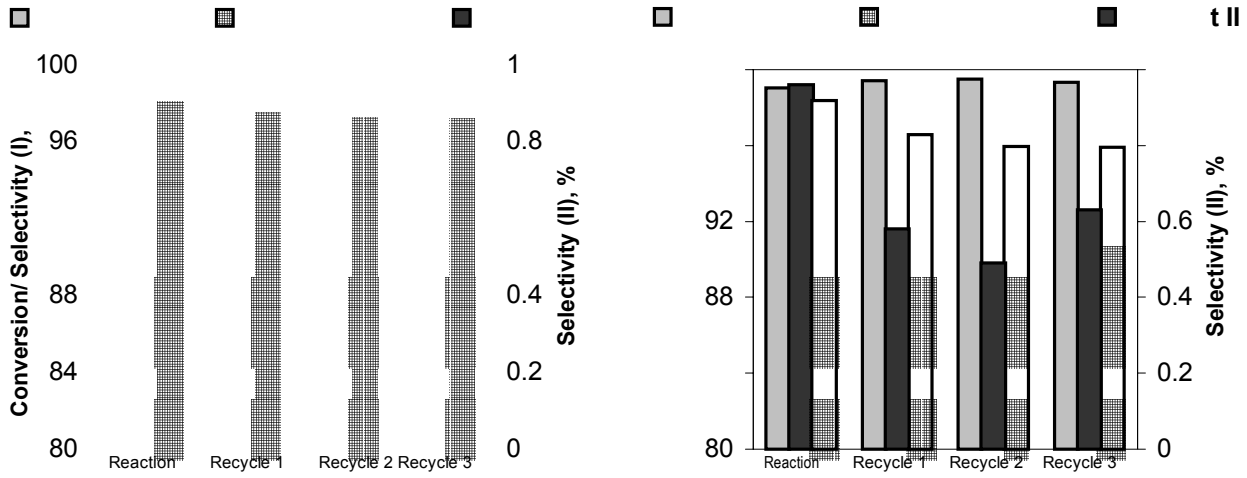

Figure 4.10. Recycle studies for styrene hydrocarboxylation using Pd-M41 catalyst (left) and Pd-M48 catalyst (right)

Reaction conditions: catalyst: 2 kg m^{-3}; styrene: 4.8 mmole; LiCl: 0.5 mmole; TsOH: 0.5 mmole; PPh_3: 0.095 mmole; H_2O: 0.01 mmole; solvent: methylethylketone; P_{CO}: 5.4 MPa; agitation speed: 18.34 Hz; temperature: 388 K; total liquid volume: 2.5×10^{-5} m^3; Pd-content: 0.18 wt% in Pd-M41; 0.20 wt.% in Pd-M48.

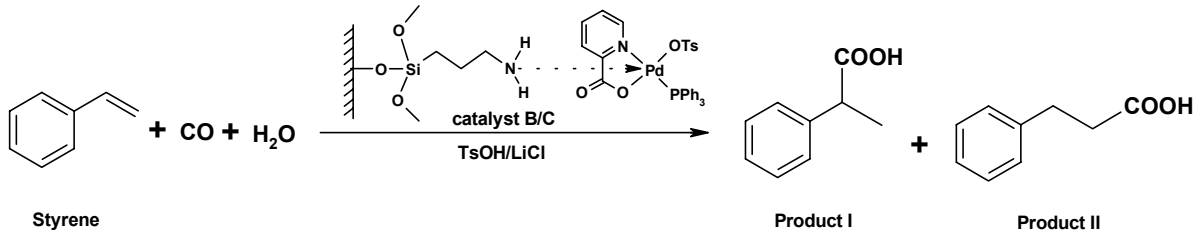

Scheme 4.4. Recycle studies for hydrocarboxylation of styrene with Pd-M41 and Pd-M48 catalysts

4.4. CONCLUSION

Novel heterogeneous catalysts consisting of encapsulated Pd-pyca comlex in the pores of cubic and hexagonal mesophases of MCM–48 and MCM–41 respectively have been reported, for hydrocarboxylation of aryl olefins and alcohols *without catalyst leaching*. This is a first case for successfully heterogenizing Pd-comlex catalysts for carbonylation or hydrocarboxylation reactions with high activity (~ 95%) and regioselectivity (~ 99%) for aryl olefins and alcohols. To minimize catalyst leaching or Pd metal deactivation of the heterogeneous Pd-bound mesoporous catalysts, selective internal grafting technique was used to anchor Pd-complex only inside the mesopores. The use of such air-stable heterogeneous catalysts showed high activity, regoselectivity, recyclability and easy catalyst-product separation from the liquid phase. Though, the reaction rates are lower compared to the homogeneous system, the cumulative turn over numbers for the anchored Pd-complex catalysts were significantly higher considering recycle experiments with complete conversion of styrene in each batch cycle. These encapsulated catalysts can open up new vistas for the industrial applications in synthesis of important intermediates used for fine chemcial industry. A detailed characterization of the catalysts specially using ^{31}P CP MAS NMR, TEM and XPS (before and after use) analyses, confirmed true heterogeneity and configuration of the Pd-complex inside the support-pores.

REFERENCES

[1] (a) Colquhoun, H. M.; Thompson, D. J.; Twigg, M. V. *Carbonylation: Direct Synthesis of Organic Compounds*; Plenum: New York, 1991. (b) Beller, M.; Bolm, C. *Transition Metals for Organic* Synthesis, Wiley-VCH, Weinheim, 1998. (c) Rieu, J. P.; Boucherle, A.; Cousse, H.; Mouzin, G. *Tetrahedron* **1986**, *42*, 4095. (d) Wu, G. G.; Wong, Y; Poirier, M. *Org. Lett.* **1999**, *1*, 745. (e) Beller, M.; Eckert, M.; Geissler, H., Napierski, B.; Rebenstock, H. P; Holla, E. W. *Chem. Eur. J.* **1998**, *4*, 935. (f) Imada, Y.; Alper, H. *J. Org. Chem.* **1996**, *61*, 6766. (g) Pisano, C.; Consiglio, G.; Sironi, A.; Moret, M. *J. Chem. Soc. Chem. Commun.* **1991**, 421.

[2] *Applied Homogeneous Catalysis with Organometallic Compounds*; Cornils, B.; Herrmann, W. A., Eds.; VCH: Weinheim, 1996; Vols. 1 and 2. (b) Sheldon, R. A. *Chem. Ind.* **1992**, 903.

[3] Armor, J. N. *Appl. Catal.* **1991**, *78*, 141.

[4] Elango, V.; Davenport, K. G.; Murphy, M. A.; Mott, G. N.; Zey, E.G.; Smith, B. L.; Moss, G. L. Eur. Pat. 400892, **1990**.

[5] (a) Seayad, A.; Kelkar, A. A.; Chaudhari, R. V. S*tud. Surf. Sci. Catal.* **1998**, *113*, 883. (b) Seayad, A.; Jayasree, S.; Chaudhari, R. V. *Catal. Lett.* **1999**, *61*, 99. (c) del Rio, I.; Ruiz, N.; Claver, C.; van der Veen, L. A.; van Leeuwen, P. W. N. M. *J. Mol. Catal. A: Chem*. **2000**, *161*, 39.

[6] Chaudhari, R. V.; Jayasree, S.; Seayad, A. M. US Patent 6,093,847, **2000**.

[7] Jayasree, S.; Seayad, A.; Chaudhari, R. V. *Org. Lett.* **2000**, *2*, 203.

[8] (a) Sheldon, R. A.; Maat, L.; Papadogianakis, G. (Hoechst Celanese Corp.) US Patent 5,536,874, **1996**. (b) Papadogianakis, G.; Maat, L.; Sheldon, R. A. *J. Chem. Tech. Biotech.* **1997**, *70*, 83.

[9] Jayasree, S.; Seayad, A.; Chaudhari, R. V. *Chem. Commun.* **2000**, 1239.

[10] Davies, I. W.; Matty, L.; Hughes, D. L.; Reider, P. J. *J. Am. Chem. Soc.* **2001**, *123*, 10139.

[11] Jayasree, S.; Seayad, A.; Chaudhari, R. V. *Chem. Commun.* **1999**, 1067.

[12] Jang, E. J.; Lee, K. H.; Lee, J. S.; Kim, Y. G. *J. Mol. Catal. A: Chem.* **1999**, *144*, 431.

[13] El Ali B.; Alper, H. *J. Org. Chem.* **1993**, *60*, 4731.

[14] Lee, C. W.; Alper, H. *J. Org. Chem.* **1995**, *60*, 250.

[15] Linsen, K. J. L.; Libens, J.; Jacobs, P. A. *Chem. Commun.* **2002**, 2728.

[16] (a) Kresge, C. T.; Leonowicz, M. E.; Roth, W. J.; Vertulli, J. C.; Beck, J. S. *Nature* **1992**, *359*, 710. (b) Beck, J. S.; Vertulli, J. C.; Roth, W. J.; Leonowicz, M. E.; Kresge, C. T.; Schmitt, K. D.; Chu, C. T.-W.; Olson, D. H.; Sheppard, E. W.; McCullen, S. B.; Higgins, J. B.; Schlenker, J. L. *J. Am. Chem. Soc.* **1992**, *114*, 10834.

[17] Mukhopadhyay, K.; Mandale, A. B.; Chaudhari, R. V. *Chem. Mater.* **2003**, *15*, 1766.

[18] Corma, A. *Chem. Rev.* **1997**, *97*, 2373.

[19] Mukhopadhyay, K.; Ghosh, A.; Kumar, R. *Chem. Commun.* **2002**, 2404.

[20] Shephard, D. S.; Zhou, W.; Maschmeyer, T.; Matters, J. M.; Caroline L. Roper, C. L.; Parsons, S.; Johnson, B. F. G.; Duer, M. J. *Angew. Chem. Int. Ed.* **1998,** *37*, 2719.

[21] (a) Thomas, J. M.; Terasaki, O.; Gai, P. L.; Zhou, W. Z.; Gonzalez–Calbet, J. *Acc. Chem. Res.* **2001**, *34*, 583. (b) Ozkaya, D.; Zhou, W. Z., Thomas, J. M.; Midgley, P. A.; Keast, V. J.; Hermans, S. *Catal. Lett.* **1999**, *60*, 113.

[22] (a) Wagner, C. D.; Riggs, W. M.; Davis, L. E.; Moulder, J. E.; Muilenberg (Eds.), *Handbook of X-ray Photoelectron Spectroscopy*; **1979**, Perkin–Elmer Corporation (USA). (b) Andersson, S. L. T.; Scurrell, M. S. *J. Catal.* **1979**, *59*, 340.

[23] Jayasree, S. *PhD Thesis submitted to the University of Pune*, **2000**.

[24] Jayasree, S.; Seayad, A.; Sarkar, B. R.; Chaudhari, R. V. *J. Mol. Catal. A: Chem.* **2002**, *181*, 221.

[25] (a) Fraile, J. M.; Garcia, J. I.; Mayoral, J. A.; Vispe, E; Brown, D. R.; Naderi, M. *Chem. Commun.* **2001**, 1510. (b) Pauwels, B.; van Tendeloo, G.; Thoelen, C.; van Rhijn, W.; Jacobs, P.A. *Adv. Mater.* **2001**, *13*, 1317.

CHAPTER 5

CATALYSIS BY TETHERED METAL COMPLEXES: HYDROFORMYLATION AND HYDROCARBOXYLATION

5.1. INTRODUCTION

Past three decades in catalysis saw various efforts to support metal complexes on inert, insoluble, inorganic matrices for '*heterogenization*' of soluble metal complexes to solid catalysts active for a variety of industrially important reactions [1]. Numerous methods of heterogenization have been investigated [2–6] for applications to various reactions. However, lower activity-selectivity, leaching of metals, limitations of the support-pore sizes and deactivation of the catalysts have limited the actual use of 'heterogenized' catalysts in industry leaving challenges to look for newer versions or modification of the heterogenized catalysts [7]. Recently, a novel approach to immobilize homogeneous catalysts on solid supports (e.g. clay, carbon, La_2O_3, Al_2O_3, SiO_2) has been proposed in which, the organometallic complex was tethered to inorganic matrices [8–10] for asymmetric hydrogenation of various alkenes, alkynes and aldehydes with enhanced catalytic activity and reusability. The authors have shown that high activity and enantioselectivity for the desired products when methyl 2-acetamidoacrylate was subjected to hydrogenation with a Rh(DiPamp) homogeneous catalyst tethered to various supports e.g. Montmorillonite K clay, Al_2O_3, carbon or Ln_2O_3, at 25 °C and 1 atm. Pressure. This anchoring procedure has also been applied to achiral complexes with similar results. For instance, hydrogenation of 1-hexene over a Wilkinson's catalyst anchored to PTA treated Al_2O_3 proceeded 2–3 times faster than the corresponding homogeneously catalyzed reaction, even on the first use of the heterogenized material. A Rh(dppb) complex anchored to a PTA modified Al_2O_3 was used for several successive hydrogenations of 1-hexene with a combined substrate: catalyst ratio of about 8000: 1. An analysis of the product mixtures from these reactions found no detectable rhodium present. One of the advantages of this approach to anchoring homogeneous catalysts is its apparent generality, in that this procedure can be used to anchor a variety of pre-formed active homogeneous catalysts onto a number of different supports. It is shown that the tethering technique leads to a true heterogeneous catalyst, which gives enhanced catalytic activity and stability compared to other methods including encapsulation.

But, no attempts were made previously to change the tethering metal complex catalysts for applications in other industrially important reactions, e.g. carbonylation, hydroformylation etc [11,12]. Recently, in our laboratory heterogeneous catalysts for hydroformylation [13] and hydrocarboxylation [14] reactions by encapsulation and anchoring (specific binding inside the pores) techniques to supports e.g. zeolite Na-Y,

MCM-41 and MCM-48 has been reported. The objective of this work was to extend and explore the tethering method for heterogenizing metal complex catalysts for catalytic applications in hydroformylation [15] and hydrocarboxylation reactions. Particularly, heterogenized Wilkinson's $HRh(CO)(PPh_3)_3$ catalyst and Pd-Pyca complex catalyst (developed in our lab) were prepared by tethering to zeolite Na-Y and other supports (e.g. SiO_2, Si-MCM-41, Al_2O_3 and MgO) through heteropolyacid [e.g. phosphotungstic acid ($H_3PW_{12}O_{40}$. xH_2O, where x = 6 – 24)] as a tethering agent. It is demonstrated that these heterogeneous catalysts thus prepared, give higher activity and stability for hydroformylation and hydrocarboxylation reactions.

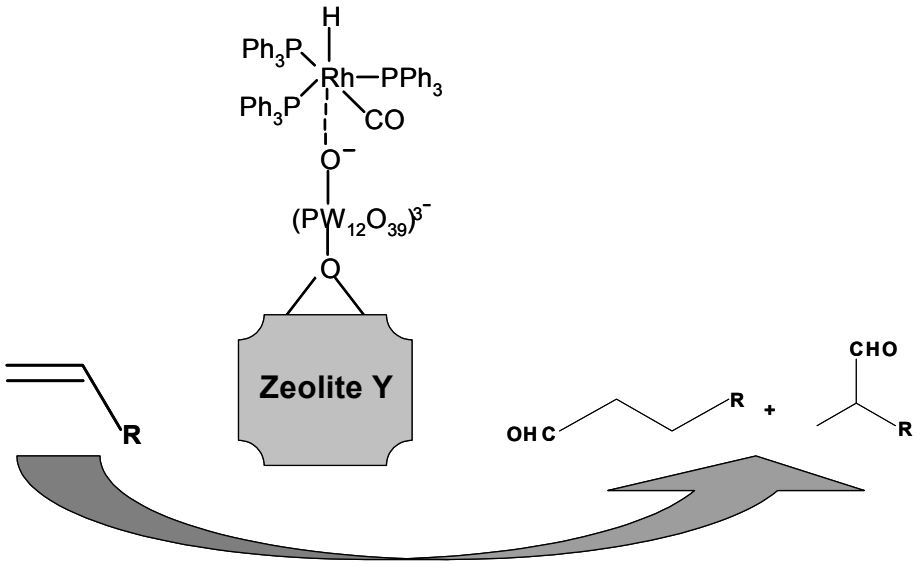

Scheme 5.1. Hydroformylation using $HRh(CO)(PPh_3)_3$ tethered to PTA on zeolite Na-Y

Zeolite Na-Y was our obvious choice as the support owing to its large cavity (12 Å supercage) accessible through four 7.4 Å windows, high surface area (~ 700 m^2 g^{-1}), high Al-content (Si/Al = 2.37), channel structures and thermo-chemical stabilities [16]. Moreover, zeolite Y particles are highly monodisperse in morphology (especially in size) with about 95 % monodispersity for 300 nm particle-size. This feature obviously helps in tethering the phosphotungstic acid (PTA) molecules on the zeolite surface in a uniform manner and hence, maximum loading of PTA molecules (hence, more of metal complex can also be anchored to the PTA surface) can be achieved on the uniform and nano-sized zeolite particles. A few catalysts tethered to alumina were also prepared to compare the catalytic activities of the Na-Y supported catalysts. A detailed characterization of the

heterogeneous catalysts using ^{31}P CP MAS NMR, powder X-ray diffraction and X-ray photoelectron spectra (XPS) is also reported to prove the catalyst heterogeneity. The performance of the tethered catalysts has also been compared with other heterogeneous catalysts reported in chapters 3 and 4.

5.2. EXPERIMENTAL METHODS

5.2.1. SYNTHESIS OF CATALYSTS AND PERFORMANCE EVALUATION

5.2.1.1. Synthesis of zeolite Na–Y, $HRh(CO)(PPh_3)_3$ and Pd-Pyca complexes

Syntheses of zeolite Na–Y, $HRh(CO)(PPh_3)_3$ and Pd-Pyca complexes were carried out as described in chapter 3 (sections 3.2.2.1 and 3.2.2.5) and chapter 4 (section 4.2.2.3) respectively.

5.2.1.2. Synthesis of tethered $HRh(CO)(PPh_3)_3$ and Pd-Pyca complexes on phosphotungstic acid (PTA) anchored to zeolite Na-Y and other supports

The preparation of the tethered catalysts was followed according to the procedure reported previously by Augustine et al. (8, 9). Specific details to synthesize metal complexes tethered to PTA-bound zeolite Na-Y [15] are described below:

$HRh(CO)(PPh_3)_3$ and Pd-Pyca complexes were synthesized according to published procedures [17, 18] as discussed in chapters 3 and 4 respectively.

In order to prepare phosphotungstic acid tethered to zeolite Na-Y support, to a solution of phosphotungstic acid (100 μmol) in 15 ml of ethanol, a slurry of zeolite Y (1.5 g of Na–Y, Si/Al = 2.37) in 45 ml ethanol was added and stirred vigorously for 6 h. The white solid (PTA–Y) obtained was filtered, washed thoroughly with ethanol to ensure complete removal of phosphotungstate anion from the solid and dried at 373 K for 6 h. A part of this solid (0.5 g) was suspended in 20 ml ethanol to which, 30 μmol of $HRh(CO)(PPh_3)_3$ was added and the mixture refluxed under stirring for 18 h. The light-grey solid product (Wk–PTA–Y) was filtered, washed with ethanol repeatedly (Soxhlet extracted for 18 h) to remove un-anchored Rh-complex to PTA–Y, dried at 353 K and used as such for hydroformylation reactions. Similarly, Wk–PTA–Al_2O_3, Wk-PTA-SiO_2, Wk-PTA-M41 and Wk-PTA-MgO catalysts were also prepared by choosing Al_2O_3, SiO_2, Si-MCM-41 and MgO supports following the same procedure (see Table 5.4 for Rh-contents).

The specifications of Wk–PTA–Y catalyst were: Rh content: 0.49% w/w; W content: 1.59% wt./wt.; average particle size: 0.5 x 0.7 μm; surface area: 720 m^2 g^{-1} for Na–Y and 372 m^2 g^{-1} for Wk–PTA–Y.

For synthesis of tethered Pd-Pyca catalyst on phosphotungstic acid bound zeolite Na-Y, 0.5 g of PTA-Y was suspended in 20 ml ethanol and 30 μmol of Pd-Pyca complex was added and refluxed under stirring for 18 h. The light-yellow solid product (Pd–PTA–Y) was then washed with ethanol repeatedly (Soxhlet extraction for 18 h) to remove un-anchored Pd-complex to PTA–Y, dried at 353 K and used as such for hydrocarboxylation reactions.

The specifications of Pd–PTA–Y catalyst were: Pd content: 0.60% w/w; W content: 1.70% wt./wt.; average particle size: 0.5 x 0.7 μm; surface area: 720 m^2 g^{-1} for Na–Y and 339 m^2 g^{-1} for Pd–PTA–Y.

5.2.2. REACTOR SET-UP AND EXPERIMENTAL PROCEDURE

All the hydroformylation and hydrocarboxylation reactions were carried out in a 50 ml microclave reactor (Parr Instrument Company, USA) with a known quantity of olefin or alcohol and the tethered catalysts (Wk–PTA–Y and Pd–PTA–Y). The hydroformylation experiments were performed at 373 K and 4.08 MPa of 1:1 (CO + H_2) mixture using cyclohexane as a solvent, while hydrocarboxylation experiments were performed at 388 K and 3.06 MPa of CO using methylethylketone as a solvent. The details have been reported in Chapter 3 (Section 3.2.3) and Chapter 4 (Section 4.2.3). In hydroformylation experiments, as the reaction progressed, CO + H_2 in 1:1 ratio was supplied from a reservoir vessel (maintained at higher pressure than the reactor) using constant pressure regulating device. Since, most of our experiments showed a material balance, between (CO + H_2) consumed and olefin conversions with the aldehyde products formed, to the extent of > 98% (see Table 5.3 and Figure 5.8), by this procedure, constant pressure as well as composition of CO and H_2 was maintained during an experiment. It was also confirmed by analysis of the CO and H_2 content in the gas phase by GC after the reaction in a few cases. Similar procedure was followed to obtain a material balance between CO consumed and olefin/ alcohol conversions with the acid products formed, to the extent of > 98% (see Table 5.5) for hydrocarboxylation reactions.

In a typical experiment, known amount of olefin with cyclohexane (AR grade, Thomas & Baker) as a solvent and heterogenized tethered Rh-catalyst were charged into

the reactor and the contents flushed with nitrogen and then with a mixture of 1:1 CO and H_2. The contents of the reactor were heated to a desired temperature, and then a mixture of CO and H_2 (1:1) was introduced slowly into the autoclave up to a desired pressure. A sample of the liquid phase mixture was withdrawn and the reaction started by switching the stirrer on. The reaction was then continued at a constant pressure of CO and H_2 by supplying CO/H_2 mixture as per consumption, from the reservoir vessel using a constant pressure regulator.

For a typical hydrocarboxylation reaction using the tethered catalyst (Pd-PTA-Y), the autoclave was charged with required amount of catalyst in required amount of water after making the total volume 25 mL with substrate in methylethylketone (MEK) as a solvent, along with required amount of promoters (TsOH, PPh_3 and LiCl). The contents were flushed few times with nitrogen followed by carbon monoxide and heated to the desired temperature. After attaining the temperature, the autoclave was pressurized with CO to the desired level and the reaction started by starting agitation. To maintain a constant pressure in the reactor, CO was fed through a constant-pressure regulator from a reservoir vessel (100 mL). Pressure drop in the reservoir vessel was recorded by means of a pressure transducer as a function of time. From these data, the conversion, selectivity turnover frequency (TOF) and selectivity of the reactions were calculated.

Both hydroformylation and hydrocarboxylation experiments should be performed with utmost care and precautions as it involves use of CO and/or H_2 at high pressures.

5.3. CHARACTERIZATION OF THE CATALYSTS

^{31}P CP–MAS NMR spectra of $HRh(CO)(PPh_3)_3$ complex (Wk), PTA and Wk–PTA–Y were obtained on a Bruker DRX 500 FT-NMR spectrometer at 202.64 MHz and 11.7 Tesla using 3 mm CP-MAS probe. The chemical shifts were referred to H_3PO_4 at 0 ppm and the spectra were collected at a spectral width of 20 kHz, with a flip angle of 45^o, 6000 real data points and 5 s relaxation delay. ^{31}P CP–MAS NMR spectra of Pd-Pyca complex, PTA and Pd-Pyca–PTA–Y (Pd-PTA-Y) were obtained on a Bruker DSX 300 FT-NMR spectrometer at 121.58 MHz and 7.05 Tesla using 89 mm CP-MAS probe. The chemical shifts were referred to H_3PO_4 at 0 ppm and the spectra were collected at a spectral width of 50 kHz, with a flip angle of 6.2 μs for 90° pulse, 6000 real data points and 5 s relaxation delay.

X-ray Photoelectron Spectroscopy (XPS) measurements of Wk–PTA–Y and Pd–PTA–Y was recorded in VG Microtech ESCA 3000 instrument, at 10^{-10} Torr pressure, a pass energy of 50 eV and using un-monochromatized Mg–K_α (photon energy of 1253.6 eV) as the radiation. Powder X-ray Diffraction (XRD) of zeolite Na–Y, PTA–Y, Wk–PTA–Y and Pd–PTA–Y were obtained at room temperature on Rigaku D MAX III VC diffractometer using Ni-filtered Cu K_α radiation, λ = 1.5404 Å, where 2 θ ranges were from 5° and 50° at a scan rate of 8°/min.

For Scanning electron microscopy (SEM), the crystalline supports were suspended in isopropanol, casted on gold plated discs followed by drying under vacuum and then were imaged on a Philips XL 30 instrument. Specific surface areas of the catalysts were determined by the BET method using N_2 adsorption measured on an Omnisorb CX–100 Coulter instrument. Prior to adsorption, the catalyst was activated at 423 K for 6 h at 10^{-4} Torr pressure. Inductively coupled plasma with atomic emission spectra (ICP-AES) analyses of Wk–PTA–Y and Pd–PTA–Y as well as reaction mixtures after hydroformylation and hydrocarboxylation reactions were performed in a Perkin Elmer 1200 instrument for determination of metal contents. Gas chromatography (GC) of the reactants and products was performed in a HP 5890 instrument fitted with a FFAP capillary column.

5.3.1. LEACHING AND RECYCLE EXPERIMENTS WITH THE TETHERED CATALYSTS, Wk–PTA–Y and Pd–PTA–Y

Catalyst leaching experiments have been performed by hot filtration of the reaction mixture at 373 K and subsequently testing the catalytic activity of the filtrate for hydroformylation without addition of catalyst. This solution and the catalysts thus recovered (dissolved in conc. HNO_3) were also analyzed for determination of Rhodium, Palladium and Tungsten content by ICP–AES analyses. For catalyst recycle experiments, the tethered catalyst was allowed to settle down and the clear supernatant liquid was decanted slowly. The residual solid catalysts were re-used with fresh charge of solvent and reactants for further recycle runs maintaining the same reaction conditions. In the recycle studies, the rhodium and palladium contents of the catalysts and subsequent hydroformylation and hydrocarboxylation reaction mixtures were analyzed for metal contents.

5.4. RESULTS AND DISCUSSION

The main objective of this work was to investigate the performance of the tethered metal complex catalysts for hydroformylation (scheme 5.1) and hydrocarboxylation reactions of olefins. A detailed characterization of the tethered catalysts on zeolite supports, their catalytic activity, selectivity and stability has been discussed.

5.4.1. CHARACTERIZATION OF Wk–PTA–Y AND Pd–PTA–Y CATALYSTS

The '*heterogenized*' Wk–PTA–Y and Pd–PTA–Y catalysts were characterized by powder XRD, SEM, ^{31}P CP MAS NMR and XPS for a possible elucidation of the structure, bonding and oxidation states of the complexes tethered to zeolite Y.

5.4.1.1. POWDER XRD AND SEM ANALYSIS

The microporous phases of zeolite Y, PTA–Y and Wk–PTA–Y catalysts were characterized by powder XRD. The distinct reflections and crystallinity remained unaltered from one another, as observed by the powder XRD patterns in Figure 5.1.

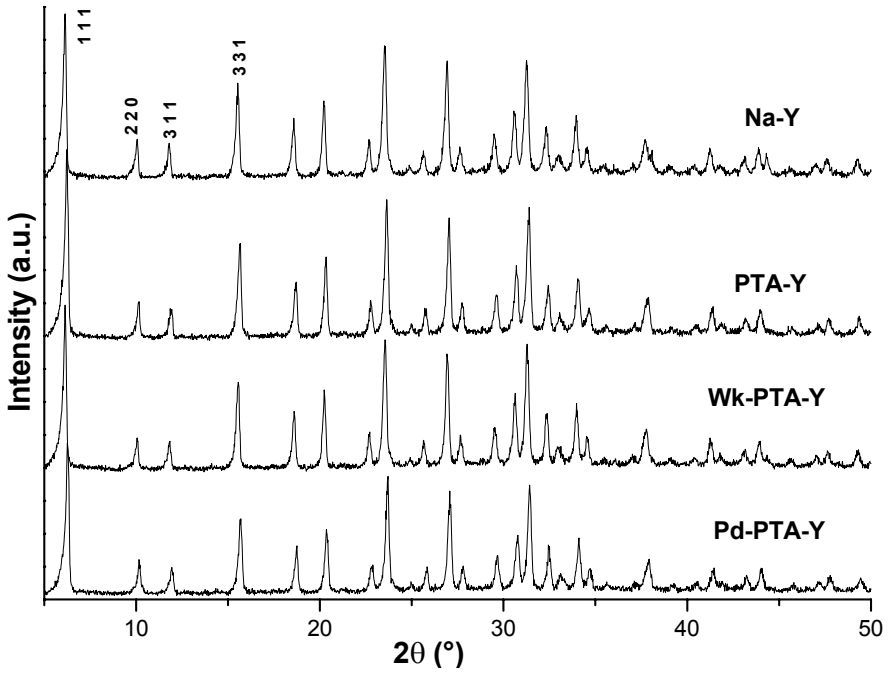

Figure 5.1. Powder XRD Patterns of (a) Na-Y, (b) PTA–Y and (c) Wk–PTA–Y

This shows that: (a) there is no change in crystallinity or morphology (determined by peak positions) of zeolite Y embedded with PTA compared to that of neat zeolite Y sample and (b) the porous framework of Wk–PTA–Y and Pd–PTA–Y catalysts were not

affected or damaged during the complex formation when $HRh(CO)(PPh_3)_3$ or Pd-Pyca complexes were tethered to the PTA–Y support.

To further consolidate this fact, we also scanned Wk–PTA–Y and Pd–PTA–Y catalysts before and after hydroformylation and hydrocarboxylation reactions by SEM (Figure 5.2). The crystalline patterns of the catalysts as well as the parent material zeolite Na-Y remained unaffected even after 6th recycle. This conclusion further supports the integrity of the Rh and Pd-complexes tethered by PTA to the zeolite matrix and retaining the crystallinity and morphology of zeolite Y even after reuse.

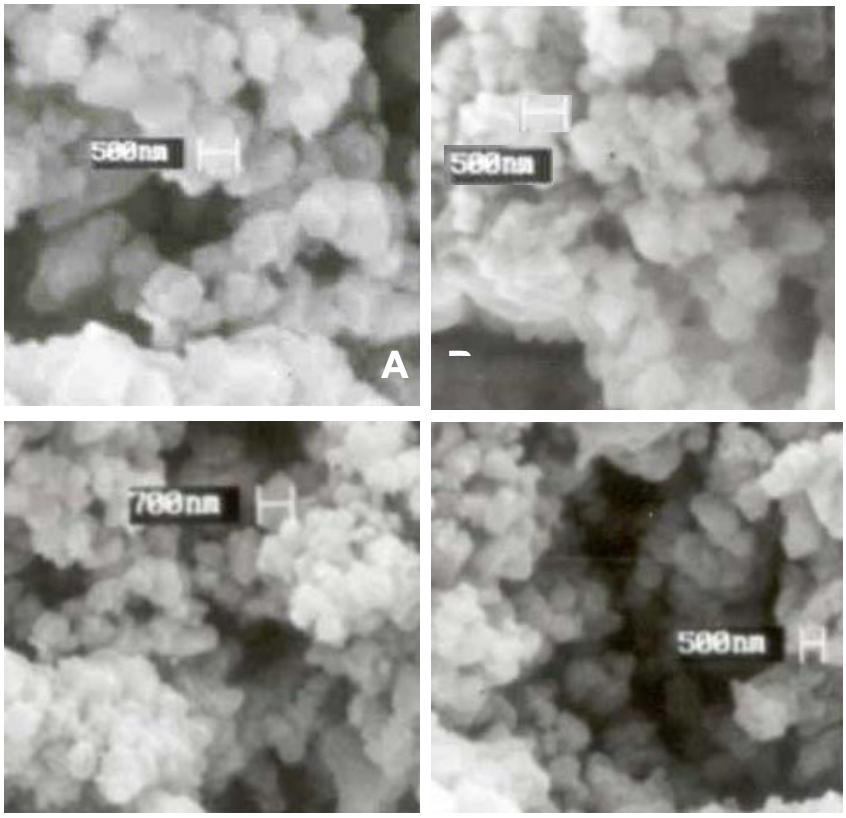

Figure 5.2. SEM of (A) zeolite Na-Y, (B) Pd-PTA-Y catalyst after 1st reaction, (C) Wk-PTA-Y catalyst before reaction and (D) Wk-PTA-Y catalyst after 6th recycle

5.4.1.2. ^{31}P CP MAS NMR: Wk-PTA-Y CATALYST

In order to understand interactions of the species and to seek conclusive evidences of true heterogeneity of complexes PTA and $HRh(CO)(PPh_3)_3$ tethered to zeolite Y, ^{31}P CP-MAS NMR spectra of PTA complex, $HRh(CO)(PPh_3)_3$ complex and Wk–PTA–Y catalyst were recorded (Figure 5.3).

There was only one major ^{31}P signal (δ_{iso} −19.8 ppm) of the PTA complex ($H_3PW_{12}O_{40}.24H_2O$ (PTA) acquired from s. d. Fine Chemicals), as envisaged from the structure, while that of the $HRh(CO)(PPh_3)_3$ complex had two major ^{31}P signals (δ_{iso}: 34.4, 45.4 ppm), each split by J-coupling to other ^{31}P and ^{103}Rh (n = 100%) nuclei; as reported earlier by us (22). The spectral pattern observed in Figure 5.3 for $HRh(CO)(PPh_3)_3$ thus, elucidated trigonal bipyramidal geometry of the complex. In comparison to ^{31}P spectra of the PTA and Rh-complex, Wk–PTA–Y catalyst showed a totally different spectrum with two distinct peaks (δ_{iso}: −12.1, 32.0 ppm). The shifts in NMR of Wk–PTA–Y catalyst may be due to a possible interaction of PTA and Rh-complex tethered to the zeolite Y matrix, where a Rh-O-W-O-Si type bond formation may have taken place (see Scheme 5.1). Interaction of this type is feasible, as bonding of types Rh-O-W in the solution phase [19] and O_{PTA}-Si [20] has been reported earlier.

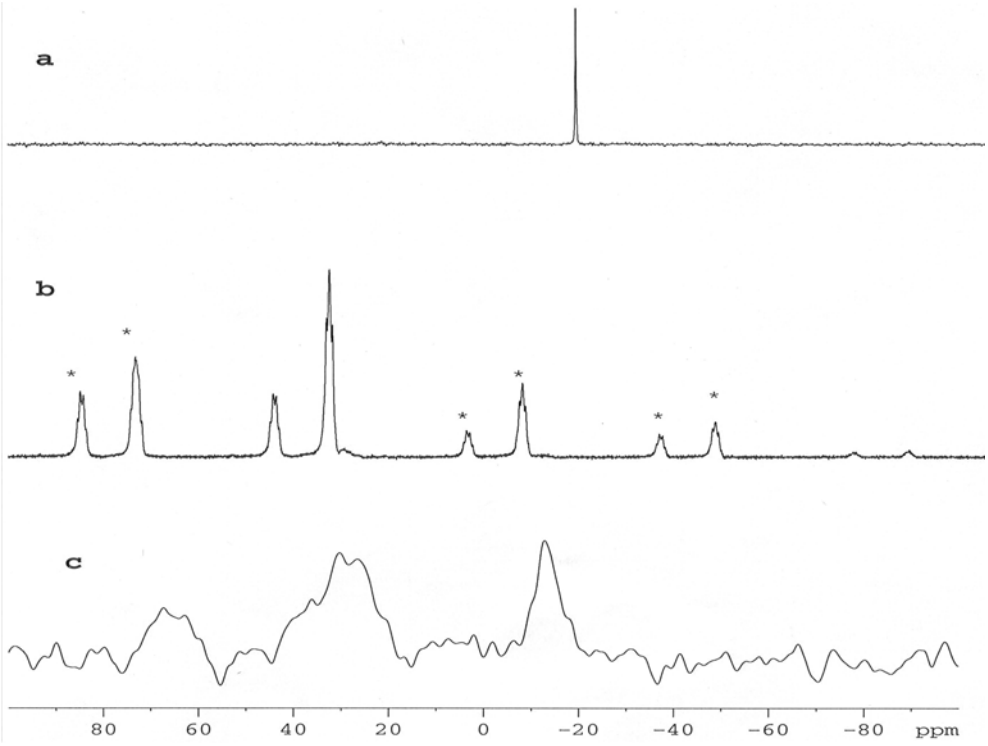

Figure 5.3. ^{31}P CP - MAS NMR of catalysts (a) PTA, (b) $HRh(CO)(PPh_3)_3$ and (c) Wk-PTA-Y ('*' indicates side bands at 8 kHz)

5.4.1.3. ^{31}P CP MAS: Pd-Pyca-PTA-Y CATALYST (Pd-PTA-Y)

In another experiment, ^{31}P CP-MAS NMR spectra of Pd-Pyca complex, PTA complex and Pd–PTA–Y solid catalyst (all the samples were referenced to H_3PO_4) were recorded on a 300 MHz NMR spectrometer to record changes in the ^{31}P peak positions. A comparison of the ^{31}P signals obtained by scanning these solid complexes and catalyst by NMR was therefore, performed to seek conclusive evidences of true heterogeneity and bonding between PTA and Pd-Pyca complexes tethered to zeolite Y (Figure 5.4).

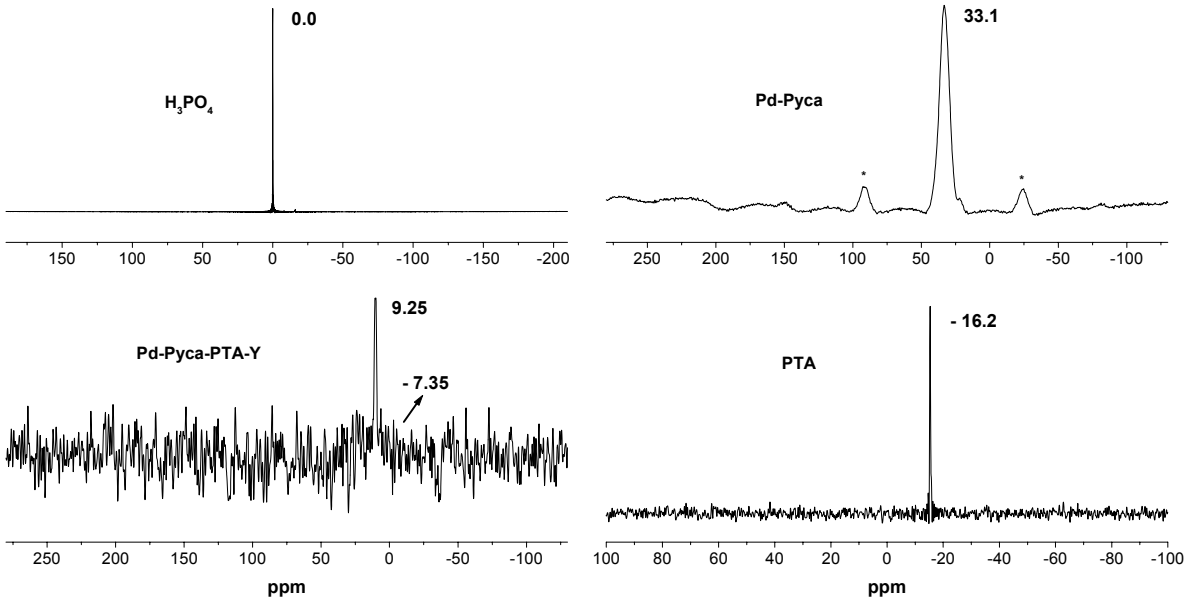

Figure 5.4. ^{31}P CP-MAS NMR of H_3PO_4, Pd-Pyca, Pd-PTA-Y and PTA

Only one major ^{31}P signal were recorded each for Pd-Pyca (δ_{iso}: 33.1 ppm) and PTA (δ_{iso}: −16.2 ppm; $H_3PW_{12}O_{40}.6H_2O$ (PTA) complexes acquired from Acros Chemicals) as envisaged from their respective structures (see Figure 5.4). There was a drastic shift in the NMR signal when the ^{31}P CP-MAS NMR of Pd-PTA-Y was carried out (δ_{iso}: 9.25 ppm and a weak signal at −7.35 ppm). Though the signal to noise ratio for this sample is poor, yet the change in the NMR shifts in the Pd-Pyca-PTA-Y catalyst from 33.1 ppm to 9.25 ppm and −16.2 ppm to −7.35 ppm observed for Pd-Pyca and PTA respectively (see Figure 5.4), validates that Pd-Pyca complex is bound to the PTA-Y support. The changes in the peak ^{31}P positions observed for Pd-PTA-Y compared to that of Pd-Pyca and PTA complexes is analogous to the tethered catalyst (Wk-PTA-Y) and Rh-complexes for hydroformylation reactions (see previous section 5.4.1.2 of this chapter). In a similar fashion, therefore, we can conclude that there is definitely a Pd-O-

W-O-Si type interaction between the Pd-Pyca complex and the PTA-Y support (similar to tethered $HRh(CO)(PPh_3)_3$ tethered to PTA-Y matrix), when tethered.

5.4.1.4. ^{29}Si MAS NMR: Wk-PTA-Y, PTA-Y and Na-Y

In order to look into the structural changes, if at all occurred while tethering metal complexes to the zeolite support, a typical ^{29}Si MAS NMR experiment of Na-Y, PTA-Y and Wk-PTA-Y supports (see Figure 5.5) were recorded on a Bruker MSL 300 FT-NMR spectrometer at 99.44 MHz and 11.7 Tesla and chemical shifts were referred to TMS (tetramethylsilane).

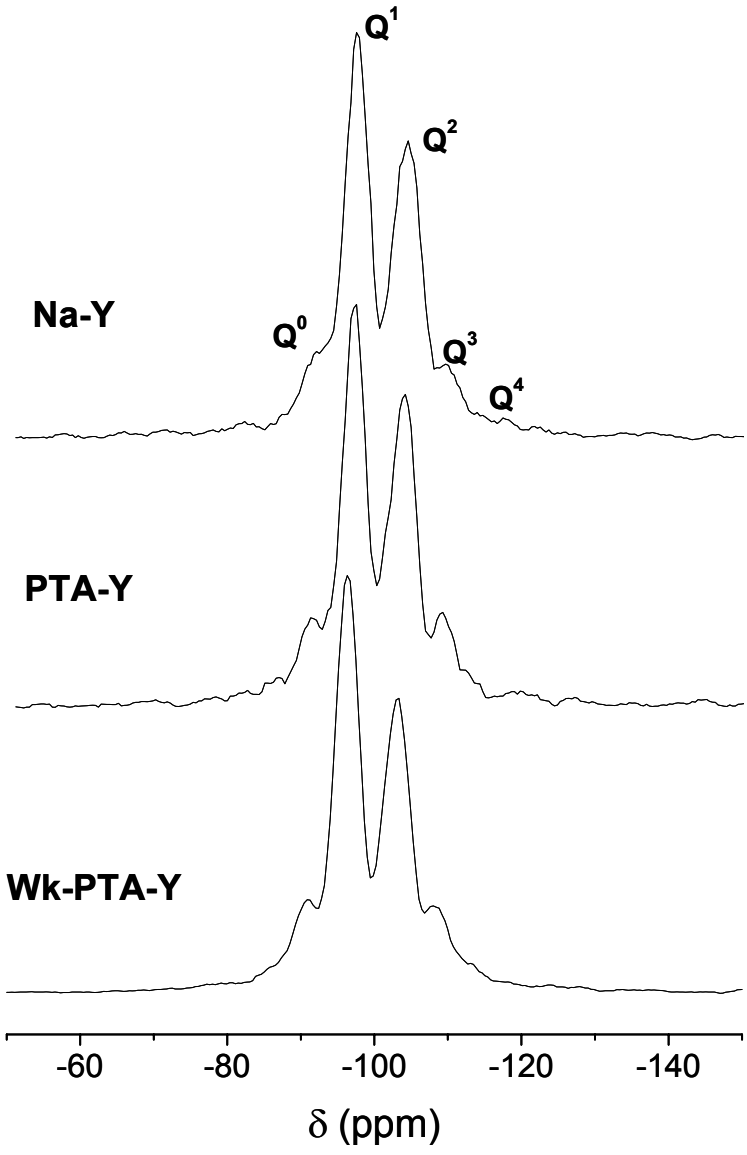

Figure 5.5. ^{29}Si MAS NMR spectra of Na-Y, PTA-Y and Wk-PTA-Y

The framework Si/Al ratio (2.37) in all the three samples (Na-Y, PTA-Y and Wk-PTA-Y) remained unaltered (see Figure 5.5), which confirmed that:

(a) the framework structure is intact after binding to PTA species to form PTA-Y,
(b) the structure is intact when Rh-complex is tethered to form Wk-PTA-Y, and
(c) there is no leaching of Al species from the zeolite Na-Y framework in the Wk-PTA-Y catalyst-synthesis process.

Thus, Al site distributions and population remain unaltered as seen from the Q^4 (nAl, wherein n = 0, 1, 2,3) environments that were detected in the above-mentioned samples in Figure 5.5.

5.4.1.5. X-RAY PHOTOELECTRON SPECTRA (XPS) ANALYSIS

Wk–PTA–Y and Pd–PTA–Y catalysts were also characterized by XPS for tungsten, silicon, aluminium, phosphorus, carbon, rhodium and palladium atoms for their respective binding energies (B. E.) and oxidation states. The B. E. values of the elements present in Wk–PTA–Y (Table 5.1 and Figure 5.6) and Pd–PTA–Y (Table 5.2 and Figure 5.7) catalysts complied well with values obtained from Rh-complex and Pd-complex supported on zeolite, as reported earlier [21]. These illustrated that rhodium and palladium were present as Rh (I) and Pd (II) without suffering from any beam damage by the catalyst and the integrity of the $HRh(CO)(PPh_3)_3$ and Pd-pyca complexes tethered to PTA-Y. Moreover, there was no change in the B. E. values or oxidation states of Rh (I) and Pd (II) to Rh (0) or Pd (0) species (B. E. values for Rh $3d_{5/2}$ is 307.1 eV and Pd $3d_{5/2}$ is 335.0 eV for Rh (0) and Pd (0) species respectively, see Ref. [22]), as often observed after the reaction or in the catalyst synthesis steps. A change in the usual B. E. values of tungsten (see Tables 5.1 and 5.2) was observed both in Wk–PTA–Y and Pd–PTA–Y catalysts, which could be possibly due to the rich electron density on tungsten atom arising from the Rh-O-W or Pd-O-W linkages in the respective systems. Decrease in B. E. values for W_{4f} species has been observed earlier [23] for reduction of W (VI) species to W (V) oxidation state, although it is indiscernible to conclude whether W (VI) of PTA has been reduced to W (V) or lower oxidation states from the XPS experiments alone due to very minimal differences among various lower oxidation states of tungsten.

Table 5.1. XPS values for different elements present in Wk–PTA–Y

Values \ Elements	W	Al	Si	P	C	Rh	
						$3d_{5/2}$	$3d_{3/2}$
Observed (eV)	29.5	77.6	106.1	133.0	288	313.2	317.8
Corrected (eV)[§]	26.5	74.6	103.1	130.0	285	310.2	314.8
Literature (eV)[‡]	31.0	74.7	103.4	130.1	285	309.1	313.9

[§] Corrected to C 1s with binding energy of 285 eV using adventitious carbon

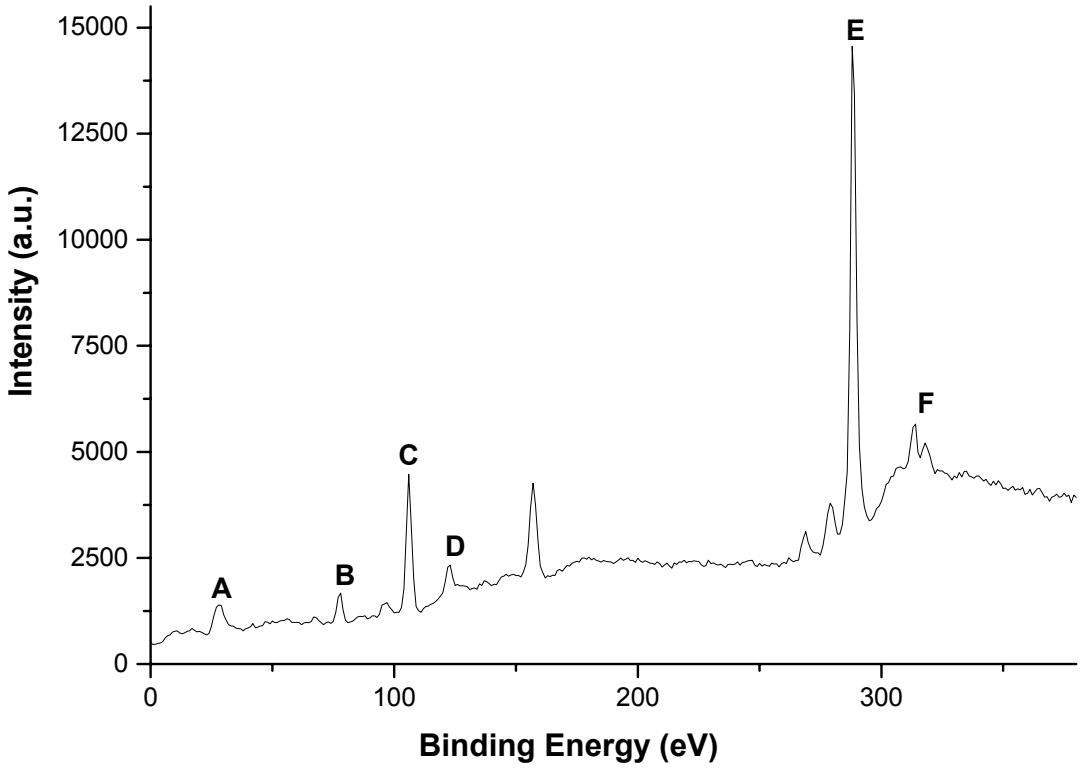

Figure 5.6. X-ray photoelectron spectra of Wk–PTA–Y catalyst (A: W $4f_{7/2}$; B: Al $2p_{3/2}$; C: Si $2p_{3/2}$; D: P $2p_{3/2}$; E: C $1s_{1/2}$; F: Rh $3d_{5/2}$ and Rh $3d_{3/2}$)

Table 5.2. XPS values for different elements present in Pd–PTA–Y

Values \ Elements	W	Al	Si	P	C	Pd	
						$3d_{5/2}$	$3d_{3/2}$
Observed (eV)	30.5	79.9	109.1	134.0	290.5	342.5	348.5
Corrected (eV)[§]	25.5	74.4	103.6	129.5	285	337.0	343.0
Literature (eV)[‡]	31.0	74.7	103.4	130.1	285	337.1	342.9

[§] Corrected to C 1s with binding energy of 285 eV using adventitious carbon

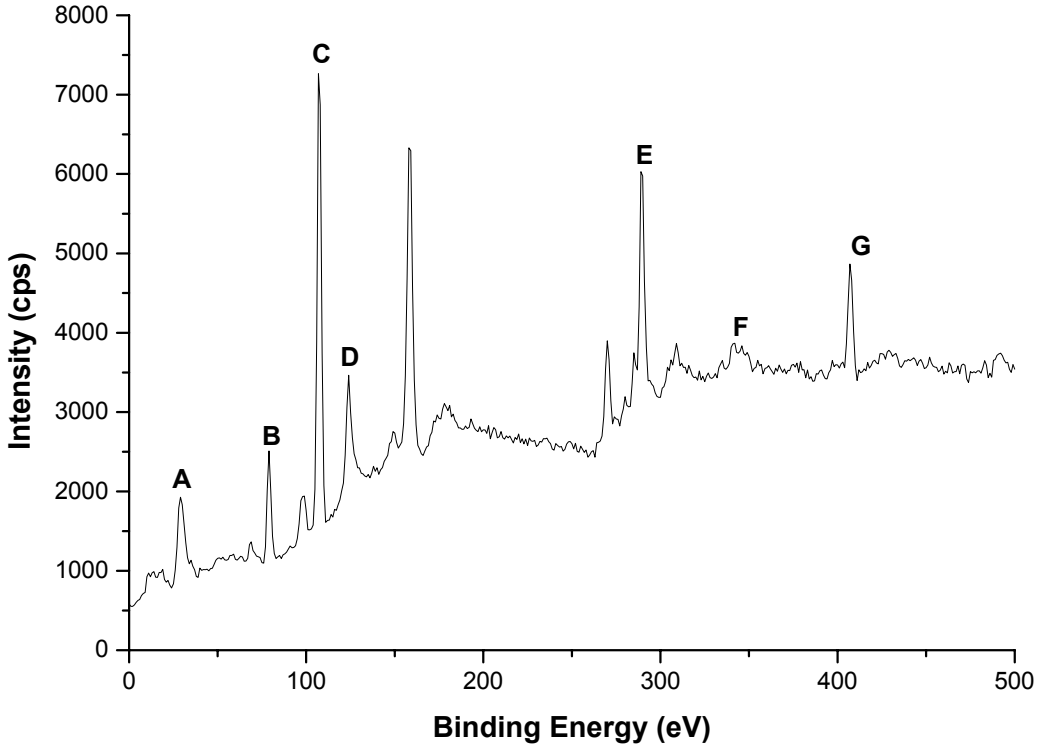

Figure 5.7. X-ray photoelectron spectra of Pd–PTA–Y catalyst (A: W $4f_{7/2}$; B: Al $2p_{3/2}$; C: Si $2p_{3/2}$; D: P $2p_{3/2}$; E: C $1s_{1/2}$; F: Pd $3d_{5/2}$ and Pd $3d_{3/2}$; G: N $1s_{1/2}$)

Crystal structures of $HRh(CO)(PPh_3)_3$ [24] and an analogous heteropolyacid (similar to PTA molecule), $H_3PW_{12}O_{40}.21H_2O$ [25] showed that the dimensions of the complexes are close to $10.8 \times 10.7 \times 10.8$ $(Å)^3$ and $7.1 \times 6.8 \times 7$ $(Å)^3$ respectively. This reflects that there could be a possible entrapment of the PTA through the zeolite Y windows (7.4 Å) inside its supercage (12 Å), but inclusion of the Rh-complex through the windows is not feasible. Since, the exact chemistry of the tethered moiety is not yet well understood, we speculate a weak coordinate-covalent interaction (similar to that observed by Burk et al. Ref. [10])) between oxygen atoms of PTA with the Rh-atom of the $HRh(CO)(PPh_3)_3$ complex. This sort of ionic interaction fastens the Rh-complex tightly with the oxygen atoms of PTA tethered to zeolite Y matrix thus, restricting the complex from leaching out in the liquid phase during reaction (see Scheme 5.1). Since, we could not obtain crystals of Pd-Pyca complex, single crystal structural data could not be obtained, but similar type of interaction between the Pd-complex and the zeolite Na-Y support is present.

5.4.2. HYDROFORMYLATION OF OLEFINS USING Wk-PTA-Y CATALYST

Wk–PTA–Y catalyst was evaluated for its activity and selectivity behaviour in hydroformylation of terminal and branched alkenes, the results of which are presented in Table 5.3.

Table 5.3. Hydroformylation of olefins with $HRh(CO)(PPh_3)_3$ and Wk–PTA–Y catalysts

Catalysts	Substrate	Conv. %	Selectivity		TOF, h^{-1}	TON	Time, h
			Ald %	n/iso			
$HRh(CO)(PPh_3)_3$	Styrene (S)	98.0	98.9	0.39	2898	2666	0.92
Wk–PTA–Y	Styrene (S)	98.1	99.8	0.51	771	1797	2.33
$HRh(CO)(PPh_3)_3$	*p*-Me-S	97.9	97.8	0.47	2073	2239	1.08
Wk–PTA–Y	*p*-Me-S	99.2	99.7	0.51	677	1578	2.33
$HRh(CO)(PPh_3)_3$	*p*-Acetoxy-S	97.9	98.3	0.43	1575	1890	1.20
Wk–PTA–Y	*p*-Acetoxy-S	99.2	99.9	0.47	680	1360	2.00
$HRh(CO)(PPh_3)_3$	*p*-*t*Bu-S	97.6	94.3	0.52	1035	1585	1.53
Wk–PTA–Y	*p*-*t*Bu-S	99.1	99.2	0.54	350	1135	3.25
$HRh(CO)(PPh_3)_3$	1-Hexene	98.8	98.8	2.57	2455	2455	1.00
Wk–PTA–Y	1-Hexene	99.3	99.1	2.48	670	1675	2.50
$HRh(CO)(PPh_3)_3$	1-Octene	98.8	98.2	2.44	1380	1835	1.33
Wk–PTA–Y	1-Octene	99.1	99.2	2.33	437	1312	3.00
$HRh(CO)(PPh_3)_3$	1-Decene	98.1	92.2	1.38	984	1506	1.53
Wk–PTA–Y	1-Decene	98.6	99.3	1.50	328	1065	3.25
$HRh(CO)(PPh_3)_3$	1-Dodecene	97.2	89.1	0.80	638	1220	1.91
Wk–PTA–Y	1-Dodecene	98.2	98.9	1.22	277	900	3.25

Reaction conditions: Wk–PTA–Y: 4 kg m^{-3} (100 mg); Rh-content in Wk–PTA–Y: 0.49% w/w; $HRh(CO)(PPh_3)_3$: 0.96 kg m^{-3} (24 mg); substrate: 0.349 kmol m^{-3}; P_{co}: 2.04 MPa; P_{H2}: 2.04 MPa; speed: 16.67 Hz; temperature: 373 K; solvent: cyclohexane; volume: $2.5x10^{-5}$ m^3; TON = kmol of substrate converted to aldehydes × $(kmol\ of\ Rh)^{-1}$; TOF = TON × $(hour)^{-1}$

The turn over frequency (TOF), conversion of olefins and selectivity values were evaluated from the concentration–time profiles, a typical example of which for hydroformylation of styrene is shown in Figure 5.8. We have observed concentration-time as well as, $(CO + H_2)$ consumed versus time data in most of the experiments. Since, the material balance of $CO + H_2$ conversion, olefin concentration and aldehydes products

formed was found to be consistent in all the cases. The data presented in Table 5.3 is for olefin conversion > 98% using the tethered catalyst.

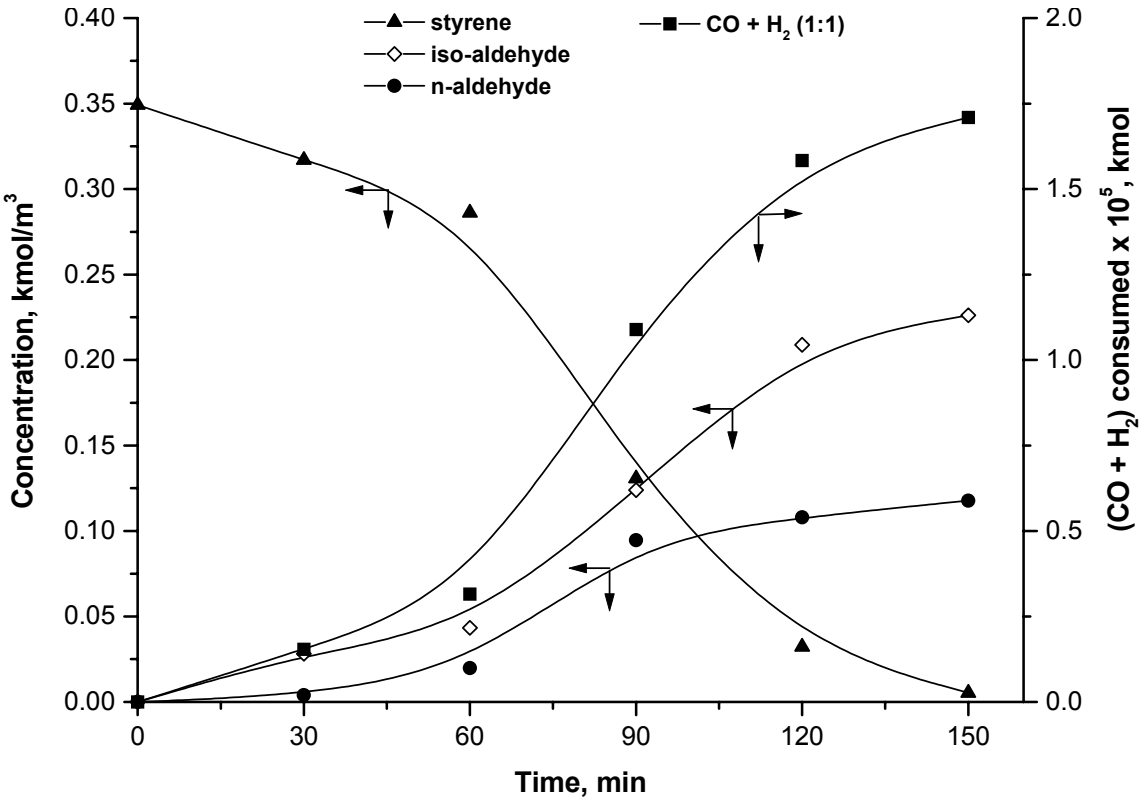

Figure 5.8. Concentration – time profile for styrene hydroformylation with Wk–PTA–Y

Reaction conditions: Wk-PTA-Y: 4 kg m^{-3} (100 mg); Rh-content in Wk–PTA–Y: 0.49% w/w; styrene: 0.349 kmol m^{-3}; P_{co}: 2.04 MPa; P_{H2}: 2.04 MPa; agitation speed: 16.67 Hz; temperature: 373 K; solvent: cyclohexane; volume: 2.5×10^{-5} m^3

Reaction products were analyzed by GC and ^{1}H NMR (where required). Hydroformylation with Wk–PTA–Y catalyst (see Table 5.3) showed excellent conversions (> 98%) of terminal and branched alkenes to respective aldehydes, high TOF (TOF ranging from 275–775 h^{-1} for various olefinic substrates), stability (after 6 recycles, the catalyst was still very active with same TOF) and high aldehyde-selectivity (> 99%) even in the absence of free PPh_3, often used in the homogenous or immobilized systems [12, 26, 34). We observed lower hydroformylation activity (TOF values) for the tethered catalyst in comparison to the $HRh(CO)(PPh_3)_3$ catalyst, which might possibly be due to the spatial restrictions of the substrate molecules to the catalytic site of Wk–PTA–Y.

To prove the catalyst stability and true heterogeneity, we performed leaching experiments, where hot reaction-mixture filtrates at 373 K were tested for hydroformylation activity without addition of fresh catalyst and adding the substrates. Since, no activity was observed for 10 h, we could conclude that metal leaching does not occur from the catalyst in the reaction medium. The hot filtrates were also subjected for ICP-AES analyses of Rh and W content (< 0.01% Rh and W loss), which exhibited almost no leaching of Rh or W metals from the tethered catalyst during reactions. The catalyst was thus found to be very stable, restoring high activity and selectivity even after 6 recycles for hydroformylation of styrene with the same batch of the catalyst (see Figure 5.9).

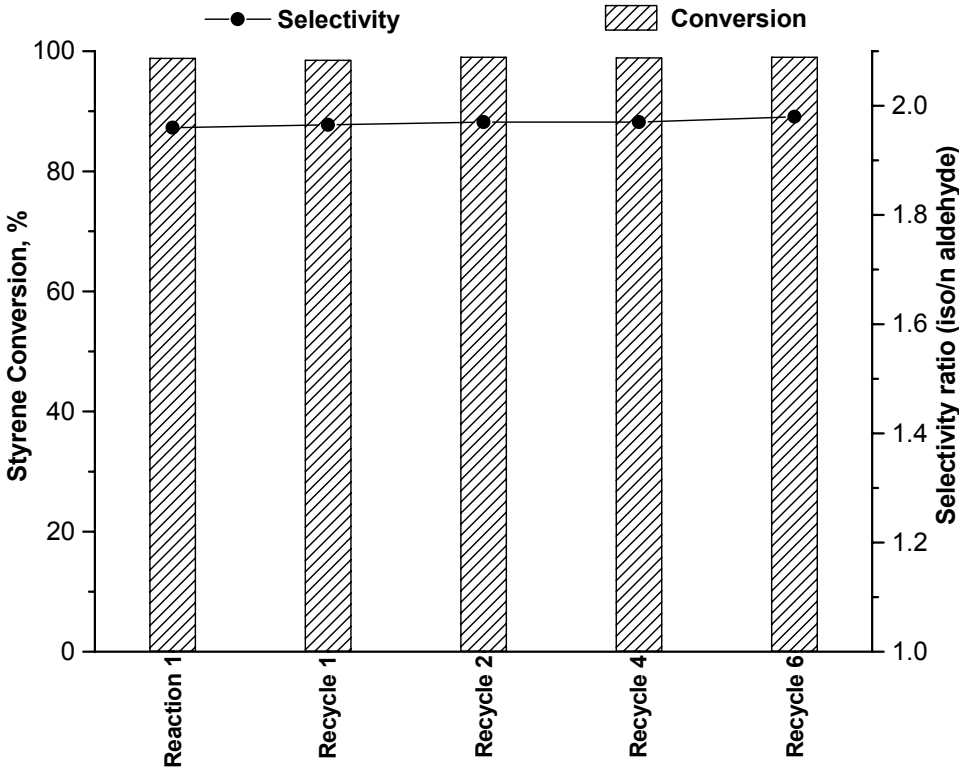

Figure 5.9. Recycle studies using Wk–PTA–Y catalyst for hydroformylation of styrene

***Reaction conditions*:** catalyst: 4 kg m^{-3} (100 mg); Rh-content in Wk–PTA–Y: 0.49% w/w; styrene: 0.349 kmol m^{-3}; P_{co}: 2.04 MPa; P_{H2}: 2.04 MPa; agitation speed: 16.67 Hz; temperature: 373 K; solvent: cyclohexane; volume: 2.5×10^{-5} m^3

5.4.2.1. HYDROFORMYLATION OF OLEFINS USING OTHER SUPPORTS

Hydroformylation of 1-Hexene was carried out with tethered $HRh(CO)(PPh_3)_3$ (abbreviated as 'Wk') on PTA anchored supports; the supports tested herein being Al_2O_3, SiO_2, MgO (all procured from Aldrich chemicals, USA) and Si-MCM-41 (synthesized as described in section 4.2.2.1 in the thesis). The tethered catalyst supports were synthesized using the same methodology as we had prepared Wk-PTA-Y catalyst. These catalysts when tested for hydroformylation of 1-Hexene were found to vary in activity (TOF) as well as selectivity (for desired aldehyde products) as presented in Table 5.4. In some cases considerable amount of Rh-metal leaching was observed in the hydroformylation reaction and subsequent recycles (e.g. SiO_2 and MCM-41 supports), whereas lower activity as well as selectivity for 1-Heptanal was observed when Al_2O_3 and MgO were used as supports (compared to the Wk-PTA-Y catalyst system in Table 5.3). It had been reported earlier that amorphous SiO_2 is a poor support for heterogenizing metal complex catalysts [28] and degradation of hexagonal structures of MCM-41 occurs on interaction with PTA [29]. Possibly these factors led to appreciable leaching of Rh-metal from the catalyst supports during the hydroformylation reaction and in subsequent recycles (Table 5.4).

Table 5.4. Hydroformylation of 1-Hexene using various Wk-PTA tethered supports

Catalysts	Rh-content (% wt./wt.)	Rh-leached [a] (%)	Conversion (%)[b]		TOF, h^{-1}	Time, h
			C_7-ald.	C_7-alc.		
Wk-PTA-SiO_2	0.47	3.10	97.3	–	581	3.00
Wk-PTA-M41	0.51	5.27	98.2	–	643	2.50
Wk-PTA-Al_2O_3	0.44	0.16	92.1	3.1[c]	537	3.25
Wk-PTA-MgO	0.39	0.21	78.8	12.9 [c]	481	3.50

Catalyst: 4 kg m^{-3} (100 mg); 1-Hexene: 0.349 kmol m^{-3}; P_{co}: 2.04 MPa; P_{H2}: 2.04 MPa; agitation speed: 16.67 Hz; temperature: 373 K; solvent: cyclohexane; volume: $2.5x10^{-5}$ m^3; TOF = kmol of 1-Hexene converted to 1-Heptanal × (kmol of Rh × h)$^{-1}$; [a] Rh-leached after 4 recycles = ppm of Rh-leached × 100 × (ppm of Rh-content in the catalyst);
[b] C_7-ald. = 1-Heptanal, C_7-alc. = 1-Heptanol;
[c]n-Hexane, n-Heptane and other olefinic products (undiagnosed) were also formed.

Choosing Al_2O_3 and MgO as supports produced undesired side products (e. g. 1-Heptanol, n-Heptane, n-Hexane and other mixed as well as higher aldehyde-products), which considerably decreased the overall conversion towards 1-Heptanal and hence TOF, although leaching of Rh-metal during the course of reaction or recycles was minimal. The yield of undesired products (1-Heptanol and alkanes) was more pronounced when MgO was chosen as support (Table 5.4).

Though, a thorough investigation is required to envisage the formation of these side products, a probable reason might be related to the basicity (as MgO is a basic oxide and possesses Frenkel defects, Al_2O_3 is an amphoteric oxide) and F-defects present in the MgO structure [30], which possibly renders reduction of the aldehyde (formed during the hydroformylation reaction) to alcohols and alkanes (Table 5.4). Earlier, an analogous report related to increased selectivity for alcohol was accounted for ethylene hydroformylation over $[H^XRu_3(CO)_9(CCO)]^{2-X}/SiO_2$-$Al_2O_3$, SiO_2 and MgO (x = 0 – 2) catalyst systems [31]. The study showed that various surface species of the title triruthenium ketenylidene cluster catalysts prepared on MgO, SiO_2, and SiO_2-Al_2O_3 showed differing activities and selectivities for oxygenates (Propanal and Propanol) and C_2H_6 in ethylene hydroformylation. Oxygenate and alcohol selectivities were 27% and 46% (MgO), 6% and 0% (SiO_2), and 2% and 0% (SiO_2-Al_2O_3), respectively.

Thus, amongst the catalyst supports surveyed in our study (Tables 5.3 and 5.4), Wk-PTA-Y was found to be an excellent choice in comparison to choice of other supports, and heterogeneous catalysts reported previously [13, 27, 32–37] in terms of hydroformylation rates, TOF, aldehyde-selectivity, stability and heterogeneity in particular. Recent reports using immobilized rhodium complexes anchored to MCM-41 matrix [32], polyelectrolyte [36] and delamellated matrix [37] for hydroformylation of olefins showed lower TOF of 165 h^{-1} for 1-hexene, as reported by Schwab et al. [36] and significant Rh leaching during recycles as compared to our system.

5.4.3. HYDROCARBOXYLATION OF ARYL OLEFINS AND ALCOHOLS USING Pd-PTA-Y CATALYST

To extend the tethering concept for other reactions, we chose to develop a Pd-based heterogeneous catalyst (using tethering methodology) using Pd-Pyca complex tethered to PTA supported zeolite Y for hydrocarboxylation reactions. Pd–PTA–Y catalyst was evaluated for its activity and selectivity behaviour in hydrocarboxylation of olefins and alcohols, the results of which are presented in Table 5.5. The mole ratio of the promoters (LiCl, TsOH) and free PPh_3 ligand to the substrate concentration was kept constant through out the reaction course at 388 K temperature and lower reaction pressures (5.4 MPa) as standardized for hydrocarboxylation reactions, discussed in the previous chapter.

Table 5.5. Hydrocarboxylation of aryl olefins and alcohols with Pd-Pyca and Pd–PTA–Y catalysts

Catalysts	Substrate	Conv. %	Selectivity (%)		TOF, h^{-1}	TON	Time, h
			iso	n			
Pd-Pyca	Styrene (S)	97.0	99.01	0.98	2600	2666	0.92
Pd–PTA–Y	Styrene (S)	98.1	99.26	0.73	279	3346	12.00
Pd-Pyca	4-Me-S	95.0	99.12	0.81	1173	2239	1.08
Pd–PTA–Y	4-Me-S	96.6	99.11	0.87	275	3298	12.00
Pd-Pyca	4-*t*Bu-S	95.0	99.00	0.98	1313	1890	1.20
Pd–PTA–Y	4-*t*Bu-S	94.1	99.32	0.67	247	3211	13.00
Pd-Pyca	IBPE	99.0	99.00	0.99	804	1585	1.53
Pd–PTA–Y	IBPE	95.1	98.12	1.86	250	3246	13.00

Reaction conditions: Pd–PTA–Y: 2 kg m^{-3} (50 mg); Pd-content in Pd–PTA–Y: 0.60 % w/w; Pd-Pyca: 0.4 kg m^{-3} (10 mg); substrate: 0.385 kmol m^{-3}; P_{co}: 5.4 MPa; agitation speed: 18.34 Hz; temperature: 388 K; PPh_3: 0.095 mmol; H_2O: 0.01 mmol; LiCl: 0.5 mmol; TsOH: 0.5 mmol; solvent: Methylethylketone; volume: 2.5×10^{-5} m^3; TON = kmol of substrate converted to acids × $(\text{kmol of Pd})^{-1}$; TOF = TON × $(\text{hour})^{-1}$

Reaction products were analyzed by GC and ^{1}H NMR (where required). It can be seen from Table 5.5 that hydrocarboxylation with Pd–PTA–Y catalyst showed almost complete conversions (> 95%) of all the substrates to the desired 2-arylpropionic acids with high TOF (TOF ranging from 245–280 h^{-1} for various substrates), stability (after 4 recycles, the catalyst was still very active with same TOF) and high regioselectivity (> 98%). We observed lower hydrocarboxylation activity for styrene ($TOF_{styrene}$ = 279 h^{-1})

using tethered Pd-PTA-Y catalyst in comparison to the homogeneous Pd-pyca catalyst ($TOF_{styrene}$ = 2600 h^{-1}) (see ref. 25), or anchored Pd-pyca complex in mesoporous MCM-41 support ($TOF_{styrene}$ = 463 h^{-1}) (see ref. 23), which might possibly be due to the spatial restrictions of the substrate molecules to the catalytic site of Pd–PTA–Y or configurational changes of the Pd-Pyca catalyst attached to the PTA supported zeolite Y. Though the exact reason for lower activity as well catalytic mechanism is yet to be experimentally revealed, the tethered approach extends a new alternative for developing heterogeneous Pd catalyst system for carbonylation reactions.

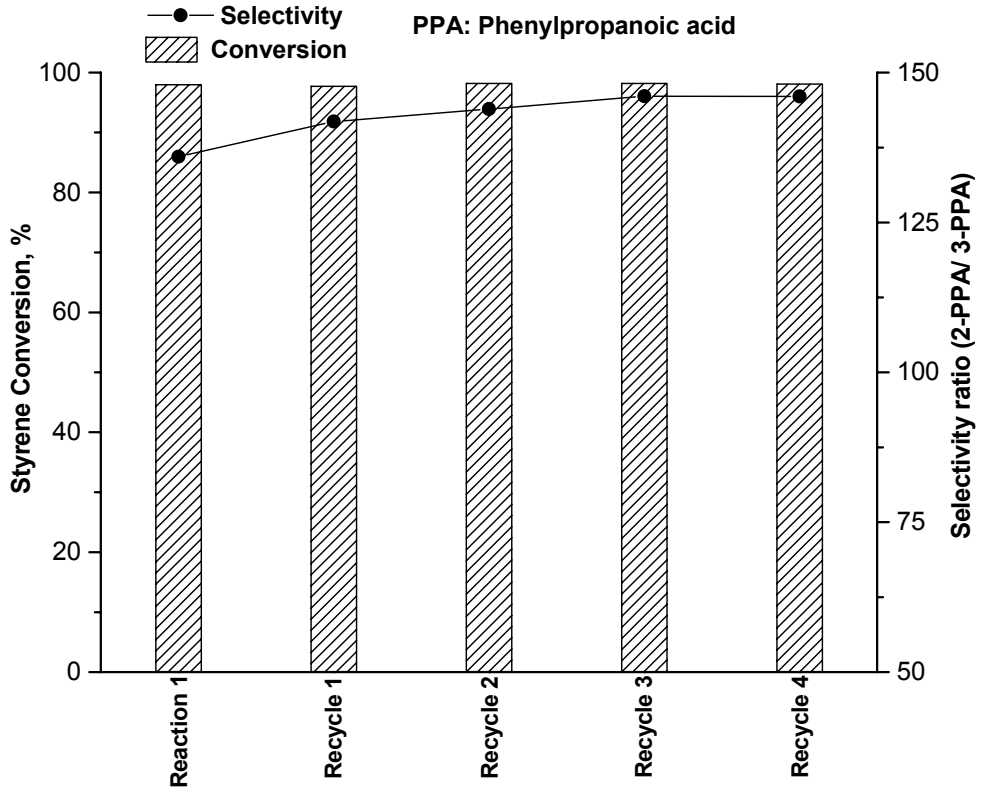

Figure 5.10. Recycle studies using Pd-PTA-Y catalyst for hydrocarboxylation of styrene

Reaction conditions: Pd–PTA–Y: 2 kg m^{-3} (50 mg); Pd-content in Pd–PTA–Y: 0.60 % w/w; substrate: 0.385 kmol m^{-3}; P_{co}: 5.4 MPa; agitation speed: 18.34 Hz; temperature: 388 K; PPh_3: 0.095 mmol; H_2O: 0.01 mmol; LiCl: 0.5 mmol; TsOH: 0.5 mmol; solvent: Methylethylketone; volume: 2.5×10^{-5} m^3.

To prove the catalyst stability and true heterogeneity, we performed leaching experiments, where hot reaction-mixture filtrates at 373 K were tested for hydrocarboxylation activity without addition of fresh catalyst and adding the substrates. Since, no activity was observed for 12 h, we could conclude that Pd-metal leaching does not occur from the catalyst in the reaction medium. The hot filtrates were also subjected

for ICP-AES analyses of Pd and W metal contents (< 0.01% Pd and < 0.01% W overall loss), which exhibited almost no leaching of Pd metal from the tethered Pd-PTA-Y catalyst during reactions or subsequent recycles. A typical recycle study (4 recycle runs) was performed for hydrocarboxylation of styrene with the same batch of the Pd-PTA-Y catalyst that was found to be very stable, retaining high activity and regioselectivity for 2-Phenylpropanoic acid (see Figure 5.10) without leaching of Pd-metal from the catalyst.

5.5. CONCLUSIONS

Thus, the novel tethered catalyst systems, consisting of a tethered $HRh(CO)(PPh_3)_3$ and Pd-Pyca complexes bound through phosphotungstic acid on zeolite Y has been reported for hydroformylation and hydrocarboxylation of olefins to aldehydes, and olefins and alcohols to acids, respectively. The tethered catalysts were found to be highly stable and recyclable for hydroformylation as well as hydrocarboxylation of a variety of olefins. By this approach, one can bind suitable homogeneous metal complex catalysts to other microporous supports to obtain stable and recyclable catalyst systems, as demonstrated by the example of hydroformylation and hydrocarboxylation of olefins.

REFERENCES

[1] Ertl, G.; Knozinger, H.; Weitkamp J., Eds.: *Handbook of Heterogeneous Catalysis*, Volumes 1 – 5, Wiley-VCH: Weinheim, **1997**.

[2] Hartley, F. R. *Supported Metal Complexes*; Reidel: Dordrecht, **1985**.

[3] Pu, L. *Chem. Rev*. **1998**, 98, 2405.

[4] Herron, N. *CHEMTECH* **1989**, 19, 542.

[5] Marks, T. J. *Acc. Chem. Res.* **1992**, *25*, 57.

[6] De Vos, D. E.; Dams, M.; Sels, B. F.; Jacobs, P. A. *Chem. Rev.* **2002**, *102*, 3615.

[7] Davies, I. W.; Matty, L.; Hughes, D. L.; Reider, P. J. *J. Am. Chem. Soc.* **2001**, *123*, 10139.

[8] Augustine, R.; Tanielyan, S.; Anderson, S.; Yang, H. *Chem. Commun.*, 1999, 1257.

[9] Tanielyan, S. K.; Augustine, R. *U. S. Patent* 6,025,295, **1999**.

[10] Burk, M. J.; Gerlach, A.; Semmerji, D. *J. Org. Chem.* **2000**, *65*, 8933.

[11] Falbe, J. *Carbon Monoxide in Organic Synthesis*, Springer-Verlag: Berlin, Heidelberg, **1970**.

[12] van Leeuwen, P. W. N. M.; Claver, C., Eds.: *Rhodium Catalyzed Hydroformylation*, Kluwer Academic: Dordrecht, **2000**.

[13] Mukhopadhyay, K; Mandale, A. B.; Chaudhari, R. V. *Chem. Mater.* **2003**, *15*, 1766.

[14] Mukhopadhyay, K; Sarkar, B. R.; Chaudhari, R. V. *J. Am. Chem. Soc.* **2002**, *124*, 9692.

[15] Mukhopadhyay, K; Chaudhari, R. V. *J. Catal.* **2003**, *1*, 73.

[16] (a) Corma, A. *Chem. Rev.* **1995**, 95, 559. (b) Breck, D. W. *Zeolite Molecular Sieves: Structure, Chemistry and Uses;* Wiley: New York, **1974**.

[17] Evans, D.; Osborn, J. A.; Wilkinson, G. J. *J. Chem. Soc. A*. **1968**, 3133.

[18] (a) Chaudhari, R. V.; Jayasree, S.; Seayad, A. M. *U. S. Patent* 6,093,847, **2000**. (b) Jayasree, S.; Seayad, A.; Chaudhari, R. V. *Org. Lett.* **1999**, *61*, 99. (c) Jayasree, S., Ph.D Thesis, submitted to Pune University, 2000.

[19] Pohl, M.; Lyon, D. K.; Mizuno, K.; Nomiya, K.; Finke, R. G. *Inorg. Chem.* **1995**, *34*, 1413.

[20] Izumi, Y.; Hasere, R.; Urabi, K. *J. Catal.* **1983**, *84*, 402.

[21] Andersson, S. L. T.; Scurrell, M. S. *J. Catal.* **1979**, *59*, 340.

[22] Wagner, C. D.; Riggs, W. M.; Davis, L. E.; Moulder, J. E., Muilenberg, Eds.; *Handbook of X-Ray Photoelectron Spectroscopy*; Perkin-Elmer Corporation: Wellesley, MA, **1979**.

[23] Maldonado-Hodar, F. J.; Perez-Cadenas, A. F.; Fierro, J. L. G.; Moreno-Castilla, C. *J. Phys. Chem. B.* **2003**, *107*, 5003.

[24] La Placa, S. J.; Ibers, J. A. *Acta Crystallogr.* **1965**, *18*, 511.

[25] Spirlet, M. –R.; Busing, W. R. *Acta Crystallogr.* **1978**, *B34*, 907.

[26] Shimizu, S.; Shirakawa, S.; Sasaki, Y.; Hirai, C. *Angew. Chem. Int. Ed. Engl.* **2000**, *39*, 1256.

[27] Sandee, A. J.; van der Veen, L. A.; Reek, J. N. H.; Kamer, P. C. J.; Lutz, M.; Spek, A. L.; van Leeuwen, P. W. N. M. *Angew. Chem. Int. Ed. Engl.* **1999**, *38*, 3231.

[28] Fraile, J. M.; Garcia, J. I.; Mayoral, J. A.; Vispe, E.; Brown, D. R.; Naderi, M. *Chem. Commun.* **2001**, 1510.

[29] Verhoef, M. J.; Kooyman, P. J.; Peters, J. A.; van Bekkum, H. *Microporous Mesoporous Mater.* **1999**, *27*, 365.

[30] Cotton, F. A.; Wilkinson, G. in *Advanced Inorganic Chemistry*, 5th Edition; Wiley: New York, 1988.

[31] Xiao, F.; Xu, R.; Ichikawa, M.; Shriver, D. F.; Guo, X. *Chin. Chem. Lett.* **1991**, *2*, 579.

[32] Nowotny, M.; Maschmeyer, T.; Johnson, B. F. G.; Lahuerta, P.; Thomas, J. M.; Davies, J. E. *Angew. Chem. Int. Ed. Engl.* **2001**, *40*, 955.

[33] Mukhopadhyay, K.; Nair V. S.; Chaudhari, R. V. *Stud. Surf. Sci. Catal.* **2000**, *130*, 2999.

[34] Davis, M. E.; Butler, P. M.; Rossin, J. A. *J. Mol. Catal.* **1985**, *31*, 385.

[35] Bianchini, C.; Burnaby, D. G.; Evans, J.; Frediani, P.; Meli, A.; Oberhauser, W.; Psaro, R.; Sordelli, L.; Vizza, F. *J. Am. Chem. Soc.* **1999**, *121*, 5961.

[36] Schwab, E.; Mecking, S. *Organometallics* **2001**, *20*, 5504.

[37] Rojas, S.; M-Mascaros, S.; Terreros, P.; Fierro, J. L. G. *New J. Chem.* **2001**, *25*, 1430.

PUBLICATIONS/ SYMPOSIA

LIST OF PUBLICATIONS/ SYMPOSIA ATTENDED/ PATENTS FILED:

PUBLISHED PAPERS:

1. *Hydroformylation of olefins using encapsulated $HRh(CO)(PPh_3)_3$ in Na-Y zeolite as a catalyst*:
   Kausik Mukhopadhyay, Vinod S. Nair and Raghunath V. Chaudhari
   Studies in Surface Science and Catalysis, 2000, 2999 – 3003.

2. *Anchored Pd Complex in MCM-41 and MCM-48: Novel Heterogeneous Catalysts for Hydrocarboxylation of Aryl Olefins and Alcohols*:
   Kausik Mukhopadhyay, Bibhas R. Sarkar, Raghunath V. Chaudhari
   ***Journal of the American Chemical Society,* 2002, 9692 – 9693.**
   ☛ **Chosen as Highlights in *SCIENCE* (EDITORS' CHOICE: CHEMISTRY), 2002, *297*, 899.**

3. *Heteropolyacids Aided Rapid and Convenient Synthesis of Highly Ordered MCM-41 and MCM-48: Exploring the Accelerated Process by ^{29}Si MAS NMR and Powder X-ray Diffraction Studies*:
   Kausik Mukhopadhyay, Anirban Ghosh, Rajiv Kumar
   ***Chemical Communications*, 2002, 2404 – 2405.**

4. *Heterogenized $HRh(CO)(PPh_3)_3$ on Zeolite Y using Phosphotungstic Acid as Tethering Agent: A Novel Hydroformylation Catalyst*:
   Kausik Mukhopadhyay, Raghunath V. Chaudhari
   ***Journal of Catalysis,* 2003, 73 – 77.**

5. *Encapsulated $HRh(CO)(PPh_3)_3$ in Microporous and Mesoporous Supports: Novel Heterogeneous Catalysts for Hydroformylation*:
   Kausik Mukhopadhyay, Anand B. Mandale, Raghunath V. Chaudhari
   ***Chemistry of Materials,* 2003, 1766 – 1777.**
   ☛ **Chosen as Research News in *THE ALCHEMIST*, 2003, *(2nd May)*.**

6. *Rh Complex Activity in Hydroformylation of 1,4–diacetoxy-butene to Vitamin-A Intermediate*:
   R. Chansarkar, **Kausik Mukhopadhyay**, A. A. Kelkar, Raghunath V. Chaudhari
   ***Catalysis Today,* 2003, 51 – 58.**

7. *Gold Nanoparticles Assembled on Amine-Functionalized Na-Y Zeolite: A Biocompatible Surface for Enzyme Immobilization*:
   Kausik Mukhopadhyay, S. Phadtare, V. P. Vinod, A. Kumar, M. Rao, Raghunath. V. Chaudhari and Murali Sastry
   ***Langmuir,* 2003, 3858 – 3863.**

PAPERS ACCEPTED:

1. *Immobilization and Biocatalytic Activity of Fungal Protease on Gold Nanoparticle-Loaded Zeolite Microspheres*:
   S. Phadtare, V. P. Vinod, **Kausik Mukhopadhyay**, A. Kumar, M. Rao, Raghunath V. Chaudhari, Murali Sastry
   ***Biotechnology and Bioengineering*, 2003, (in press)**

LIST OF PRESENTATIONS IN NATIONAL/ INTERNATIONAL CONFERENCES:

1. *Trapezing Effect between Microporous and Mesoporous Materials by Tuning the Surfactant Concentration*:
   Kausik Mukhopadhyay
   ***International Symposium on Chemistry** for Platinum Jubilee Celebration of Indian Chemical Society, Calcutta, 11th–16th December 1999; (**POSTER** presentation)*.

2. *Hydroformylation of Olefins Using Encapsulated $HRh(CO)(PPh_3)_3$ in Na-Y Zeolite as a Catalyst*:
   Kausik Mukhopadhyay, Vinod S. Nair and Raghunath V. Chaudhari
   ***12th International Congress on Catalysis**, Granada, SPAIN, 9th–14th July 2000 (**POSTER** presentation)*

3. *High Resolution ^{31}P Solid State NMR of Triphenyl Phosphine Complexes*:
   K. Damodaran, Kausik Mukhopadhyay**, S. Ganapathy**
   Symposium on Spatially Resolved Magnetic Resonance and 7th National Magnetic Resonance Society Symposium, ***Chennai, 7th–10th February 2001 (**POSTER** presentation)*.**

4. **Attended** *National Workshop on Materials Characterization and Testing* **organized by** *Centre for Materials for Electronic Technology, **Pune, 22nd February 2002.***

5. *Rh Complex Activity in Hydroformylation of 1,4–diacetoxy-butene to Vitamin-A Intermediate*:
   R. Chansarkar, Kausik Mukhopadhyay**, A. A. Kelkar, Raghunath V. Chaudhari**
   4th International Symposium on Catalysis in Multiphase Reactors, ***Lausanne, Switzerland, 22nd– 25th September 2002 (**Keynote Lecture**)*.**

6. *Keggin Anions Promoted Synthesis of Zeolites and Mesoporous Materials*:
   Kausik Mukhopadhyay, **Anirban Ghosh, Rajiv Kumar**
   *14th International Zeolite Association, **Capetown, South Africa, April 2004, (accepted for** POSTER **presentation).***

7. *Encapsulation of Metal Complexes in Inorganic Supports – New Concepts, Chemistry and Applications*:
   Kausik Mukhopadhyay
   *1st Royal Society of Chemistry Students Symposium, **NCL Pune, 19th – 20th September 2003 (**ORAL **presentation).***

LIST OF PATENTS FILED:

1. *An improved process for the preparation of zeolites and mesoporous materials*:
   Kausik Mukhopadhyay, Anirban Ghosh, Rajiv Kumar
   (**Filed for US patent**)

2. *Improved catalysts and process for hydroformylation*:
   Kausik Mukhopadhyay, R. V. Chaudhari
   (**Filed for US patent**)

3. *Novel Immobilized Metal Complex Catalysts for Carbonylation Reactions*:
   Kausik Mukhopadhyay, Bibhas R. Sarkar, R. V. Chaudhari
   (**Filed for US patent**)